CORA Cork Open Research Archive
Cartlann Taighde Oscailte Chorcaí

Title	The taphonomy of feathers
Authors	Slater, Tiffany S.
Publication date	2022-08-18
Original Citation	Slater, T. S. 2022. The taphonomy of feathers. PhD Thesis, University College Cork.
Type of publication	Doctoral thesis
Rights	© 2022, Tiffany S. Slater. - https://creativecommons.org/licenses/by-nc-nd/4.0/
Download date	2026-11-15 03:32:19
Item downloaded from	https://hdl.handle.net/10468/13657

UCC
University College Cork, Ireland
Coláiste na hOllscoile Corcaigh

Ollscoil na hÉireann, Corcaigh

National University of Ireland, Cork



The taphonomy of feathers

Thesis presented by

Tiffany Slater

ORCiD: 0000-0003-1475-8376

for the degree of

Doctor of Philosophy

University College Cork

School of Biological, Earth and Environmental Sciences

Head of School/Department: Prof. Astrid Wingler

Supervisor(s): Prof. Maria E. McNamara, Prof. Patrick J. Orr

2022

CONTENTS

List of figures 4
List of tables....8
Abstract 12
Outline 13
Project aims 14
1. Introduction 15
1.1 Feather function and development 15
1.2 Melanosomes 21
1.3 Melanins 22
1.4 Feather proteins 26
1.5 Soft tissue preservation 31
1.6 Organic preservation 32
1.7 Fossil feathers 34
1.8 Experimental taphonomy 45
2. Material and methods 51
2.1 Material 51
2.2 Taphonomic experiments 53
2.3 Resin embedding and ultramicrotomy 56
2.4 Scanning electron microscopy (SEM) 57
2.5 Transmission electron microscopy (TEM) 59
2.6 Alkaline hydrogen peroxide oxidation-high-performance liquid chromatography (AHPO-HPLC) 59
2.7 X-ray absorption near-edge structure spectroscopy (XANES) 63
2.8 Fourier-transform infrared spectroscopy (FTIR) 67
2.9 Pyrolysis-gas chromatography-mass spectrometry (py-GC-MS) 69
3. Taphonomic experiments resolve controls on the preservation of melanosomes and keratinous tissues in feathers 70
3.1 Introduction 71
3.2 Materials and methods 73
3.3 Results 79
3.4 Discussion 84
3.5 References 89
3.6 Supplementary information 95
4. Taphonomic experiments reveal authentic molecular signals for fossil melanins and verify preservation of 10 million year old phaeomelanin in fossils 97

4.1 Introduction....98
4.2 Results and discussion....101
4.3 Materials and methods....123
4.4 References....127
4.5 Supplementary information....132
5. Preservation of corneous beta proteins in Mesozoic feathers....151
5.1 Introduction....151
5.2 Results and discussion....152
5.3 Materials and methods....162
5.4 References....166
5.5 Supplementary information....170
6. Degradation experiments reveal a melanin-based bias in the preservation of corneous beta proteins in fossil feathers....176
6.1 Introduction....177
6.2 Materials and methods....178
6.3 Results....182
6.4 Discussion....195
6.5 References....200
6.6 Supplementary information....206
7. Discussion....213
7.1 Taphonomic processes vary in the extent to which they control the preservation of primary feather components....213
7.2 Feather intrinsic chemistry influences the preservation potential of feather CBPs and melanins....226
7.3 Evidence of phaeomelanin and feather CBPs can survive in deep time....232
7.4 Model for the preservation of fossil feathers....240
7.5 Limitations of taphonomic experiments....245
8. Conclusion....251
8.1 Concluding remarks....251
8.2 Future directions....253
References....256
Appendix I....289
Appendix II....289
Supplementary dataset 1....289
Supplementary dataset 2....289

List of figures

Fig. 1.1 Illustration showing the anatomy of a pennaceous feather (modified from the Cornell Bird Academy [Thompson, 2014]). ……16

Fig. 1.2 Illustrations of the common feather morphologies observed in extant birds (from the Cornell Bird Academy [Thompson, 2014]). ……17

Fig. 1.3 A schematic illustration of a pennaceous feather in the early phase of its development. The distal end of the feather develops before the proximal end (from Prum and Brush [2002]). ……18

Fig. 1.4 Schematic illustration showing the development of a feather papilla and follicle (modified from Chen et al. [2015]). The dashed line in part d indicates the position of the plane of the transverse sections in e–h. ……19

Fig. 1.5 Schematic illustration showing an adult feather follicle in the initiation, growth and rest phases of feather generation, collectively termed endysis (modified from Chen et al. [2015]). ……20

Fig. 1.6 Stages I–IV of melanogenesis for eumelanosomes and phaeomelanosomes (from D'Alba and Shawkey [2019]). ……22

Fig. 1.7 Chemical pathways for the synthesis of eumelanin and phaeomelanin (modified from Galván and Solano [2016]). ……23

Fig. 1.8 Schematic illustration of feather corneous beta proteins (CBPs). The 45° angle between each polypeptide chain in a dimer and β-filaments is omitted in order to highlight the disulfide bonds (in red in b–d). ……28

Fig. 1.9 Schematic illustration of intermediate filament-keratin (IF-keratin). (a) polypeptide chain, (b) dimer and (c) protofilament. ……30

Fig. 1.10 Evolutionary developmental model of feathers (from Prum [1999]). ……35

Fig. 2.1 Schematic diagram showing design of taphonomic experiments using black and orange (*Gallus gallus*) and white (*Egretta garzetta*) feathers. ……54

Fig. 2.2 Degradation products of eumelanin and phaeomelanin (modified from Ito et al. [2011]. Oxidation of eumelanin using alkaline hydrogen peroxide oxidation (AHPO) generates pyrrole-2,3,5-tricarboxylic acid (PTCA), pyrrole-2,3,4,5-tetracarboxylic acid (PTeCA) and pyrrole-2,3-dicarboxylic acid (PDCA) markers. AHPO treatment of phaeomelanin produces thiazole-2,4,5-tricarboxylic acid (TTCA) and thiazole-4,5-dicarboxylic acid (TDCA). Hydroiodic acid hydrolysis (HI) treatment of phaeomelanin produces 4-amino-3-hydroxylphenylalanine (4-AHP), 3-amino-4-hydroxyphenylalanine (3-AHP) and benzothiazole-amino acid (BZ-AA). ……61

Fig. 2.3 Setup of experimental beamline station 14-3 at the Stanford Synchrotron Radiation Lightsource facility (Menlo Park, CA, USA). ……64

Variation in the formatting of the figure and table captions among chapters is due to differences in the formatting requirements of the journals.

Fig. 2.4 X-ray absorption spectrum showing the primary features in a XANES spectrum and associated EXAFS region (modified from Wang et al. [2019]). ……..……65

Fig. 2.5 Unprocessed FTIR spectrum of a feather sample showing the two primary spectral regions. ……68

Fig. 3.1 Experimental sequences. Schematic showing potential natural scenarios incorporating experimental pathways 8–16. Sequence 1 is based on oxidation prior to maturation (where used); Sequence 2 is based on oxidation following maturation. Experiments included some, or all, of decay, maturation and oxidation (with various parameters used for decay and maturation; for details see Table 3.1 and Supplementary Fig. 3.1). ……76

Fig. 3.2 SEM images of feather barbules. A, pathway 1. B, pathway 2. C, pathway 3. D, pathway 4. E, pathway 5. F, untreated. G, pathway 6. H, pathway 7. A, C, F–H, transverse fractured surfaces. B, D, E, transverse microtomed surfaces. a, decay at pH 12.2; d, decay at pH 6; o, oxidized; p, matured with pressure; t, matured without pressure; u, untreated. Black arrowheads, 3D melanosomes. All scale bars represent 1 µm. ……80

Fig. 3.3 SEM images of feather barbules. D, G, H, transverse fractured surfaces. A–C, E–F, transverse microtomed surfaces. A, pathway 8. B, pathway 9. C, pathway 10. D, pathway 11. E, pathway 12. F, pathway 13. G, pathway 14. H, pathway 15. d, decay at pH 6; o, oxidized; p, matured with pressure; t, matured without pressure. Black arrowheads, 3D melanosomes. White arrowheads, mouldic melanosomes. All scale bars represent 1 µm. …… 81

Fig. 3.4 TEM images of feather barbules. A, untreated. B, pathway 2. C, pathway 8. D, pathway 12. Melanosomes appear black; moulds appear as light-toned ovoids. a, decay in alkaline conditions (pH 12.2); d, decay at pH 6; o, oxidized; u, untreated. All scale bars represent 500 nm. ……82

Fig. 3.5 Additional features of experimentally treated feathers. A–B, SEM images of transverse microtomed surfaces in untreated feathers (A) and feathers from pathway 3 (B). C, TEM image of feather barbule from pathway 8 (see Fig. 3.4C for additional examples of compressed voids at higher resolution). D, light micrograph of feather barbs following experimental treatment in pathway 16. Black arrowheads, blade marks showing direction of cutting during microtomy. White arrow, compressed moulds. White arrowheads, translucent barbs. d, decayed; o, oxidized; t, matured; u, untreated. All scale bars represent 1 µm except D (1 mm). ……..83

Fig. 3.6 AHPO analysis of *Gallus gallus* feathers and their experimental media. PTCA and PTeCA are eumelanin markers (PTeCA is a marker for diagenetically altered melanin). ……..84

Fig. 3.7 The impact of various taphonomic conditions on melanosome preservation. Grey ovoid denotes transverse section of feather barbule. Arrows indicate time. Brackets indicate that a particular taphonomic process is not always present. ……87

Fig. 4.1 Eumelanin and phaeomelanin molecules and their respective constituent monomers. Key eumelanin monomer units are DHI and DHICA; phaeomelanin monomer

units are benzothiazine (BT) and benzothiazole (BZ). Chemical degradation of these units by alkaline hydrogen peroxide oxidation (AHPO) generates PDCA, PTCA, PTeCA, TTCA and TDCA markers. Hydroiodic acid (HI) hydrolysis generates 4-AHP (and 3-AHP, not shown here) and BZ-AA[33-35,39,40]. ……100

Fig. 4.2 AHPO-HPLC data for black, orange and white feathers from extant birds with and without thermal treatment. Bar charts show melanin marker concentrations in black and orange (*Gallus gallus*) and white (*Egretta garzetta*) feathers; data are shown for untreated feathers and feathers thermally matured at 200°C and 250°C. Melanin markers are generated during alkaline hydrogen peroxide oxidation (AHPO) and hydroiodic (HI) acid hydrolysis. Filled bars indicate the mean values per treatment; floating bars indicate standard deviation per treatment. ……102

Fig. 4.3 HCl-AHPO-HPLC data for black, orange and white feathers from extant birds with and without thermal treatment. Bar charts show melanin marker concentrations for untreated feathers and feathers thermally matured at 200°C and 250°C. Melanin markers are generated during HCl-alkaline hydrogen peroxide oxidation (AHPO). Filled bars indicate the mean values per treatment; floating bars indicate standard deviation per treatment. Black and orange feathers are from the domestic chicken (*Gallus gallus*) and white feathers are from the little egret (*Egretta garzetta*). ……112

Fig. 4.4 HCl-AHPO-HPLC data for fossil melanins. Eumelanin (A) and phaeomelanin (B) marker concentrations in samples of melanosomes. Fossil feathers are from the early bird *Confuciusornis* and the feathered dinosaur *Sinornithosaurus* from the Jehol biota. Fossil frog samples are of internal melanosomes from *Pelophylax pueyoi* from the Libros biota. ……115

Fig. 4.5 Authentic chemical signals for fossil melanins. Schematic showing chemical degradation of eumelanin and phaeomelanin during fossilisation based on AHPO-HPLC analysis of experimentally matured black and orange (*Gallus gallus*) and white (*Egretta garzetta*) feathers. Dashed line separates data with and without HCl treatment. The long horizontal arrows illustrate the relative concentrations of melanin markers before treatment and after maturation at 250°C without HCl treatment. The short horizontal arrows (on the right) depict the relative concentrations of markers following maturation at 250°C with HCl treatment. Concentration values (in ng/mg) indicate absolute concentrations of melanin markers. ……117

Fig. 5.1 Sulfur-XANES spectra for fossil feathers and untreated and experimentally degraded white (*Egretta garzetta*) and black (*Gallus gallus*) feathers. ……153

Fig. 5.2 FTIR spectra for fossil feathers and untreated and experimentally degraded white (*Egretta garzetta*) and black (*Gallus gallus*) feathers. Amide bands are indicated in brown boxes and all other bands in grey boxes. ……155

Fig. 5.3 Deconvoluted amide I and II regions from FTIR data for fossil feathers and untreated and experimentally degraded white (*Egretta garzetta*) and black (*Gallus gallus*) feathers. a – f, feathers from extant birds. a, untreated black feathers. b, untreated white feathers. c, black feathers matured at 200°C. d, white feathers matured at 200°C. e, black feathers matured at 250°C. f, white feathers matured at 250°C. g – j, fossil feathers. g, h, Green River feather (YPM VP 58657). i, *Confuciusornis* (IVPP V 13171). j, *Sinornithosaurus* (IVPP V 12811). Black, processed spectra; green, resolved peaks; blue, deconvolution fit. 157

Fig. 5.4 Schematic representation of the hierarchical structure of feather corneous beta proteins (CBPs). Disulfides can occur in four component structures: β-bundles, β-filaments, dimers and β-sheets. Limited data are available on the orientation of β-strands in CBPs (but see[29]). 159

Fig. 6.1 S-XANES spectra of experimentally degraded black and orange (*Gallus gallus*) and white (*Egretta garzetta*) feathers. 184

Fig. 6.2 PCA of S-XANES spectra shown in Fig. 6.1. Chemospace plots show data fields for A) different experimental treatments and B) different feather types. Chemospace plots in C–E show data fields for experimental treatments using C) black, D) orange and E) white feathers. F) Spectra for PC2 and PC3. G – H) Chemospace plots of black, orange and white untreated feathers (G) and feathers matured at 150°C, 135 bar (with and without decay (H)), 200°C (I)and 250°C (J). 187

Fig. 6.3 Py-GC-MS pyrograms of black and orange (*Gallus gallus*) and white (*Egretta garzetta*) feathers degraded in sulfurization experiments. 189

Fig. 6.4 FTIR spectra of experimentally degraded black and orange (*Gallus gallus*) and white (*Egretta garzetta*) feathers. 191

Fig. 6.5 PCA of FTIR spectra shown in Fig. 6.4. A – B) Chemospace plots show data fields for different experimental treatments (A) and different feather types (B). Chemospace plots in C–E show data fields for experimental treatments using black (C), orange (D) and white (E) feathers. F) Spectra for components 2 and 3. G – J) Chemospace plots for black, orange and white untreated feathers (G) and feathers matured at 150°C, 135 bar (with and without decay (H)), 200°C (I) and 250°C (J). 194

List of tables

Table 2.1 Mean A650 : A500 values in black and orange (*Gallus gallus*) and white (*Egretta garzetta*) feathers after soluene-350 solubilisation. A650 and A500 values relate to the spectrophotometric absorption of the soluene-350 solution at 650 nm and 500 nm, respectively (Ozeki et al., 1996). A higher A650 : A500 ratio indicates greater eumelanin content. Black and orange feathers: n = 3; white feathers: n = 2. ……52

Table 2.2 Fossil specimens studied in this thesis. Burial history information as reported by McNamara et al. (2013). ……53

Table 2.3 List of material from extant birds and the techniques used on each sample. a, untreated; b, decayed; c, oxidised; d, sulfurised; e, thermally matured; f, matured with high pressure. 1, scanning electron microscopy; 2, transmission electron microscopy; 3, alkaline hydrogen peroxide oxidation-high performance liquid chromatography (AHPO-HPLC); 4, hydroiodic acid hydrolysis-HPLC; 5, HCl-AHPO-HPLC; 6, X-ray absorption near edge structure spectroscopy; 7, Fourier-transform infrared spectroscopy; 8, pyrolysis-gas chromatography-mass spectrometry. *, not all samples from taphonomic experiments were analysed using each technique listed. ……55

Table 2.4 List of fossil material and the techniques used on each sample. 1, HCl-AHPO-HPLC; 2, X-ray absorption near edge structure spectroscopy; 3, Fourier-transform infrared spectroscopy; 8, pyrolysis-gas chromatography-mass spectrometry. ……56

Table 3.1 Experimental setup showing taphonomic sequences, experimental conditions used and natural scenarios corresponding to experimental pathways. ……75

Table 4.1 AHPO-HPLC data for total melanin marker concentrations in black, orange and white feathers. Mean and standard deviation data (in ng/mg) for concentrations of total melanin, total eumelanin (PTCA + PDCA + PTeCA) and total phaeomelanin markers (TTCA + TDCA + 4-AHP + BZ-AA) obtained using alkaline hydrogen peroxide oxidation (AHPO) and hydroiodic (HI) acid hydrolysis. Untreated and experimentally matured black and orange feathers, *Gallus gallus*; white feathers, *Egretta garzetta.* ……103

Table 4.2 AHPO-HPLC data for individual melanin marker concentrations in black, orange and white feathers. Mean and standard deviation data for individual melanin markers in untreated and experimentally matured black and orange (*Gallus gallus*) and white (*Egretta garzetta*) feathers following alkaline hydrogen peroxide oxidation (AHPO) and hydroiodic (HI) acid hydrolysis. Percentage data denote the mean change in concentrations of specific markers between untreated feathers and those matured at 200°C and 250°C. ……105

Table 4.3 HCl-AHPO-HPLC data for individual melanin marker concentrations in fossil soft tissues and host sediments. ……116

Table 4.4 Predictions of authentic signals for fossil melanins in eumelanin- and phaeomelanin-dominated systems. Predictions are based on AHPO-HPLC and HCl-AHPO-HPLC data from untreated and experimentally matured black and orange (*Gallus gallus*) and white (*Egretta garzetta*) feathers. These feathers represent eumelanin-dominated and phaeomelanin-dominated systems, respectively. Data for non-melanin systems indicate

signals for diagenetic artefacts produced by thermal maturation of melanin-poor, protein-rich systems. Predictions for moderate maturation are derived from the data from the 200°C experiment; predictions for strong maturation are derived from trends extrapolated from the 250°C experiment. ……..118

Table 6.1 Peak assignments for py-GC-MS spectra of black and orange (*Gallus gallus*) and white (*Egretta garzetta*) feathers degraded in sulfurization experiments. ……..190

Table 6.2 Peak assignments for FTIR spectra of experimentally degraded black and orange (*Gallus gallus*) and white (*Egretta garzetta*) feathers. ……192

Declaration

This is to certify that the work I am submitting is my own and has not been submitted for another degree, either at University College Cork or elsewhere. All external references and sources are clearly acknowledged and identified within the contents. I have read and understood the regulations of University College Cork concerning plagiarism.

Digital signature of the candidate: 

Acknowledgements

This thesis would not be possible without the support of so many people.

First and foremost, I would like to thank my supervisor, Prof. Maria E. McNamara, for her invaluable supervision and support throughout my PhD programme, which challenged me to achieve more than I ever dreamed possible. I would also like to thank my co-supervisor, Prof. Paddy J. Orr, for his support and thoughtful conversation. I am especially grateful to Prof. Mike Benton, Kate Ashbrook and Mike Wheeler for being such inspiring mentors and for granting me opportunities that enabled me to pursue a PhD.

My gratitude extends to my examiners, Prof. Philip Donoghue and Dr David Jarvis, for their time spent reviewing my thesis. I sincerely appreciate their comments and suggestions, which made for a very enjoyable viva voce.

I also wish to thank Dr David Jarvis for lending me his ears and sharing his wisdom over many cups of tea, and Dr Russell Garwood, for providing so much support from a distance.

I am deeply thankful for Andy Ingamells – your love, support and laughter helped me through each day of my studies. You gave me the courage to pursue a PhD and motivated me every day to complete it. I am happily indebted to my ma (Resa Kay), dad (Rick Slater), my beloved gram (Gail Slater), Jennifer Gaynor, Natasha Gaynor-Loos, Hank Loos, Tatum, Riley, Bobby, Stephen and Lesley Ingamells, Chris Kuell, Christine DiMeglio and (last but not least) Blue dog for all of their love and support.

I would like to give a special thanks to my chosen family: Enrico, Conor, Pisco and the six friendly beavs – Philippa, John, Keith, Linda, Aoife and Seán. You have made Ireland home.

My thesis would not be possible without my colleagues (in no particular order): Tara Foley, Naomi O'Reilly, Dr Aude Cincotta, Dr Jess Franklin, Dr Zixiao Yang, Dr Valentina Rossi, Daniel Falk, Hannah Binner, Beatriz Carazo del Hoyo, Dr Ninon Robin, Dr Luke McDonald, Dr James Jepson, Dr Chris Rogers, Dr Thomas Clements, Dr Fleur Noailles, Dr Giliane Odin and Shengyu Wang. Thank you for all your support and, ultimately, your friendship.

Desi Richter, Alison Miller and (the epic) Kathryn Peterson – I am truly grateful for all your wisdom and kind words. Each of you has left a lasting impression on the way that I work, how I relate to my work and on my life. You are rock stars.

I would also like to thank the following members of the TAWS community (in no particular order): Rebecca Schwartz, Melissa Schwartz, Melinda Valente, Deirdre Rogers, Kevin Hylton, Kate Vacek, Dhvani Badwaik, Paige Madison, Brian Kootte, Andréa Craft, Madeline McKenna, Laura Copeland, Kristen Daly Mosier, Katrina Pasierbek, Tiara Walz, Laura Santander, Sofia Marques de Silva, Olivia Benowitz, Adriana, Michael Schwartz, Becky Bivens, Laura Weimer, Kristi Boone, Ciara O'Higgins, Dawn Lazerte, Motomori Lewis, Tasha Z, Silvia Clark, Christine Mayor, Anna Mooney, Amy Hellem, Rahul Yadav, Polly Cook, Andrew Roesch, Elizabeth Fox, Katie Lazarowicz, Dhvani, Zainab Al Qaisi, Michael Munroe, Tamanda Walker, Natalie Chong and every other person that helped make TAWS such a wonderful space to work. Each of you has shown me so much compassion during the pandemic and have helped me stay motivated to cross the finish line.

Abstract

Fossil feathers harbour key information for understanding the evolution of feathers through deep time. The ability of fossil feathers to inform on the biochemical evolution of feathers is, however, restricted due to an incomplete understanding of feather taphonomy. Accurate interpretation of data from fossil feathers requires a comprehensive understanding of the fate of key feather components – melanosomes, melanins and feather corneous beta proteins (CBPs) – during fossilization, but this is not fully characterized. Further, whether the preservation of different feather components is inter-dependent, and whether certain components impact preservation of others, is unknown. Unsurprisingly, reports of preserved feather chemistry in fossils are controversial. This thesis addresses these issues using taphonomic experiments incorporating decay, sulfurisation, oxidation, thermal maturation and high temperature-high pressure maturation on black, white and orange feathers from extant birds. The results resolve the controls on the preservation of melanosomes and melanins (in decreasing order of importance: oxidation, maturation and decay) and the proteinaceous component of feathers (in decreasing order of importance: maturation, oxidation and decay). The experimental results also support new fossil evidence for the preservation of disulfides and amides, which are indicative of feather CBPs, in Mesozoic fossil feathers and the preservation of phaeomelanin molecular residues in Miocene fossil frogs. Collectively, the results form the basis for a new integrated model for feather preservation that is firmly grounded in quantitative empirical data and encompasses all major feather components. This model explains variations in the preservation of fossil feathers and represents a major advance in our understanding of the preservation of feathers and of structural proteins. Critically, the model highlights the power of combining systematic and quantitative taphonomic experiments with a holistic, whole-tissue approach, to resolve long-standing issues relating to the preservation of soft tissues in the fossil record.

Outline

This thesis comprises eight chapters. Chapter 1 provides an overview of the components and evolution of feathers in addition to a summary of fossil feathers and the role of experimental taphonomy in elucidating fossil soft-tissue preservation. Chapter 2 details the material and methods used to perform the research presented in this thesis. Chapters 3–6 present four studies investigating the taphonomy of feathers. These four chapters follow the formatting requirements of specific journals for publication. Chapter 3 presents a paper that has been published in the journal *Palaeontology.* Chapter 4 presents a study that is prepared for re-submission to *Nature Communications.* Chapter 5 presents a study that is prepared for submission to *Nature.* Chapter 6 presents a study that is prepared for submission to *Current Biology.* Each chapter is presented as a complete study, with references and supplementary information following the main text in each case. Chapter 7 provides a brief overview of the findings of this project and discusses each finding in relation to relevant literature. Chapter 8 concludes the thesis and highlights important avenues for future research. UK English is used throughout the thesis.

References cited in Chapters 1, 2 and 7 are provided following Chapter 8.

Appendix I provides the following publication:
McNamara, M. E., Rossi, V., Slater, T., Rogers, C., Ducrest, A.-L., Dubey, S., & Roulin, A. (2021). Decoding the evolution of melanin in vertebrates. *Trends in Ecology & Evolution*, *36*(5), 430–443. https://doi.org/10.1016/j.tree.2020.12.012

Candidate contribution to the study. TSS contributed to the writing of the paper.

Appendix II provides the links to supplementary datasets for Chapters 3 and 4.

Project aims

The aims of the thesis are to test the following hypotheses:

1. Oxidation promotes melanosomes degradation
2. Proteinaceous feather tissue can survive maturation under conditions that simulate diagenesis
3. Feather corneous beta proteins can survive maturation under conditions that simulate diagenesis
4. Chemical evidence of feather CBPs can be detected in fossil feathers using FTIR and S-XANES
5. The degradation of eumelanin and phaeomelanin monomers follows predictable pathways during thermal maturation
6. Chemical evidence of phaeomelanin monomers can survive in fossils

The research in this thesis demonstrates that hypotheses 1–6 are true.

1. Introduction

This chapter contains eight sections. Section 1.1 considers the development, structure and evolution of feathers andis followed by three sections describing the primary components of feathers – melanosomes (section 1.2), melanins (section 1.3) and feather proteins (section 1.4). Section 1.5 reviews the preservation of fossil soft tissues and section 1.6 reviews the organic preservation of fossil soft tissues. Collectively, these sections provide the foundation for a review of the fossil record of feathers in section 1.7. Finally, section 1.8 provides an overview of experimental taphonomy and its essential role in palaeontology.

1.1 Feather function and development

Feathers are highly complex and evolutionarily novel integumentary structures that comprise predominantly feather corneous beta proteins (CBPs) and pigments. Feather CBPs (previously termed β-keratins [Alibardi, 2016b]) are fibrous structural proteins containing abundant disulfide bonds (Wang et al., 2016; see Chapter 1.4). Pigments are organic molecules that produce colour via the selective absorption of different wavelengths of light. The most common feather pigments are melanins (McGraw et al., 2005; see Chapters 1.2 and 1.3) but feathers can also contain carotenoids (Brush, 1978; McGraw, 2006), psittacofulvins (as in parrots [McGraw, 2006]) porphyrins (as in turacos [McGraw, 2006]), and spheniscins (as in penguins [Thomas et al., 2013]).

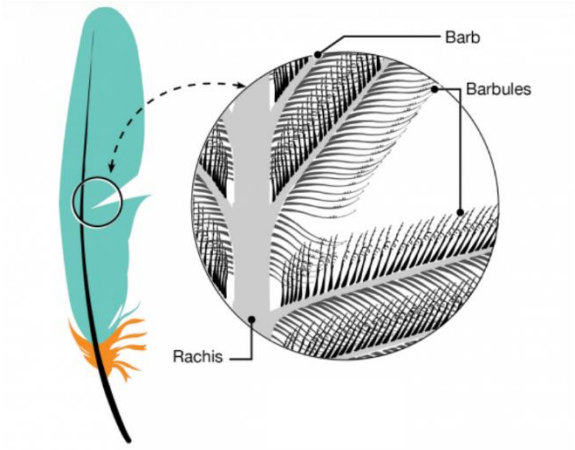


Fig. 1.1 *Illustration showing the anatomy of a pennaceous feather (modified from the Cornell Bird Academy [Thompson, 2014]).*

Feathers possess a hierarchical branching structure with a calamus, rachis, barbs and barbules (Fig. 1.1; Lucas & Stettenheim, 1972). At the proximal end of a feather stalk is a calamus held by the feather follicle (i.e., an invagination of living epithelial cells into the dermis) in the skin; the rest is called the rachis. Barbs proximally fuse to the rachis and barbules fuse to the barbs to form the feather vane. Variations on this structure create diverse feather morphologies that serve many functions (Fig. 1.2; Prum, 1999). Down feathers exhibit a short calamus and rachis with long barbs and barbules. Semiplume feathers possess a longer calamus and rachis than down feathers. The barbs in down and semiplume feathers do not interlink via barbules, generating plumulaceous feathers with either no vane (as in down feathers) or a soft open vane (as in semiplumes); such plumulaceous feathers function in thermoregulation. Contour feathers, remiges (wing feathers) and rectrices (tail feathers) are pennaceous feathers that contain stiffer and more abundant barbs than plumulaceous feathers. Pennaceous feathers can exhibit open or closed feather vanes. In the latter case, barbules possess pennulae with ventral hooks interlock with proximal barbules (Lucas & Stettenheim, 1972). Unlike other pennaceous feathers, contour feathers have plumulaceous barbs in the proximal feather region to create an open vane structure; hooked pennulae on barbules in the distal region create a closed feather vane structure. This structure supports functions in both thermoregulation and display (Prum, 1999). Remiges can be either primary or secondary flight feathers. Primary flight feathers tend to be longer and thinner than secondaries and are on the distal portion of a wing. Secondary flight feathers have a more proximal position on the wing than primary feathers. Remiges and rectrices possess an elongated rachis with stiff

barbs and barbules. Pennulae with ventral hooks are present on all barbules in remiges and rectrices to form a closed feather vane that provides strength for flight; remiges and rectrices, however, also function in display (Prum, 1999). Remiges and rectrices can be either symmetrical or asymmetrical depending on the position of the rachis. The outer vane of an asymmetrical feather is toward the leading edge of the wing. Primary remiges and proximal rectrices are asymmetrical and exhibit a thinner outer vane than the inner vane to improve flight capability. In crown birds, the outer vane exhibits barbs with a smaller angle to the rachis than the barbs of the inner vane. Bristles have a long and stiff rachis with few short, stiff barbules whereas filoplumes have a short, flexible rachis with few barbs on their distal ends. Bristles and filoplumes primarily serve a sensory function.



Fig. 1.2 Illustrations of the common feather morphologies observed in extant birds (from the Cornell Bird Academy [Thompson, 2014]).

Feathers form in pterylae, or feather tracts, and in a distal to proximal fashion (i.e., the distal end of a feather forms before the proximal end) through the generation of keratinocytes [Prum, 1999]; Fig. 1.3). Birds shed feathers through ecdysis whereas endysis is the process of feather generation (Lucas & Stettenheim, 1972). Feather regeneration serves many physiological purposes, such as colour rejuvenation (Chuong et al., 2012) and eliminating heavy metals from the organism (Burger, 1995).

The development of natal down feathers, i.e., the first generation of feathers formed during development, occurs before that of mature feathers. During the initial development of natal down feathers, the Wnt/β-catenin signalling pathway leads to a local thickening of the dermis, termed a placode, that gives rise to a feather (Prum, 1999; Prum & Brush, 2002; Lucas & Stettenheim, 1972; Fig. 1.4a). The genes Shh, myc and myb determine the

proximal-distal axis of the placode (Chen et al., 2015) and outgrowth of the placode generates a papilla, which can also be referred to as a feather bud (Fig. 1.4b). The papilla possesses an epidermal collar at the base of the follicle (Fig. 1.4c). The innermost epidermal layer of the collar creates the tubular epidermis of the papilla, which differentiates into various layers: the pulp, outer epidermal layer, inner epidermal layer and the intermediate epidermal layer (Foth, 2020; Prum & Dyck, 2003). Dermal cells in the proximal end of the follicle comprise the dermal pulp and the dermal cells in the distal end comprise the pulp (Inaba & Chuong, 2020; Fig. 1.4c). The intermediate epidermal layer generates barb ridges in a distal to proximal fashion (Prum & Dyck, 2003; Fig. 1.4d). The generation of barb ridges is followed quickly by the epidermal invagination of part of the follicle into the dermis (Prum & Brush, 2002; Fig. 1.4d). Genes essential to the formation of feathers include fibroblast growth factors (FGFs), sonic hedgehog (Shh), wingless integrated proteins (Wnt; e.g., Wnt-2 and Wnt-6), bone morphogenic proteins (BMPs; e.g., BMP4), noggin and neural-cell adhesion molecules (N-CAM; Chu et al., 2014; Dhouailly, 2009; Lin et al., 2013; Yu et al., 2002).

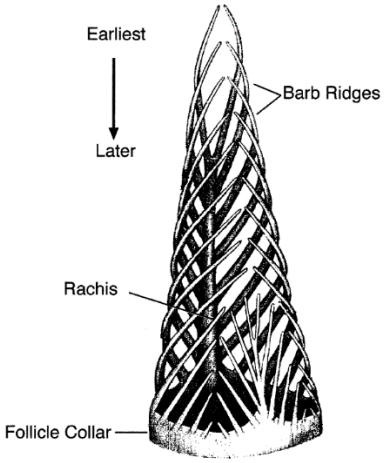


Fig. 1.3 A schematic illustration of a pennaceous feather in the early phase of its development. The distal end of the feather develops before the proximal end (from Prum and Brush, 2002).

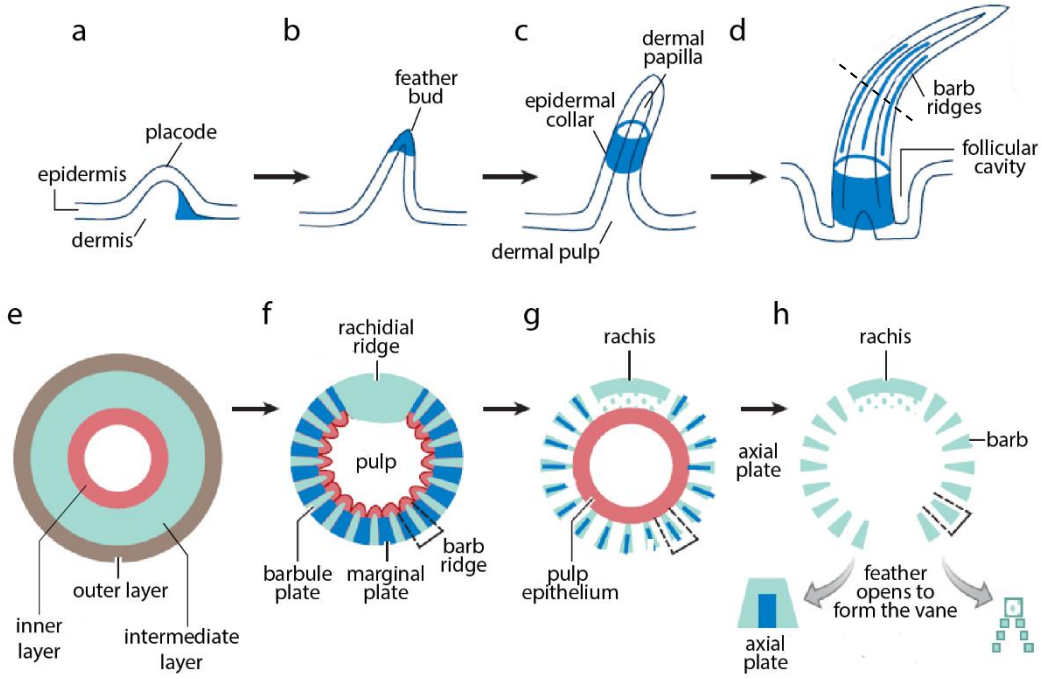


Fig. 1.4 Schematic illustration showing the development of a feather papilla and follicle (modified from Chen et al. [2015]). The dashed line in part d indicates the position of the plane of the transverse sections in e–h.

Blood vessels in the dermal pulp supply the developing feather with nutrients. The outer epidermal layer forms a sheath to protect the germinating feather whereas the inner epidermal layer plays a critical role in the production of barb ridges (Prum & Dyck, 2003; Fig. 1.4e). In conjunction with the dermal pulp, the inner epidermal layer produces cornified pulp caps (Prum & Dyck, 2003). Folding of the inner epidermal layer creates marginal plates and a central axial plate (Fig. 1.4f). Barb ridges are generated from the intermediate epidermal layer and differentiate into the proliferation and ramogenic zones. The ramogenic zone generates the ramogenic column, which forms the ramus of the barb and two lateral barbule plates (Lin et al., 2013; Prum & Brush, 2002; Fig. 1.4f). Lateral barbule plates are separated by the central axial plate and form plumulaceous barbules that proximally fuse with the ramogenic columns (Prum & Brush, 2002). Several barbs join in the rachidial ridge region to form the rachis and the calamus forms from the sheath and the pulp epithelium of the collar (Alibardi, 2017; Prum, 1999; Fig. 1.4g). The axial plates separating the barbule plates degenerate once the rachis, rami and barbule cells are cornified (Prum, 1999; Fig. 1.4h).

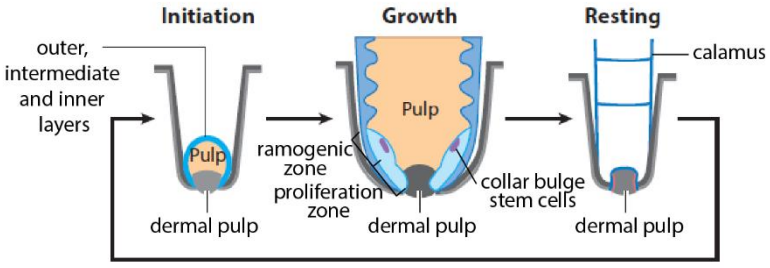


Fig. 1.5 Schematic illustration showing an adult feather follicle in the initiation, growth and rest phases of feather generation, collectively termed endysis (modified from Chen et al. [2015]).

In general, the generation of mature feathers occurs as described for the generation of natal down feathers, except that stem cells within the proliferation zone first thicken the collar surrounding the dermal pulp (Alibardi, 2017; Prum & Dyck, 2003; Fig. 1.5). The genetic signalling involved in feather regeneration is not fully understood (Alibardi, 2017) but sprouty RTK signalling antagonist 4 (Spry4) and the Wnt inhibitors Dkk2 and Frzb (Chu et al., 2014) play a crucial role in addition to the genes acting in natal down formation (Lin et al., 2020).

The feather follicles that generate down feathers can also form other feather morphologies (except filoplumes; Prum & Dyck, 2003). If the position of the barb generative zone, which gives rise to barb ridges, is directly opposite the rachidial ridge, a symmetric feather develops (Prum, 1999). When the barb generative zone is not directly opposite the rachidial ridge, an asymmetric feather develops (Prum, 1999). The position of the barb generative zone ultimately controls the extent of asymmetry in asymmetric pennaceous feathers (Prum, 1999). Further, Wnt-3a controls the tilt of the stem cell ring, which is associated with feather morphology (Lin et al., 2020; Yue et al., 2006). Tilting of the stem cell ring angles the barb ridges toward the anterior side of the papilla to form a rachis and also determines the angle of the barbs on either side of the rachis (Yue et al., 2006). The production of asymmetric feathers also requires differential barb growth on either side of the rachis (Feo & Prum, 2014), which occurs via the local expression of CRABP1 and the enzyme CYP26B1 in the pulp (Li et al., 2017).

The dermal pulp of a papilla is essential to endysis as it supplies the developing feather with nutrients (Chu et al., 2014) and acts as the source of feather pigments (Prum, 1999; Prum & Dyck, 2003), of which melanins dominate (see Chapters 1.2 and 1.3). The germinal epithelium in the collar produces keratinocytes – cells that generate the structural proteins, namely feather CBPs, that form feather tissue (see Chapter 1.4).

1.2 Melanosomes

Melanosomes are organelles that synthesise melanin pigments and derive from melanocytes. Melanocytes arise from melanoblasts, which in turn derive from neural crest cells (NCCs; Inaba & Chuong, 2020). In birds, melanoblasts are present in the lower collar bulge at the base of the feather follicle (Fig. 1.5); following their migration into barb ridges, melanoblasts differentiate into melanocytes that synthesise melanosomes (Lin et al., 2013; Fig. 1.5). Melanocytes express enzymes that are essential for melanogenesis (i.e., melanin synthesis): tyrosinase (TYR) and tyrosinase-related proteins (TYRPs; Inaba & Chuong, 2020). Melanocytes then transfer pigmented melanosomes to keratinocytes (Prum & Williamson, 2002; Lucas & Stettenheim, 1972) but how this occurs is unclear (Galván & Solano, 2016). Eumelanosomes (ca. 1–2 μm long) are often ellipsoidal to rod-shaped and are rich in the pigment eumelanin that imparts black, brown and grey colouration to tissues. Phaeomelanosomes (ca. 0.5–0.8 μm diameter) are generally (sub-)spherical and are rich in the pigment phaeomelanin that produces orange, rufous and grey colouration. Melanosomes, however, do not exist in binary states and usually contain both eumelanin and phaeomelanin (Ito et al., 2018; Wakamatsu & Ito, 2002). Nevertheless, the terms eumelanosomes and phaeomelanosomes are used here as current understanding indicates that melanosome morphology and chemistry are linked in feathers (D'Alba & Shawkey, 2019). Melanosomes can also impart structural colouration, especially those that are elongate (Babarović et al., 2019), hollow (Greenewalt et al., 1960; Shawkey et al., 2015) and that exhibit dense and geometric packing (Xiao et al., 2020) and/or layering (Shawkey et al., 2006). Layers of melanosomes generate iridescence via the different refractive indices of air, melanin and structural proteins.

Eumelanogenesis is a four-step process (Fig. 1.6). In stage I, a membrane-bound vesicle develops fibrils comprising the protein PMEL17 (D'Alba & Shawkey, 2019). Eumelanosome

fibrils possess a β-sheet organisation and form within multivesicular bodies (MVBs; Hurbain et al., 2008). Fibrils are fully developed during stage II when the melanosome becomes ellipsoidal. Stages III and IV include the synthesis of eumelanin molecules and their deposition (and storage) on the fibrils (D'Alba & Shawkey, 2019).

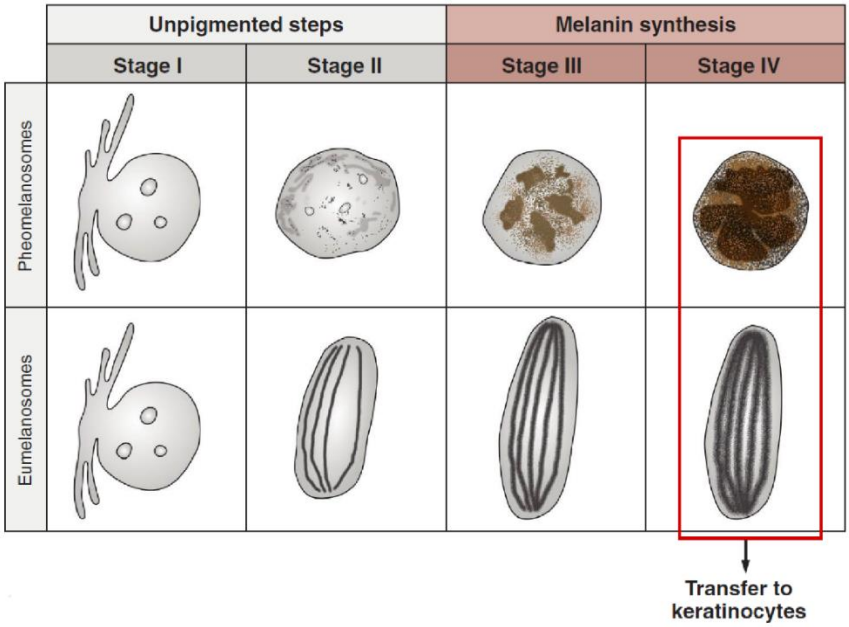


Fig. 1.6 Stages I–IV of melanogenesis for eumelanosomes and phaeomelanosomes (from D'Alba and Shawkey [2019]).

Phaeomelanogenesis can also be characterised as a four-stage process, but PMEL17 proteins do not organise into fibrils (D'Alba & Shawkey, 2019). The lack of fibrillar organisation of PMEL17 is likely due to the weaker expression of PMEL17 in melanocytes that produce phaeomelanosomes than in melanocytes that produce eumelanosomes (Furumura et al., 1998; Kobayashi et al., 1994). The presence of organised fibrils may be responsible for the ellipsoidal shape of eumelanosomes in birds and mammals (D'Alba & Shawkey, 2019; Kushimoto et al., 2001).

1.3 Melanins

Melanin pigments are biopolymers that impart colour and strength to tissues and act in metal sequestration, homeostasis, UV protection and as antioxidants (Bush & Simon, 2007; Dubey & Roulin, 2014; Hong & Simon, 2007; Solano, 2020).

Melanogenesis is regulated primarily by the melanocortin 1 receptor (MC1R) gene and the melanocortin pathway. MC1R regulates the expression of TYRP1 and TYRP2 within the melanocyte and PMEL within the melanosome (see Chapter 1.2; Galván & Solano, 2016). The melanocortin pathway involves hormones secreted by the pituitary gland, such as adrenocorticotropin hormone (ACTH) and melanocyte-stimulating hormones (MSH); these hormones bind to MC1R in the melanocyte (Galván & Solano, 2016; Inaba & Chuong, 2020). Cellular cyclic adenosine monophosphate (cAMP) increases when **α**-MSH binds to MC1R, resulting in eumelanogenesis (Inaba & Chuong, 2020). Phaeomelanogenesis arises from the inhibition of MC1R by agouti signalling protein (ASIP; Inaba & Chuong, 2020). Eumelanogenesis and phaeomelanogenesis begin with the same reactions. L-dopaquinone forms from the oxidation of L-tyrosine by tyrosinase (tyrosine hydroxylase) and L-dopa by tyrosinase (dopa oxidase; Galván & Solano, 2016; Wakamatsu & Ito, 2002; 1 in Fig. 1.7).

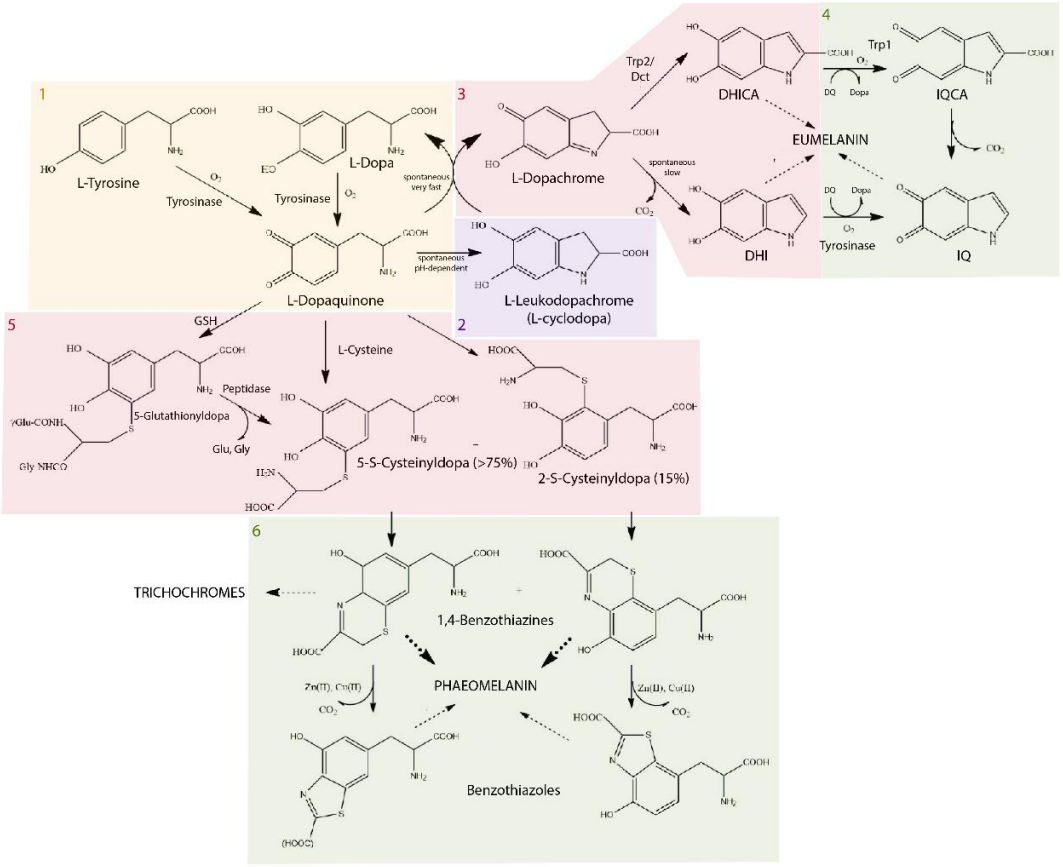


Fig. 1.7 Chemical pathways for the synthesis of eumelanin and phaeomelanin (modified from Galván and Solano [2016]).

Eumelanogenesis continues with the oxidation of dopaquinone to create L-leukodopachrome (Galván & Solano, 2016; 2 in Fig. 1.7). An acidic environment inhibits

this pH-dependent process within the melanosome (Ancans et al., 2001). L-leukodopachrome can quickly reduce to L-dopa and L-dopachrome (Galván & Solano, 2016); L-dopachrome generates the indolic orthodiphenols (o-diphenols) DHI and DHICA (Galván & Solano, 2016; Wakamatsu & Ito, 2002; 3 in Fig. 1.7). Tyrosinase-related protein 2 (Tyrp2) catalyses the isomerisation of L-dopachrome to DHICA (Ito & Wakamatsu, 2008; Wakamatsu & Ito, 2002). The generation of the DHI and DHICA o-diphenols, and the resulting DHI:DHICA ratio present in a melanosome, depends on the activity of TYRP2, melanosomal pH and the presence of metal ions (Galván & Solano, 2016). DHI and DHICA undergo further oxidation to the orthoquinones (o-quinones) 5,6-indolequinone (IQ) and indole-2-carboxylic acid-5,6-quinone (IQCA), respectively (Galván & Solano, 2015; part 4 in Fig. 1.7). Hair eumelanin containing predominantly DHI+IQ appears black whereas the dominance of DHICA+IQCA results in grey colouration (Urabe et al., 1994). DHI, DHICA, IQ and IQCA combine to generate a heterogeneous eumelanin polymer, with DHI and DHICA crosslinked via IQ (Kishida et al., 2021), but the spatial architecture of the cross-linked macromolecular structure is not resolved (Galván & Solano, 2015; Ito et al., 2011; Wakamatsu & Ito, 2002). Eumelanogenesis generates reactive oxygen species (ROS) that are likely toxic to melanocytes, especially during the decarboxylative generation of DHI and IQ (Galván & Solano, 2015); further, cells containing more DHI+IQ melanin than DHICA+IQCA melanin have lower rates of survival (Galván & Solano, 2015; Urabe et al., 1994). DHI+IQ eumelanin and DHICA+IQCA eumelanin have different UV and visible light absorption properties due to their different molecular branching structures; DHI+IQ eumelanin is more branched and able to absorb a larger range of wavelengths than DHICA+IQCA eumelanin (Galván & Solano, 2015; Panzella et al., 2013). DHI+IQ eumelanin consequently offers superior UV protection to tissues but at a greater cost due to the increased ROS production of its respective monomers (Galván & Solano, 2015; Urabe et al., 1994).

The presence of glutathione and L-cysteine favours phaeomelanogenesis over eumelanogenesis. Before L-dopaquinone can generate L-leukodopachrome, L-dopaquinone reacts very quickly with glutathione and L-cysteine to form 5-glutathionyldopa and cysteinyldopas (Galván & Solano, 2016; Ito & Wakamatsu, 2008) – the first step in phaeomelanogenesis (part 5 in Fig. 1.7). L-cysteine and L-dopaquinone bond in various ways to form cysteinyldopas; one of these, 5-*S*-cysteinyldopa (5-*S*-CD),

accounts for >75% of the cysteinyldopas created (2-S-CD accounts for 15%; Galván & Solano, 2016; part 5 in Fig. 1.7). The bonding of L-dopaquinone to glutathione produces 5-*S*-glutathionyl-dopa, which converts to 5-*S*-CD (Galván & Solano, 2016). Oxidation of cysteinyldopa produces benzothiazine (BT) units (Napolitano et al., 1999); decarboxylation of BT units forms benzothiazole (BZ) units (Galván & Solano, 2016; part 6 in Fig. 1.7). Tissues with higher BT/BZ ratios appear pale orange whereas a lower BT/BZ ratio results in darker orange-red colouration (Galván & Solano, 2015; Wakamatsu et al., 2009). The BT monomers in phaeomelanin generate more ROS than BZ monomers in response to ionising radiation (Galván & Solano, 2015; Wakamatsu et al., 2009). Birds exposed to high amounts of radiation possess a low BT/BZ ratio (Galván et al., 2014). Unlike eumelanogenesis, however, the process of phaeomelanogenesis does not generate ROS (Galván & Solano, 2015; Wakamatsu et al., 2009) and is beneficial to organisms as it depletes toxic cysteine levels (Galvan et al., 2012).

Reports suggest two additional types of phaeomelanin pigments: trichochromes and erythromelanins (Galván & Solano, 2016; Hudon, 2005). Trichochromes form via the binding of two BZ monomers (Rorsman, 1979) but erythromelanins have not been characterised (Galván & Solano, 2016). Trichochromes and erythromelanins, however, have not been identified independently of these reports (Hudon, 2005; Rorsman, 1979).

Environmental factors can influence melanin synthesis. For example, diet can alter metal ion concentrations and oxidative stress can deplete glutathione (Galvan & Alonso-Alvarez, 2009; Galvan & Solano, 2009). Hormones can also alter the melanocortin pathway and influence melanogenesis (Inaba & Chuong, 2020).

Molecular control of melanin synthesis can produce complex colour patterning across different body regions and even within a single feather (Galván et al., 2017; Inaba & Chuong, 2020). ASIP plays a key role in various feather patterns that include pairwise combinations of black, white and rufous colours (Haupaix & Manceau, 2020; Inaba & Chuong, 2020; Lin et al., 2013). For example, spatiotemporal heterogeneity of ASIP expression in the dermal pulp of feather follicles produces black and white patterning within a single feather, whereby the inhibition of melanocyte differentiation produces white regions (Lin et al., 2013). White regions in black and white Barred Plymouth Rock

chicken feathers result from the premature differentiation of melanoblasts due to mutations in the gene CDKN2A/B (Hellström et al., 2010; Lin et al., 2013). Notably, most tissues – including feathers – contain melanin copolymers and a mixture of eumelanin and phaeomelanin (Ito et al., 2018; Wakamatsu & Ito, 2002).

1.4 Feather proteins

Feathers – in addition to scales, claws and beaks – are composed predominantly of the protein keratin, which is rich in the amino acid cysteine (Wang et al., 2016). In particular, feathers comprise mostly proteins that are traditionally referred to as "β-keratins"; feathers contain minor amounts of other proteins traditionally termed "α-keratins" (Alibardi, 2016b). Despite the nomenclature, β-keratins and α-keratins are phylogenetically unrelated; there is also inconsistent application of the terms in the literature, as α-keratins with a β-sheet conformation are occasionally referred to as β-keratins (Alibardi, 2016b). This thesis uses the terminology of Alibardi (2016b), who recommends the use of the term "corneous β-proteins" (CBPs) for β-keratins and "intermediate filament-keratins" (IF-keratins) for α-keratins.

1.4.1 Corneous beta proteins

CBPs are small proteins (8–30kDa) encoded by genes located in the epidermal differentiation complex (EDC) that, in the chicken, is on chromosome 25 (Alibardi, 2017; Holthaus et al., 2018). The EDC contains many genes that encode for proteins acting in the differentiation and cornification of keratinocytes, the predominant cells of the epidermis (Alibardi, 2017; Holthaus et al., 2018; Mischke et al., 1996).

All CBPs derive from the EDC (Greenwold & Sawyer, 2010) and each sequence of a CBP contains a pre-core box epitope, a core box region and a β-universal motif within the core box region (Holthaus et al., 2018). The β-universal motif of proline-glycine-proline is a major feature of the 34-amino acid pleated β-sheet in the CBP polypeptide chain (Alibardi, 2016b; Calvaresi et al., 2016; Fraser & Parry, 2011; Fig. 1.8a). Proline-glycine-proline forms the β-turns in β-sheets due to the cyclic structure of proline and the steric flexibility of glycine since it has the smallest side chain of all amino acids. Avian CBPs can be divided

into the phylogenetically distinct subfamilies of keratinocyte-, claw-, scale- and feather CBPs. Feather CBPs differ from scale-, claw- and keratinocyte CBPs in the near- or complete absence of glycine-rich regions that usually follow the core box region within the molecular sequence of other CBPs (Alibardi, 2017; Gregg & Rogers, 1986).

The chicken genome contains 149 CBP genes (Ng et al., 2014), with 65 located in the EDC (Holthaus et al., 2018). Several reports hypothesise that avian CBP genes located on chromosomes 1, 2, 5, 6, 7, 9, 10 and 27 (Ng et al., 2014) translocated from the EDC (Gregg & Rogers, 1986; Holthaus et al., 2018; Ng et al., 2014). This translocation of avian CBP genes may have facilitated the evolution of feathers capable of supporting flight (Alibardi, 2017; Greenwold & Sawyer, 2011; Holthaus et al., 2018).

Hypotheses on the origin of feather CBPs. There are two competing hypotheses for the origin of feather CBPs and both are based primarily on molecular data. One hypothesis proposes that feather CBPs arose after the origin of feathers. Phylogenies of crocodile, lizard, turtle and bird CBPs reveal a resemblance between reptilian CBPs and avian scale CBPs (Greenwold & Sawyer, 2011). Greenwold and Sawyer (2011) interpret this similarity between reptilian and avian scale CBPs to suggest that avian scale CBPs arose from reptilian scale/claw CBPs, presumably on the basis that reptiles evolved before birds. Further, phylogenies of the avian CBP subfamilies show that avian scale CBPs are ancestral to feather CBPs (Greenwold & Sawyer, 2010, 2013; Ng et al., 2014), with an estimated divergence time of ca. 125 Ma for feather CBPs (Greenwold & Sawyer, 2011). These data collectively give rise to the hypothesis that feather CBPs arose from avian scale CBPs after the origin of feathers, suggesting that basal avemetatarsalian feathers were composed of ancient, undifferentiated CBPs (Greenwold & Sawyer, 2011).

The alternative hypothesis is that feather CBPs arose from reptilian scale CBPs before the origin of feathers (Dalla Valle et al., 2009; Dhouailly, 2009). Developmental studies show that embryonic epidermal tissues in archosaurs possess a protein epitope characteristic of feathers (Alibardi, 2017). The presence of a feather epitope in an archosaur embryo suggests that the organism can synthesise feather CBPs and that feather CBPs arose in early archosaurs ca. 250 Ma (Dalla Valle et al., 2009; Dhouailly, 2009). The alternative hypothesis also proposes that avian scale CBPs originate from feather CBPs. Molecular

data show that avian scale CBPs are dissimilar to reptilian scale CBPs but similar to feather CBPs (Dhouailly, 2009). Developmental data showing that the inhibition of feather morphogenesis generates avian scales support this proposal and an independent origin of squamate scales and feathers (Dalla Valle et al., 2009; Dhouailly, 2009; Lucas & Stettenheim, 1972). Developmental data also show that lepidosaur and crocodile scales lack a placode and pulp during development; this contrasts with avian scales and feathers (Dhouailly, 2009) and further supports the "feather first" hypothesis.

In sum, the origin of feather CBPs is still unresolved and it is uncertain whether the first feathers were composed primarily of feather CBPs, as in modern feathers, or undifferentiated CBPs.

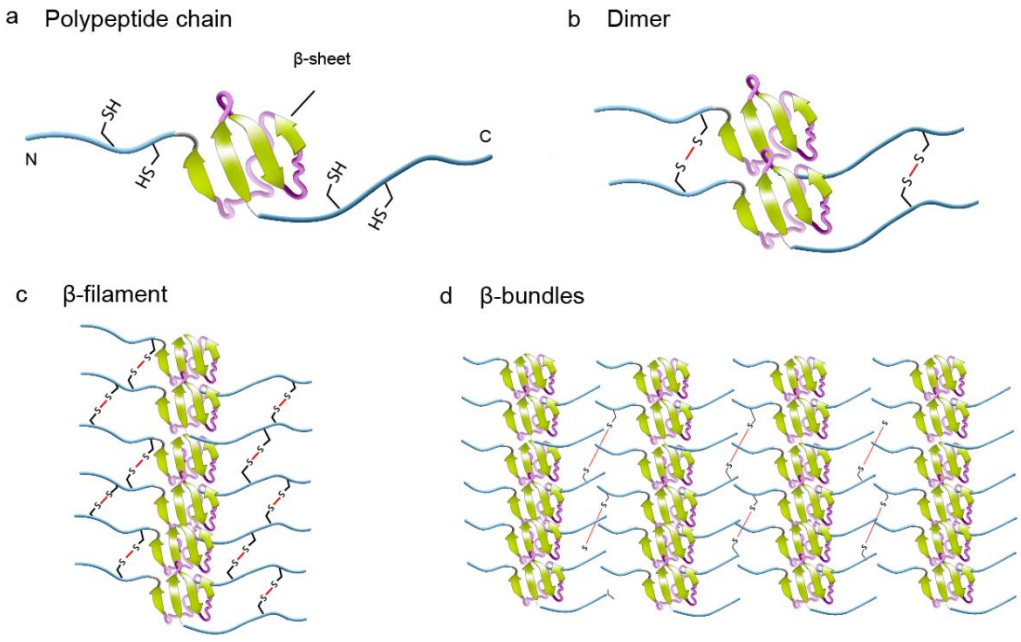


Fig. 1.8 Schematic illustration of feather corneous beta proteins (CBPs). The 45° angle between each polypeptide chain in a dimer and β-filaments is omitted in order to highlight the disulfide bonds (in red in b–d).

Assembly of feather corneous β-bundles. The β-sheets of two feather CBPs can combine via disulfide bonds to form a dimer (Alibardi, 2017; Fig. 1.8b). Dimers then polymerise linearly via disulfide bonds to form twisted helical filaments (3–4 nm wide; Fig. 1.8c), with each dimer at a 45° angle to the last and four dimers producing a 180° turn (Alibardi, 2017; Calvaresi et al., 2016; Fraser & Parry, 2011). The absence of glycine-rich loops in feather CBPs facilitates the linear formation of β-filaments, potentially allowing more direct

interaction between monomers (Alibardi, 2017). The N-regions in one β-filament form disulfide bonds with the adjacent C-regions of another β-filament (Bragulla & Homberger, 2009). Several β-filaments join to produce a β-bundle that in feathers is highly regular in structure (Alibardi, 2017; Fig. 1.8d). In contrast, the β-bundles of scale-, claw- and keratinocyte CBPs possess an irregular structure that potentially results from the glycine-rich regions (Alibardi, 2017; Gregg & Rogers, 1986; see Chapter 1.4.1). N- and C-terminal regions form the interfilamentous matrix in β-bundles of feather CBPs (Fraser & Parry, 2008; Fig. 1.8d). The N- and C-terminals of feather CBPs differ from other CBPs in their high cysteine content; disulfide bonds link two adjacent cysteine amino acids (to form cystine), which imparts structural stability to the protein (Alibardi, 2016a; Alibardi et al., 2009; Fraser et al., 1972). Non-CBP proteins, such as corneous-associated proteins, are also present in the barbs and barbules of feathers (Alibardi, 2016b; Gregg & Rogers, 1986). Differential expression of non-CBPs and CBPs may partly be responsible for the variation in strength among feather structures (Alibardi, 2016b). Further, variation in CBP expression during feather development may contribute to the morphological diversity of feathers (Holthaus et al., 2018; Kowata et al., 2014).

1.4.2 Intermediate filament-keratins

Feathers contain IF-keratins in addition to feather CBPs (Alibardi, 2016b). In contrast to CBPs, IF-keratins arise from a protein cluster outside the EDC (Alibardi, 2016b). IF-keratins are larger (40–70kDa) than CBPs and possess an α-helix conformation (Galván & Solano, 2016; Fig. 1.9a). However, IF-keratins can transform from an α-helix to a β-sheet conformation in certain conditions, e.g., where the strain level exceeds ca. 20–25% (Kreplak et al., 2004). In contrast to CBPs, most IF-keratins are cysteine-poor, with high concentrations of cysteine occurring only in trichocyte IF-keratins (present in hair, wool, hoof, horn, claw and baleen; Eckhart & Ehrlich, 2018; Holthaus et al., 2018). IF-keratins are abundant during the early stages of feather development but are rapidly replaced by CBPs (Alibardi, 2017; Alibardi & Toni, 2008). The small amount of residual IF-keratins in a mature feather are located primarily in the feather sheath and rachis (Ng et al., 2012; Wu et al., 2015), with very few in barbs and barbules (Alibardi, 2016b). It is uncertain how much residual IF-keratin remains in a mature feather but the number of genes encoding IF-

keratins in the avian genome are less than 40 and only a few encode for IF-keratins in feathers (Alibardi, 2016b).

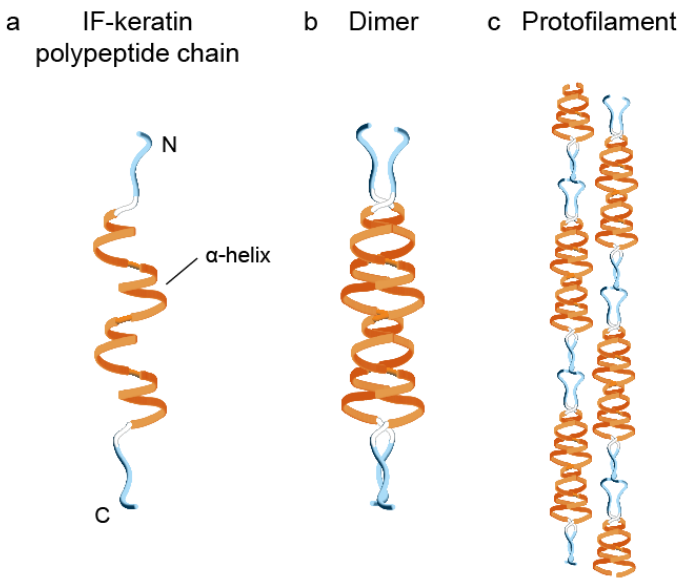


Fig. 1.9 Schematic illustration of intermediate filament-keratin (IF-keratin). (a)polypeptide chain, (b) dimer and (c) protofilament.

Assemblies of IF-keratins with an α-helix conformation form the primary component of several epidermal tissues. Two IF-keratin polypeptide chains bond to form a dimer (Fig. 1.9b), which join to produce a protofilament (Alibardi, 2017; Fig. 1.9c). Several protofilaments join to form IFs (8–12 nm wide); tonofilaments are formed by multiple IFs (Calvaresi et al., 2016; Holthaus et al., 2018).

Soft and hard epidermal tissues form via different processes. The accumulation of keratin proteins produces soft IF-keratin-dominated tissues via the process of keratinisation (Alibardi, 2016b). Hard epidermal tissues (e.g., hair, nails, feathers) form via the process of cornification (Alibardi, 2016b), which requires the addition of keratin-associated proteins (KAPs) to IF-keratin filaments. KAPs are a separate family of proteins to IF-keratins and CBPs that form the interfilamentous matrix between the IF-keratin filaments in mammalian epidermal tissues (Alibardi, 2006; Fraser & Parry, 2014). Interestingly, certain sequence regions of CBPs closely resemble KAPs (Alibardi, 2006; Fraser & Parry, 2014). Cornification of hard epidermal tissues can also require the addition of non-beta corneous proteins (CPs), such as involucrin and filaggrin, to IF-keratin filaments (Alibardi, 2006, 2016b; Kalinin

et al., 2002). Feathers cornify via the accumulation of CBPs and the association of corneous proteins (CPs) to the (low amount of) IF-keratin filaments present (Alibardi, 2016b).

1.5 Soft tissue preservation

Konservat-Lagerstätten are fossil deposits characterised by an unusually high fidelity of preservation, frequently preserving near-complete skeletons and/or evidence of soft tissues (i.e., non-biomineralised parts of an organism; Muscente et al., 2017; Seilacher, 1970). These deposits paint a more accurate picture of past biodiversity (such as the Cambrian explosion [Butterfield, 2003]) and inform on the origin of vertebrates, the evolutionary history of soft-bodied organisms (e.g., Burgess Shale [Conway Morris, 2008] and Chengjiang [Shu et al., 1999] biotas) and the origins of enigmatic taxa (Clements et al., 2017; Rogers et al., 2019). In particular, Konservat-Lagerstätten that bear fossil feathers (e.g., Jehol biota; Benton et al., 2008) have led to major advances in understanding macroevolutionary events such as the transition of non-avialan dinosaurs to birds. The mode(s) of preservation of fossil soft tissues can vary among and within Konservat-Lagerstätten. Different modes of preservation reflect variation in the biochemistry of the soft tissues, the surrounding environment and the impact of taphonomic processes on soft tissues. Accurately interpreting evidence of fossil soft tissues thus requires an understanding of how taphonomic processes can influence soft-tissue preservation.

Taphonomy is the branch of palaeontology that focuses on the processes an organism experiences during and after death and post-fossil collection. The primary taphonomic processes are disarticulation, transport, decay, mineralisation, mechanical alteration, alteration by diagenetic fluids and maturation. These processes do not necessarily occur in succession and can interact to produce variation in the quality of fossil preservation. Taphonomic processes generally result in a biased fossil record toward recalcitrant, biomineralised tissues such as bones, meaning that fossils retaining evidence of labile, soft tissues are rare (Gabbott et al., 2021).

The taphonomy of an organism is affected by factors that are intrinsic (i.e., factors that result from the biochemical composition of the organism) and extrinsic (i.e., factors that result from the external environment of an organism) to the organism. The biochemical

composition of an organism can be influenced by age, diet, anatomy and mode of life of an animal. The biochemical composition of an organism is a strong control on whether its soft tissues preserve organically (McNamara et al., 2010, 2012) or preserved via their replication in authigenic minerals (Wilby & Briggs, 1997; see Chapter 1.8.1). Extrinsic factors that can influence taphonomic processes can be biological in nature (e.g., the ecosystem structure, predation, scavenging by larger organisms, microbial decay and bioturbation), physical (e.g., the depth, current and stratification of water, fair weather and storm wave base and pressure due to burial depth), or chemical (e.g., ion and O_2 concentrations, sediment chemistry and temperature). Extrinsic factors can determine whether soft tissues are deposited in an anoxic, oxic or euxinic environment or entombed (e.g., in amber [McCoy et al., 2019, 2016]).

Taphonomic processes can be constructive and destructive, depending on the time and rate that they occur. For example, when thermal maturation occurs prior to extensive decay it can stabilise biomolecules and facilitate the organic preservation of soft tissues (Barden et al., 2011; Glass et al., 2013; Gupta et al., 2006, 2009; McNamara et al., 2006; Stankiewicz et al., 2000; see Chapter 1.8.2); thermal maturation, however, results in the loss of volatiles. Similarly, authigenic mineralisation is constructive to soft tissue preservation yet it requires degradation. Authigenic mineralisation of soft tissues requires the generation of steep geochemical gradients via intense and early decay of soft tissues (Briggs, 2003).

1.6 Organic preservation

Organically preserved fossils are those that preserve soft tissues as carbonaceous remains. The preservation potential of a tissue or character is its likelihood of preserving in the fossil record. In general, the preservation potential of soft tissues can be ranked in decreasing order from integumentary and connective tissues, skeletal muscle, neural tissue, organ tissue to blood and bone marrow; this ranking reflects the rate at which these tissues decay (Gill-King, 1997). Various scenarios may favour the preservation of fossil soft tissue: deposition in an anoxic environment (Allison, 1988; Seilacher, 1970), adsorption of clay minerals (McMahon et al., 2016) and heavy metal ions (Petrovich, 2001), and rapid

entombment in microbes (Varejão et al., 2019) or resin (McCoy et al., 2016), but these processes are not requirements of soft-tissue preservation.

Organically preserved soft tissues can potentially yield molecular information about ancient organisms. Different molecules degrade via enzymatic hydrolysis and oxidation at different rates depending on their structure and composition; preservation potential decreases progressively from lipids, polysaccharides and proteins to nucleic acids (Eglinton & Logan, 1991). Lipids can survive for billions of years (Cappellini et al., 2018) primarily due to their polymerisation during maturation, forming long-chain polymers that are highly resistant to chemical degradation (Briggs, 1999; Glass et al., 2013; Gupta et al., 2006, 2009; McNamara et al., 2006; Stankiewicz et al., 2000; see Chapter 1.8.2). Polymerisation during maturation can also incorporate sulfur from sulfides and polysulfides into tissues, a process termed sulfurisation. Sulfurisation promotes molecular crosslinking that increases resistance to chemical degradation (De Graaf et al., 1992; Kok et al., 2000; McNamara et al., 2016b; Schouten et al., 1994; Sinninghe Damsté et al., 2007; van Dongen et al., 2003, 2006). Remnants of the polysaccharide chitin are preserved in the cuticle of a 310 Ma scorpion and 417 Ma eurypterid, likely due to their interaction with fatty acids (Cody et al., 2011). Protein remnants can survive for millions of years; for instance, a ~3.5 Ma camel yields up to 80% of the protein sequence of collagen (Buckley et al., 2019). The oldest genomic data reported are from a ca. 1 Ma mammoth tooth (van der Valk et al., 2021) but most reports of ancient DNA come from specimens that are only tens of thousands of years old (Bada et al., 1999; Poinar et al., 1996).

Broadly speaking, the preservation potential of biomolecules in the geological record is inversely proportional to the amount of biochemically relevant information that they can provide but this is untrue when studying macroevolution. Compared to nucleic acids, proteins evolve more slowly and provide useful information on evolutionary processes occurring above the species level. For example, sequencing of ancient collagen from the extinct ‘Malagasy aardvark’ (Late Quaternary, Madagascar) led to its reclassification from the order Bibymalagasia, which is phylogenetically close to aardvarks, to Tenrecoidea – an order containing tenrecs (Buckley, 2013). Although proteins seldom survive for more than a few million years, protein remnants can survive in Mesozoic fossils via their interaction with stabilising substances such as certain minerals (Demarchi et al., 2016). Investigation

into the survival of proteins in deep time is thus critical to future palaeontological discoveries regarding the biochemical underpinnings of macroevolutionary events (Cappellini et al., 2018).

1.7 Fossil feathers

Our knowledge of the fossil feather record commenced with the discovery of *Archaeopteryx* (Late Jurassic, Solnhofen limestone; Meyer, 1861), which possesses feathers with similar morphology to those of modern birds (e.g., curved rachis, barbs, differentiated barbules and vane asymmetry; Wellnhofer, 2009). *Archaeopteryx* feathers do not, therefore, fill any knowledge gap in the evolution of feathers or reveal new feather morphologies and are thus limited in their ability to inform on feather evolution. A much better understanding of feather origins has emerged from studies of dinosaurs and early birds associated with organically preserved feathers of various morphologies (Chen et al., 1998; Hou et al., 1995; Ji et al., 2001; Norell et al., 2002; Qiang et al., 1998; Xu & Zhang, 2005; Xu et al., 1999, 2000, 2001, 2009, 2010). The interpretation of integumentary structures in a pterosaur as feathers suggests that feathers evolved ca. 250 Ma (Benton et al., 2019; Yang et al., 2019). The identification of pterosaur feathers is consistent with comparative genomic estimates that feather regulatory elements and nonkeratin feather genes were present in the genome before the origin of dinosaurs (Lowe et al., 2015).

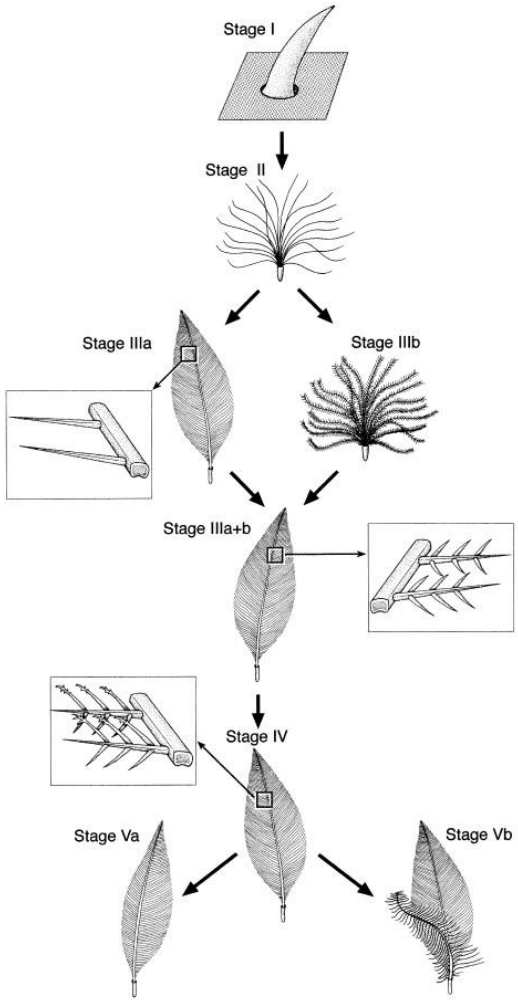


Fig. 1.10 *Evolutionary developmental model of feathers (from Prum [1999]).*

Fossil discoveries to date are consistent with the general sequence of feather evolution proposed by Prum (1999). Stage I of the model involves the development of the feather follicle (Prum, 1999; Fig. 1.10); this results in an unbranched and hollow tube resembling structures in *Sinosauropteryx* (Early Cretaceous, Jehol Biota; Chen et al., 1998) and *Beipiaosaurus* (Early Cretaceous, Jehol Biota; Chen et al., 2015; Xu et al., 1999). In stage II the collar differentiates into barb ridges to generate barbs, generating a tuft of barbs that fuse to a calamus. Stage II represents the basally branched feathers in *Dilong* (Early Cretaceous, Jehol Biota; Xu et al., 2004) and *Sinornithosaurus* (Early Cretaceous, Jehol Biota; Xu et al., 2001). At Stage III it is uncertain whether a rachis or barbules develops first; these options are presented as stage IIIa and -IIIb. Stage IIIa involves the development of helical separation of barb ridges with regular spacing to form a feather with a rachis and barbs, such as the serially branched feathers in *Sinornithosaurus* (Xu et al., 2001). In stage IIIb the barbule plates differentiate, forming a tuft of barbs and barbules. Stage IIIa+b features an open pennaceous feather with a rachis, barbs and barbules. Stage IV involves

the differentiation of barbules to form both distal and proximal barbule plates to create a pennaceous feather with a closed vane; the feathers of *Caudipteryx* and *Protoarchaeopteryx* (Early Cretaceous, Jehol Biota; Qiang et al., 1998) represent this stage. Stage V features a feather with an asymmetrical vane, such as the feathers in *Microraptor* (Early Cretaceous, Jehol Biota; Dyke et al., 2013), *Confuciusornis* (Late Jurassic/Early Cretaceous, Jehol Biota; Hou et al., 1999) and *Archaeopteryx* (Wellnhofer, 2009).

The fossil record reveals the existence of several feather morphologies that are not present in extant taxa or the developmental model proposed by Prum (1999). For example, *Similicaudipteryx* (Early Cretaceous, Jehol Biota; Xu et al., 2010) and *Kulindadromeus* (Middle/Late Jurassic, southeastern Siberia; Godefroit et al., 2014) possess ribbon-like feathers. *Kulindadromeus* also possesses feathers that comprise several filaments associated with a basal plate (Godefroit et al., 2014). Further, a dinosaur tail preserved in amber (middle Cretaceous, Myanmar) exhibits feathers with barbs that alternate in position along a rachis (i.e., are not directly across from each other; Xing et al., 2016). Notably, the developmental model does not account for the development of an asymmetric feather vane without different barb-rachis angles for the inner and outer vane (see Chapter 1.1). Asymmetric feathers in *Confuciusornis, Sapeornis* (Early Cretaceous, Jehol Biota) and *Archaeopteryx* and of the hindlimbs of *Microraptor* exhibit the same barb-rachis angle on both the inner and outer vane (Feo et al., 2015).

There is debate on whether feathers first evolved for signalling, thermoinsulation or flight. The presence of asymmetric pennaceous feathers in *Microraptor* demonstrates that highly complex feathers evolved prior to powered flight (Dyke et al., 2013). Further, the occurrence of monofilaments and feathers in pterosaurs suggests that feathers originally evolved for thermoinsulation in the common avemetatarsalian ancestor of Dinosauria and Pterosauria (Benton et al., 2019) and only later were co-opted for signalling and flight.

1.7.1 Fossil melanosomes or bacteria?

Fossil microbodies are often found in fossil soft tissues. Microbodies in a fossil feather (Middle Eocene, Germany) were originally identified as bacteria due to their similarity in shape and size to modern decay bacteria (Wuttke, 1983). Vinther et al. (2008) later

reinterpreted microbodies associated with a fossil feather (Early Cretaceous, Brazil) and the eyespot of a fossil bird as preserved melanosomes due to their morphological similarity to melanosomes in extant birds. The range of geometries of extant bacteria and melanosomes in feathers of extant taxa overlaps (Moyer et al., 2014), rendering the misinterpretation of fossil melanosomes as fossil bacteria based on morphological data possible. Principal components analysis of melanosome and bacteria geometry, however, reveals that the overlap is minor (Roy et al., 2020).

Many researchers agree that geochemical data on fossil soft tissues and the surrounding sediment should support interpretations of fossil microbodies (Lindgren, Moyer, et al., 2015a; Marshall et al., 2011; Moyer et al., 2014; Vinther, 2016). Early reports of fossil melanosomes did not provide chemical data (Vinther et al., 2008; Zhang et al., 2010). Many reports of organically preserved bacteria did not provide chemical evidence of carbonaceous matter within the microbodies (De Gregorio et al., 2011; Pacton et al., 2006; Schopf et al., 1965; Westall et al., 2001). Nevertheless, permineralised bacteria can retain organic residues (Alleon et al., 2018; Preston et al., 2011; Preston & Genge, 2010; Ye et al., 2020), suggesting that organic remains of bacteria may survive in the fossil record. Taphonomic experiments (see Chapter 1.8) demonstrate that organic remains of melanosomes can survive under various conditions (Colleary et al., 2015; Jarenmark et al., 2021; McNamara et al., 2013, 2018) but whether organic remains of bacteria can survive is unknown.

The primary chemical techniques used to identify evidence of melanin, or residues thereof, in fossils are time-of-flight secondary ion mass spectrometry (ToF-SIMS), Fourier-transform infrared (FTIR) and Raman spectroscopy and, especially, alkaline hydrogen peroxide oxidation-high-performance liquid chromatography (AHPO-HPLC; Galván & Jorge, 2015; Glass et al., 2012; Jarenmark et al., 2021; McNamara et al., 2016b; Wakamatsu & Ito, 2002). Each of these techniques can detect molecular signatures indicative of melanin or its degraded and altered remains. Notably, chemical spectra for fossil melanosomes and bacteria are similar when studied using FTIR (Preston & Genge, 2010; Preston et al., 2011) and Raman (Alleon et al., 2018). In contrast, Tof-SIMS and especially AHPO-HPLC spectra are more diagnostic of melanin (Jarenmark et al., 2021; Wakamatsu & Ito, 2002) and reveal widespread evidence of melanin in carbonaceous fossils (Barden et al., 2015, 2011;

Colleary et al., 2015; Gabbott et al., 2016; Glass et al., 2012; Gren et al., 2017; Lindgren et al., 2012, 2014, 2018, 2019; McNamara et al., 2016b, 2018; Pinheiro et al., 2019; Rossi et al., 2019). Synchrotron-based analyses, such as synchrotron-rapid scanning X-ray fluorescence (SRS-XRF), X-ray absorption near-edge structure (XANES) and extended X-ray absorption fine structure (EXAFS), can also support evidence of fossil melanin via the detection of metals that are typically associated with eumelanin and phaeomelanin (Edwards et al., 2016; Manning et al., 2019; Wogelius et al., 2011; see Chapter 1.7.2).

1.7.2 Fossil melanosomes and melanins

The survival of melanins in the fossil record has been attributed to their inherent recalcitrance (Glass et al., 2012). Borovanský and Riley (2011) suggest that the chemical properties of melanin are conferred to melanosomes. Melanin biopolymers are resistant to enzymatic digestion (Ohtaki & Seiji, 1971) and acid hydrolysis (Borovanský et al., 1977) and are insoluble under most pH conditions. Analysis of melanosomes preserved in 3D in fossil frogs from the Libros Biota (Late Miocene) using pyrolysis-gas chromatography-mass spectrometry (py-GC-MS) reveals the presence of alkylated thiophenes – i.e., long aliphatic chains with sulfur-containing heterocyclic compounds (McNamara et al., 2016b). Alkylated thiophenes result from the incorporation of environmentally derived sulfides and polysulfides into organic material. The presence of alkylated thiophenes in fossil frog melanosomes confirms that sulfurisation can contribute to the preservation of melanosomes (McNamara et al., 2016b). The preservation of fossil melanosomes thus may not result exclusively from the inherent recalcitrance of melanin.

Heavy metals can associate with and even confer stability to organic matter. The association of Cu and Pb with hair has enabled keratin fibrils to survive in archaeological settings that would ordinarily lead to their degradation (Bertrand et al., 2014). It is possible that heavy metals may also confer stability to melanin and melanosomes and promote their preservation in fossils (Wogelius et al., 2011). In contrast to 3D fossil melanosomes, melanosomes can also preserve as external moulds, termed mouldic melanosomes (Gren et al., 2017; Li et al., 2010; Zhang et al., 2010). Importantly, this indicates that soft tissues can preserve under taphonomic scenarios that are not conducive to 3D melanosome

preservation. Fossil feathers can possess heavy metals that are associated with eumelanin molecules even where no 3D melanosomes are preserved (Wogelius et al., 2011).

The discovery of fossil melanosomes, both 3D and mouldic, has facilitated reconstructions of the original melanin-based colouration of many extinct animals. Reconstructions of the original colouration of early birds (Li et al., 2018; Zhang et al., 2010), non-avialan feathered dinosaurs (Hu et al., 2018; Li et al., 2012, 2010; Zhang et al., 2010) and a mouse (Manning et al., 2019) have helped elucidate ancient animal behaviour. In extant animals, colour patterns and visually striking colours aid in camouflage and visual communication, such as sexual signalling (Gluckman & Cardoso, 2010; Stuart-Fox et al., 2021). The tail of *Sinosauropteryx* features dark and light regions that produce stripes, with dark regions containing spheroidal melanosomes that Zhang et al. (2010) interpret as phaeomelanosomes. Li et al. (2010) similarly interpret the spheroidal melanosomes in the headcrest of *Anchiornis huxleyi* (Jurassic, Jehol Biota) as phaeomelanosomes. Evidence of fossil phaeomelanosomes in feathers of *Sinosauropteryx* and the headcrest feathers of *Anchiornis* supports interpretations that the feathers in these regions were rufous in colour and functioned in visual communication (Li et al., 2010; Zhang et al., 2010). Eumelanosomes in the feathers of *Microraptor* (Li et al., 2012) and *Caihong juji* (Late Jurassic, Daohugou Biota; Hu et al., 2018) are very long and thin and are densely packed; Li et al. (2012) and Hu et al. (2018) interpret this as evidence of iridescent structural colour that may have served in signalling. Babarović et al. (2019) report non-iridescent structural blue colouration in the bird *Eocoracias brachyptera* (Eocene, Messel shale). Body regions possessing very long and wide eumelanosomes (ca. 1200 x 400 nm) and that are blue in ancestral state reconstructions were interpreted to have original blue colouration (Babarović et al., 2019).

Although fossil pigments can provide information about ancient organisms, there are many limitations to reconstructing original fossil colour. Critically, there is no correlation between melanosome shape and chemistry in non-avian taxa (Pinheiro et al., 2019). The link between melanosome geometry and chemistry in avian taxa (Babarović et al., 2019; Carney et al., 2012; Li et al., 2012, 2014), however, has not been adequately characterised to determine if the relationship can be extrapolated to extinct avian taxa. Importantly, Babarović et al. (2019) show that feather colour predictions are only 61.9% accurate when

based on melanosome morphology. Further, the melanosome geometries that produce grey and non-iridescent structural blue colouration are indistinguishable (Babarović et al., 2019). Another key limitation is that most original colour reconstructions of extinct animals use data from small regions of fossil soft tissue. Small samples from disparate parts of the body, even if numerous, are unlikely to form an accurate picture of the integumentary colour for an entire organism (Edwards et al., 2014).

An additional caveat concerning the accuracy of most original colour reconstructions is that they have a bias toward eumelanin pigments. Most reconstructions exclude non-melanin pigments, which rarely preserve in fossil soft tissues (but see McNamara et al., 2016a). Moreover, chemical evidence of phaeomelanin has been reported only in the 3 Ma fossil mouse *Apodemus* (Manning et al., 2019). The paucity of evidence for fossil phaeomelanin reported to date indicates that melanin-based reconstructions may be biased towards eumelanin since most tissues in extant vertebrates contain at least both eumelanin and phaeomelanin (see Chapter 1.3).

Colour reconstructions of extinct animals may inform on palaeobiology regardless of whether they include non-melanin pigments or not. Dark and light regions in the fossil soft tissues of *Psittacosaurus* (Early Cretaceous, Jehol Biota; Vinther et al., 2016), *Sinosauropteryx* (Smithwick et al., 2017) and *Borealopelta markmitchelli* (Early Cretaceous, Alberta; Brown et al., 2017) indicate dorso-ventral patterning. A quantitative study on dorso-ventral patterning in extant taxa, as in deer, suggests that dorso-ventral patterning in fossils can inform on palaeoecology (Allen et al., 2012). In general, strong countershading in animals is associated with the occupation of open and well-lit environments (Allen et al., 2012). Countershading in the dinosaur *Psittacosaurus* suggests that it occupied a forested habitat (Vinther et al., 2016), whereas the countershading in *Sinosauropteryx* indicates occupation of an open and well-lit habitat (Smithwick et al., 2017). Brown et al. (2017) interpret the countershading in *Borealopelta* as evidence of predation pressure on the dinosaur but do not propose a particular habitat. Fossil melanosomes and chemical evidence of eumelanin in the cyclostome *Mayomyzon pieckoensis* (Late Carboniferous, Mazon Creek Lagerstatte) indicate vertical striping and countershading, suggesting that *Mayomyzon* inhabited clear waters (Gabbott et al., 2016). Melanophores and chemical residues of eumelanin are present in the ichthyosaur

Stenopterygius (Early Jurassic, Holzmaden; Lindgren et al., 2018) and the turtle *Tasbacka danica* (Eocene, Fur Formation; Lindgren et al., 2017). The pigmentation patterns in *Stenopterygius* and *Tasbacka* indicate countershading that was likely used for camouflage in pelagic waters (Lindgren et al., 2017, 2018). Conversely, melanosomes and chemical evidence of eumelanin indicate a uniform dark colouration for an unidentified ichthyosaur (Early Jurassic, Yorkshire) that may have provided camouflage during deep-diving (Lindgren et al., 2014). Interpreting selection pressures, such as camouflage, from dorso-ventral patterning is contentious. The functions of melanin are not necessarily mutually exclusive. Further, dorso-ventral patterning can protect tissues from UV radiation while minimising the costly production of melanosomes in areas that UV protection is not needed (Negro et al., 2018). Dorso-ventral patterning is therefore not always suggestive of a particular habitat (Negro et al., 2018).

Nevertheless, evidence of dark- and light-coloured regions in ancient animals provides valuable information on the functional evolution of melanin (McNamara et al., 2021). The preservation of patterning in the fossil record informs on the evolution of specific genes such as ASIP, which is involved in dorso-ventral patterning (Haupaix & Manceau, 2020; Inaba & Chuong, 2020; Manceau et al., 2011; McNamara et al., 2021). Other important evolutionary findings include the convergent evolution of melanin in secondarily aquatic reptiles (Lindgren et al., 2014) and the use of melanin to strengthen the tips of feathers mechanically, as evidenced by darker feather tips in *Archaeopterx* (Manning et al., 2013).

Fossil melanins can also support hypotheses on feather evolution. Melanins outside of melanosomes are sometimes present in the dermis below the collagen layers (Prum & Torres, 2003). The presence of melanin and melanosomes in fossil integumentary structures consequently supports the interpretation of structures as feathers (Yang et al., 2019; Zhang et al., 2010), as opposed to degraded collagen (Feduccia et al., 2005; Lingham-Soliar, 2003a, b, 2007) or actinofibrils (Unwin & Martill, 2020). Critically, detecting melanins in fossil integumentary structures that span the hypothesised timeframe of feather origins may support the identification of feather-like structures as primitive feathers.

The increasing application of analytical chemical techniques to fossil soft tissues has provided more opportunities for fossil melanin to inform on melanin evolution (McNamara et al., 2021). Trace metals can potentially support interpretations of integumentary colouration. SRS-XRF analysis of feathers from extant birds has revealed the presence of Cu in black regions and Zn in orange regions (Edwards et al., 2016). SRS-XRF of the 3 Ma fossil mouse *Apodemus* (Pliocene, Germany) revealed the presence of Zn in preserved hair that also contains evidence of phaeomelanin (Manning et al., 2019). Interestingly, EXAFS data of Cu-rich feathers in *Confuciusornis* suggests that the Cu may be bound to eumelanin (Wogelius et al., 2011).

Trace metals can also help infer the anatomy of ancient organisms. Extant amphibians, reptiles, mammals and birds show tissue-specific melanin-metal associations (Rossi et al., 2019, 2020). Data on tissue-specific melanin-metal associations support the interpretation of the internal anatomy of a fossil tadpole and suggest an important role for melanins in metal homeostasis early in vertebrate evolution (Rossi et al., 2019, 2020). However, melanin-metal associations can alter depending on the surrounding chemical environment (Hong & Simon, 2007). Maturation of melanin extracts (from tissues of extant animals) in Cu- or Zn- rich solutions alters the original trace metal signature of melanin extracts (Rogers et al., 2021; Rossi et al., 2021). This alteration during maturation indicates that diagenetic processes can overprint the original trace metal chemistries of fossil melanins (Rogers et al., 2021; Rossi et al., 2021). Melanin-metal associations may alter during diagenesis but tissue-specific signals can still preserve in the fossil record (Rossi et al., 2019).

The functional evolution of phaeomelanin is debated as the pigment produces toxic ROS in response to ionising radiation (see Chapter 1.3). Phaeomelanin may be ancestral to eumelanin based on current knowledge of its phylogenetic distribution and the model for melanin biosynthesis (Hoekstra, 2006; McNamara et al., 2021). Chemical detection of phaeomelanin in Mesozoic fossils is thus critical to elucidating its role in the integument as it is phototoxic to organisms.

1.7.3 Fossil feather proteins

Fossil feathers usually preserve as carbonaceous compressions (Benton et al., 2008; Godefroit et al., 2014; Gren et al., 2017; Hu et al., 2018; Li et al., 2010; Lindgren et al., 2015b; Vinther et al., 2008; Zhang et al., 2010). Despite extensive study (McNamara, 2013; McNamara et al., 2013; Moyer et al., 2016; Saitta et al., 2017a, b, 2018; Zhao et al., 2020), there is no consensus on the interpretation of ultrastructural and chemical data of fossil feathers and the chemistry of fossil feathers has not been fully characterised.

The matrix in which mouldic eumelanosomes and phaeomelanosomes occur (Gren et al., 2017; Li et al., 2010; Lindgren et al., 2015b; Zhang et al., 2010) has been interpreted as the remains of degraded keratin (Gren et al., 2017; Li et al., 2010; Zhang et al., 2010), raising questions concerning its chemical composition. Indeed, there are reports of CBPs in fossil feathers from *Shuvuuia deserti* (Schweitzer et al., 1999) and *Eoconfuciusornis* (Early Cretaceous, Jehol Biota; Pan et al., 2016). Pan et al. (2019) report CBPs in addition to IF-keratins in feathers of *Anchiornis.* Evidence of fossil feather proteins, however, is controversial (Saitta et al., 2017a, b, 2018) as (1) laboratory experiments have not confirmed that feather proteins, or remnants thereof, can survive maturation (see Chapter 1.8) (2) reports of remnant feather CBPs in fossils (Pan et al., 2016, 2019; Schweitzer et al., 1999) do not provide a taphonomic model for their survival (3) the purported remnants of feather CBPs in fossil feathers are hundreds of millions of years older than proteins are expected to survive (Eglinton & Logan, 1991; see Chapter 1.6) and (4) it has not been demonstrated that the methodology used (immunohistochemistry) to report ancient feather proteins is appropriate for use on fossil soft tissues.

Definitive evidence of ancient feather proteins requires, among many things, a taphonomic model for their preservation. Relative to many other proteins, feather CBPs are particularly robust. Feather CBPs are fibrous proteins with extensive cross-linking via cystine disulfide bonds (see Chapter 1.4; Wang et al., 2016). The highly cross-linked nature of feather CBPs renders the degradation of feathers from poultry waste difficult (Pahua-Ramos et al., 2017). The inherent biochemistry of feather CBPs may facilitate the preservation of remnant feather CBPs in deep time.

Despite industrial difficulties with degrading feathers (Pahua-Ramos et al., 2017), various recent reports suggest that proteinaceous components of feathers do not preserve in fossils (Saitta et al., 2018; Smithwick et al., 2017; Vinther et al., 2008). Moreover, Saitta et al. (2017b, 2019) hypothesise that melanosomes are the main feather component to survive fossilisation. Additional reports suggest that pigmented feathers are less decay-prone than white feathers (Goldstein et al., 2004; Gunderson et al., 2008), potentially due to melanin-keratin interactions (Lindgren, et al., 2015; Zhao et al., 2020). A separate report, however, shows that white feathers are less decay-prone than pigmented feathers (Saitta et al., 2017a). Whether melanin content can influence the preservation of feather CBPs remains unclear and requires comprehensive study. Also unclear is the potential of other taphonomic processes to contribute to the preservation of feather CBPs remnants. Barden et al. (2011) hypothesise that the aliphatic component of feathers from the bird *Gansus yumenensis* (Early Cretaceous, Xiagou Formation) reflects *in situ* polymerisation. Nevertheless, experiments on feathers to date have not focused on processes such as *in situ* polymerisation and sulfurisation.

Identifying fossil feather CBPs, or remnants thereof, requires the use of appropriate techniques. Evidence for the survival of feather CBP remnants in fossil feathers stems largely from positive results using immunohistochemistry that show fluorescence of the fossil feather tissue (Benton et al., 2019; Pan et al., 2016, 2019; Saitta & Vinther, 2019; Schweitzer et al., 1999). The use of immunohistochemistry on fossils, however, remains controversial as it requires rigorous testing on experimentally degraded feathers, which has not yet been done (Smithwick, 2017). Pan et al. (2019) support their interpretation of keratin preservation in *Anchiornis* with elemental maps showing co-localisation of sulfur with fossil feather tissue; bulk elemental chemistry, however, can be altered during diagenesis, e.g., via sulfurisation (McNamara, et al., 2016; Rogers et al., 2021; Rossi et al., 2020, 2021).

Remnants of ancient feather CBPs in the fossil record could yield insights into the biomolecular evolution of feathers and flight. The origin of feather CBPs is still uncertain as there are two competing hypotheses for the evolution of feather CBPs (Dhouailly, 2009; Greenwold & Sawyer, 2011, 2013; see Chapter 1.4). Notably, the hypothesis of a deeper

origin for CBPs is consistent with the identification of feathers in pterosaurs (Yang et al., 2019).

Controlled taphonomic experiments assessing the preservation potential of feather CBPs and IF-keratins can determine whether they are likely to preserve in fossils. Further, the study of experimentally degraded and fossil samples should use alternative techniques to immunohistochemistry (such as sulfur-XANES spectroscopy; Benton et al., 2019).

1.8 Experimental taphonomy

Taphonomic research aims to accurately interpret fossils through the applied knowledge of taphonomic processes (see Chapter 1.5). Taphonomic processes can promote either the retention or loss of structural and biochemical information (see Chapter 1.5). Further, taphonomic processes can interact to produce variation in the quality of fossil preservation within and among fossil deposits. The generation of taphonomic artefacts during diagenesis may result in fossil characteristics that do not inform on the palaeobiology of the organism. Therefore, the accurate interpretation of fossils requires consideration of the taphonomic history of a fossil.

Controlled laboratory experiments can facilitate investigations on the impact of intrinsic and extrinsic factors on the preservation of organic remains (Briggs, 1995, 2003; Briggs & McMahon, 2016; Sansom, 2014). The control of intrinsic and extrinsic factors in controlled laboratory experiments and study of taphonomic processes in isolation and, potentially, in combination can yield a framework for interpreting fossil data.

1.8.1 Decay

Decay experiments on organelles (Carlisle et al., 2021) and many taxa of invertebrates (Briggs & Kear, 1993; Butler et al., 2015; McNamara, 2013; Odin et al., 2018; Sansom et al., 2010, 2011, 2013) and vertebrates (Davis & Briggs, 1998; Gäb et al., 2020) have provided critical insights into the inorganic and organic preservation of fossils.

Decay experiments have revealed several major controls on the inorganic preservation of fossil soft tissues. Importantly, decay promotes the authigenic mineralisation of decay-prone soft tissues (Briggs & Kear, 1994; Briggs & Wilby, 1996; Gabbott et al., 2021). The authigenic mineralisation of soft tissues depends, in part, on the relative concentrations of specific mineral ions (Briggs & Wilby, 1996). Decomposition of an organism can generate anoxia and low pH (due to the release of CO_2 and volatile fatty acids) and, if the pH drops below 6.38, can promote the precipitation of calcium phosphate (Briggs & Kear, 1994). The replication of soft tissues in calcium carbonate proceeds when the pH increases above 6.38 (Briggs & Wilby, 1996). Authigenic mineralisation is also contingent on the decay microenvironment in an organism. For example, experimental decay of cephalopods shows that taxa using ammonia to regulate buoyancy are unlikely to preserve soft tissues via phosphatisation due to the alkaline environment generated by ammonia during decay (Clements et al., 2017; Voight et al., 1995).

Decay experiments on chordates and basal vertebrates provide insights into the interpretations of organically preserved soft-bodied fossils (Sansom et al., 2010, 2011, 2013). Notably, synapomorphic characters degrade before plesiomorphic characters in lancelets (Sansom et al., 2010). This decay pattern can potentially result in misinterpreting an early diverging vertebrate taxon as phylogenetically more basal than it is, termed 'stemward slippage' (Sansom et al., 2010).

Previous experiments on isolated feathers elucidate the role of decay in fossil feather preservation to varying degrees (Moyer et al., 2016; Saitta et al., 2017a, b, 2018). Decay experiments in Saitta et al. (2017a) use a cultured microbial broth to accelerate the decay process. Interestingly, Saitta et al. (2017a) report extensive degradation of tissue macrostructure in decayed black feathers, in which barbs and barbules are only partially fused. The loss of tissue macrostructure in decayed black feathers (Saitta et al., 2017a), which are likely eumelanin-rich, may indicate that eumelanin-rich fossil feathers bearing original tissue macrostructure did not experience extensive decay. The decay of feathers as per Saitta et al. (2017a) may thus not be appropriate for the study of most fossil feathers. In contrast to the results from black feathers, the macrostructure of decayed white feathers resembles that of untreated white feathers (Saitta et al., 2017a). This result for decayed white feathers contrasts with previous interpretations that white feathers are

more decay-prone than pigmented feathers (Goldstein et al., 2004; Gunderson et al., 2008; see Chapter 1.7.3). Moyer et al. (2016) degraded feathers over ten years under various conditions and in natural settings; it is difficult, however, to assess the impact of decay in these experiments for various reasons. The experiments introduce variables (such as burial, 'periodic' watering and the storage of samples under different conditions and for different lengths of time) in combination without analysing the impact of each variable in isolation. Further, uncontrolled experiments (such as the burial of a bird near a stream [Moyer et al., 2016]) prevent an exact replication of the experiment. The decay experiments in Moyer et al. are therefore limited in their potential to inform on the impact of decay on feather tissue.

Sulfurisation can occur during decay as well as during maturation (see Chapter 1.6). Sulfurisation involves the incorporation of environmentally derived sulfides and polysulfides into biomolecules, forming disulfide bridges that can link aliphatic chains (see Chapter 1.7.2). Sulfurisation can also result in the replacement of a C atom within a heterocyclic ring with a S atom to form alkylated thiophenes, which are diagnostic of sulfurisation (Kok et al., 2000; McNamara et al., 2016b; van Dongen et al., 2003, 2006; see Chapters 1.6 and 1.7.2). Evidence of sulfurisation in the fossil record stems from the presence of organosulfur compounds (OSCs), including alkylated thiophenes, in fossil melanosomes (McNamara et al., 2016b). Further, the presence of OSCs in 10 Ma bone marrow and the soft tissues of a mosasaur (Late Cretaceous) indicate that sulfurisation promoted the preservation of organics (Lindgren et al., 2014; McNamara et al., 2006).

There are currently no reports of the sulfurisation of feather tissue but previous experiments can inform on the conditions favourable to their sulfurisation. The decay of carbohydrates with elemental S and sulfides at 50°C transforms carbohydrates into thermally stable OSCs (van Dongen et al., 2003). The use of conditions favourable to sulfurisation in decay experiments may shed light on the potential role of sulfurisation in the preservation of fossil feathers.

1.8.2 Maturation

Analysing the impact of diagenesis on soft-tissue preservation in laboratory timescales requires the use of elevated temperatures, alone or in combination with elevated pressures. Elevated temperatures are known to accelerate the morphological and chemical changes that occur at much lower temperatures over longer geological timescales (Briggs & McMahon, 2016).

Previous taphonomic experiments serve as a guide on how to define experimental conditions that are appropriate for simulating diagenetic burial on a certain tissue (Cody et al., 2011; Gupta et al., 2006; Stankiewicz et al., 1997, 2000). For example, the *in situ* polymerisation of lipids and free fatty acids in arthropod cuticles is known to occur at temperatures of 250°C–360°C combined with pressures of up to 700 bars for durations of 24 hours; critically, these conditions generate aliphatic macromolecules that resemble the type I/II kerogen composition of Palaeozoic arthropod cuticles (Gupta et al., 2006; Stankiewicz et al., 1997, 2000). Maturation conditions that are appropriate for arthropod cuticles, however, are not suitable for all tissues.

Most fossil feathers are readily identifiable as feathers due to the preservation of their hierarchical branching structure. Experimentally matured feathers that retain feather macrostructure are useful analogues for fossil feathers. Feathers matured at 150°C–250°C and 250 bar for 1–24 hours retain tissue macrostructure (McNamara et al., 2013; Zhao et al., 2020). These conditions also result in a melanin chemical composition similar to several Mesozoic fossil feathers (Colleary et al., 2015) from deposits with low maximum burial temperatures (i.e., <60°C; McNamara, 2013; McNamara et al., 2013). Experiments using similar maturation conditions have informed on specific aspects of fossil feather taphonomy. For example, the preservation of mouldic melanosomes that are larger than closely juxtaposed 3D fossil melanosomes indicates diagenetic shrinkage of melanosomes (McNamara et al., 2013; Colleary et al., 2015). Maturation experiments reveal that this phenomenon is due to diagenetic shrinkage. Experimental maturation of feathers shows that melanosomes shrink up to 20% after 1 hour at the relatively mild conditions of 200°C, 250 bar and 250°C, 250 bar (McNamara et al., 2013).

Temperature is the key factor in the physical and chemical preservation of melanin. Temperature impacts on the structure of melanosomes more than pressure as melanosomes exhibit more shrinkage under conditions of 250°C, 250 bar than 200°C, 250 bar (McNamara et al., 2013). Further, temperature impacts on melanin chemistry more than age (Glass et al., 2013). Fossil ink sacs from the Posidonia Shale preserve fewer chemical markers for melanin than ink sacs from the Oxford Clay or Blue Lias formations, which have lower thermal maximum temperatures than the Posidonia Shale (Glass et al., 2013). Data from taphonomic experiments and fossils demonstrate the greater importance of temperature than pressure when performing maturation experiments.

Data from previous maturation experiments suggest that feather proteins can survive extensive degradation (Moyer et al., 2016; Schweitzer et al., 2018), supporting evidence of CBPs and IF-keratins in Mesozoic fossil feathers (Pan et al., 2016, 2019; Schweitzer et al., 1999). The maturation experiment in Moyer et al. (2016) however, uses the extreme temperature of 350°C for ten years. These temperatures and durations are inconsistent with the conditions known to produce feather samples comparable to fossil feathers in terms of feather macrostructure (Colleary et al., 2015; McNamara et al., 2013; Zhao et al., 2020). Further, the maturation experiments in Moyer et al. (2016) did not incorporate elevated pressure. Although pressure has little impact on feather degradation (McNamara et al., 2013), all fossil feathers have experienced pressures above atmospheric pressure during burial so where possible, pressure should be considered in the design of maturation experiments involving feathers.

Additional maturation experiments on feathers (Saitta et al., 2017a, b, 2018) cast doubt on reports of feather CBPs and IF-keratins in the fossil record (Pan et al., 2016, 2019; Schweitzer et al., 1999). Saitta et al. (2017a, b) report that the maturation of feathers at 250°C, 250 bar for 24 hours generates a thick water-soluble fluid. Electron microscopy and py-GC-MS data of the fluid show evidence for melanin pigments only (Saitta et al., 2017a, b). Maturation conditions that eliminate feather hierarchical structure, however, cannot inform on the taphonomy of fossil feathers that preserve gross feather structure. In contrast, moderate maturation (100°C, 250 bars for 24 hours) of feathers results in the preservation of tissue macrostructure (Saitta et al., 2017a). Nevertheless, the lack of evidence for feather CBPs in py-GC-MS data of highly matured (250°C, 250 bars for 24

hours) feathers and fossil feathers from thermally immature deposits (Messel Shale and Fur Formation) was used to support the argument that feather CBPs cannot survive in deep time (Saitta et al., 2017b). Py-GC-MS, however, does not produce diagnostic signatures for both feather CBPs and melanins (Zhao et al., 2020). Therefore, the absence of evidence for feather CBPs in the fossil feathers studied (Saitta et al., 2017b) is not necessarily evidence of their absence in the fossils studied or, especially, in other fossils with different diagenetic histories.

Maturation can also induce chemical alterations to soft tissues. Melanin-metal associations can alter during maturation due to interactions with metal ions (Rogers et al., 2021; Rossi et al., 2021; see Chapter 1.7.2). Previous reports suggest that fossil mouldic melanosomes may result from the interaction of melanosomes with reactive pore fluids during maturation (McNamara, 2013; Vinther, 2016). The full impact of different fluid chemistries on feather components remains unclear.

This thesis uses taphonomic experiments that incorporate as temperatures, high-pressures and oxidising fluids to investigate the impact of these extrinsic variables on the preservation potential of feather structural proteins, melanosomes and melanin. The use of different coloured feathers in several experiments allows for an assessment of the impact of melanin chemistry on the morphological and chemical degradation of feather structural proteins and melanins. Fossil analyses examine the extent to which fossils can retain morphological and chemical evidence of feather proteins, melanosomes and melanin. The data from taphonomic experiments form a foundation for the interpretation of fossil data.

2. Material and methods

This chapter describes the material and methods used in this project. Each section considers the basic principles of each method and explains any key benefits and limitations.

2.1 Material

The material chosen for study includes extant taxa and fossils. Feathers from extant taxa were studied in their native state, i.e., untreated, and after experimental degradation. Degradation experiments in this study simulate different fossilisation processes and untreated feathers serve as controls . Fossil data were compared to data from untreated- and experimentally degraded feathers. This three-fold approach to understanding fossil feather taphonomy grounds the interpretation of fossils.

2.1.1 Extant material

Feathers from extant *Gallus gallus domesticus* (common chicken) were kindly supplied by Liam Hayes. Feathers from *Egretta garzetta* (little egret) were obtained from a bird found less than 24 hours after its death near the School of Biological, Earth and Environmental Sciences at University College Cork. The zebra finch (*Taeniopygia guttata*) was sourced from a local pet shop for a previous unrelated study and was euthanised with approval from the Health Products Regulatory Authority of Ireland via authorisation AE19130-IO87. Feathers were dissected from each specimen and stored at -80°C.

The morphological degradation of melanosomes was assessed using black feathers from the zebra finch only (see Chapter 3). Black zebra finch feathers were chosen as they contain solid melanosomes; hollow melanosomes or melanosomes with large internal vacuoles (as in *Gallus*) might be difficult to distinguish from degraded melanosomes.

Black and orange feathers from the common chicken and white feathers from the little egret were used to characterise the chemical degradation of eumelanin, phaeomelanin

and feather proteins (see Chapters 4, 5 and 6). All feather types contain both eu- and phaeomelanin (see Chapter 1.3) but ratios of the two are linked to feather colour (McGraw et al., 2005). Black and orange feathers from the common chicken were used as they are readily obtainable and represent eumelanin- and phaeomelanin-dominated systems, respectively (Table 2.1). White feathers from the little egret have minimal melanin content and were used to analyse the degradation of feather components in what is effectively a zero-melanin system.

Table 2.1 *Mean A650 : A500 values in black and orange (*Gallus gallus domesticus*) feathers after soluene-350 solubilisation. A650 and A500 values are from the spectrophotometric absorption of the soluene-350 solution at 650 nm and 500 nm, respectively (Ozeki et al., 1996). A higher A650 : A500 ratio indicates greater eumelanin content. Black and orange feathers: n = 3.*

Feather colour	A650 : A500
Black	0.3 ± 0
Orange	0.1 ± 0

2.1.2 Fossil material

Access limitations and sampling restrictions influenced the selection of fossils. Most fossils chosen for study were sourced previously for unrelated studies and readily accessible in the laboratory. A single specimen (YPM VP 58657) was loaned for this study and sampling of organic soft tissue over 1 mm^2 in size was not permitted. The most appropriate specimens for study contain the phenomena of interest, e.g., fossil melanosomes and a filamentous matrix that comprises proteins in extant animals. Fossils from the Jurassic (ca. 125 Ma) to the Miocene (ca. 10 Ma) were chosen for study and capture variation in burial history (McNamara et al., 2013; Table 2.2). Fossil melanosomes and filamentous matrices have been reported in fossil feathers from the Jehol Biota (Gren et al., 2017; Li et al., 2010; Lindgren et al., 2015b; Zhang et al., 2010). Fossil feathers from Jehol were thus chosen to test for chemical evidence of fossil melanins and residues of structural proteins in Mesozoic fossils. A fossil feather from the Green River biota (Middle Eocene, USA) was also studied as an example of a younger deposit that is more thermally mature than Jehol (Table 2.2) and known to preserve melanosomes in fossil feathers (Ksepka et al., 2013). Frog fossils from the Libros Biota were chosen for study as the biota is relatively young in

geological terms and thermally immature; further, fossils from the deposit show chemical evidence of melanin (McNamara et al., 2016b; Rossi et al., 2019).

Fossil specimens were loaned from the following institutions: Institute of Vertebrate Paleontology and Paleoanthropology (IVPP), Yale Peabody Museum of Natural History (YPM) and Museo Nacional de Ciencias Naturales de Madrid (MNCN).

Table 2.2 Fossil specimens studied in this thesis. Burial history information as reported by McNamara et al. (2013).

Taxon	Accession number	Age	Locality	Burial history
Sinornithosaurus	IVPP V 12811	Lower Cretaceous	Yixian Formation, China	649–3706 m, 60–185°C, 200–12200 bar
Confuciusornis	IVPP V 13171	Lower Cretaceous	Yixian Formation, China	
Confuciusornis	CKGM F 6433	Lower Cretaceous	Yixian Formation, China	
Pelophylax pueyoi	MNCN 63773	Upper Miocene	Libros, Spain	100 m, <40°C, 33 bar
Pelophylax pueyoi	MNCN 63678	Upper Miocene	Libros, Spain	
Pelophylax pueyoi	MNCN 63694	Upper Miocene	Libros, Spain	
Pelophylax pueyoi	CKGM F 6434	Upper Miocene	Libros, Spain	
Unidentified isolated feather	YPM VP 58657	Middle Eocene	Green River Formation, USA	1200–6700 m, 65–180°C, 400–2200 bar

2.1.3 Analytical standards

The sulfur chemistries of fossil feathers and untreated and experimentally degraded feathers were compared to the sulfur chemistries of select S-containing compounds. Commercially available standards representing different sulfur species (Sigma Aldrich; ≥98% purity) were mixed with BN to obtain a sulfur concentration of ca. 5 wt%, ground with a pestle and mortar and pressed into a pellet.

2.2 Taphonomic experiments

Taphonomic experiments (see Chapter 1.8) form the core of this thesis and were designed to produce phenomena observed in the fossil feathers of interest. Fossil feathers often exhibit gross feather structure (i.e., distinct rachis, barbs and barbules) and preserved melanosomes. Experiments incorporated one or more of the following taphonomic processes: decay, sulfurisation, oxidation and maturation (Fig. 2.1).

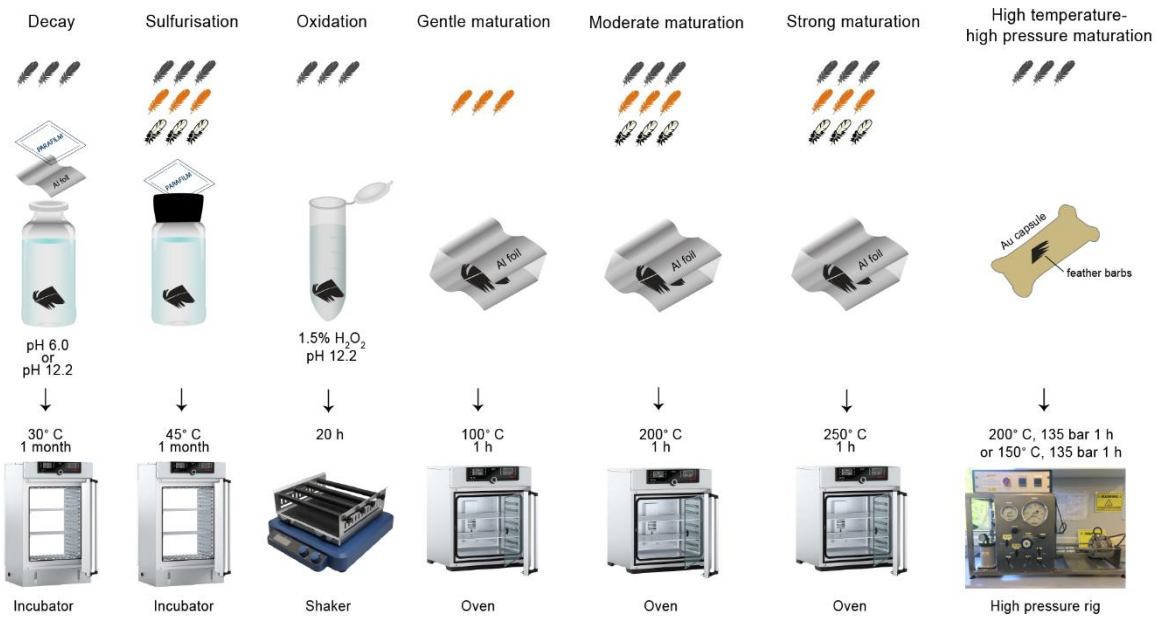


Fig. 2.1 *Schematic diagram showing design of taphonomic experiments using black and orange (*Gallus gallus*) and white (*Egretta garzetta*) feathers.*

Decay experiments were performed for 1 or 12 months at 30 ± 1°C with no added inoculum. Feathers were experimentally sulfurised in vials with N-flushed DD water, NaHS and elemental S for 1 month at 45 ± 1°C under a N atmosphere (van Dongen et al., 2003). Feathers were oxidised in a 1.5% H_2O_2 solution for 20 h at room temperature as in previous studies (Ito et al., 2011; Wakamatsu & Ito, 2002). Maturation experiments were performed with or without pressure using temperatures that are known to retain gross feather structure and melanosomes (Colleary et al., 2015; McNamara et al., 2013), as in the fossils of interest. For maturation without pressure, feather pieces (2 cm^2) were placed in Al foil (sterilised with 70% ethanol) folded into a packet and matured in a Memmert convection oven at either 200 ± 1°C or 250 ± 1°C for 1 h. Feathers matured with pressure used Au capsules. Au tubing (2 mm diameter) was cut into 10 mm lengths and one end welded using a Lambert PUK U4 microscope. Feather pieces (2 x 4 mm) were inserted into the Au capsules with sterile tweezers and the capsules welded shut. Capsules were inspected using a Leica EZ4W microscope and any poorly welded capsules likely to rupture under pressure were not used and replacement capsules welded. Au capsules were weighed and placed in an Inconel reaction chamber (8 mm internal diameter) in a custom-built cold-seal high-pressure rig (StrataTech Ltd. (UK)). Oxygen was removed from 1 l DD water by flushing with N for 15 min. The water was then pumped through the rig and, using compressed air, placed under 135 bar of pressure. The furnace was set to maintain a

temperature of either 150°C or 200°C in the reaction chamber. The experiment was terminated after 1 h and the rig left to cool before the Au capsules were removed from the reactor. Capsules were weighed again to assess for any damage incurred during the experiment. Capsules were opened using a sterile scalpel and, if wet inside, were left unused.

*Table 2.3 List of material from extant birds and the techniques used on each sample. a, untreated; b, decayed; c, oxidised; d, sulfurised; e, thermally matured; f, matured with high pressure. 1, scanning electron microscopy; 2, transmission electron microscopy; 3, alkaline hydrogen peroxide oxidation-high performance liquid chromatography (AHPO-HPLC); 4, hydroiodic acid hydrolysis-HPLC; 5, HCl-AHPO-HPLC; 6, X-ray absorption near edge structure spectroscopy; 7, Fourier-transform infrared spectroscopy; 8, pyrolysis-gas chromatography-mass spectrometry. *, not all samples from taphonomic experiments were analysed using each technique listed.*

Sample	Feather colour	Feather type	Body region	Common name	Taphonomic experiments	Replicates per treatment	Technique*	Chapter
Taeniopygia gutatta	Black	Contour	Uropygial	Zebra finch	a,b,c,e,f	3	1,2,3	3
Gallus gallus domesticus	Black	Contour	Torso	Common chicken	a,e	5	3,4,5	4
Gallus gallus domesticus	Orange	Contour	Torso	Common chicken	a,e	5	3,4,5	4
Egretta garzetta	White	Primary	Wing	Little egret	a,e	4	3,4,5	4
Gallus gallus domesticus	Black	Contour	Torso	Common chicken	a,b,c,d,e,f	3	6,7,8	5,6
Gallus gallus domesticus	Orange	Contour	Torso	Common chicken	a,b,c,d,e,f	3	6,7,8	5,6
Egretta garzetta	White	Primary	Wing	Little egret	a,b,c,d,e,f	3	6,7,8	5,6

Table 2.4 *List of fossil material and the techniques used on each sample. 1, HCl-AHPO-HPLC; 2, X-ray absorption near edge structure spectroscopy; 3, Fourier-transform infrared spectroscopy; 8, pyrolysis-gas chromatography-mass spectrometry.*

Sample	Accession number	Technique	Chapter
Sinornithosaurus	IVPP V 12811	1,2,3	4,5
Sediment	IVPP V 12811	1,2,3	4,5
Confuciusornis	IVPP V 13171	1,2,3	4,5
Sediment	IVPP V 13171	2,3	5
Confuciusornis	CKGM F 6433	1	4
Sediment	CKGM F 6433	1	4
Pelophylax pueyoi	MNCN 63773	1	4
Pelophylax pueyoi	MNCN 63678	1	4
Pelophylax pueyoi	MNCN 63694	1	4
Pelophylax pueyoi	CKGM F 6434	1	4
Sediment	CKGM F 6434	1	4
Pelophylax pueyoi (tadpole)	?	1	4
Sediment	?	1	4
Unidentified isolated feather	YPM VP 58657	2,3	5
Sediment	YPM VP 58657	2,3	5

Samples of all untreated and experimentally degraded feathers were obtained using a sterile scalpel and used in one or several of the following ways: 1) embedded in LR White resin for ultramicrotomy, 2) analysed using scanning electron microscopy (SEM), 3) analysed using transmission electron microscopy (TEM), 4) placed directly in glass vials and analysed using AHPO-HPLC, HCl-AHPO-HPLC and hydroiodic acid hydrolysis-HPLC (HI-HPLC), 5) placed on low-sulfur tape for S-XANES spectroscopy, 6) placed in glass vials for py-GC-MS and 7) analysed using FTIR spectroscopy without further treatment (Tables 2.3 and 2.4). Host sediment from fossil slabs were also analysed using HCl-AHPO-HPLC, XANES and FTIR to test whether chemical signatures in fossil feather tissues are autochthonous.

2.3 Resin embedding and ultramicrotomy

The dissection of feather barbs and barbules from extant birds using a scalpel can artificially generate melanosome moulds (i.e., some melanosomes remain in the part and others in the counterpart), making the morphological assessment of melanosome degradation via SEM difficult. To resolve this problem, samples of barbs (2–3 mm^2) were dehydrated and embedded in LR White resin (medium grade hardness); the resin blocks were then cut using a Leica EM UC7 ultramicrotome with a 45° diamond knife to produce 80 nm transverse sections of the feather tissue and a smooth sample/resin block surface.

Resin blocks were analysed using SEM and ultrathin sections of the samples were analysed using TEM.

2.4.1 Protocol

The following resin embedding protocol was used:

1. Place feather tissues in separate sterile glass vials and fix with 2.5% glutaraldehyde. Agitate using a shaker for 1 h at room temperature (RT).
2. Wash in 0.1 M PB for 1 h (x3).
3. Wash in DD water for 20 min (x3).
4. Dehydrate in 30% ETOH on a shaker for 30 min.
5. Dehydrate in 50% ETOH on a shaker for 30 min.
6. Dehydrate in 70% ETOH on a shaker for 30 min.
7. Place tissue in 2:1 mixture of LR White:70% ETOH. Agitate using a shaker for 1 h at RT.
8. Place tissue in 100% LR White and cover glass vials with Al foil. Agitate using a shaker overnight at RT.
9. Place tissue in 100% LR White and cover glass vials with Al foil. Agitate using a shaker for 30 min.
10. Place tissue in 100% LR White and cover glass vials with Al foil. Agitate using a shaker for 30 min.
11. Place tissue in new sterile glass vials with 100% LR White and cover with Al foil. Agitate using a shaker for 30 min.
12. Place tissue in coffin moulds and cover coffin moulds with LDPE, ensuring no oxygen is present under the LDPE.
13. Place covered coffin moulds in an oven at 60°C under a low vacuum for 48–72 h.

2.4 Scanning electron microscopy (SEM)

SEM is frequently used in palaeontology for the imaging of melanosomes in extant and fossil tissues (Lindgren et al., 2014, 2017; McNamara, 2013; McNamara et al., 2016b; Rossi et al., 2019; Vinther et al., 2008).

Scanning electron microscopes contain either an electron gun with a cathode or a field emission gun as sources of (primary) electrons. A series of magnets, apertures and condenser lenses focus the electron beam at different voltages. Inelastic interactions of the incident beam with the upper few nanometres of the sample surface generate secondary electrons; these secondary electrons have low energy and provide detailed information on surface topography. A detector located at an angle to the sample stage maximises the detection of secondary electrons and produces a shadow effect to emphasise surface topography. The secondary electron signal produces an image with a resolution of up to 1–20 nm. Back-scattered electrons (BSE) are higher energy than secondary electrons and penetrate deeper into the sample. Unlike secondary electrons, BSE are not sensitive to the topography of a sample as the BSE detector sits directly above the sample. BSE imaging is most helpful in providing information about the elemental composition of a sample. BSE imaging was not used here as it cannot provide information regarding the oxidation state of an element.

Most scanning electron microscopes can accommodate samples of ca. 5 cm^2 in the sample chamber, permitting the analysis of many fossils without destructive sampling. The imaging of a small fossil, however, can be restricted to areas within the boundaries of the sample stage, limiting the areas that can be analysed without sampling.

Organic materials are not conductive and can exhibit charging during SEM analyses. High-quality SEM images of organic materials are most easily achieved by sputter coating the sample with a conductive metal (e.g., Au). Sputter coating of samples can be problematic if other analyses are planned to follow SEM as the coating may obstruct features in the sample or mask a chemical signal.

SEM was used to image melanosomes and fibrous tissues in untreated and experimentally degraded feathers in this project. SEM images facilitated the examination of the extent to which melanosomes and fibrous tissues were preserved during each treatment.

2.5 Transmission electron microscopy (TEM)

TEM is regularly used in palaeontology to image fossil melanosomes (Lindgren et al., 2012; McNamara et al., 2016b; Tanaka et al., 2014), fossil feather ultrastructure (Lindgren et al., 2015b; Pan et al., 2016, 2019) and photonic structures in fossil insects (McNamara et al., 2011, 2014).

The basic principles of TEM are similar to those of SEM but the electrons transmit through the sample. The electron source at the top of the instrument transmits electrons through the sample chamber; a detector near the bottom of the instrument uses the electrons transmitted through the sample to generate an image.

TEM allows the imaging of nanometre-scale details of the internal structure of a sample. As with SEM, organic material can be unstable under the electron beam. TEM permits analysis of the internal chemical composition of a sample using energy-dispersive X-ray spectroscopy or high-angle annular dark-field imaging but these techniques were not used in this study. Samples for TEM should be ultrathin, i.e., 80–100 nm thick, for electrons to transmit through the sample. The preparation of ultrathin sections is time-consuming and destructive as samples are embedded in resin and sectioned using an ultramicrotome. Sample preparation of fossil soft tissues for TEM can be challenging as fossil material is often friable and prone to lifting out of the resin sections. Sample preparation and use of the TEM microscope require extensive training.

In this project, ultrathin sections of resin-embedded untreated and experimentally degraded feathers were imaged using TEM.

2.6 Alkaline hydrogen peroxide oxidation-high-performance liquid chromatography (AHPO-HPLC)

AHPO-HPLC is used increasingly for the detection of fossil melanin as it can detect degradation products that are unique to melanin and provide support for the identification of fossil melanosomes or melanin granules (Glass et al., 2012; Lindgren et al., 2018, 2019; McNamara et al., 2018; Rossi et al., 2019) as opposed to bacteria (see Chapter 1.7.1).

AHPO-HPLC analysis identifies melanin pigments via the chemical detection of the degradation products of the eumelanin units DHI and DHICA and the phaeomelanin unit BZ (Ito et al., 2011, 2013). Application of an alkaline hydrogen peroxide solution to samples that contain melanosomes ruptures melanosome membranes and oxidises melanin. HPLC analysis of a homogenised sample solution produces a chromatogram with peaks that correspond to the degradation products of melanin. DHI and DHICA (see Chapter 1.3) are oxidised to produce pyrrole-2,3,5-tricarboxylic acid (PTCA), pyrrole-2,3,4,5-tetracarboxylic acid (PTeCA) and pyrrole-2,3-dicarboxylic acid (PDCA) markers (Ito et al., 2011, 2013) (Fig. 2.2). PTCA is a degradation product of the DHICA monomer whereas DHI generates PTeCA and PDCA. The PTCA/PTeCA ratio informs on the degree to which DHI and DHICA are crosslinked (Glass et al., 2012, 2013; Ito et al., 2013). Similarly, oxidation of the phaeomelanin unit BZ (benzothiazole) generates the degradation products thiazole-2,4,5-tricarboxylic acid (TTCA) and thiazole-4,5-dicarboxylic acid (TDCA; Ito et al., 2011, 2013). IQ and IQCA absorb light at specific ultraviolet A wavelengths (Ito et al., 2016) but UVA irradiation was not used here.

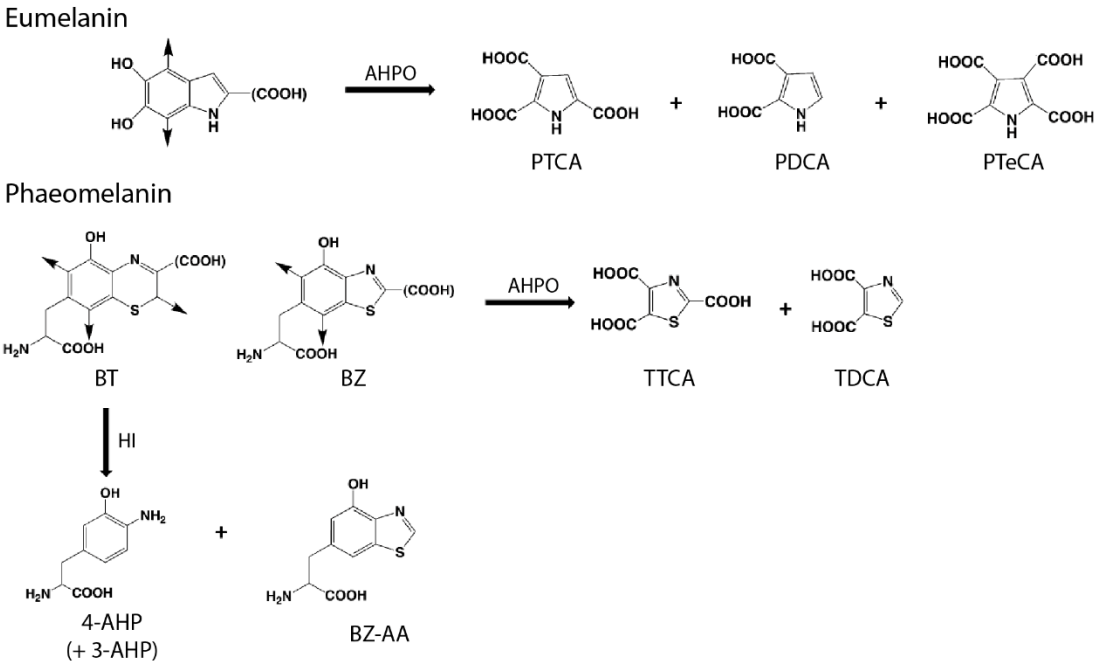


Fig. 2.2 Degradation products of eumelanin and phaeomelanin (modified from Ito et al. [2011]. Oxidation of eumelanin using alkaline hydrogen peroxide oxidation (AHPO) generates pyrrole-2,3,5-tricarboxylic acid (PTCA), pyrrole-2,3,4,5-tetracarboxylic acid (PTeCA) and pyrrole-2,3-dicarboxylic acid (PDCA) markers. AHPO treatment of phaeomelanin produces thiazole-2,4,5-tricarboxylic acid (TTCA) and thiazole-4,5-dicarboxylic acid (TDCA). Hydroiodic acid hydrolysis (HI) treatment of phaeomelanin produces 4-amino-3-hydroxylphenylalanine (4-AHP), 3-amino-4-hydroxyphenylalanine (3-AHP) and benzothiazole-amino acid (BZ-AA).

Following AHPO-HPLC, HI treatment of the sample aliquots yields additional phaeomelanin degradation products that can be detected using HPLC. The degradation of BZ generates the marker benzothiazole-amino acid (BZ-AA) whereas degradation of 5-*S*-cysteinyldopa and 2-*S*-cysteinyldopa in benzothiazine (BT) generate 4-amino-3-hydroxylphenylalanine (4-AHP) and 3-amino-4-hydroxyphenylalanine (3-AHP), respectively (Wakamatsu et al., 2002, 2009).

The demineralisation of samples before AHPO-HPLC analysis uses HCl treatment (Ito et al., 2018). Demineralisation is routine for fossil samples as they are likely to include mineralised components from the soft tissues and/or host sediment. HCl pre-treatment

can also be used on samples from extant taxa as it prevents the generation of peaks in the HPLC chromatogram from materials such as proteins that interfere with the melanin signal.

AHPO-HPLC is considered the only method to yield diagnostic markers that can identify and quantify melanin (Ito et al., 2011; Jarenmark et al., 2021; Wakamatsu & Ito, 2002). Oxidative degradation can, however, extensively alter melanin monomers to produce molecules dissimilar to melanin markers (Jarenmark et al., 2021). Moreover, AHPO-HPLC is a destructive technique that requires ca. 4 mg of sample. Fossil soft tissues are often only several microns thick. To acquire a sample of ca. 4 mg a substantial portion of the carbon film, up to 10 mm^2, may have to be removed. AHPO-HPLC is thus not possible when there is no permission to sample fossils or the collection of ca. 4 mg is not possible due to the size of the fossil. A disadvantage of HCl-AHPO-HPLC is that the phaeomelanin markers BZ-AA, 3-AHP and 4-AHP cannot be analysed after demineralisation via HCl treatment. HCl-AHPO-HPLC cannot detect the BT unit via its direct degradation products of 3-AHP and 4-AHP; any BT present can only contribute to the melanin signal if it converts to BZ via ring contraction. Ultimately, AHPO-HPLC analysis of HCl-treated fossils can only detect TTCA and TDCA that are primarily indicative of phaeomelanin BZ.

This thesis investigates the AHPO degradation products of melanin in untreated and experimentally degraded feathers. Samples (3–5 mg) of untreated and experimentally treated feathers from extant birds and freeze-dried aliquots (100 µl) of oxidising solutions were shipped to Fujita Health University (Japan) for chemical analyses performed by Prof. S. Ito and Prof. K. Wakamatsu. AHPO-HPLC analysis was performed as described by Ito et al. (2011, 2013). In brief, samples were homogenised with a Ten-Broeck glass homogeniser at a 5 mg/ml concentration. Aliquots (100 µl) from each homogenate were placed in screw-capped conical test tubes to which 375 µl 1 M K_2CO_3 and 25 µl 30% H_2O_2 were added, creating a 1.5% H_2O_2 solution in each tube. Tubes were agitated on a test-tube mixer at 25°C for 20 h. The experiment terminated with the addition of 50 µl 10% Na_2SO_3 and 140 µl 6 M HCl to each tube and the tubes were centrifuged at 4000 g for 1 min. An aliquot (80 µl) from each tube was directly injected into an HPLC system to detect H_2O_2 oxidation products.

HI-HPLC was performed on samples of untreated and experimentally matured feathers following AHPO-HPLC to detect additional phaeomelanin markers. Aliquots (100 µL) from each homogenate were placed in screw-capped conical test tubes to which 30 µl 30% H_3PO_2 and 500 µl 57% HI was added and the tubes were heated at 130°C for 20 h. The mixture was cooled and 100 µl was transferred to a test tube, dried and dissolved in 200 µl 0.1 M HCl. An aliquot (10–20 µl) from each tube was directly injected into an HPLC system.

Untreated and experimentally degraded feathers from extant birds, fossil soft-tissue and host sediments were analysed using HCl-AHPO-HPLC in addition to AHPO-HPLC and HI-HPLC. For HCl-AHPO-HPLC analysis samples were placed in screw-capped test tubes to which 4 ml 6 M HCl was added and the tubes heated at 110°C for 16 h. Data was handled and interpreted by T. S. Slater.

2.7 X-ray absorption near-edge structure spectroscopy (XANES)

Analytical chemical techniques, such as synchrotron-based XANES, are increasingly relied upon for the study of organically preserved fossils (Alleon et al., 2018; Gueriau et al., 2015; Muscente et al., 2017; Strullu-Derrien et al., 2019). XANES analysis has been used to support the identification of phaeomelanin in the 3 Ma fossil mouse *Apodemus* (Pliocene, Germany; Manning et al., 2019) and to show that the melanosome chemistry of the enigmatic fossil *Tullimonstrum* from the Mazon Creek biota (Upper Carboniferous, Illinois) is more consistent with that of extant cephalopods than vertebrates (Rogers et al., 2019).

Synchrotron facilities and their beamline stations vary in their layouts. In general, accelerated photons in a storage ring supply a radiation source to each experimental station. The following description is of beamline 14-3 at the Stanford Synchrotron Radiation Lightsource (SSRL; Fig. 2.3). The electron radiation source interacts with a monochromator that uses one or multiple silicon crystals to diffract and isolate a selected wavelength of an element. Through a process termed mirror pitch feedback (MPF), two blades (top and bottom) downstream of the monochromator focus the electrons as the beam oscillates. Soller slits further downstream can move horizontally or vertically to focus the beam into the first ion chamber, termed I0. Ion chambers are purged with gas and measure the intensity of the incident beam. The number of photons present in the beam is

termed the flux. The order of magnitude of the flux, termed the gain, is controlled in I0 to provide MPF to the blades. Following I0 is another set of slits and I1 to register any attenuation of the beam. A standard or filter can follow I1; I2 measures any signal from the standard or filter. An Rh-coated Kirkpatrick-Baez pair of mirrors then focuses the beam to a spot size of either 5 µm or 25 µm. Photons aim toward a sample holder at a 45° angle to the incident beam; the detector is at a 60° angle from the sample. Beamline 14-3 uses a multi-element silicon drift detector to detect fluorescent X-rays. The four-element silicon drift detector collects data in four single-channel analysers (SCAs) according to a quantum detector processor. Synchrotron analyses of the elemental chemistry in a sample rely on the principle that elements possess different energies at which an electron in their innermost shell, i.e., the K-shell, is excited by X-rays. In general, the X-ray energy required to excite a K-shell electron is greater for heavy elements relative to light elements. The SCAs produce a spectrum from the data by measuring the pulse amplitudes within user-defined windows that correspond to the excitation energies of an element.

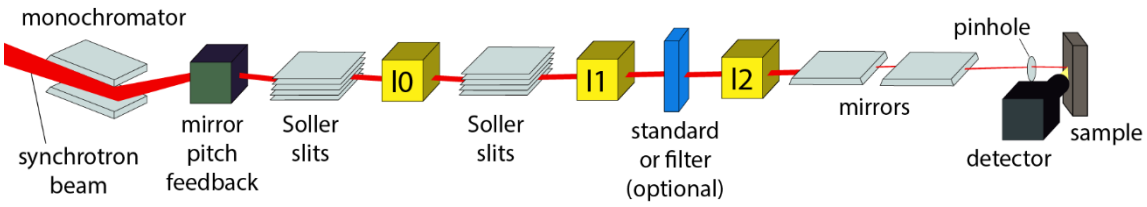


Fig. 2.3 Setup of experimental beamline station 14-3 at the Stanford Synchrotron Radiation Lightsource facility (Menlo Park, CA, USA).

Synchrotron-based XANES is a spectroscopic technique that provides information on the oxidation state, also termed species, of multivalent elements. All atoms of a particular element within a micron-sized sample region may not possess the same oxidation state. A XANES absorption spectrum represents an average of all the oxidation states in the sample region analysed and can offer detection limits of parts per million (Cutler et al., 2001). XANES data incorporate sub-surface information. The following characteristics influence the extent to which the beam penetrates: 1) beam energy, 2) beam angle, 3) the chemical heterogeneity in the sample, 4) sample thickness and 5) molecular density of the sample. The molecular density of the sample influences the penetration depth as elements in high concentrations absorb X-rays more quickly, resulting in a lower penetration depth. Penetration depth can be calculated easily for inorganic and homogeneous samples for

which the general molecular composition is known. The penetration depth for the organic and heterogeneous samples studied here is unknown but the signal may contain sub-surface information. The intensity of a peak within a XANES spectrum indicates the relative abundance of the oxidation state to which the peak corresponds. The presence of multiple oxidation states in the sample region analysed generates a spectrum with multiple peaks. In general, less energy is required to eject a K-shell electron from a reduced atom than a more oxidised atom; peaks for reduced species are therefore present in the spectrum at lower energies whereas peaks for more oxidised species are present at higher energies.

A XANES spectrum comprises three regions: 1) the pre-edge region where the incident energy of the beam is lower than the binding energy of the core electrons, 2) the main edge at which the energy is greater or equal to the binding energy of a core electron and 3) the near edge region (Fig. 2.4). The region beyond the XANES spectrum is termed the extended X-ray absorption fine structure (EXAFS) region. This thesis focuses on spectral features within XANES spectra as the pre-edge, main edge and near edge regions can be used to identify the atomic oxidation state(s) present for a particular atom.

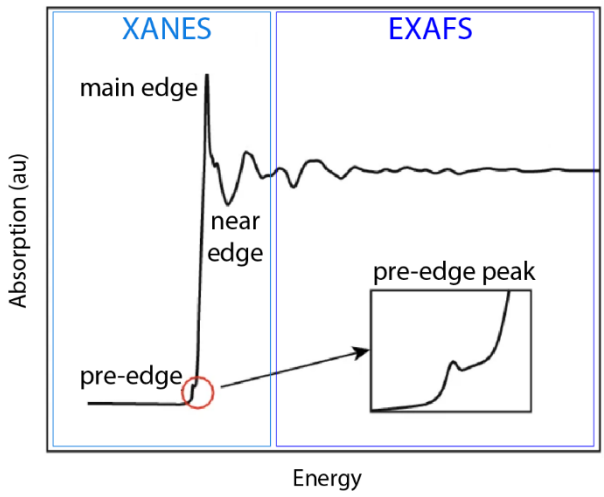


Fig. 2.4 X-ray absorption spectrum showing the primary features in a XANES spectrum and associated EXAFS region (modified from Wang et al. [2019]).

To generate a XANES spectrum the monochromator generates a beam of incident electrons that is user-defined and known to excite a K-shell electron in the atom of interest (Calvin, 2013). The excited K-shell electron is ejected, creating a core hole (i.e., an innermost electron shell missing an electron). An electron from another shell fills the core

hole and the silicon drift detector records the resulting fluorescent photon. Alternatively, an excited K-shell electron can transmit its energy to an electron in the outer shell of the atom. The silicon drift detector records the ejection of the outer electron, which is termed an Auger electron once ejected. To excite all species of an element the monochromator progressively increases the energy of the beam; the silicon drift detector simultaneously records all fluorescent photons and Auger electrons ejected.

Sulfur XANES (S-XANES) targets organic and inorganic sulfur oxidation states, ranging between -2 and +6. S-XANES has been used to characterise the sulfur chemistry in feathers from extant birds (Edwards et al., 2016): feathers contain a high content of S-containing cysteine amino acids (Wang et al., 2016; see Chapter 1.4) and can contain S-rich phaeomelanin. Sulfur in fossil feathers may derive from this original biological sulfur or from the incorporation of sulfides and/or polysulfides (derived from the environment) into organic molecules (Kok et al., 2000; van Dongen et al., 2003).

The sample size needed for XANES analysis is minimal (ca. 2 mm^2 or ca. 2 mg). Further, beamline 6-2 at the Stanford Synchrotron Radiation Lightsource (SSRL) can accommodate fossils that are up to 600 x 300 mm in size. Although S-XANES can analyse fossil soft tissue *in situ*, the ionising radiation generated during analysis can alter the biochemistry of samples; sulfur species in particular are prone to oxidation during analysis. Ionising radiation can also change the chemistry of a sample via the loss of electrons, which alters chemistry at the atomic level, and the loss of hydrogen or gain of oxygen, which alters molecular structure (Gueriau et al., 2016). Another limitation of S-XANES is that it cannot target feather CBPs exclusively and thus other S-bearing feather components, such as phaeomelanin, inevitably contribute to the S-XANES signal if present.

Samples of analytical standards, fossil feathers and untreated and experimentally degraded feathers from extant birds were analysed using S-XANES to test for the presence of reduced sulfur species. Samples on low-sulfur tape and fossil feathers were mounted on a stage in a He chamber for analysis. Data were collected with a spot size of 0.15 x 0.4 mm^2 and using different energy step sizes across the scan range (2450–2470 eV: 0.2 eV, 0.1 s; 2470–2480 eV: 0.1 eV, 0.2 s; 2480–2490 eV: 0.5 eV, 0.1 s; as in Edwards et al. [2016]) to prevent beam damage but also to ensure adequate resolution of the sulfur K-edge. Data

collected during separate beam runs were aligned using the calibration spectrum and normalisation was performed by defining the pre- and post-edges and with E_0 set to the energy of the first peak in the first derivative of μ(E).

2.8 Fourier-transform infrared spectroscopy (FTIR)

FTIR is commonly used to analyse the organic and inorganic chemistry of biological and geological samples, including cultural heritage materials such as paintings and fossils. Palaeontologists most often use mid-IR spectroscopy for the analysis of organic molecules, with many reports on the chemistry and taxonomy of fossil palynomorphs (Dutta et al., 2013; Fraser et al., 2014; Jardine et al., 2021). FTIR has also been used to support the presence of eumelanin in fossil frogs (McNamara et al., 2016b) and residues of collagen in a 195 Ma dinosaur and keratins in a 50 Ma reptile (Edwards et al., 2011).

The collection of FTIR data can use transmission, reflection and attenuated total reflectance (ATR). Transmission FTIR generates a spectrum via the conduction of IR through the sample to the detector whereas, in reflection, the detector registers the light reflected from the sample. ATR-FTIR was chosen to analyse all samples as it collects data in reflectance mode but requires no sample preparation and can analyse samples ≥2 mm^2 in size or that weigh ≥2 mg. A further benefit of analysing samples in reflectance mode is that it removes any potential absorption effects induced by the thickness of the sample. FTIR instruments that attach to a microscope possess the additional advantage of being non-destructive and can accommodate small to medium-sized fossils (up to ca. 300 x 400 mm^2). The quantification of chemical bonds in a sample, however, requires destructive grinding of a sample to a fine powder to mix the sample with a known quantity of a chemical "spike" in powder form. The choice of spike for quantifying chemical bonds in a sample should ensure no peak overlap with the peaks for the sample.

FTIR analysis can inform on the molecular composition of inorganic and organic samples. Molecules absorb IR light if the IR frequency is greater or equal to the energy required to produce a vibrational mode in a molecule. The primary vibration modes are stretching, bending, wagging, rocking and twisting of chemical bonds. Bonds in functional groups (i.e., groups such as carboxylic acids, amides and amines that impart specific properties to

compounds) absorb IR light at characteristic frequencies (Smith, 2011). IR spectroscopy records the absorbance of infrared light by a sample in an interferogram and the interferogram is then converted into a spectrum using a Fourier-transform (Smith, 2011). In general, lighter atoms absorb lR at higher frequencies (i.e., peaks occur at higher wavenumbers) than heavier atoms. The 4000–1200 cm^{-1} region in a mid-IR spectrum contains peaks corresponding to the primary functional groups in a sample whereas 1200–400 cm^{-1} is the fingerprint region, containing many peaks unique to a given compound (Fig. 2.5).

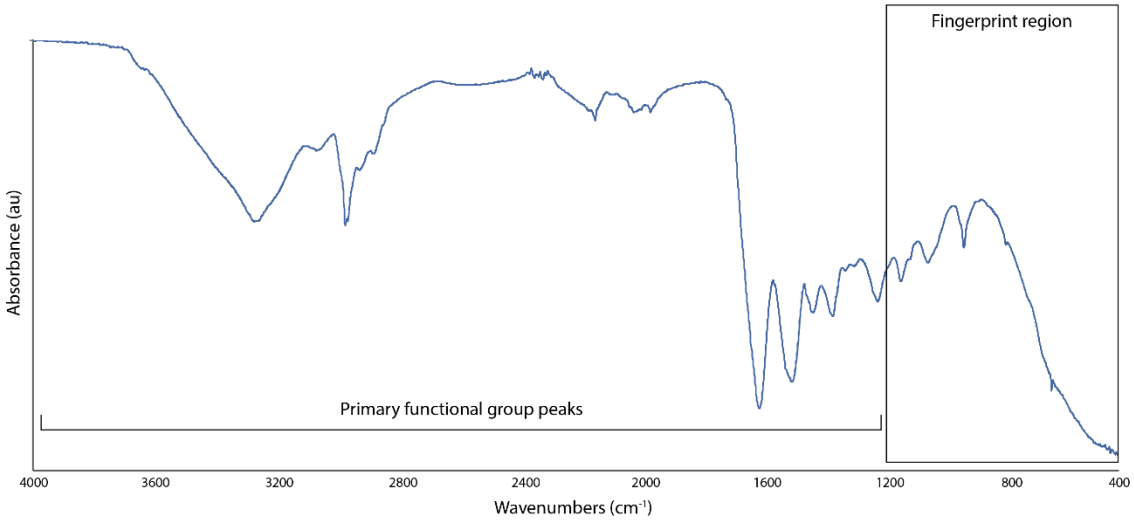


Fig. 2.5 *Unprocessed FTIR spectrum of a feather sample showing the two primary spectral regions.*

The intensity of an FTIR peak reflects the concentration (per unit volume) of the functional group that corresponds to the molecular bond(s). For example, a stronger peak reflects a higher concentration of the functional group assigned to the frequency of the peak. The frequency at which bonds in proteins vibrate during FTIR analysis reflects their secondary structure. For example, the frequency of the amide I and II peaks can vary depending on whether the protein is comprised predominantly of α-helices or β-sheets. Further, prominent peaks can be generated by the summation of several smaller peaks that can carry information on secondary structure. Smaller peaks and their size can be estimated by deconvoluting the spectral data across the range of interest. In this thesis, the secondary structures that correspond to deconvolution peak positions are characterised primarily for amide I and, to a lesser extent, amide II bands.

Fossil feathers and untreated and experimentally degraded feathers were analysed using FTIR to test for the presence of amides. Samples (4 mm^2) of untreated and experimentally degraded feathers were placed on a sterile diamond/KRS-5 crystal in a universal ATR accessory fitted to a PerkinElmer Frontier FTIR spectrometer. Pressure was applied to the sample using the pressure arm until the live reading of the spectrum was stable. Fossil material was fixed to the stage of a Spotlight 400 microscope fitted to a PerkinElmer Frontier FTIR spectrometer. The resulting spectra were used to investigate the protein secondary structures present in the samples.

2.9 Pyrolysis-gas chromatography-mass spectrometry (py-GC-MS)

Py-GC-MS involves the analysis of samples through a series of steps. First, the GC gradually heats the sample to 600–1000°C in an anaerobic environment. During thermal maturation, molecules within the sample decompose into smaller fragments. A gas chromatography column possesses an inert gas as the mobile phase and a bound liquid as the stationary phase to separate the smaller molecular fragments. Molecular fragments vary in the amount of time spent interacting with the stationary phase in the column, resulting in different retention times. A mass spectrometer detects the molecular fragments and produces a chromatogram with peaks on the x-axis based on the retention time of molecules. The mass spectrum of the chromatogram shows the mass to charge ratio corresponding to each peak, which aids in the characterisation of macromolecules and helps determine their molecular structure. If many degradation products are present, py-GC-MS can yield complex chromatograms that can be difficult to interpret. Further, the retention time of volatiles, which influences peak identification, can depend on various factors such as the temperature of pyrolysis and ramp rate of the temperature.

In this thesis, samples (30–50 mg or ca. 15–25 mm^2) of feathers degraded in sulfurization experiments were shipped to Manchester University (UK) for py-GC-MS analysis by Prof. B. van Dongen. Py-GC-MS was used to test for the presence of OSCs indicative of sulfurisation such as alkylated thiophenes (McNamara et al., 2016b; van Dongen et al., 2003).

3. Taphonomic experiments resolve controls on the preservation of melanosomes and keratinous tissues in feathers

This chapter comprises a paper that is published in the journal *Palaeontology* (Slater et al., 2019: https://onlinelibrary.wiley.com/doi/full/10.1111/pala.12445). This chapter is organised as follows: introduction, materials and methods, results, discussion, references and supplementary information.

The term 'keratin' is used in Chapter 3 to refer to proteinaceous feather tissue composed of β- and α-keratins. This study was published prior to the widespread adoption of the term feather CBPs for feather β-keratins and IF-keratins for α-keratins (Alibardi, 2016b; Holthaus et al., 2018).

Candidate contribution to the study. TSS contributed to the design of the study and performed all experiments and the following sample preparation and analyses: resin embedding, scanning electron microscopy and, with assistance, transmission electron microscopy. TSS co-wrote the paper with input from all other authors.

Abstract. Fossils are a key source of data on the evolution of feather structure and function through deep time, but their ability to resolve macroevolutionary questions is compromised by an incomplete understanding of their taphonomy. Critically, the relative preservation potential of two key feather components, melanosomes and keratinous tissue, is not fully resolved. Recent studies suggesting that melanosomes are preferentially preserved conflict with observations that melanosomes preserve in fossil feathers as external moulds in an organic matrix. To date, there is no model to explain the latter mode of melanosome preservation. We addressed these issues by degrading feathers in systematic taphonomic experiments incorporating decay, maturation and oxidation in isolation and combination. Our results reveal that the production of mouldic melanosomes requires interactions with an oxidant and is most likely to occur prior to strong maturation. This constrains the taphonomic conditions under which melanosomes are likely to be fossilized. Critically, our experiments also confirm that keratinous feather structures have a higher preservation potential than melanosomes under a range of diagenetic conditions,

supporting hitherto controversial hypotheses that fossil feathers can retain degraded keratinous structures.

3.1 Introduction

Fossil feathers play a pivotal role in our understanding of the evolutionary processes underlying the transition from non-avian dinosaurs to birds. Feathers comprise primarily melanosomes embedded in a keratinous matrix, both of which have been the subject of extensive research (Schweitzer *et al.* 1999*a*; Vinther *et al.* 2008; McNamara *et al.* 2013; Moyer *et al.* 2016; Pan *et al.* 2016, 2019) in both modern and palaeontological contexts in order to understand better the underlying drivers in the evolution of feathers and flight. Keratin is a fibrous protein rich in cysteine, which promotes extensive cross-linking (and thus confers chemical stability) via disulfide bonds (Wang *et al.* 2016). Keratinous tissues can be preserved in fossils by replacement in authigenic minerals (Benton *et al.* 2008; Briggs *et al.* 1997; Manning *et al.* 2009; McNamara *et al.* 2018*a*). Reports of organically preserved keratinous tissues (Schweitzer *et al.* 1999*a*; Moyer *et al.* 2016; Pan *et al.* 2016, 2019), however, are disputed (Saitta *et al.* 2017*a*, *b*). The other key component of many (but not all) feathers are melanosomes, micron-sized organelles rich in melanin pigments that occur in two primary forms: eumelanin, a heterogenous polymer derived from oxidation of the amino acid tyrosine (Solano 2014) and phaeomelanin, derived from tyrosine and sulfur-rich L-cysteine (Ito and Wakamatsu 2008). Melanosomes and chemical evidence for melanin have been reported from soft tissues associated with many exceptionally preserved fossils (Vinther *et al.* 2008; Wogelius *et al.* 2011; Barden *et al.* 2015; Lindgren *et al.* 2015). Such discoveries have stimulated attempts to reconstruct the original coloration of fossil birds, reptiles and avian and non-avian dinosaurs (Li *et al.* 2010; Zhang *et al.* 2010; Lindgren *et al.* 2014; McNamara *et al.* 2016*a*; Vinther *et al.* 2016; Lindgren *et al.* 2017; Hu *et al.* 2018) and have provided insights into palaeoecology (Brown *et al.* 2017; Smithwick *et al.* 2017) and the evolution of communication strategies (McNamara *et al.* 2016*a*; Lindgren *et al.* 2017).

Despite such extensive research, the taphonomy of melanin and melanosomes is incompletely understood. Chemical evidence for preservation of the melanin molecule has been reported from fossil fish eyes (Lindgren *et al.* 2012), reptile skin (Lindgren *et al.*

2014), frog internal tissues (McNamara et al. 2018*b*) and cephalopod ink sacs (Glass *et al.* 2012). This, plus the preservation of melanosomes, has been attributed to the inherent resistance of melanin to alteration (Glass *et al.* 2012) by enzymatic digestion (Ohtaki and Seiji 1971) and acid hydrolysis (Borovanský *et al.* 1977). Recent work, however, demonstrates that diagenetic processes can impact the chemistry of melanosomes, e.g., the incorporation of sulfur (sulfurization) can promote preservation (McNamara *et al.* 2016*b*); conversely, certain processes, especially oxidation, can degrade melanin (Korytowski and Sarna 1990).

Little is known about the physical taphonomy of melanosomes. Experiments have demonstrated that maturation of melanosomes results in diagenetic shrinkage (McNamara *et al.* 2013). Paradoxically, despite the inherent recalcitrance of melanosomes, many fossil feathers display extensive regions where melanosomes are preserved as external moulds; the melanosomes themselves are degraded (Li *et al.* 2010, figs 1c–g, 2a–b, e–f; Zhang *et al.* 2010, figs 1b–c, 2b–e, 3b, 4b–d; Lindgren *et al.* 2015, supplementary figs 2a–h, 3a–e). The physical and chemical conditions under which this occurs are unknown, and hypotheses relating to the nature of the diagenetic processes responsible (Vinther 2015, 2016) remain untested. The chemistry of the mould-bearing matrix is particularly controversial. Previous studies have speculated that mouldic melanosomes are embedded in the degraded remains of the originally keratinous matrix (Zhang *et al.* 2010), but this hypothesis is not universally accepted (Saitta *et al.* 2017*a*, *b*); rather, the matrix surrounding some fossil melanosomes has been interpreted as sediment infill following keratin decay (Saitta *et al.* 2017*b*). Moulds in fossil feathers have been interpreted as sites formerly occupied by decay bacteria (Moyer *et al.* 2014), but the taphonomic mechanism responsible is unknown.

Here, we address these issues by experimentally degrading feathers from extant birds in controlled laboratory experiments. We analyzed feather microstructure using SEM and TEM and feather chemistry using alkaline hydrogen peroxide oxidation (AHPO) followed by high-performance liquid chromatography (HPLC). Our results reveal the taphonomic pathways that favour preservation of melanosomes and keratinous feather components and the conditions under which melanosome degradation can produce moulds in a keratinous matrix.

3.2 Materials and methods

3.2.1 Justification for experimental design

Decay and maturation were integrated in our experiments as both processes impact preservation (Briggs 2003). For experiments using temperature only, samples were placed in Al foil packets; samples for experiments combining temperature and pressure were placed within Au capsules. It has been proposed that maturation of tissues in Al foil packets may result in the potential loss of labile and recalcitrant materials (Saitta *et al.* 2019). While loss of volatiles (gases and water) may occur in this scenario, previous experiments demonstrate that more recalcitrant materials – including melanosomes and the surrounding keratinous matrix – can survive maturation (McNamara *et al.* 2013). One criticism of maturation in sealed Au capsules is that these may prevent loss of labile materials (Saitta *et al.* 2019). In natural systems, however, confining sediment may prevent at least localized loss of labile materials from tissues.

The optimum experimental conditions are those that are geologically realistic and that generate the phenomena or processes being investigated. Our goal was to investigate the controls on melanosome degradation in feathers that retain recognizable branching structure after experimentation, as in the fossils of interest. We therefore used similar experimental conditions to those of McNamara *et al.* (2013), which are known to retain gross feather structure and melanosomes. Conditions using higher temperature and pressure (such as those used in Saitta *et al.* 2017*a, b*) do not preserve recognizable feather structure.

3.2.2 Simulated taphonomic pathways

Taphonomic experiments simulated a suite of pathways (1–16; Table 3.1) under oxic conditions using the following variables: decay, pH, oxidation, temperature and pressure (Fig. 3.1 and Supplementary Fig. 3.1). Untreated feathers were used as a control. Pathways 1–7 test individual variables. Pathways 8–11 test various combinations of decay (at pH 6), oxidation and maturation, where oxidation precedes maturation (where used). These

collectively comprise taphonomic sequence 1 (Table 3.1 and Supplementary Fig. 3.1). Taphonomic sequence 2 is based on maturation prior to, or simultaneous with, oxidation and incorporates pathways 12– 16 (Table 3.1 and Supplementary Fig. 3.1).

Table 3.1 *Experimental setup showing taphonomic sequences, experimental conditions used and natural scenarios corresponding to experimental pathways.*

	Pathway	Decay		Oxidation		Maturation		Natural analogue
		pH 6	pH 12.2	Occurrence	Timing	Without pressure	With pressure	
	Control							–
	1	X						Decay in slightly acidic sediments / pore waters
	2		X					Decay in highly alkaline fluids
	3					X		Thermal maturation
	4						X	High temperature-high pressure maturation
	5			X				Oxidation by pore fluids
	6	X				X		Decay followed by high temperature maturation
	7	X					X	Decay followed by high temperature-high pressure maturation
Sequence 1	8	X		X				Decay followed by oxidation by pore fluids
Sequence 1	9	X		X	Before maturation	X		Decay followed by oxidation by pore fluids and then by high temperature maturation
Sequence 1	10			X	Before maturation	X		Oxidation by pore fluids followed by high temperature maturation
Sequence 1	11			X	Before maturation		X	Oxidation by pore fluids followed by high temperature-high pressure maturation
Sequence 2	12	X		X	After maturation	X		Decay followed by high temperature maturation and then by oxidation by pore fluids upon exhumation
Sequence 2	13			X	After maturation	X		Thermal maturation followed by oxidation by pore fluids upon exhumation
Sequence 2	14	X		X	After maturation		X	Decay followed by high temperature-high pressure maturation and then by oxidation by pore fluids upon exhumation
Sequence 2	15			X	After maturation		X	High temperature-high pressure maturation followed by oxidation by pore fluids upon exhumation
Sequence 2	16			X	Simultaneous with maturation	X		Oxidation by pore fluids and thermal maturation occur simultaneously

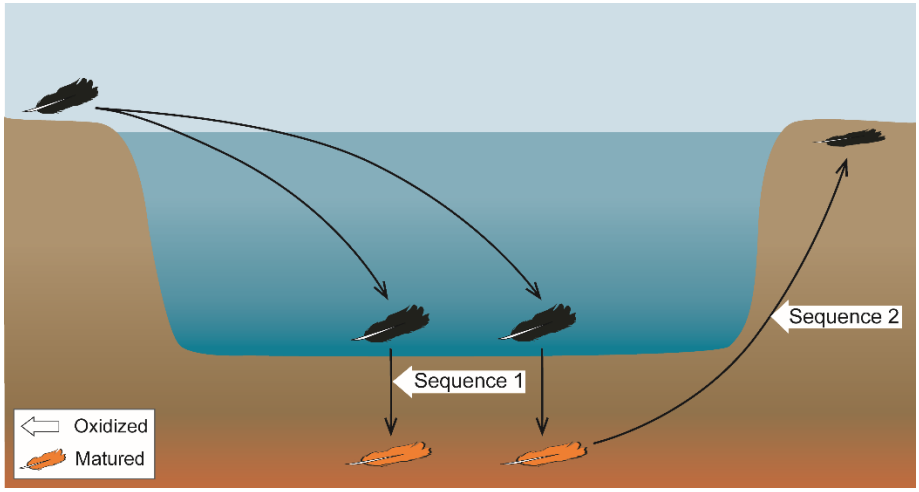


Fig. 3.1 *Experimental sequences. Schematic showing potential natural scenarios incorporating experimental pathways 8–16. Sequence 1 is based on oxidation prior to maturation (where used); Sequence 2 is based on oxidation following maturation. Experiments included some, or all, of decay, maturation and oxidation (with various parameters used for decay and maturation; for details see Table 3.1 and Supplementary Fig. 3.1).*

3.2.3 Material

Black contour feathers from the uropygial region of the zebra finch, *Taeniopygia gutatta* (n = 3) were stored at -80°C prior to treatment via pathways 1–16. Black primary feathers from *Gallus gallus* (common chicken, n = 3) were used for AHPO analysis due to the large sample size required (individual specimens of *T. guttata* yielded insufficient black regions from tail feathers); feather samples from this taxon were treated to pathways 5, 8, 12 and 13. For all experiments, three replicate feather samples (one from each of three specimens) of similar colour (as assessed visually) were used. Replicate *G. gallus* samples for individual pathways were combined for AHPO analyses.

3.2.4 Decay experiments

Feathers were placed in sterile glass vials containing 5 ml distilled deionized water with no added inoculum. Decay experiments in pathways 1, 6–9, 12 and 14 used a starting pH of 6.0. Decay experiments in pathway 2 used a starting pH of 12.2; pH was adjusted via the addition of K_2CO_3. Pathway 2 tested in isolation the impact of the elevated pH used in the oxidation experiment. Vials were sealed loosely with aluminium foil, covered by parafilm

and placed in a Memmert constant temperature incubator for one month at 30°C +/- 1°C. Decayed feathers were stored in 70% ethanol prior to analysis.

3.2.5 Maturation experiments

Feathers were experimentally matured using one of two approaches: (i) high temperature and (ii) high temperature combined with high pressure. (i) Feathers were placed in Al foil and matured in a standard laboratory convection oven at 200°C +/- 1°C for 1 h. (ii) Feathers were placed in Au tubes and matured in a customized StrataTech water-pressurized cold-seal autoclave at 200°C, 135 bar for 1 h.

3.2.6 Oxidation experiments

Degradation of melanosomes in a laboratory context is difficult. Lysosomal digestion (Ohtaki and Seiji 1971) removes melanosomal proteins but does not alter the melanin molecule; acid hydrolysis decarboxylates melanin (Ito *et al.* 2018) but does not alter melanosome geometry (Borovanský *et al.* 1977). The only treatment known to degrade melanosomes in a laboratory context is oxidation in a highly alkaline solution, which ruptures the melanosomal membrane and solubilizes melanin (Smith *et al.* 2017). Feather samples were oxidized using a modified version of the AHPO protocol described in Ito *et al.* (2011). Samples (0.5–1 mg) were placed in an Eppendorf tube to which 100 µl DD water, 375 µl 1 M K_2CO_3 and 25 µl 30% H_2O_2 were added to produce a final concentration of 1.5% H_2O_2 at a pH of 12.2. The tubes were agitated at 175 rpm for 20 h, and the experiment stopped by adding 50 µl 10% Na_2SO_3 and 140 µl of 6 M HCl. The tubes were centrifuged for 1 min at 5500 rpm and samples placed in an ultrasonic bath with DD water for 15–30 s to remove precipitates. Experiments for pathway 16 (synchronous oxidation and high temperature maturation) were carried out at 150°C until the solution fully evaporated (30 min) without addition of Na_2SO_3 and HCl as in other experiments using oxidation.

3.2.7 AHPO

AHPO is a chemical assay that allows identification and quantification of melanin via diagnostic chemical markers that are derived from the 5,6-dihydroxyindole (DHI) parent

subunits of the melanin molecule. The markers for eumelanin are pyrrole-2,3,5-tricarboxylic acid (PTCA), pyrrole-2,3-dicarboxylic acid (PDCA) and pyrrole-2,3,4,5-tetracarboxylic acid (PTeCA); PTCA is a marker for the 5,6-dihydroxyindole-2-carboxylic acid (DHICA) unit with a carboxyl group attached at the 2-position of DHI (Ito *et al.*, 2011) and PTeCA is a marker for thermally altered (cross-linked) DHI units and is thus used as a marker for eumelanin in fossils (Glass *et al.* 2012; McNamara *et al.* 2018*b*). Feather samples (4 mg) treated as per experimental pathways 5, 8, 12 and 13, and aliquots (100 µl) of the oxidizing solution were analyzed via HPLC as follows. Feather tissue (4 mg) from each pathway was homogenized in distilled water with a Ten-Broeck glass homogenizer at a concentration of 10 mg/ml. Aliquots (100 µl) of this and the oxidizing solution were then subjected to AHPO (Ito *et al.* 2011).

3.2.8 SEM

Small (2–3 mm^2) fragments of barbs were dissected using sterile tools, dehydrated and embedded in LR White resin using standard protocols (Pan *et al.* 2016). Resin blocks were cut using a Leica EM UC7 ultramicrotome with a 45° diamond knife and mounted on Al stubs with carbon tape. Blocks were then sputter coated with Au/Pd and analyzed using an FEI Inspect SEM at an accelerating voltage of 10 kV and working distance of 8 mm. Where melanosomes could not be readily observed (e.g. on the surface of the resin block), barbs were fractured and mounted on carbon conductive tape on Al stubs.

3.2.9 TEM

Ultrathin (80 nm) sections were placed on Cu grids. Sections were stained with 3% uranyl acetate (5 min) and 0.3% lead citrate (2 min) using standard protocols (Lewis and Knight 1977) and examined using a JEOL 2000FXII transmission electron microscope at 80 kV.

3.2.10 Statistical analysis

Quantitative data on the abundance of mouldic melanosomes was collected from transverse sections through barbules as follows. The number of moulds was calculated per unit area for untreated samples and for samples that were treated with oxidation

(pathways 8–15). Differences in the number of moulds between samples were assessed using an unpaired t-test.

3.3 Results

3.3.1 Generation of mouldic melanosomes

Three-dimensional micron-sized moulds are apparent in many of the experimentally treated feathers (Figs 3.2E, 3.3, 3.4C, 3.5C). Similar features reported previously in decay experiments were interpreted as moulds of decay bacteria by Moyer *et al.* (2014). The moulds generated in our experiments are not of decay bacteria as they (1) are visible in feathers that were not decayed, (2) occur only internally within the feather cortex, and (3) no bacteria were observed on decayed feather surfaces. Further, the geometry of the moulds produced in our experiments is consistent with that of melanosomes in transverse sections of feathers (Supplementary Table 3.1). The structures we observed are thus clearly mouldic melanosomes; this is supported by our chemical data, which confirm the presence of melanin markers in the experimental media (see below).

SEM images show that the feather barb cortex contains densely packed melanosomes. In all of our experiments moulds are less abundant per unit area than are the melanosomes, suggesting not all melanosomes were degraded. The relative abundance of moulds, however, varies among experimental treatments: these variations are discussed below.

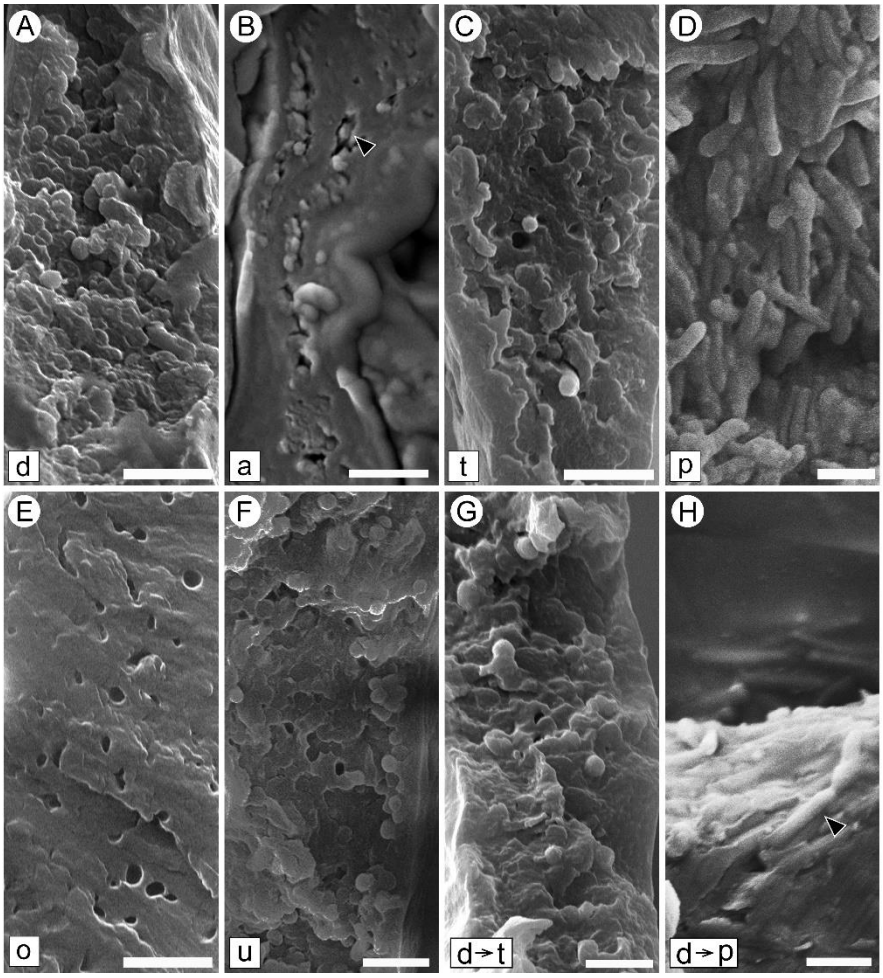


Fig. 3.2 SEM images of feather barbules. A, pathway 1. B, pathway 2. C, pathway 3. D, pathway 4. E, pathway 5. F, untreated. G, pathway 6. H, pathway 7. A, C, F–H, transverse fractured surfaces. B, D, E, transverse microtomed surfaces. a, decay at pH 12.2; d, decay at pH 6; o, oxidized; p, matured with pressure; t, matured without pressure; u, untreated. Black arrowheads, 3D melanosomes. All scale bars represent 1 µm.

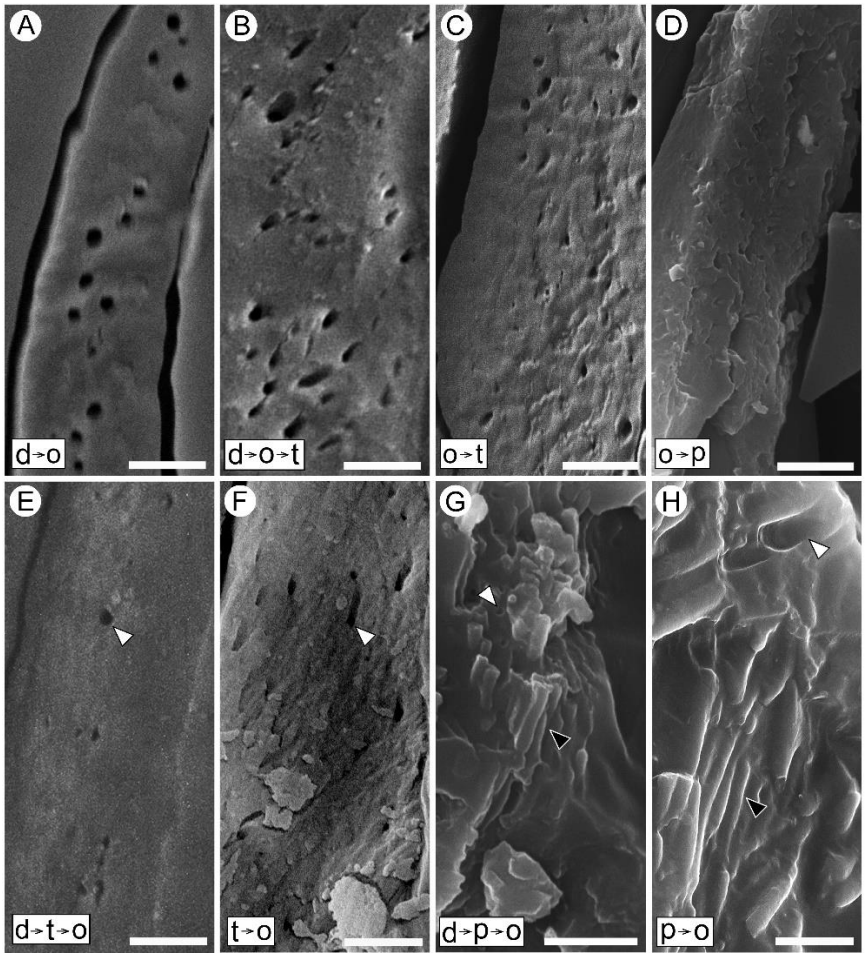


Fig. 3.3 SEM images of feather barbules. D, G, H, transverse fractured surfaces. A–C, E–F, transverse microtomed surfaces. A, pathway 8. B, pathway 9. C, pathway 10. D, pathway 11. E, pathway 12. F, pathway 13. G, pathway 14. H, pathway 15. d, decay at pH 6; o, oxidized; p, matured with pressure; t, matured without pressure. Black arrowheads, 3D melanosomes. White arrowheads, mouldic melanosomes. All scale bars represent 1 µm.

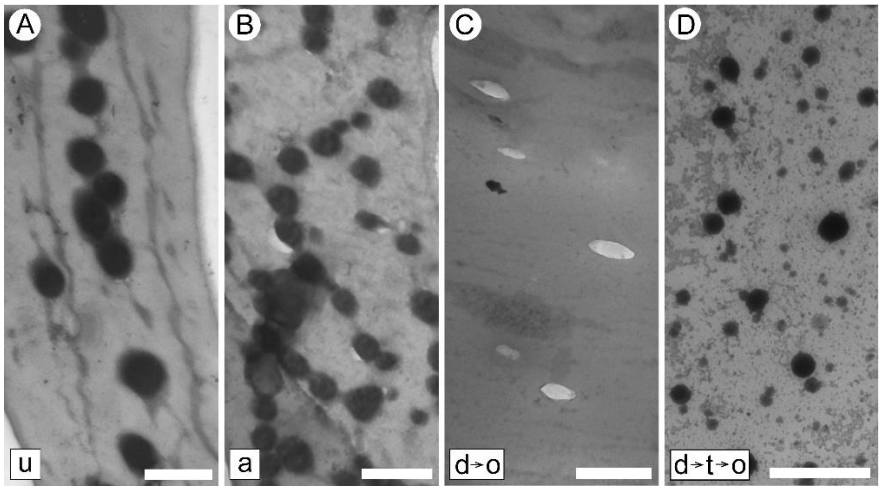


Fig. 3.4 TEM images of feather barbules. A, untreated. B, pathway 2. C, pathway 8. D, pathway 12. Melanosomes appear black; moulds appear as light-toned ovoids. a, decay in alkaline conditions (pH 12.2); d, decay at pH 6; o, oxidized; u, untreated. All scale bars represent 500 nm.

3.3.2 Pathways 1–7

Moulds are absent in all samples prepared from untreated feathers and pathways 1–4, 6 and 7 (Table 3.1, Figs 3.2A–D, F–H, 3.4A–B, 3.5A–B). The presence of moulds in feathers from pathway 5 is thus not an artefact of preparation (Fig. 3.2E). It is also consistent with the variation seen in the experimental data (see below). Some distortion of the shape of the moulds is difficult to prevent when sectioning such material for TEM (as opposed to imaging SEM samples; see Fig. 3.4C).

3.3.3 Taphonomic sequence 1

Abundant moulds were generated via pathways 8–11 (0.55 moulds / μm^2, 1.23 moulds / μm^2, 1.53 moulds / μm^2 and 1.03 moulds / μm^2, respectively; Figs 3.3A–D, 3.4C, 3.5C). In TEM images, feathers from pathway 8 exhibit moulds and few intact melanosomes (Fig. 3.4C; feathers from pathways 9–11 were not analyzed using TEM). Maturation did not destroy moulds generated during a previous oxidation step (pathways 9, 10 and 11; Fig. 3.3B–D).

3.3.4 Taphonomic sequence 2

Mouldic melanosomes are absent or rare in feathers degraded via pathways 12–15 (0.05 moulds / μm^2, 0.52 moulds / μm^2, 0.31 moulds / μm^2 and 0.01 moulds / μm^2, respectively; Figs 3.3E–H, 3.4D). Three-dimensional melanosomes, however, are abundant (Figs 3.3G–H, 3.4D). Feathers treated via pathway 16 were degraded to a translucent residue that lacked obvious barbs and barbules (Fig. 3.5D); melanosomes and moulds could not be identified.

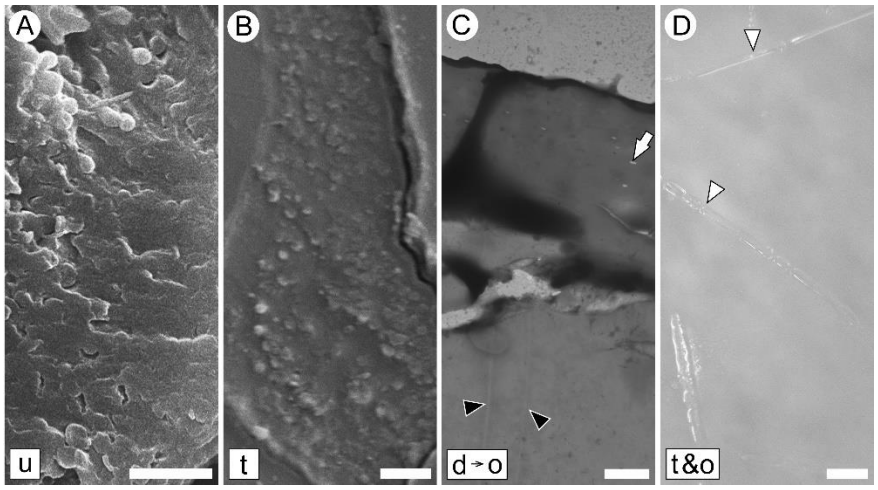


Fig. 3.5 Additional features of experimentally treated feathers. A–B, SEM images of transverse microtomed surfaces in untreated feathers (A) and feathers from pathway 3 (B). C, TEM image of feather barbule from pathway 8 (see Fig. 3.4C for additional examples of compressed voids at higher resolution). D, light micrograph of feather barbs following experimental treatment in pathway 16. Black arrowheads, blade marks showing direction of cutting during microtomy. White arrow, compressed moulds. White arrowheads, translucent barbs. d, decayed; o, oxidized; t, matured; u, untreated. All scale bars represent 1 µm except D (1 mm).

3.3.5 Abundance of mouldic melanosomes and melanin concentrations

Fewer moulds were produced in taphonomic sequence 2 (0.22 ± 0.24 moulds/μm^2) than sequence 1 (1.09 ± 0.41 moulds/μm^2; these differences are statistically significant (t-test result: $t(6) = 3.62$, $p = 0.01$). We analyzed feather samples and experimental media from pathways 5, 8, 12 and 13 using AHPO. All feathers analyzed contain lower concentrations of the eumelanin markers PTCA (244.4 ± 91.8 ng/mg) and PTeCA (106.4 ± 27.6 ng/mg) than the corresponding experimental media (1313.2 ± 420 ng/mg and 349.9 ± 169 ng/mg,

respectively; Fig. 3.6); these differences are statistically significant ($t(14) = 3.08$, $p = 0.008$). Higher quantities of eumelanin markers are present in the experimental media from treatments lacking maturation (pathways 5 and 8) relative to treatments including a maturation step (pathways 12 and 13). Feathers treated to decay and oxidation only (pathway 8), and their experimental media, contain higher concentrations of eumelanin markers than in any other experimental treatment; further, media from these and other decayed samples (i.e., pathway 12) show higher PTeCA/PTCA ratios than non-decayed feathers (pathways 5 and 13; Supplementary Table 3.3). The significant differences in the abundance of both melanin and melanosomes between feathers treated via sequences 1 and 2 strongly suggest that our data reflect real experimentally-induced differences and not original variations in melanin content (McGraw *et al.* 2005) among the individual feathers analyzed.

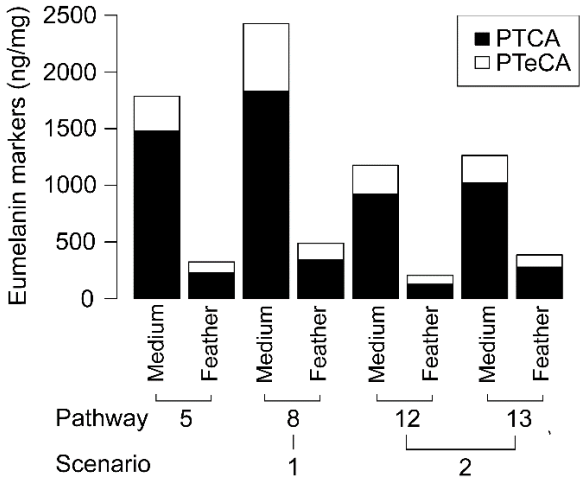


Fig. 3.6 AHPO analysis of Gallus gallus feathers and their experimental media. PTCA and PTeCA are eumelanin markers (PTeCA is a marker for diagenetically altered melanin).

3.4 Discussion

Sample preparation was consistent for each treatment and so relative differences in the abundance of moulds among samples are almost certainly real and not artefacts. Compressed moulds in ultrathin sections from pathway 8 (Fig. 3.4C) are an artefact of microtomy and may reflect enhanced susceptibility of the feather to mechanical damage during sectioning due to experimental treatment (Fig. 3.5C).

3.4.1 Controls on melanosome preservation

The restriction of moulds to oxidized feathers (Figs 3.2–3.4) strongly suggests that interaction with an oxidant is prerequisite to the formation of mouldic melanosomes in fossils. Decay does not result in the production of mouldic melanosomes, even under alkaline conditions (which are known to enhance melanin solubility; Figs 3.2, 3.4; Wakamatsu *et al.* 2012). The lower concentrations of eumelanin markers in feathers relative to experimental media (Fig. 3.6) demonstrate that all treatments analyzed using AHPO resulted in loss of melanin from feathers. Nevertheless, the presence of melanin markers in all experimentally treated feathers analyzed provides robust experimental evidence that fossil feathers with diverse taphonomic histories have the potential to retain melanin and/or its diagnostic alteration products. This supports the hypothesis that the melanin identified in fossil feathers derives from melanosomes and not decay bacteria (contra Moyer *et al.* 2014).

The preservation of abundant moulds following maturation (including maturation at high pressure) in pathways 9–11 confirms that moulds that form early during the diagenetic process can survive subsequent thermal alteration and elevated pressures. Preservation of mouldic melanosomes does not, therefore, imply little or no maturation during burial.

Published images of fossil feathers typically show broad regions where adjacent melanosomes are preserved predominantly either as moulds or as intact microbodies (Li *et al.* 2010, figs 1c–g, 2a–b, e–f; Zhang *et al.* 2010, figs 1b–c, 2b–e, 3b, 4b–d; Lindgren *et al.* 2015, supplementary figs 2a–h, 3a–e). This contrasts with our results from pathways 12–15, which show that oxidation after maturation with pressure results in a heterogeneous distribution (at a micron-scale) of intact and mouldic melanosomes and overall fewer moulds than where oxidation precedes maturation. Instead, patterns in melanosome preservation in fossils are more consistent with our results from sequence 1 and strongly suggest the presence of a taphonomic switch from a system favouring preservation of melanosomes as 3D bodies to one favouring preservation as moulds that is controlled by the timing of oxidant availability relative to maturation.

To date, mouldic melanosomes have been reported from Konservat-Lagerstätten that are hosted in sediments interpreted to have been deposited within oxic (Zhou *et al.* 2016) or dysoxic/anoxic bottom waters (Pedersen 1981). Various chemical species, however, can act as oxidants. Manganese-based oxidants are strongest in alkaline (Messaoudi *et al.* 2001; Dash *et al.* 2009) and oxic (Antoniou *et al.* 2014) environments and also at oxic-anoxic interfaces (Jones *et al.* 2018). Nitrates are strong oxidants under both acidic and alkaline conditions (Quin *et al.* 2015), while halogens, e.g., chlorine and fluorine, can maintain a high oxidation potential under various pH conditions when present in high quantities (Steininger and Pareja 1996). Copper is an oxidant under acidic and alkaline conditions (Celante and Freitas 2010) and is known to accelerate the oxidation of melanin via Fenton-like reactions (Korytowski and Sarna 1990).

The AHPO results provide further insights into the preservation of melanosomal melanin. The higher quantity of PTeCA in the experimental medium from pathway 8 relative to that from pathway 5 suggests that decay enhances melanosome degradation. In addition, the higher PTeCA:PTCA values for pathway 12 relative to pathway 13 indicate that melanosome oxidation may be enhanced when feathers have undergone some decay. Despite this, the lower concentrations of eumelanin markers in treatments including both decay and maturation relative to treatments involving decay but not maturation suggest that maturation is a more important control on melanin preservation than decay (Glass *et al.* 2013). The preservational mechanism for the remnant melanosomes presumably reflects, at least in part, *in situ* polymerization processes, which are responsible for the organic preservation of various fossil tissues (McNamara *et al.* 2016*b*). Collectively, our experimental results suggest that feathers exposed to (an) oxidizing agent(s) prior to strong maturation will likely possess more mouldic melanosomes than feathers that experienced maturation prior to oxidation (Fig. 3.7). This does not exclude the possibility that some moulds may form following maturation; further, if feathers experience decay following exposure to strong oxidising agents, it is possible that moulds may be occluded by collapse of the feather. Our experiments show that the primary controls on melanosome and melanin preservation are (in decreasing order of importance): exposure to an oxidant, the extent of maturation, and decay.

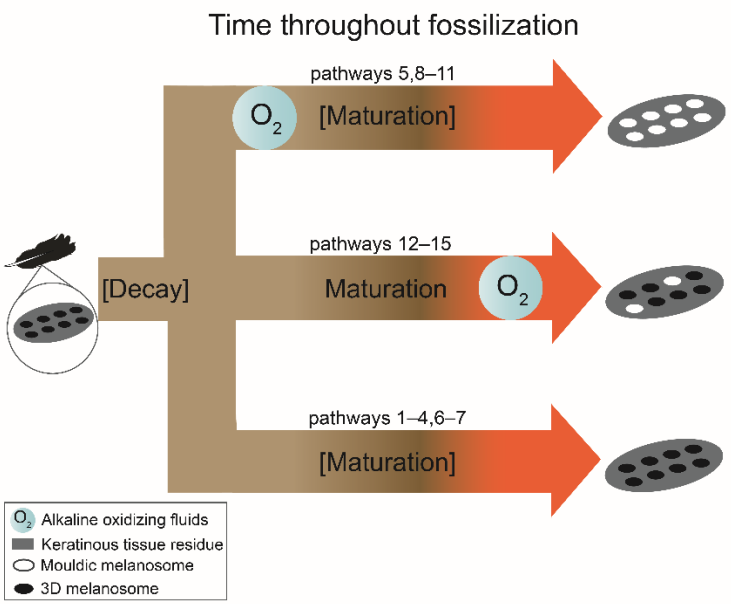


Fig. 3.7 The impact of various taphonomic conditions on melanosome preservation. Grey ovoid denotes transverse section of feather barbule. Arrows indicate time. Brackets indicate that a particular taphonomic process is not always present.

3.4.2 Keratin preservation

The survival of feather residues in the fossil record (Zhang *et al.* 2010; Pan *et al.* 2016, 2019) is controversial (Saitta *et al.* 2017*a*, *b*). Chemical evidence of keratin has been reported from various Mesozoic and Cenozoic fossils (Edwards *et al.* 2011; Schweitzer *et al.* 1999*a*, *b*; Pan *et al.* 2016, 2019) and organic matrices surrounding fossil feather melanosomes have been interpreted as degraded residues of originally keratinous feather tissue (Gren *et al.* 2017; Li *et al.* 2010; Zhang *et al.* 2010) or diagenetic replacements thereof (Lindgren *et al.* 2015). These findings have been disputed on the basis of recent taphonomic experiments on feathers (Saitta *et al.* 2017*a*, *b*, 2019). Maturation experiments on black feathers in Au cells for 24 h at 100°C, 250 bar resulted in the transformation of the tissue to a black pellet (Saitta *et al.* 2017*b*); at 250°C, 250 bar, feather structure transformed to a fluid (Saitta *et al.* 2017*a*). Further, Saitta *et al.* (2019) report loss of keratinous tissues in feather barbs experimentally matured in sediment. The pellets and barb imprints were not tested for chemical evidence of keratin or its residues (Saitta *et al.* 2017*b,* 2019). Pyrolysis-GC-MS analyses of the fluid failed to provide unequivocal evidence for keratin (Saitta *et al.* 2017*a*); this, however, is not unexpected as (1) keratin and melanin produce similar pyrolysates and (2) it is unlikely that keratinous

components would survive the elevated temperatures used in such analyses. The microstructure of fossil feathers has also been the basis of hypotheses relating to the preservation of keratinous residues. Exposure of melanosomes in fossils has been interpreted as evidence that keratin components should rarely be preserved (Saitta *et al.* 2017*a*). While examples of fossil feathers preserving only melanosomes certainly exist (e.g. fig. 5c in Hu *et al.* (2018), our experiments confirm that three-dimensional melanosomes and keratinous components of feathers can both persist under various taphonomic conditions. Critically, our experiments also identify a suite of taphonomic conditions where keratinous components of feathers can survive, yet melanosomes do not. These results support previous interpretations that organic matrices surrounding fossil melanosomes represent degraded residues of originally keratinous feather tissue (Li *et al.* 2010; Zhang *et al.* 2010; McNamara *et al.* 2013; Pan *et al.* 2016).

Our findings suggest that organic residues preserved in some fossil feathers are ideal targets for chemical and immunohistochemical analyses for remnants of keratin. Such residues have been reported in Cretaceous fossils with primitive feather types (Li *et al.* 2010; Zhang *et al.* 2010; Lindgren *et al.* 2015); analysis of these, and older, fossils has the potential to yield important insights into feather chemistry at key stages of feather evolution. Our investigation into the differential preservation of feather components provides a robust framework for future experiments as it allows the impact of different taphonomic factors (and their relative timing) on feather preservation to be assessed. Combination of this rigorous experimental approach with chemical analyses will provide critical empirical data to test fossil-based models for the survival of keratin and melanin in the fossil record.

Acknowledgements. The research was funded by European Research Council Starting Grant 2014-ERC-StG-637691-ANICOLEVO awarded to MEM. We thank Giliane Odin, Suzanne Crotty, Vince Lodge and Joe Tobin for assistance with SEM and TEM and Jack Connell and Liam Hayes for supplying feathers. Johan Lindgren and an anonymous referee are thanked for useful comments.

Author contributions. TSS performed all analyses with assistance from MEM and TBF; TSS, MEM and PJO co-wrote the paper with input from all other authors; MEM and PJO

conceived the study; MEM and TSS designed the research; SI and KW performed AHPO analyses.

3.5 References

ANTONIOU, A., BREUKELEN, B. M. VAN and STUYFZAND, P. J. 2014. Aquifer pre-oxidation using permanganate to mitigate water quality deterioration during aquifer storage and recovery. *Applied Geochemistry,* **50**, 25–36.

BARDEN, H. E., BERGMANN, U., EDWARDS, N. P., EGERTON, V. M., MANNING, P. L., PERRY, S., VEELEN, A. VAN, WOGELIUS, R. A. and DONGEN, B. E. VAN 2015. Bacteria or melanosomes? A geochemical analysis of micro-bodies on a tadpole from the Oligocene Enspel Formation of Germany. *Palaeobiodiversity and Palaeoenvironments*, **95**, 33–45.

BENTON, M. J., ZHOU, Z., ORR, P. J., ZHANG, F. and KEARNS, S. L. 2008. The remarkable fossils from the Early Cretaceous Jehol Biota of China and how they have changed our knowledge of Mesozoic life: Presidential Address, delivered 2nd May 2008. *Proceedings of the Geologists' Association*, **119**, 209-228.

BOROVANSKÝ, J., HACH, P. and DUCHOŇ, J. 1977. Melanosome: an unusually resistant subcellular particle. *Cell biology international reports*, **1**, 549–554.

BRIGGS, D. E. G. 2003. The role of decay and mineralization in the preservation of soft-bodied fossils. *Annual Review of Earth and Planetary Sciences*, **31**, 275–301.

BRIGGS, D. E. G., WILBY, P. R., PÉREZ-MORENO, B. P., SANZ, J. L. and FREGENAL-MARTÍNEZ, M. 1997. The mineralization of dinosaur soft tissue in the Lower Cretaceous of Las Hoyas, Spain. *Journal of the Geological Society*, **154**, 587–588.

BROWN, C. M., HENDERSON, D. M., VINTHER, J., FLETCHER, I., SISTIAGA, A., HERRERA, J. and SUMMONS, R. E. 2017. An exceptionally preserved three-dimensional armored dinosaur reveals insights into coloration and Cretaceous predator-prey dynamics. *Current Biology*, **27**, 2514–2521.e3.

CELANTE, V. G. and FREITAS, J. G. 2010. Electrodeposition of copper from spent Li-ion batteries by electrochemical quartz crystal microbalance and impedance spectroscopy techniques. *Journal of Applied Electrochemistry,* **40**, 233–239.

DASH, S., PATEL, S. and MISHRA, B. K. 2009. Oxidation by permanganate: synthetic and mechanistic aspects. *Tetrahedron,* **65**, 707–739.

EDWARDS, N. P., BARDEN, H. E., DONGEN, B. E. VAN, MANNING, P. L., LARSON, P. L., BERGMANN, U., SELLERS, W. I. and WOGELIUS, R. A. 2011. Infrared mapping resolves soft tissue preservation in 50 million year-old reptile skin. *Proceedings of the Royal Society B: Biological Sciences*, **278**, 3209–3218.

GLASS, K., ITO, S., WILBY, P. R., SOTA, T., NAKAMURA, A., BOWERS, C. R., VINTHER, J., DUTTA, S., SUMMONS, R., BRIGGS, D. E., WAKAMATSU, K. and SIMON, J. D. 2012. Direct chemical evidence for eumelanin pigment from the Jurassic period. *Proceedings of the National Academy of Sciences USA*, **109**, 10218–10223.

GLASS, K., ITO, S., WILBY, P. R., SOTA, T., NAKAMURA, A., BOWERS, C. R., MILLER, K. E., DUTTA, S., SUMMONS, R. E., BRIGGS, D. E. G., WAKAMATSU, K. and SIMON, J. D. 2013. Impact of diagenesis and maturation on the survival of eumelanin in the fossil record. *Organic Geochemistry,* **64**, 29–37.

GREN, J. A., SJÖVALL, P., ERIKSSON, M. E., SYLVESTERSEN, R. L., MARONE, F., SIGFRIDSSON CLAUSS, K. G. V., TAYLOR, G. J., CARLSON, S., UVDAL, P. and LINDGREN, J. 2017. Molecular and microstructural inventory of an isolated fossil bird feather from the Eocene Fur Formation of Denmark. *Palaeontology*, **60**, 73–90.

HU, D., CLARKE, J. A., ELIASON, C. M., QIU, R., LI, Q., SHAWKEY, M. D., ZHAO, C., D'ALBA, L., JIANG, J. and XU, X. 2018. A bony-crested Jurassic dinosaur with evidence of iridescent plumage highlights complexity in early paravian evolution. *Nature Communications*, **9**, 1–12.

ITO, S. and WAKAMATSU, K. 2008. Chemistry of mixed melanogenesis—pivotal roles of dopaquinone. *Photochemistry and Photobiology*, **84**, 582–592.

ITO, S., NAKANISHI, Y., VALENZUELA, R. K., BRILLIANT, M. H., KOLBE, L. and WAKAMATSU, K. 2011. Usefulness of alkaline hydrogen peroxide oxidation to analyze eumelanin and pheomelanin in various tissue samples: application to chemical analysis of human hair melanins. *Pigment Cell & Melanoma Research*, **24**, 605–613.

ITO, S., MIYAKE, S., MARUYAMA, S., SUZUKI, I., COMMO, S., NAKANISHI, Y., WAKAMATSU, K. 2018. Acid hydrolysis reveals a low but constant level of pheomelanin in human black to brown hair. *Pigment Cell & Melanoma Research*, **31**, 393–403.

JONES, M., NICO, P., YING, S., REGIER, T., THIEME, J. and KEILUWEIT, M. 2018. Manganese-driven carbon oxidation at oxic-anoxic interfaces. *Environmental Science & Technology,* **52**, 12349–12357.

KORYTOWSKI, W. and SARNA, T. 1990. Bleaching of melanin pigments. Role of copper ions and hydrogen peroxide in autooxidation and photooxidation of synthetic dopa-melanin. *Journal of Biological Chemistry*, **265**, 12410–12416.

LEWIS, P. and KNIGHT, D. 1977. Staining methods for sectioned material. *In* GLAUERT A. M. (ed.). *Practical Methods in Electron Microscopy Series. Volume 5.* North-Holland Publishing Company, Amsterdam, 547 pp.

LI, Q., GAO, K. Q., VINTHER, J., SHAWKEY, M. D., CLARKE, J. A., D'ALBA, L., MENG, Q., BRIGGS, D. E. G. and PRUM, R. O. 2010. Plumage color patterns of an extinct dinosaur. *Science*, **327**, 1369–1372.

LINDGREN, J., UVDAL, P., SJÖVALL, P., NILSSON, D. E., ENGDAHL, A., SCHULTZ, B. P. and THIEL, V. 2012. Molecular preservation of the pigment melanin in fossil melanosomes. *Nature Communications*, **3**, 1–7.

LINDGREN, J., SJÖVALL, P., CARNEY, R. M., UVDAL, P., GREN, J. A., DYKE, G., SCHULTZ, B. P., SHAWKEY, M. D., BARNES, K. R. and POLCYN, M. J. 2014. Skin pigmentation provides evidence of convergent melanism in extinct marine reptiles. *Nature*, **506**, 484–488.

LINDGREN, J., SJÖVALL, P., CARNEY, R. M., CINCOTTA, A., UVDAL, P., HUTCHESON, S. W., GUSTAFSSON, O., LEFÈVRE, U., ESCUILLIÉ, F., HEIMDAL, J., ENGDAHL, A., GREN, J. A., KEAR, B. P., WAKAMATSU, K., YANS, J., and GODEFROIT, P. 2015. Molecular composition and ultrastructure of Jurassic paravian feathers. *Scientific Reports*, **5**, 1–13.

LINDGREN, J., KURIYAMA, T., MADSEN, H., SJÖVALL, P., ZHENG, W., UVDAL, P., ENGDAHL, A., MOYER, A. E., GREN, J. A., KAMEZAKI, N., UENO, S. and SCHWEITZER, M. H. 2017. Biochemistry and adaptive colouration of an exceptionally preserved juvenile fossil sea turtle. *Scientific Reports*, **7**, 13324.

MANNING, P. L., MORRIS, P. M., McMAHON, A., JONES, E., GIZE, A., MACQUAKER, J. H. S., WOLFF, G., THOMPSON, A., MARSHALL, J. and TAYLOR, K. G. 2009. Mineralized soft-tissue structure and chemistry in a mummified hadrosaur from the Hell Creek Formation, North Dakota (USA). *Proceedings of the Royal Society B: Biological Sciences*, **276**, 3429–3437.

McGRAW, K. J., SAFRAN, R. J. and WAKAMATSU, K. 2005. How feather colour reflects its melanin content. *Functional Ecology*, **19**, 816–821.

McNAMARA, M. E., BRIGGS, D. E. G., ORR, P. J., FIELD, D. J. and WANG, Z. 2013. Experimental maturation of feathers: implications for reconstructions of fossil feather colour. *Biology Letters*, **9**, 1–6.

McNAMARA, M. E., DONGEN, B. E. VAN, LOCKYER, N. P., BULL, I. D. and ORR, P. J. 2016b. Fossilization of melanosomes via sulfurization. *Palaeontology*, **59**, 337–350.

McNAMARA, M. E., ORR, P. J., KEARNS, S. L., ALCALÁ, L., ANADÓN, P. and PEÑALVER, E. 2016a. Reconstructing carotenoid-based and structural coloration in fossil skin. *Current Biology*, **26**, 1075–1082.

McNAMARA, M. E., KAYE, J. S., BENTON, M. J., ORR, P. J., ROSSI, V., ITO, S. and WAKAMATSU, K. 2018b. Non-integumentary melanosomes can bias reconstructions of the colours of fossil vertebrates. *Nature Communications* **9**, 1–9.

McNAMARA, M. E., ZHANG, F., KEARNS, S. L., ORR, P. J., TOULOUSE, A., FOLEY, T., HONE, D. W. E., ROGERS, C. S., BENTON, M. J., JOHNSON, D. and XU, X. 2018a. Fossilized skin reveals coevolution with feathers and metabolism in feathered dinosaurs and early birds. *Nature Communications*, **9**, 1–7.

MESSAOUDI, B., JOIRET, S., KEDDAM, M. and TAKENOUTI, H. 2001. Anodic behaviour of manganese in alkaline medium. *Electrochemical Acta,* **46**, 2487–2498.

MOYER, A. E., ZHENG, W. and SCHWEITZER, M. 2016. Keratin durability has implications for the fossil record: results from a 10 year feather degradation experiment. *PlosOne,* **11**, e0157699.

MOYER, A. E., ZHENG, W., JOHNSON, E. A., LAMANNA, M. C., LI, D.-Q., LACOVARA, K. J. and SCHWEITZER, M. H. 2014. Melanosomes or microbes: testing an alternative hypothesis for the origin of microbodies in fossil feathers. *Scientific Reports*, **4**, 1–9.

OHTAKI, N. and SEIJI, M. 1971. Degradation of melanosomes by lysosomes. *Journal of Investigative Dermatology*, **57**, 1–5.

PAN, Y., ZHENG, W., MOYER, A. E., O'CONNOR, J. K., WANG, M., ZHENG, X., WANG, X., SCHROETER, E. R., ZHOU, Z. and SCHWEITZER, M. H. 2016. Molecular evidence of keratin and melanosomes in feathers of the Early Cretaceous bird *Eoconfuciusornis*. *Proceedings of the National Academy of Sciences USA*, **113**, E7900–E7907.

PAN, Y., ZHENG, W., SAWYER, R. H., PENNINGTON, M. W., ZHENG, X., WANG, X., WANG, M., HU, L., O'CONNOR, J., ZHAO, T., LI, Z., SCHROETER, E. R., WU, F., XU, X., ZHOU, Z. and SCHWEITZER, M. 2019. The molecular evolution of feathers with direct

evidence from fossils. *Proceedings of the National Academy of Sciences USA,* **116**, 3018–3023.

PEDERSEN, G. K. 1981. Anoxic events during sedimentation of a Palaeogene diatomite in Denmark. *Sedimentology,* **28**, 487–504.

QUIN, P., JOSEPH, S., HUSSON, O., DONNE, S., MITCHELL, D., MUNROE, P., PHELAN, D., COWIE, A. and ZWIETEN, L. VAN. 2015. Lowering N2O emissions from soils using eucalypt biochar: the importance of redox reactions. *Scientific Reports,* **5**, 1–14.

SAITTA, E. T., KAYE, T. G. and VINTHER, J. 2019. Sediment-encased maturation: a novel method for simulating diagenesis in organic fossil preservation. *Palaeontology,* **62**, 135–150.

SAITTA, E. T., ROGERS, C. S., BROOKER, R. A. and VINTHER, J. 2017b. Experimental taphonomy of keratin: a structural analysis of early taphonomic changes. *Palaios*, **32**, 647–657.

SAITTA, E. T., ROGERS, C. S., BROOKER, R. A., ABBOTT, G. D., KUMAR, S., O'REILLY, S. S., DONOHOE, P., DUTTA, S., SUMMONS, R. E. and VINTHER, J. 2017a. Low fossilization potential of keratin protein revealed by experimental taphonomy. *Palaeontology*, **60**, 547–556.

SCHWEITZER, M. H., WATT, J. A., AVCI, R., KNAPP, L., CHIAPPE, L., NORELL, M. and MARSHALL, M. 1999a. Beta-keratin specific immunological reactivity in feather-like structures of the Cretaceous alvarezsaurid, *Shuvuuia deserti*. *Journal of Experimental Zoology*, **285**, 146–157.

SCHWEITZER, M. H., WATT, J. A., AVCI, R., FORSTER, C. A., KRAUSE, D. W., KNAPP, L., ROGERS, R. R., BEECH, I. and MARSHALL, M. 1999b. Keratin immunoreactivity in the Late Cretaceous bird *Rahonavis ostromi*. *Journal of Vertebrate Paleontology*, **19**, 712–722.

SMITH, R. A. W., GARRETT, B., NAQVI, K. R., FÜLÖP, A., GODFREY, S. P., MARSH, J. M. and CHECHIK, V. 2017. Mechanistic insights into the bleaching of melanin by alkaline hydrogen peroxide. *Free Radical Biology and Medicine*, **108**, 110–117.

SMITHWICK, F. M., NICHOLLS, R., CUTHILL, I. C. and VINTHER, J. 2017. Countershading and stripes in the theropod dinosaur *Sinosauropteryx* reveal heterogeneous habitats in the Early Cretaceous Jehol Biota. *Current Biology*, **27**, 1–7.

SOLANO, F. 2014. Melanins: skin pigments and much more—types, structural models, biological functions, and formation routes. *New Journal of Science*, **2014**, 1–28.

STEININGER, J. M. and PAREJA, C. 1996. ORP sensor response in chlorinated water. *NSPI Water Chemistry Symposium, Phoenix*.

VINTHER, J. 2015. A guide to the field of palaeo colour: melanin and other pigments can fossilise: reconstructing colour patterns from ancient organisms can give new insights to ecology and behaviour. *BioEssays*, **37**, 643–656.

VINTHER, J. 2016. Fossil melanosomes or bacteria? A wealth of findings favours melanosomes. *BioEssays*, **38**, 220–225.

VINTHER, J., BRIGGS, D. E., PRUM, R. O. and SARANATHAN, V. 2008. The colour of fossil feathers. *Biology Letters*, **4**, 522–525.

VINTHER, J., NICHOLLS, R., LAUTENSCHLAGER, S., PITTMAN, M., KAYE, T. G., RAYFIELD, E., MAYR, G. and CUTHILL, I. C. 2016. 3D camouflage in an ornithischian dinosaur. *Current Biology*, **26**, 2456–2462.

WAKAMATSU, K., NAKANISHI, Y., MIYAZAKI, N., KOLBE, L. and ITO, S. 2012. UVA-induced oxidative degradation of melanins: fission of indole moiety in eumelanin and conversion to benzothiazole moiety in pheomelanin. *Pigment Cell & Melanoma Research*, **25**, 434–445.

WANG, B., YANG, W., MCKITTRICK, J. and MEYERS, M. A. 2016. Keratin: structure, mechanical properties, occurrence in biological organisms, and efforts at bioinspiration. *Progress in Materials Science*, **76**, 229–318.

WOGELIUS, R. A., MANNING, P. L., BARDEN, H. E., EDWARDS, N. P., WEBB, S. M., SELLERS, W. I., TAYLOR, K. G., LARSON, P. L., DODSON, P. and YOU, H. 2011. Trace metals as biomarkers for eumelanin pigment in the fossil record. *Science*, **333**, 1622–1626.

ZHANG, F., KEARNS, S. L., ORR, P. J., BENTON, M. J., ZHOU, Z., JOHNSON, D., XU, X. and WANG, X. 2010. Fossilized melanosomes and the colour of Cretaceous dinosaurs and birds. *Nature*, **463**, 1075–1078.

ZHOU, L., ALGEO, T. J., FENG, L., ZHU, R., PAN, Y., GAO, S., ZHAO, L. and WU, Y. 2016. Relationship of pyroclastic volcanism and lake-water acidification to Jehol Biota mass mortality events (Early Cretaceous, northeastern China). *Chemical Geology*, **428**, 59–76.

3.6 Supplementary information

3.6.1 Supplementary figures

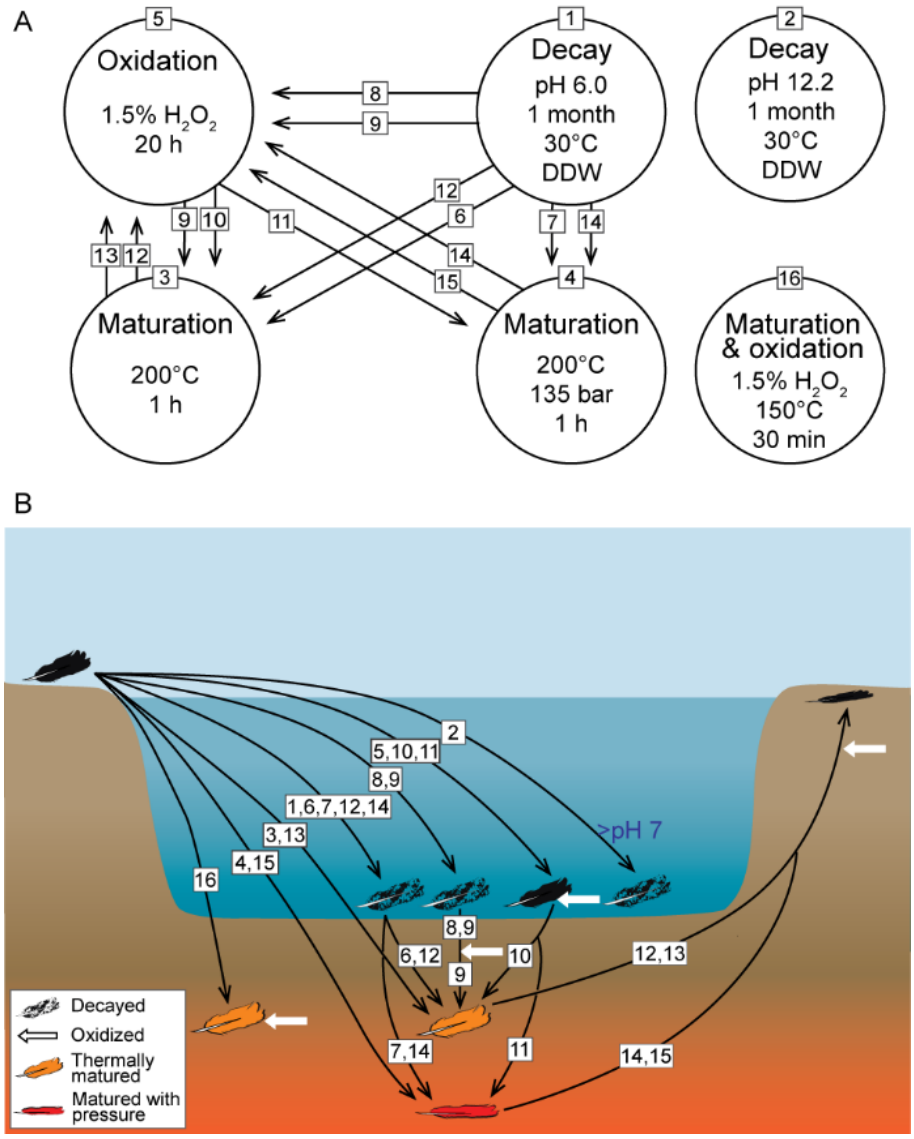


Fig. S3.1 *Experimental setup. A, schematic showing experimental pathways used. B, detailed schematic showing potential natural scenarios corresponding to each experimental pathway (indicated by numerals). DDW, distilled-deionized water.*

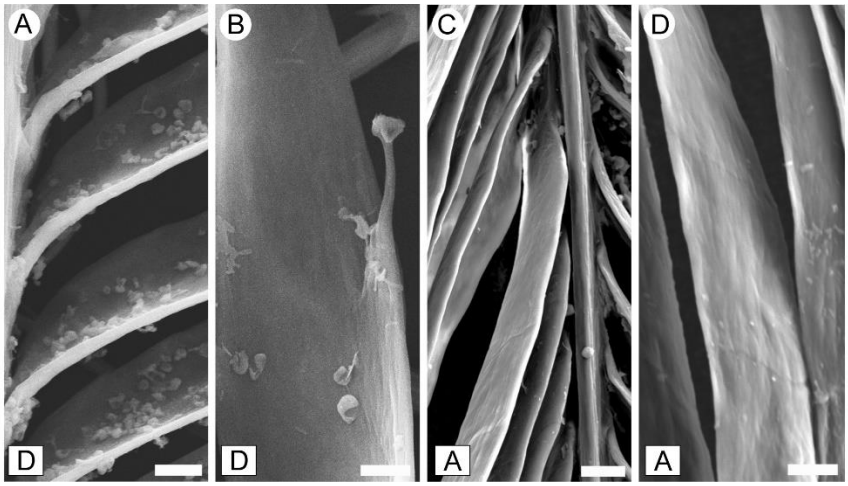


Fig. S3.2 SEM images of feather barbules showing the paucity of obvious decay bacteria in feathers decayed in pH 6 and 12.2. A–B, pathway 1. C–D, pathway 2. A, decay at pH 12.2; D, decay at pH 6. Scale bars in A, C = 10 µm, B, D = 5 µm.

4. Taphonomic experiments reveal authentic molecular signals for fossil melanins and verify preservation of 10 million year old phaeomelanin in fossils

This chapter comprises a paper that is prepared for re-submission to the journal *Nature Communications.* This chapter is organised as follows: introduction, results and discussion, materials and methods, references and supplementary information.

As in Chapter 3, the term 'keratin' is used in Chapter 4 to refer to proteinaceous feather tissue composed of β- and α-keratins as opposed to the term feather CBPs for β-keratins and IF-keratins for α-keratins.

Candidate contribution to the study. TSS contributed to the design of the study and performed all experiments and interpreted AHPO-HPLC and HCl-AHPO-HPLC data. TSS co-wrote the paper with input from all other authors.

Abstract. Melanin pigments play a critical role in physiological processes and shaping animal behaviour. Fossil melanin is therefore a unique resource for understanding the functional evolution of melanin. Accurate evolutionary models require robust fossil evidence, but the impact of fossilisation on molecular signatures for eumelanin and, especially, phaeomelanin is not fully understood. Here we present a new model for the chemical taphonomy of fossil eumelanin and phaeomelanin based on thermal maturation experiments using feathers from extant birds. Our results reveal which molecular signatures are honest signals for thermally matured eumelanin and phaeomelanin, which signatures are artefacts derived from the maturation of non-melanin proteins, and how these chemical data are impacted by sample preparation. Our model correctly predicts the molecular composition of melanins in diverse vertebrate fossils from the Miocene and Cretaceous and, critically, identifies direct molecular evidence for phaeomelanin in these fossils. This new taphonomic framework is an essential addition to the geochemical toolbox that underpins reconstructions of melanin evolution and of melanin-based coloration in fossil vertebrates.

4.1 Introduction

Melanin pigments are heterogenous polymers that have critical functions in animal homeostasis[1,2] and behaviour[3] and are implicated in key transitions in vertebrate evolution[4]. Integumentary melanins sequester metals and shield tissues from photo-oxidation and mechanical abrasion while providing visual signals that thwart predators and/or attract mates[4,5]. Diverse melanin-based integumentary colours are achieved using eumelanin, which generates black and brown hues, and/or phaeomelanin, which generates rufous and grey colours[6,7]. These pigments are stored in melanosomes – organelles that, in feathers, can have relatively elongate (eumelanosomes) to spherical (phaeomelanosomes) shapes. Evidence of melanosomes and of melanins in the fossil record has fuelled interpretations of the original colours of diverse ancient animals[8-12], yielding potential insights into behavioural ecology[13-19] and the functional evolution of melanin[4,20,21].

Reconstructions of melanin-based animal colour and of melanin macroevolution are accurate only where eumelanin and/or phaeomelanin – or their degraded remains – can be identified with confidence in fossils[22,23]. Ideally, chemical evidence of ancient melanin should be supported by morphological evidence of melanosome preservation[23]. Evidence of eumelanin has been recovered from various fossils using time-of-flight secondary ion mass spectrometry (ToF-SIMS), which yields characteristic ion fragmentation patterns for eumelanin[13,15,24-29] and can map spatial distributions of specific melanin-associated ions onto fossil melanosomes[15,25]. Evidence of eumelanin in fossils can also be inferred from associations between preserved melanosomes and specific metal species, e.g. Cu^{2+}, and/or metal coordination complexes[30]. Neither of these methods, however, can confirm the preservation of eumelanin molecular units in fossils.

Chemical evidence of fossil phaeomelanin is even more elusive. The ornithischian dinosaur *Borealopelta* preserves evidence for the phaeomelanin subunit benzothiazole (BZ) in ToF-SIMS spectra but lacks preserved melanosomes[16]; whether the BZ signal is original, or a diagenetic or anthropogenic contaminant, has not been conclusively demonstrated. Evidence of BZ has also been reported in hair of the 3 Ma fossil mouse *Apodemus* based on synchrotron-S-XANES spectra and Zn-organosulfur associations[12]. Melanosomes are

preserved, but molecular data from the fossil were not reported. Elevated concentrations of S and/or organosulfur compounds in fossil melanosomes have also been interpreted as evidence of phaeomelanin[26], but this could reflect chemical alteration of eumelanin during fossilisation, e.g., via sulfurisation[28]. A phaeomelanin-dominated composition has been inferred for putative melanosomes from two bats from the 47 Ma Messel biota based on their small and subrounded geometries[26]. The chemistry of the structures, however (i.e., the plotted position of the fossils in the principal components chemospace), is not consistent with enrichment in sulfur-bearing molecular fragments[26].

Identifying honest signals for fossil melanins, and discriminating these from the effects of fossilisation, is therefore essential to understanding the fossil record of melanin. The pathways by which fossilisation can impact chemical evidence of melanin, however, are not fully understood. Taphonomic experiments on melanosomes have yielded insights into how fossilisation processes can alter melanosome morphology and geochemistry[26,31,32]. Recent experiments on synthetic melanins[24] suggested that different eumelanin subunits converge in chemistry during thermal maturation. It is unclear, however, whether the latter changes also apply to natural melanins, especially in the complex chemical environment represented by intact melanosomes and tissues.

The most diagnostic chemical assay for eumelanin is alkaline hydrogen peroxide oxidation treatment followed by high-performance liquid chromatography (AHPO-HPLC)[33]. This assay quantifies derivatives of discrete eumelanin monomers (Fig. 4.1)[34,35] and has revealed molecular preservation of eumelanin in fossil squid[33,36], insects[37], an ichthyosaur[38] and a frog[20]. Phaeomelanin monomers can be identified using both AHPO-HPLC and HPLC following HI hydrolysis of samples[39], but these approaches have not been applied to the detection of phaeomelanin in fossils.

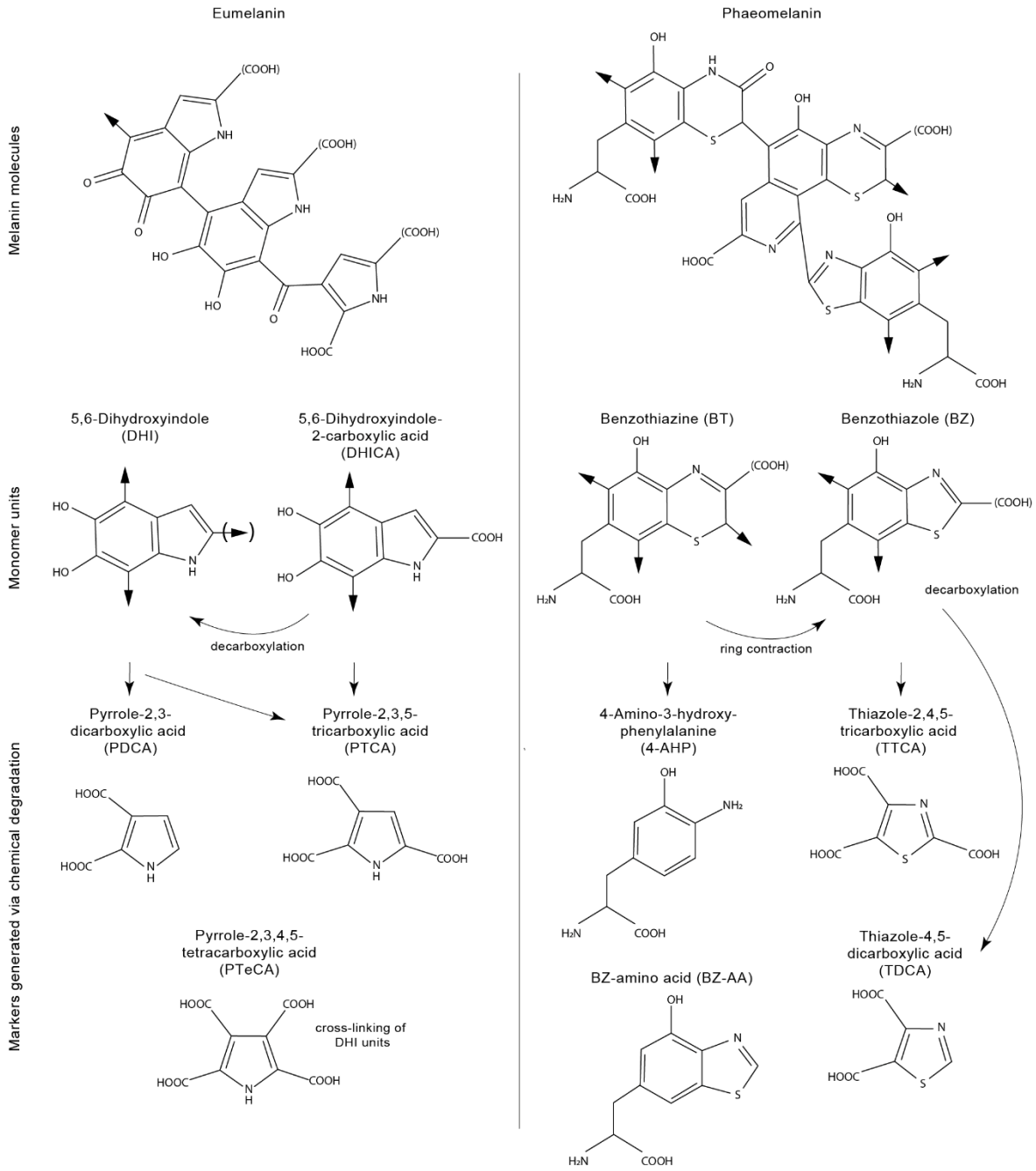


Fig. 4.1 Eumelanin and phaeomelanin molecules and their respective constituent monomers. Key eumelanin monomer units are DHI and DHICA; phaeomelanin monomer units are benzothiazine (BT) and benzothiazole (BZ). Chemical degradation of these units by alkaline hydrogen peroxide oxidation (AHPO) generates PDCA, PTCA, PTeCA, TTCA and TDCA markers. Hydroiodic acid (HI) hydrolysis generates 4-AHP (and 3-AHP, not shown here) and BZ-AA[33-35,39,40].

Here we use taphonomic experiments on feathers from extant birds and AHPO-HPLC analysis to examine the impact of thermal maturation on eumelanin and phaeomelanin, including their respective monomers, in a whole-tissue context. Our results reveal which

molecular signatures generated by AHPO-HPLC are authentic signals for thermally matured melanin. Our empirical model is tested using new data from the non-avian dinosaur *Sinornithosaurus*, the fossil bird *Confuciusornis* and specimens of the fossil frog *Pelophylax pueyoi* (Supplementary Fig. 4.1). Critically, our experimental data support evidence for the preservation of phaeomelanin in all fossils analyzed. Our predictive model of eumelanin and phaeomelanin degradation in whole tissues thus provides a unique taphonomic framework for the identification of eumelanin and phaeomelanin monomers in fossils that will underpin future investigations of the evolution of melanin and its functions through deep time.

4.2 Results and discussion

4.2.1 Melanin chemistry of untreated feathers

Eumelanin comprises 5,6-dihydroxyindole (DHI) and 5,6-dihydroxyindole-2-carboxylic acid (DHICA) units[34,35] (Fig. 4.1). AHPO-HPLC of DHI yields primarily pyrrole-2,3-dicarboxylic acid (PDCA) and pyrrole-2,3,4,5-tetracarboxylic acid (PTeCA) cross-linked at the C2 and C3 positions[24,35]; minor pyrrole-2,3,5-tricarboxylic acid (PTCA) reflects cross-linking at the C2 position[34,35]. AHPO-HPLC of DHICA yields primarily PTCA[34,35] and PTeCA cross-linked at the C3 position[24,35]. Phaeomelanin comprises benzothiazine (BT) and BZ units (Fig. 4.1), the latter generating thiazole-2,4,5-tricarboxylic acid (TTCA) and, if decarboxylated, thiazole-4,5-dicarboxylic acid (TDCA)[34]. Hydroiodic acid (HI) hydrolysis of PM allows direct identification of the BZ monomer 6-(2-amino-2carboxyethyl)-4-hydroxybenzothiazole (BZ-amino acid, BZ-AA) and the degradation products of BT, 4-amino-3-hydroxyphenylalanine (4-AHP) and 3-amino-4-hydroxyphenylalanine (3-AHP)[39,40]. 3-AHP is a minor degradation product of phaeomelanin but is not diagnostic[39]; data for this monomer are thus discussed in the supplementary material (see also Supplementary Fig. 4.2).

As expected, our AHPO-HPLC data reveal that black and orange feathers are dominated by eumelanin and phaeomelanin markers, respectively (Fig. 4.2, Table 4.1 and Supplementary Fig. 4.3). Phaeomelanin markers also occur in black feathers, and eumelanin markers in orange feathers, albeit as minor components in each case. ToF-SIMS spectra from the feathers are dominated by peaks for proteins and lipids with no distinct signatures for

melanins; and are not discussed further here (Supplementary Fig. 4.4; see Supplementary text).

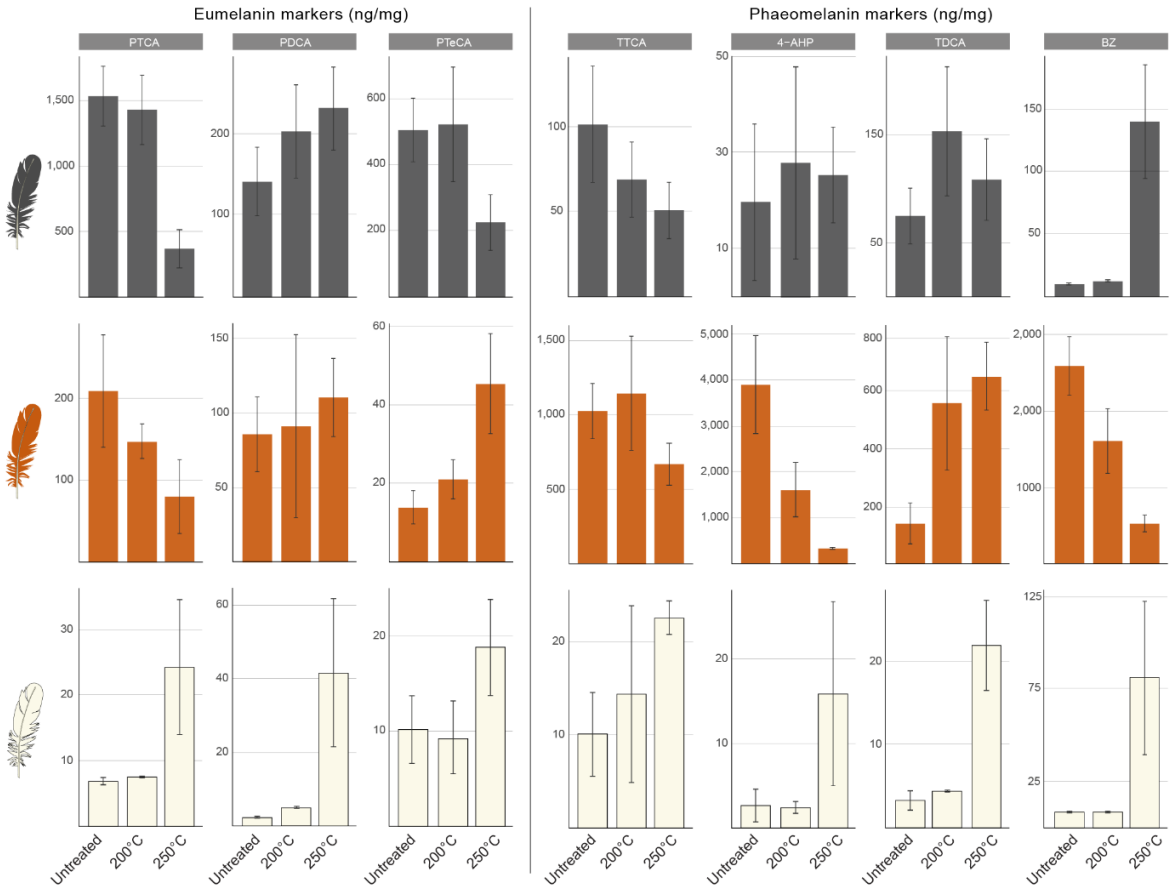


*Fig. 4.2 AHPO-HPLC data for black, orange and white feathers from extant birds with and without thermal treatment. Bar charts show melanin marker concentrations in black and orange (*Gallus gallus*) and white (*Egretta garzetta*) feathers; data are shown for untreated feathers and feathers thermally matured at 200°C and 250°C. Melanin markers are generated during alkaline hydrogen peroxide oxidation (AHPO) and hydroiodic (HI) acid hydrolysis. Filled bars indicate the mean values per treatment; floating bars indicate standard deviation per treatment.*

Table 4.1 *AHPO-HPLC data for total melanin marker concentrations in black, orange and white feathers. Mean and standard deviation data (in ng/mg) for concentrations of total melanin, total eumelanin (PTCA + PDCA + PTeCA) and total phaeomelanin markers (TTCA + TDCA + 4-AHP + BZ-AA) obtained using alkaline hydrogen peroxide oxidation (AHPO) and hydroiodic (HI) acid hydrolysis. Untreated and experimentally matured black and orange feathers,* Gallus gallus*; white feathers,* Egretta garzetta.

Feather type		HCl pre-treatment	Total melanin	Eumelanin	Phaeomelanin
Black	Untreated	no	2377 ± 309	2173 ± 315	204 ± 29
		yes	1059 ± 170	988 ± 143	71 ± 28
	200°C	no	2408 ± 474	2146 ± 410	261 ± 89
	250°C	no	1144 ± 249	819 ± 215	325 ± 53
		yes	786 ± 204	702 ± 179	83 ± 28
Orange	Untreated	no	7984 ± 1411	308 ± 67	7676 ± 1356
		yes	583 ± 60	84 ± 16	499 ± 54
	200°C	no	5178 ± 1041	258 ± 54	4920 ± 1005
	250°C	no	2412 ± 379	235 ± 40	2177 ± 381
		yes	1263 ± 91	195 ± 29	1068 ± 68
White	Untreated	no	43 ± 7	20 ± 2	24 ± 5
		yes	21 ± 4	8 ± 0	13 ± 4
	200°C	no	51 ± 13	22 ± 4	29 ± 10
	250°C	no	226 ± 19	85 ± 31	141 ± 48
		yes	173 ± 36	152 ± 39	22 ± 4
Percentage change in marker concentration relative to untreated samples					
Black	200°C	no	+1	-1	+28
	250°C	no	-52	-62	+59
		yes	-26	-28	+18
Orange	200°C	no	-35	-16	-36
	250°C	no	-69	-24	-72
		yes	+116	+132	+114
White	200°C	no	+18	+12	+22
	250°C	no	+420	+333	+491
		yes	+712	+1807	+63

Untreated black feathers contain 2377 ng/mg total melanin markers, which are predominantly eumelanin markers (91%: 2173 ng/mg; Table 4.1), in turn dominated by PTCA (1531 ng/mg), with minor PTeCA (505 ng/mg) and PDCA (138 ng/mg; Fig. 4.2, Table 4.2 and Supplementary Fig. 4.3). The PDCA : PTCA ratio is 0.09, indicating that eumelanin in the black feather comprises ca. 66% DHI and 34% DHICA[41]. The PTeCA : PTCA ratio is 0.33.

The accessory phaeomelanin signal in the black feathers is dominated by TTCA and TDCA with minor 4-AHP and BZ-AA (Fig. 4.2, Table 4.2 and Supplementary Fig. 4.3).

Total melanin markers are more abundant in untreated orange feathers (7984 ng/mg) than in black feathers (Table 4.1). Most markers (96%) are derived from phaeomelanin markers (7676 ng/mg), predominantly 4-AHP (3907 ng/mg), BZ-AA (2598 ng/mg) and TTCA (1032 ng/mg), with minor TDCA (139 ng/mg; Fig. 4.2, Table 2 and Supplementary Fig. 4.3). This composition indicates that phaeomelanin in the orange feathers comprises approximately equal quantities of BT and BZ units (the conversion factors of 34 for TTCA and 9 for 4-AHP yield estimated quantities of 35163 ng/mg BT and 35088 ng/mg BZ, respectively[34,40]). The accessory eumelanin signal is dominated by PTCA with minor PDCA and PTeCA (Fig. 4.2, Table 2 and Supplementary Fig. 4.3).

Untreated white feathers show total melanin concentrations of only 43 ng/mg, close to detection limits (Table 4.1). The dominant markers are TTCA (10 ng/mg) and PTeCA (10 ng/mg); all other markers are present in negligible quantities that approach detection limits (Fig. 4.2, Table 4.2 and Supplementary Fig. 4.3).

Table 4.2 *AHPO-HPLC data for individual melanin marker concentrations in black, orange and white feathers. Mean and standard deviation data for individual melanin markers in untreated and experimentally matured black and orange (*Gallus gallus*) and white (*Egretta garzetta*) feathers following alkaline hydrogen peroxide oxidation (AHPO) and hydroiodic (HI) acid hydrolysis. Percentage data denote the mean change in concentrations of specific markers between untreated feathers and those matured at 200°C and 250°C.*

			Eumelanin markers				Phaeomelanin markers				
Feather type		HCl pre-treatment	PTCA	PDCA	PTeCA	PTeCA : PTCA	TTCA	TDCA	TTCA : TDCA	BZ-AA	4-AHP
Black	Untreated	no	1531 ± 203	138 ± 38	505 ± 87	0.33 ± 0.03	101 ± 31	75 ± 23	1.6 ± 0.96	8 ± 0.93	20 ± 14
		yes	463 ± 111	83 ± 21	443 ± 79	1.01 ± 0.31	17 ± 5	54 ± 24	0.34 ± 0.08	X	X
	200°C	no	1427 ± 239	198 ± 50	521 ± 156	0.36 ± 0.06	69 ± 20	154 ± 54	0.46 ± 0.09	11 ± 2	28 ± 18
	250°C	no	367 ± 133	226 ± 45	226 ± 75	0.66 ± 0.22	51 ± 15	109 ± 34	0.51 ± 0.22	140 ± 42	25 ± 9
		yes	289 ± 85	108 ± 22	305 ± 77	1.07 ± 0.09	19 ± 7	64 ± 22	0.31 ± 0.1	X	X
Orange	Untreated	no	209 ± 62	86 ± 22	14 ± 4	0.07 ± 0.04	1032 ± 169	139 ± 63	9.2 ± 4	2598 ± 346	3907 ± 961
		yes	59 ± 11	16 ± 5	9 ± 4	0.14 ± 0.05	356 ± 33	143 ± 27	2.6 ± 0.5	X	X
	200°C	no	146 ± 20	91 ± 55	21 ± 5	0.14 ± 0.02	1149 ± 350	555 ± 206	2.12 ± 0.22	1613 ± 383	1603 ± 553
	250°C	no	80 ± 41	110 ± 24	45 ± 11	0.70 ± 0.3	673 ± 128	647 ± 108	1.03 ± 0.11	384 ± 102	185 ± 74
		yes	100 ± 20	39 ± 11	56 ± 9	0.59 ± 0.17	612 ± 80	456 ± 77	1.4 ± 0.4	X	X
White	Untreated	no	7 ± 1	2 ± 1	10 ± 3	1.5 ± 1	10 ± 4	3 ± 1	3.89 ± 2.47	8 ± 1	3 ± 2
		yes	3 ± 1	2 ± 0	3 ± 0	1.13 ± 0.33	8 ± 3	5 ± 1	1.59 ± 0.19	X	X
	200°C	no	8 ± 0	5 ± 2	9 ± 3	1.22 ± 0.43	14 ± 8	4 ± 0	3.23 ± 1.81	8 ± 1	2 ± 1
	250°C	no	24 ± 9	42 ± 17	19 ± 4	0.82 ± 0.12	23 ± 2	22 ± 5	1.09 ± 0.31	81 ± 36	16 ± 9
		yes	73 ± 22	36 ± 6	43 ± 15	0.60 ± 0.11	11 ± 1	11 ± 5	1.24 ± 0.60	X	X
			Percentage change in marker concentration relative to untreated samples								
Black	200°C	no	-7	+44	+3	+10	-32	+105	-71	+34	+41
	250°C	no	-76	+64	-55	+99	-50	+45	-69	+1620	+28
		yes	-37	+31	-31	+5	+14	+19	-10	X	X
Orange	200°C	no	-30	-46	+53	+94	+11	+299	-77	-38	-59
	250°C	no	-62	+29	+231	+855	-35	+365	-89	-85	-95
		yes	+69	+140	+530	+311	+72	+219	-45	X	X
White	200°C	no	+9	+108	-9	-20	+43	+35	-17	0	-6
	250°C	no	+251	+1595	+85	-46	+125	+575	-72	+914	+501
		yes	+2328	+1934	+1250	-47	+30	+117	-22	X	X

4.2.2 Maturation of black feathers

Following maturation at 200°C for 1 h (herein termed “moderate” maturation), concentrations of total melanin markers and eumelanin markers are almost identical to untreated feathers (total melanin: 2408 ng/mg, +1% (relative to untreated); eumelanin: 2146 ng/mg, -1%; Table 4.1). As with untreated samples, eumelanin markers are dominated by PTCA (1427 ng/mg, -7%; Fig. 4.2, Table 4.2 and Supplementary Fig. 4.3). PTeCA (521 ng/mg, +3%) and PDCA (198 ng/mg, +44%) are minor components and the associated PTeCA : PTCA ratio is 0.36. The minor decrease in PTCA and increase in PDCA

likely reflect limited decarboxylation of DHICA, giving rise to DHI (that, in turn, yields primarily PDCA during AHPO-HPLC analysis; Fig. 4.1)[24,35]. The accessory phaeomelanin signal is dominated by TDCA (Fig. 4.2, Table 4.2 and Supplementary Fig. 4.3).

In contrast, maturation at 250°C for 1 h (i.e., "strong" maturation) results in a dramatic loss of markers for total melanin and for eumelanin (total melanin: 1144 ng/mg, -52%; eumelanin: 819 ng/mg, -62%; Table 4.1). Further, the various eumelanin markers differ in their response to treatment: PTCA and PTeCA decrease (PTCA: 367 ng/mg, -76%; PTeCA: 226 ng/mg, -55%), whereas PDCA increases (226 ng/mg, +64%; Fig. 4.2, Table 4.2 and Supplementary Fig. 4.3). The changes in PDCA and PTCA (Fig. 4.1) likely reflect extensive decarboxylation of DHICA (resulting in the loss of PTCA and increase in PDCA), yielding abundant non-crosslinked DHI[35]. The decrease in concentration of PTeCA is less than that for PTCA and reflects less extensive thermal degradation of cross-linked DHI and/or DHICA units; the associated increase of the PTeCA : PTCA ratio (to 0.61) indicates selective preservation of cross-linked DHI units[33,35,36].

Following strong maturation, the accessory phaeomelanin signal in black feathers is dominated by BZ-AA and TDCA. TTCA and 4-AHP are minor components (Fig. 4.2, Table 4.2 and Supplementary Fig. 4.3).

4.2.3 Maturation of orange feathers

After moderate maturation, concentrations of total melanin and phaeomelanin markers decrease markedly (total melanin: 5178 ng/mg, -35%; phaeomelanin: 4920 ng/mg, -36%; Table 4.1). Phaeomelanin markers are dominated by BZ-AA (1613 ng/mg, -38%) and 4-AHP (1603 ng/mg, -59%); TTCA (1149 ng/mg, +11%) and TDCA (555 ng/mg, +299%) are present in minor amounts (Fig. 4.2, Table 4.2 and Supplementary Fig. 4.3). The increase in TDCA during maturation likely reflects progressive decarboxylation of BZ (Fig. 4.1). The loss of 4-AHP is probably due to the conversion of BT to BZ via ring contraction[40]; decarboxylation of BZ is likely to further contribute to the increase in TDCA. As in untreated feathers, the accessory eumelanin signal is dominated by PTCA (Fig. 4.2, Table 4.2 and Supplementary Fig. 4.3).

Following strong maturation, concentrations of total melanin and phaeomelanin markers decrease further (total melanin: 2412 ng/mg, -69%; phaeomelanin: 2177 ng/mg, -72%; Table 4.1; Fig. 4.2, Table 4.2 and Supplementary Fig. 4.3). Markers are dominated by TTCA (673 ng/mg, -35%) and TDCA (647 ng/mg, +365%). BZ-AA (384 ng/mg, -85%) and 4-AHP (185 ng/mg, -95%) are present in minor quantities. As with moderately matured samples, the increase in concentrations of TDCA (and decrease in BZ) likely reflect decarboxylation of BZ; the continued loss of 4-AHP probably reflects the conversion of BT to BZ[39].

Following strong maturation, the accessory eumelanin signal in orange feathers is dominated by PDCA. PTCA and PTeCA are present in minor amounts and exhibit a marked decrease (PTCA) and increase (PTeCA) compared to untreated feathers (Fig. 4.2, Table 4.2 and Supplementary Fig. 4.3).

4.2.4 Maturation of white feathers

Moderately matured white feathers show a minor increase in concentrations of total melanin (51 ng/mg, +18%), eumelanin (22 ng/mg, +12%) and phaeomelanin (29 ng/mg, +22%) markers (Table 4.1); except for TTCA (14 ng/mg), all markers show concentrations < 9 ng/mg (Fig. 4.2, Table 4.2 and Supplementary Fig. 4.3). In contrast, strongly matured white feathers show substantial increases in total melanin (226 ng/mg, +420%), eumelanin (85 ng/mg, +333%) and especially phaeomelanin (141 ng/mg, +491%) markers (Table 4.1). The most abundant marker following maturation at 250°C is BZ-AA (81 ng/mg, +914%), with minor PDCA (42 ng/mg, +1595%), PTCA (24 ng/mg, +251%), TTCA (23 ng/mg, +125%), TDCA (22 ng/mg, +575%), PTeCA (19 ng/mg, +85%) and 4-AHP (16 ng/mg, +501%; Fig. 4.2, Table 4.2 and Supplementary Fig. 4.3).

The white feathers represent a melanin-poor, protein-rich system. The dramatic increase in concentration of most melanin markers in these samples with progressive maturation is inconsistent with our experimental results for degradation of eumelanin in eumelanin-dominated systems and of phaeomelanin in phaeomelanin-dominated systems. The chemical changes thus cannot be explained by degradation of specific melanin monomers. Instead, the white feather data strongly suggest that limited quantities of melanin markers are generated from non-melanin feather components, most likely proteins[42], during

thermal maturation. This process is enhanced at relatively elevated temperatures, but total marker concentrations remain very low relative to those of black and orange feathers.

4.2.5 Comparative changes in melanin marker abundance among feather types

Overall, eumelanin and phaeomelanin degrade at broadly similar rates during maturation, albeit with a slight bias towards survival of eumelanin (during strong maturation, concentrations of total markers decrease by 62% for eumelanin and by 72% for phaeomelanin; Table 4.1). These data indicate that phaeomelanin markers should be detectable (in at least certain fossils) using AHPO-HPLC.

Individual melanin markers lack a consistent response to maturation in black and orange feathers. PTCA (and thus DHICA) dominates the composition of all black feathers analysed (regardless of experimental treatment) and is the most abundant eumelanin marker in untreated and moderately matured orange feathers (Fig. 4.2 and Table 4.2). In contrast, concentrations of PTCA decrease steadily with progressive maturation in orange feathers (200°C: -30%; 250°C: -62%) but decrease markedly in black feathers only upon maturation at 250°C (200°C: -7%; 250°C: -76%).

The eumelanin marker PDCA is present in low quantities in all feathers analysed, but is the only eumelanin marker to increase substantially in concentration with progressive maturation in black feathers and is the most abundant eumelanin marker in strongly matured orange and white feathers (Fig. 4.2 and Table 4.2). Unexpectedly, PDCA concentrations increase during moderate maturation in black feathers and decrease in orange feathers (+44% and -46%, respectively), but increase in both feather types during strong maturation (orange: +29%; black: +64%). The enhanced loss of both PDCA and PTCA in moderately matured orange feathers (relative to black feathers) cannot be explained readily using the eumelanin-rich feather data (and well-established chemical mechanisms for degradation of eumelanin monomers[24,33-36]) as a model. Instead, these data indicate a heterogeneous response of DHI and DHICA units to thermal maturation in feathers of different colour. This could reflect differences in the extent to which DHI and DHICA units are stabilised by cross-linking, both within the monomers themselves and with other

moieties in the local chemical environment, e.g., melanoproteins, keratin proteins and/or metals, in feathers of different colour.

PTeCA concentrations decrease with strong maturation in black feathers but increase with both moderate and strong maturation in orange feathers (Fig. 4.2 and Table 4.2). The associated increase in PTeCA : PTCA in orange feathers (200°C: +94%; 250°C: +855%) far exceeds that in black feathers (200°C: +10%; 250°C: +99%). This could reflect more crosslinking of eumelanin in orange relative to black feathers[33,35,36] or generation of PTeCA via thermal degradation of melanoproteins or other proteins specific to phaeomelanin-dominated systems.

Phaeomelanin markers also exhibit different trends during maturation in orange and black feathers. In orange feathers, TTCA decreases in concentration after strong maturation but is the most abundant phaeomelanin marker. TDCA is the only phaeomelanin marker to increase in concentration with progressive maturation (Fig. 4.2 and Table 4.2). In contrast, similar trends are not observed for TDCA and TTCA in black feathers with progressive maturation (TTCA: -32% at 200°C and -50% at 250°C; TDCA: +105% at 200°C and +45% at 250°C). These changes in phaeomelanin marker concentrations in black feathers cannot readily be explained using the phaeomelanin-rich feather data as a model. As with the eumelanin markers discussed above, the heterogeneous response of phaeomelanin markers to maturation may reflect differences in local chemical environment between eumelanin- and phaeomelanin-dominated systems.

4-AHP and BZ-AA are the most abundant phaeomelanin markers in untreated and moderately matured orange feathers (Fig. 4.2, Table 4.2 and Supplementary Fig. 4.3). During maturation, concentrations of 4-AHP progressively decrease in orange feathers (200°C: -59%; 250°C: -95%) but increase in black feathers (200°C: +41%; 250°C: +28%). BZ-AA concentrations decrease progressively with maturation in orange feathers (200°C: -38%; 250°C: -85%). Black feathers show a similar increase in this monomer following moderate maturation (+34%) but a dramatic increase during strong maturation (+1620%). This may reflect, in part, natural variation in a minor component of the feather melanin chemistry. As with TTCA and TDCA, these differences in the response of 4-AHP and BZ-AA in black and orange feathers are difficult to explain using the well-established chemical

mechanisms outlined above[39] for degradation of phaeomelanin. Instead, the increase in 4-AHP and BZ-AA in black feathers likely reflects minor generation of these moieties from non-melanin feather components, i.e., melanoproteins or keratin proteins.

Melanin markers in white feathers are present in sufficiently high concentrations to facilitate comparisons with other feather types only for strongly matured samples (Fig. 4.2 and Table 4.2). The dominant trend in the data are for substantial increases in the concentrations of all markers. Given the low abundance of melanin markers in untreated white feathers, the only plausible explanation is that the increase in eumelanin and phaeomelanin markers reflects generation from non-melanin proteinaceous moieties in the feathers during thermal degradation.

The progressive decrease in PTCA with increasing maturation observed in black feathers here is supported by recent maturation experiments using synthetic melanin[24]. There are some differences between the results of the latter experiments and our study, e.g. maturation of synthetic melanins did not yield a progressive increase in PDCA[24]. Here, the increase in PDCA is attributed to DHICA degradation (generating DHI and, upon AHPO-HPLC analysis, PDCA; Fig. 4.1)[35]. Overall, our data on matured black feathers more closely resemble previously reported data for experimentally matured *Sepia* melanin than those for isolated synthetic melanin units and mixtures thereof[24]. The ratio of phaeomelanin in black feathers increases with strong maturation (untreated: 9%; 250°C: 28%), due primarily to the dramatic increase in BZ-AA (which likely reflects degradation of non-melanin proteins). Collectively, our data indicate that both eumelanin and phaeomelanin follow distinct chemical pathways during thermal maturation, at least when hosted within tissues.

4.2.6 HCl-AHPO-HPLC data

In fossils, melanins and/or melanosomes may potentially be incorporated or encapsulated into diagenetic minerals. HCl treatment prior to AHPO-HPLC is therefore commonly applied to fossil tissue samples to improve the detection of melanin; the treatment has also been applied to biological samples to remove potentially interfering compounds such as proteins[42]. The potential impact of acid treatment on AHPO-HPLC data from fossils is,

however, unknown. We therefore applied this method to a duplicate set of experimental samples.

Following HCl treatment, unmatured black feathers contain 1059 ng/mg total melanin markers (Table 4.1). Eumelanin markers dominate (988 ng/mg) with abundant PTCA (463 ng/mg) and PTeCA (443 ng/mg) and minor PDCA (83 ng/mg; Tables 4.1, 4.2, Fig. 4.3 and Supplementary Fig. 4.5). The PTeCA : PTCA ratio is 1.01 and the accessory phaeomelanin signal is dominated by TDCA (Fig. 4.3, Table 4.2 and Supplementary Fig. 4.5). HCl-treated, unmatured orange feathers contain fewer melanin markers (583 ng/mg) than black feathers. Phaeomelanin markers dominate (499 ng/mg), especially TTCA (356 ng/mg); TDCA is a minor component (143 ng/mg). Untreated white feathers possess very few melanin markers (total 21 ng/mg), which are dominated by TTCA (8 ng/mg) and TDCA (5 ng/mg).

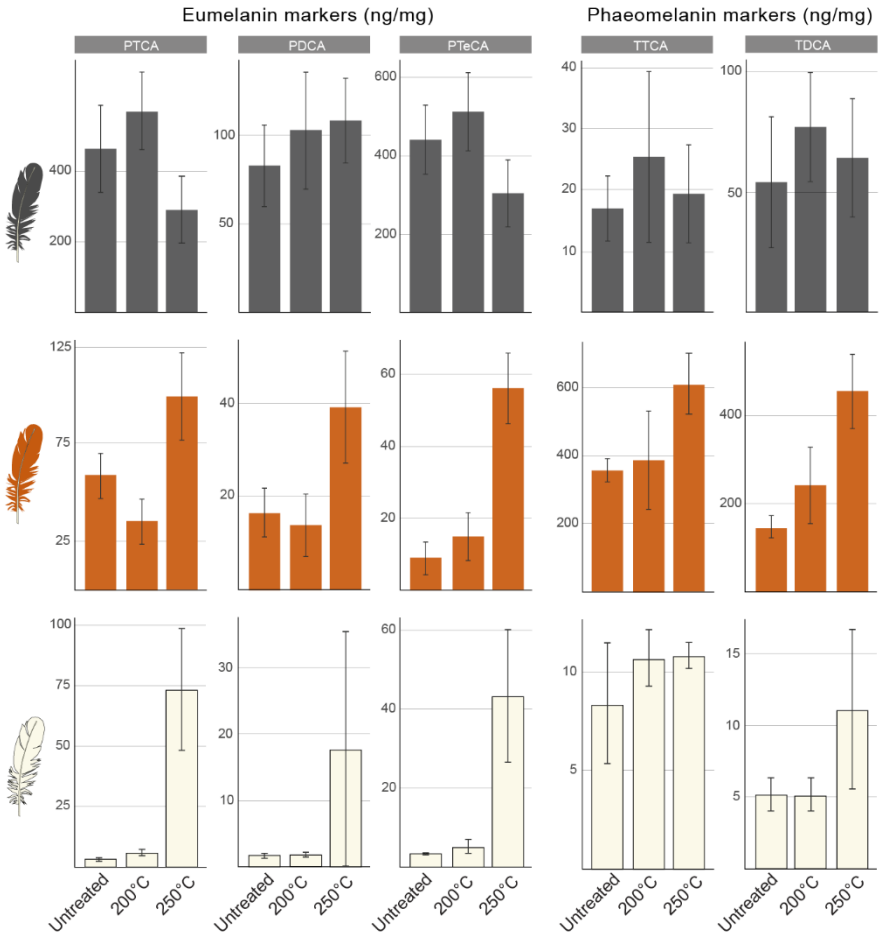


*Fig. 4.3 HCl-AHPO-HPLC data for black, orange and white feathers from extant birds with and without thermal treatment. Bar charts show melanin marker concentrations for untreated feathers and feathers thermally matured at 200°C and 250°C. Melanin markers are generated during HCl-alkaline hydrogen peroxide oxidation (AHPO). Filled bars indicate the mean values per treatment; floating bars indicate standard deviation per treatment. Black and orange feathers are from the domestic chicken (*Gallus gallus*) and white feathers are from the little egret (*Egretta garzetta*).*

Following moderate maturation, HCl-treated feathers show broadly similar total, and relative, concentrations of melanin markers to untreated feathers (Fig. 4.3, Table 4.2 and Supplementary Fig. 4.5). Following strong maturation, HCl-treated black feathers contain markedly fewer melanin and eumelanin markers relative to HCl-treated unmatured samples (total melanin: 786 ng/mg, -26%; eumelanin: 702 ng/mg, -28%; Table 4.1). Eumelanin markers are dominated by PTeCA (305 ng/mg, -31%) and PTCA (289 ng/mg, -37%) with minor PDCA (108 ng/mg, +31%; Fig. 4.3, Table 4.2 and Supplementary Fig. 4.5).

TDCA dominates the accessory phaeomelanin signal (Fig. 4.3, Table 4.2 and Supplementary Fig. 4.5).

Strongly matured, HCl-treated orange feathers contain more melanin markers than black feathers (total melanin: 1263 ng/mg, +116%; phaeomelanin: 1068 ng/mg, +114%; Table 4.1). Unlike black feathers, phaeomelanin markers show higher concentrations of TTCA (612 ng/mg, +72%) than TDCA (456 ng/mg, +219%). The accessory eumelanin signal is dominated by PTCA with minor PTeCA and PDCA (Fig. 4.3, Table 4.2 and Supplementary Fig. 4.5).

Strongly matured, HCl-treated white feathers contain substantially more total melanin and, especially, eumelanin markers (total melanin: 173 ng/mg, +712%; eumelanin: 152 ng/mg, +1807%); PTCA (73 ng/mg, +2328%), PTeCA (43 ng/mg, +1250%) and PDCA (36 ng/mg, +1934%) concentrations are particularly high (Fig. 4.3, Table 4.2 and Supplementary Fig. 4.5). Concentrations of all other markers are relatively unchanged.

These experimental data reveal important differences in the response of melanins to thermal maturation following, and without, acid treatment. Firstly, fewer melanin markers are recovered following acid treatment (-31%, -48% and -23% for strongly matured black, orange and white feathers, respectively). This may reflect degradation of melanin markers. Secondly, the relative proportions of the various markers differ markedly between acid-treated and non-acid treated samples. HCl-treated, strongly matured black feathers retain more PTeCA than samples lacking acid treatment. HCl-treated orange feathers contain less TTCA and especially TDCA than samples lacking acid treatment. HCl-treated and strongly matured white feathers contain more PTeCA and especially PTCA relative to samples lacking acid treatment, but total melanin concentrations remain low. This probably reflects the generation of minor amounts of melanin monomers from non-melanin components.

4.2.7 Melanin chemistry in fossils

HCl-AHPO-HPLC analysis of fossil melanosomes (Fig. 4.4 reveals that melanin markers are most abundant in the internal melanosomes from the Miocene frogs. Eumelanin marker concentrations are typically 21.8 – 60.8 ng/mg but are particularly high in CKGM F 6434

(354.1 ng/mg); high concentrations have been reported in other fossils[33]. Marker concentrations are much lower in the sedimentary matrix (Table 4.4), indicating that the markers in the fossil soft tissues are autochthonous and do not derive from the sediment. In the other frog samples, PTCA (7–26 ng/mg, mean 18 ng/mg) and PTeCA (12–31 ng/mg, mean 21 ng/mg) are similar and PDCA is a minor component (2–5 ng/mg, mean 4 ng/mg). Concentrations of eumelanin markers are lower in the fossil feathers relative to the frogs and show consistently higher concentrations of PTeCA relative to PTCA and especially PDCA (PTeCA: 2.6–12.8 ng/mg, mean 6.7 ng/mg; PTCA: 1.5–7.3 ng/mg, mean 2 ng/mg; PDCA: 4 ng/mg). In general, the PTeCA : PTCA ratio is higher for markers from the fossil feathers (mean 1.66) than frogs (mean 1.21), which suggests a greater degree of polymerisation[33].

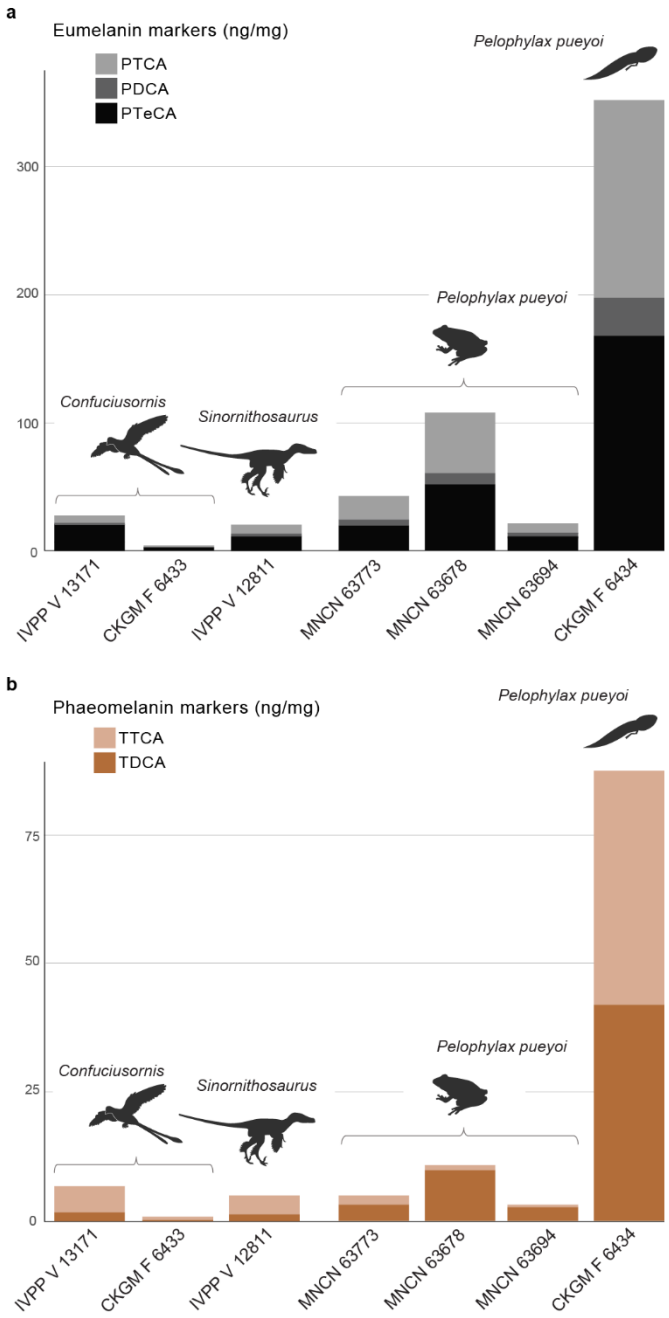


Fig. 4.4 *HCl-AHPO-HPLC data for fossil melanins. Eumelanin (A) and phaeomelanin (B) marker concentrations in samples of melanosomes. Fossil feathers are from the early bird* Confuciusornis *and the feathered dinosaur* Sinornithosaurus *from the Jehol biota. Fossil frog samples are of internal melanosomes from* Pelophylax pueyoi *from the Libros biota.*

Table 4.3 *HCl-AHPO-HPLC data for individual melanin marker concentrations in fossil soft tissues and host sediments.*

	Eumelanin markers				Phaeomelanin markers		
Fossil	PTCA	PDCA	PTeCA	PTeCA : PTCA	TTCA	TDCA	TTCA : TDCA
Sinornithosaurus IVPP V 12811	3.71 ± 1.08	0.79 ± 0.04	5.78 ± 1.88	1.54 ± 0.06	3.13 ± 0	1.13 ± 0	2.77 ± 0
Sediment IVPP V 12811	1.05	0.52	2.26	2.15	<0.3	<0.2	1.5
Confuciusornis IVPP V 13171	5.72 ± 1.54	1.02 ± 0.15	10.02 ± 2.78	1.75 ± 0.01	4.59 ± 0	1.47 ± 0	3.12 ± 0
CKGM F 6433	1.51	0.29	2.59	1.72	0.73	0.25	2.92
Sediment CKGM F 6433	0.7	0.16	1.14	1.63	0.11	0.2	0.55
Pelophylax pueyoi (adult) MNCN 63773	18.6	4.61	20	1.08	1.62	3.29	0.49
(adult) MNCN 63678	23.75 ± 3.05	4.43 ± 0.51	26.15 ± 6.58	1.09 ± 0.13	-	4.99 ± 1.29	-
(adult) MNCN 63694	7.51	2.31	12	1.6	<0.5	2.79	0.18
(tadpole) CKGM F 6434	155	30.1	169	1.09	45.4	42.1	1.08
Sediment CKGM F 6434	4.84	5.42	13.4	2.77	11.4	5.29	2.16

The phaeomelanin markers TTCA and TDCA are detected in low quantities in both fossil feathers and frogs (Fig. 4.4). The markers are below detection limits for two feather samples; in the remaining three feather samples, TTCA is consistently more abundant than TDCA (TDCA: 0.25–1.5 ng/mg, mean 0.95 ng/mg; TTCA: 0.7–4.6 ng/mg, mean 2.82 ng/mg). In contrast, in the fossil frog samples, TDCA is consistently more abundant than TTCA (TDCA: 2.8–5.9 ng/mg, mean 4 ng/mg; TTCA: below detection limit–1.6 ng/mg) except in CKGM F 6434, where TTCA ≈ TDCA.

4.2.8 Predictive model for fossil melanin chemistry

Our data form the basis of a predictive model for authentic signals for eumelanin and phaeomelanin in fossil tissues (Fig. 4.5 and Table 4.4). We first present the model for strongly matured samples analysed with AHPO-HPLC, and then show how the model predictions are modified by acid treatment. In our model, the key markers for eumelanin are PTCA and PTeCA (as the relationship between the two is an indicator of the extent of maturation[35]); those for phaeomelanin are TTCA and TDCA (as BZ-AA and 4-AHP have yet to be analysed using HI hydrolysis-HPLC).

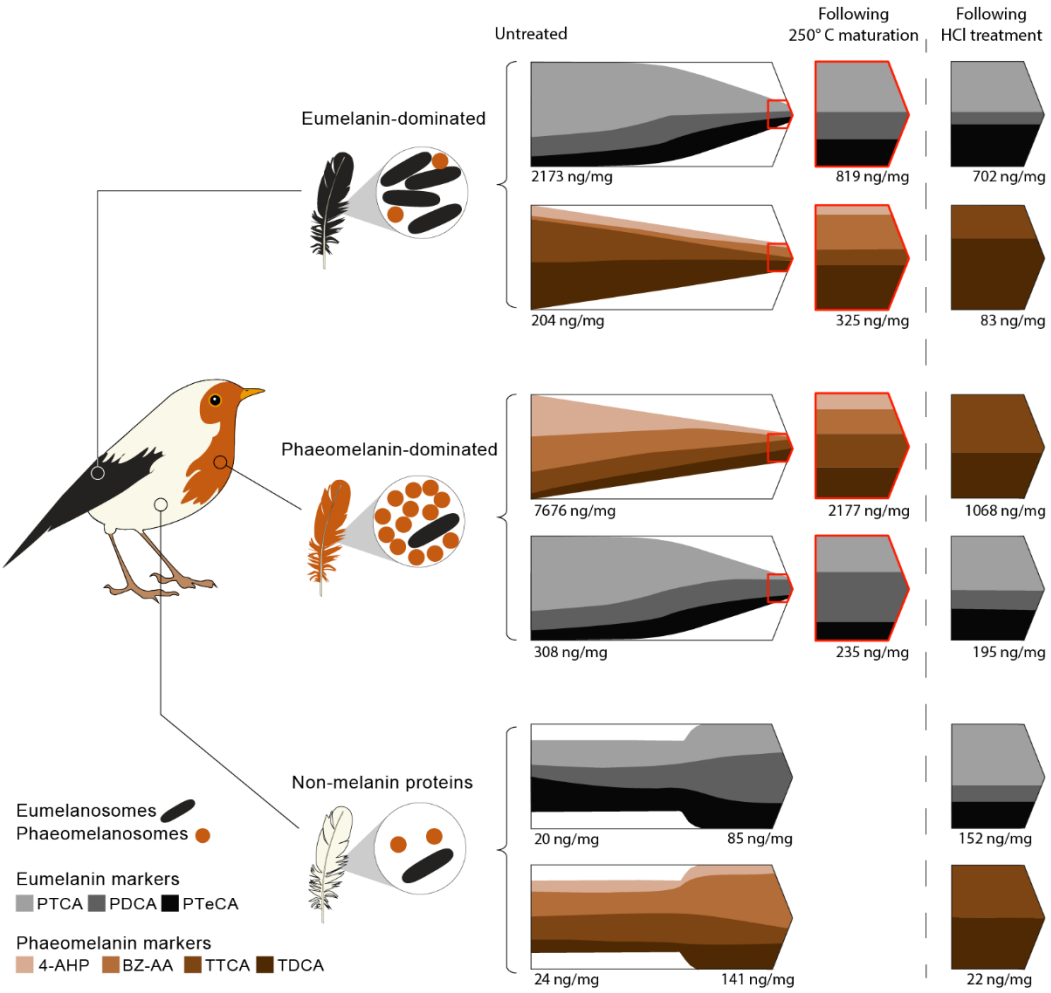


*Fig. 4.5 Authentic chemical signals for fossil melanins. Schematic showing chemical degradation of eumelanin and phaeomelanin during fossilisation based on AHPO-HPLC analysis of experimentally matured black and orange (*Gallus gallus*) and white (*Egretta garzetta*) feathers. Dashed line separates data with and without HCl treatment. The long horizontal arrows illustrate the relative concentrations of melanin markers before treatment and after maturation at 250°C without HCl treatment. The short horizontal arrows (on the right) depict the relative concentrations of markers following maturation at 250°C with HCl treatment. Concentration values (in ng/mg) indicate absolute concentrations of melanin markers.*

*Table 4.4 Predictions of authentic signals for fossil melanins in eumelanin- and phaeomelanin-dominated systems. Predictions are based on AHPO-HPLC and HCl-AHPO-HPLC data from untreated and experimentally matured black and orange (*Gallus gallus*) and white (*Egretta garzetta*) feathers. These feathers represent eumelanin-dominated and phaeomelanin-dominated systems, respectively. Data for non-melanin systems indicate signals for diagenetic artefacts produced by thermal maturation of melanin-poor, protein-rich systems. Predictions for moderate maturation are derived from the data from the 200°C experiment; predictions for strong maturation are derived from trends extrapolated from the 250°C experiment.*

		No HCl treatment		HCl treatment
Feather type	Type of markers	Gentle maturation	Strong maturation	Strong maturation
Eumelanin-dominated	Eumelanin	PTCA >> PTeCA > PDCA	PTCA > PDCA ≥ PTeCA	PTeCA ≈ PTCA >> PDCA
	Phaeomelanin	TDCA > TTCA	TDCA > TTCA	TDCA >> TTCA
Phaeomelanin-dominated	Eumelanin	PTCA > PDCA > PTeCA	PDCA > PTCA > PTeCA	PTCA > PTeCA > PDCA
	Phaeomelanin	TTCA >> TDCA	TTCA ≥ TDCA	TDCA > TTCA
Non-melanin	Eumelanin	PTCA ≈ PTeCA > PDCA	PDCA > PTCA > PTeCA	PTCA > PTeCA >> PDCA
	Phaeomelanin	TTCA > TDCA	TDCA ≈ TTCA	TTCA ≈ TDCA

The chemistry of fossil melanins can be predicted by examining changes in the relative proportions of the different melanin markers during experimental maturation (Supplementary Text and Supplementary Figs. 2, 5). Where samples have not been acid treated, our experimental data indicate that an authentic signal for strongly matured eumelanin should show PTCA > PDCA ≥ PTeCA. This is supported by an accessory phaeomelanin signal dominated by BZ-AA and TDCA, with minor TTCA and especially 4-AHP (i.e., BZ-AA > TDCA > > TTCA > 4-AHP and the key signal TDCA > TTCA).

Authentic signals for strongly matured phaeomelanin should exhibit abundant TTCA and TDCA, with BZ-AA and 4-AHP as minor components, i.e., TTCA ≥ TDCA > BZ-AA > 4-AHP. This is supported by an accessory eumelanin signal dominated by PDCA with minor PTCA and PTeCA, i.e., PDCA > PTCA > PTeCA.

Data from matured white feathers show that most melanin markers increase in concentration when matured at 250°C, with eumelanin markers dominant. The relative

proportion of PDCA and, to a lesser extent, PTCA also increases. These changes are not consistent with thermal degradation of melanin, but rather suggest minor generation of melanin monomers from non-melanin compounds. An “artificial” melanin signal in fossils will thus be dominated by eumelanin markers, with PDCA > PTCA > PTeCA. Accessory phaeomelanin markers will be dominated by BZ-AA, with minor amounts of all other markers, i.e. yielding BZ-AA >> TTCA ≈ TDCA > 4-AHP (i.e. TDCA ≈ TTCA).

The predictive model requires modifications for HCl-treated samples (Fig. 4.3 and Supplementary Fig. 4.5). In eumelanin-dominated systems, strongly matured HCl-treated samples generate a signal dominated by eumelanin markers, especially PTeCA and PTCA (in similar proportions) with minor PDCA. An authentic signal for strongly matured eumelanin after HCl treatment of samples should therefore show PTeCA ≈ PTCA >> PDCA, with accessory TDCA >> TTCA.

HCl-treated and strongly matured samples from phaeomelanin-dominated systems should be dominated by phaeomelanin markers and should contain more TTCA than TDCA, i.e. TTCA > TDCA, with an accessory eumelanin signal showing PTCA > PTeCA > PDCA.

An artificial melanin signal will be dominated by eumelanin markers, with PTCA > PTeCA >> PDCA; phaeomelanin markers will be minor components (with TTCA ≈ TDCA).

4.2.9 Testing the model: fossil melanin chemistry

The fossil frog melanosomes analysed are ovoid (0.75–1.2 µm long) to spherical (0.40–0.55 µm long)[43]. Preserved melanosome morphology, however, is unlikely to inform on original melanin chemistry in these specimens: melanosomes in extant amphibians lack differentiation into substantially elongate and spherical forms, which is likely a feature ancestral to the group[4,20]. The HCl-treated fossil frog melanosomes are dominated by eumelanin markers, especially PTeCA and PTCA, with PTeCA ≈ PTCA; except in CKGM F 6434 (where TDCA ≈ TTCA), phaeomelanin markers are consistently dominated by TDCA (Fig. 4.4; Table 4.4). The HCl-AHPO-HPLC signal in the fossil data is therefore not consistent with artificially generated eumelanin (where the model predicts PTCA > PTeCA >> PDCA) nor with an original composition dominated by phaeomelanin (where the model predicts

dominant phaeomelanin markers and accessory PTCA > PTeCA > PDCA). Instead, the eumelanin marker data are consistent with an original eumelanic composition (where PTeCA ≈ PTCA is predicted). This is supported by the eumelanin-dominated composition of melanosomes in extant amphibians[20]. The dominant phaeomelanin signal in the fossil frogs (TTCA < TDCA) is not consistent with artificial generation from non-melanin components, for which the model predicts TTCA ≈ TDCA in HCl-treated fossil samples. Instead, the fossil phaeomelanin signal is consistent with an original accessory phaeomelanin component, for which the model predicts TTCA < TDCA. This is supported by the presence of minor quantities of phaeomelanin in melanosomes of extant amphibians[20] and by the presence of elevated concentrations of Zn in melanosomes from the Libros frogs[21], which is indicative of phaeomelanin[12].

The fossil feather melanosomes are dominated by eumelanin markers, with PTeCA > PTCA >> PDCA, and an accessory phaeomelanin signal with TTCA > TDCA. Melanin markers are also present in the host sediment, albeit at much lower levels than in the soft tissues of the corresponding specimen (Table 4.4), indicating that the markers in the fossil soft tissues do not derive from the sediment. The bulk AHPO signal is not consistent with a phaeomelanin-dominated system; further, the eumelanin signal is not consistent with artificial generation of melanin (where the model predicts PTCA > PTeCA > PDCA in HCl-treated samples). Instead, the fossil feather signal is most consistent with an original eumelanin-rich system. The higher PTeCA : PTCA ratio in the fossil feathers relative to the model (which predicts PTeCA ≈ PTCA, with a slight dominance of PTeCA over PTCA) probably reflects more extensive crosslinking of DHI units during fossilisation over long geological timescales. This suggests that DHI is more robust than DHICA during thermochemolysis[33,35,36].

An original eumelanin component in the fossil feathers is supported by the presence of rod-shaped melanosomes – presumably eumelanosomes – at least locally in *Confuciusornis*[9,44]. Given reports of abundant melanosomes with ovoid to spheroid geometries (Supplementary Fig. 4.6) – presumably phaeomelanosomes[9,44] – in *Confuciusornis*, it is somewhat surprising that phaeomelanin markers are very low in concentration (although the relative proportions of presumed eumelanosomes to phaeomelanosomes in *Confuciusornis* has not been estimated). This is consistent with our experimental data that demonstrate enhanced degradation of phaeomelanin relative to

eumelanin during thermal maturation and is supported by the diagenetic history of the host sediment: fossils from the Jehol biota experienced relatively high burial temperatures[31]. Other potential contributing factors include oxidation during diagenesis[45], which may preferentially degrade phaeomelanin[31]; our experimental data presented here also suggest a further bias against recovery of phaeomelanin markers from HCl-treated samples. Given these biases, it is plausible that the *Confuciusornis* feathers analysed originally had a higher proportion of phaeomelanin than the eumelanin-dominated feathers matured in our experiments. This could also reconcile the TTCA > TDCA signal in the fossil feathers with our model, which is consistent with a phaeomelanin-dominated composition (it is also consistent with artificial marker generation, but the dominance of PTeCA over PTCA in the fossil feathers renders this unlikely).

4.2.10 Broader implications

Our study provides the first empirical and comparative models for the degradation of eumelanin and phaeomelanin during thermal maturation and, in doing so, identifies authentic molecular signals for these forms of melanin in fossils. Analysis of fossil melanosomes, combined with a holistic consideration of preserved melanosome morphology and the chemistry of melanosomes in extant analogues, confirms the validity of our model. Our experiments demonstrate that phaeomelanin monomers can survive strong maturation and can be detected in thermally matured tissues using (HCl-)AHPO-HPLC. Critically, our study provides strong empirical support for the survival of phaeomelanin in Miocene fossils (for which chemical data are fully consistent with our model). Our data also support the preservation of phaeomelanin Mesozoic fossils that have survived extensive thermal degradation and/or oxidation, but further work is required to characterise the confounding effects of diagenesis over long intervals and/or high temperatures, oxidation and HCl treatment on feathers with different proportions of melanin markers.

Differences in the response of eumelanin and phaeomelanin markers to thermal maturation in eumelanin- and phaeomelanin-rich feathers, respectively, highlight the importance of the local chemical environment on the degradation of melanin. Interpretations of melanin chemistry in fossils should therefore apply a holistic approach to

data interpretation that combines molecular data with data on the morphology of associated fossil melanosomes and on melanosome morphology and melanin chemistry in extant relatives.

The increase in 4-AHP and BZ-AA in black feathers, and of all melanin markers in white feathers during strong maturation, probably reflects artificial formation due to degradation of keratin and/or other non-melanin components. Concentrations of these artificial melanin markers are especially high where samples are treated with HCl. The formation of markers from non-melanin components is unlikely to make a major contribution to data from fossil eumelanin as concentrations of artificially generated eumelanin markers are predicted to be much lower than for originally eumelanin-rich fossils, even after HCl treatment. Particular caution is required, however, when interpreting data on phaeomelanin markers in fossils, as our data suggest that such markers can be readily generated during HCl treatment of melanin-poor tissue samples. Interpretations of authentic fossil phaeomelanin are, however, supported by preservation of melanosomes, especially those with spheroidal shapes in feathers, and by consideration of melanin chemistry in relevant tissues in extant analogues. Future studies on fossil melanins should clearly incorporate an understanding of the potential impact of diagenetic artefacts on molecular data.

Emerging data on taxonomic and tissue-specific trends in the distribution of melanin in vertebrates suggest important shifts in the functions of melanin in immunity, homeostasis and visual communication over geological time[4]. It is therefore critical that studies of the macroevolutionary history of melanin and its functions are not undermined by controversy regarding the validity of the fossil evidence[23,46]. Our results provide an essential framework for the interpretation of fossil melanosome chemistry, thus constraining future hypotheses on melanin evolution through deep time.

4.3 Materials and methods

4.3.1 Maturation experiments

Black (*n* = 5) and orange (*n* = 5) contour feathers from the domestic chicken, *Gallus gallus domesticus*, and white (*n* = 4) primary feathers from the little egret, *Egretta garzetta*, were stored at -80°C prior to experimental treatment. Feathers were selected based on their high content of eumelanin or phaeomelanin (black and orange feathers, respectively), or near-lack of melanin (white feathers)[6]. Feather pieces (ca. 45 x 25 mm) were wrapped in Al foil and thermally matured in a standard laboratory convection oven for 1 h at 100°C, 200°C or 250°C (each +/- 1°C).

4.3.2 Experimental justification

For any taphonomic experiment, the optimum conditions are those that generate the phenomena of interest in fossils[45]. The purpose of our experiments was to investigate the impact of thermal maturation on the chemistry of feather melanin. The ultimate aim is to apply the experimental results to the interpretation of melanin chemistry in fossil feathers that retain gross feather structure (e.g. rachis and barbs) and melanosomes. The most appropriate conditions for our experiments are therefore those that ensure the survival of melanosomes and the surrounding keratinous tissue (or at least residues thereof) at the end of the experiment[31,45] yet involve sufficiently high temperatures and/or pressures to ensure geochemical alteration of melanin. In other words, the experiments should achieve a taphonomic "sweet spot" between too much, and too little, degradation.

***Experimental maturation and feather structure*.** Previous maturation experiments on feathers have used various combinations of pressure and temperature, with feathers enclosed in foil or Au capsules. Substantial deterioration of feather macrostructure (including thinning, convolution and loss of barbules, and merging of barbs) occurs after 1 h in foil at 200°C 200 bar (following a 1 h-long ramp-up of temperature to 200°C[47,48]) and 1 h in foil at 200°C 250 bar[31]. Fluidization of feather tissue occurs after 1 h in foil at 250°C 250 bar (following a 1 h-long ramp-up of temperature to 250°C[47,48]; also reported in separate experiments in Au capsules for 24 h at 250°C 250 bar[49]). Retention of

melanosomes but loss of the keratinous feather cortex occurred during experiments for 12–24 h at 210–250°C 225–300 bar[49]. All of these conditions are clearly too extreme for the purposes of our experiments. In contrast, feather macrostructure survives maturation in Au capsules for 24 h at 100°C 250 bar[50]; also reported in separate experiments using these conditions (but in foil) for 1 hr[47,48] with little or no appreciable damage; some contortion of barbules is evident after 1 h at 150°C 250 bar[47]. Use of lower pressures, even when coupled with higher temperatures, promotes retention of intact feather structures, as in our previous experiments for 1 h at 200°C, 135 bar[45]. Collectively these data suggest that retention of feather macrostructure is best achieved in experiments at relatively low pressures, i.e. at 135 bar or less.

Maturation experiments and melanin chemistry. Previous experiments have not systematically analyzed melanin monomer chemistry (but see ref. 45). Conditions promoting geochemical alteration of melanosomes can, however, be inferred from published data. Previous experiments at 100°C 250 bar for 24 h did not result in major differences between the chemistry of matured and untreated feathers, as evidenced by gas chromatography-mass spectrometry analyses[50]. These experimental temperatures are clearly too low to induce substantial chemical alteration of melanosomes, especially since elevated pressures enhance degradation of tissue ultrastructures[51]. Experiments at 200°C 250 bar and 250°C 250 bar induced shrinkage of melanosomes[31], which presumably is associated with altered melanosome chemistry. Such elevated temperatures are therefore optimal for our experiments, albeit not in conjunction with elevated pressures as this combination induces substantial feather degradation (see above). We tested this using a set of pilot experiments on orange feathers at 100°C for 1 h (Supplementary Figs. 7, 8). As predicted, after maturation, the TTCA : TDCA ratio is unchanged in HCl-treated samples (0.71 for both untreated and matured samples) and very similar in samples lacking acid treatment (0.93 (untreated) and 0.88 (matured)); the 4-AHP : BZ : AA ratio is similar in untreated (0.5) and matured (0.6) samples lacking acid treatment. Our experiments therefore used relatively elevated temperatures of 200°C and 250°C and atmospheric pressure. Although our experiments were conducted in air and can thus be classed as broadly oxidising, they did not incorporate reaction with a strong oxidant as our previous experiments have shown that this destroys melanosomes[45].

Chemical analysis of such thermally matured melanosomes can inform on the geochemistry of preserved melanosomes associated with eumelanin- and phaeomelanin-rich fossil feathers. White feathers were used to test whether markers generated by AHPO and HI hydrolysis are unique to melanin. Experiments were performed under oxic conditions to enhance thermal degradation (relative to anoxic conditions[51]). No additional experimental media were used as the focus of the experiments is the analysis of feather residues resulting from autochthonous *in situ* chemical changes, not changes induced by extrinsic fluids.

4.3.3 Fossil material

This study used several specimens from the Jehol (Early Cretaceous, NE China) and Libros (Late Miocene, NE Spain) biotas. Fossils analyzed from the Jehol Biota are two specimens (CKGM F 6433 and IVPP V 13171) of *Confuciusornis* and one specimen of *Sinornithosaurus* (IVPP V 12811). Fossils from Libros are four specimens of *Pelophylax pueyoi* (CKGM F 6434, MNCN 63678, MNCN 63694 and MNCN 63773). Institutional abbreviations: CKGM, Cork Geological Museum; IVPP, Institute of Vertebrate Paleontology and Paleoanthropology, Beijing, China; MNCN, Museu Nacional de Ciencias Naturales, Madrid, Spain.

4.3.4 SEM

Samples of preserved soft tissue were dissected from fossil specimens using sterile tools, mounted on Al stubs with carbon tape, sputter coated with C or Au and analysed using a Hitachi S-3500N scanning electron microscope at accelerating voltages of 15–25 kV.

4.3.5 HPLC analyses

Feather samples (each 3–5 mg) were homogenised in distilled water with a Ten-Broeck glass homogeniser at a concentration of 5 mg/mL. Separate aliquots (100 µL) of this homogenate were subjected to AHPO or HI hydrolysis. AHPO tests for the presence of the eumelanin markers PTCA, PDCA and PTeCA and the phaeomelanin markers TTCA and TDCA[34,35]; HI hydrolysis tests for the phaeomelanin markers 3-AHP, 4-AHP[39] and BZ-AA[40]. 3-AHP is a minor component of phaeomelanin degradation products[39] and can be derived

from proteins (i.e., it is not melanin-specific)[52]; 3-AHP data are thus not of major focus here and are provided in the supplementary material instead. Fossil samples (4–8 mg each) were ground to a powder and analysed using HCl-AHPO[42]. HCl-AHPO was developed[42] in order to demineralize samples and purify analytical results by removing interfering materials such as proteins. Products from AHPO and HCl-AHPO were analysed by a modified HPLC protocol using an ion pair reagent[53]. BZ-AA and 4-AHP cannot be analysed following acid treatment. A different HPLC column was used to analyse feathers matured at 100°C than untreated and feathers matured at 200°C and 250°C due to regular replacement of the column as per standard protocols.

Values cited herein for percentage change in monomer concentrations (ng/mg) for experimentally matured feathers of a particular colour are relative to mean concentrations of that monomer in untreated feathers of the same colour.

4.3.6 ToF-SIMS analyses

Samples were mounted on ToF-SIMS sample holders without prior treatment, ToF-SIMS analyses were conducted in the static SIMS mode on a TOFSIMS IV instrument (IONTOF GmbH) using 25 keV Bi^{3+} primary ions and low energy electron flooding for charge compensation. Positive and negative ion data were acquired with instrument optimization for high mass-resolution (m/Δm ~5,000, spatial resolution ~3–4 µm). The pulsed primary ion current was set at 0.10 pA.

4.3.7 Enzymatic melanin extraction

Melanin was extracted from untreated and strongly matured feathers (lacking acid treatment) using the protocol in ref. 20. In brief, samples were treated with nine cycles of solutions using 1,4-DTT (DTT), proteinase-K, and papain while incubated at 37.5°C at 200 rpm for 9 d.

Acknowledgements. We thank Naomi O'Reilly for assistance and Jack Connell and Liam Hayes for supplying feathers. The research was funded by ERC Starting Grant H2020-ERC-

2014-StG-637691-ANICOLEVO and ERC Consolidator Grant H2020-ERC-COG-10103293 PALAEOCHEM awarded to M.E.M.

Author contributions. M.E.M. conceived the research and designed the study with T.S.S. F.Z. provided fossil material. T.S.S. performed maturation experiments. S.I. and K.W. performed AHPO-HPLC analyses. J. L., P. S. and M. J. performed ToF-SIMS analyses. T.S.S. and M.E.M. wrote the manuscript with input from S.I., K.W. and F.Z.

4.4 References

1 D'Alba, L. & Shawkey, M. D. Melanosomes: biogenesis, properties, and evolution of an ancient organelle. *Physiol. Rev.* **99,** 1–19 (2019).

2 Hong, L. & Simon, J. D. Current understanding of the binding sites, capacity, affinity, and biological significance of metals in melanin. *J. Phys. Chem. B* **111,** 7938–7947 (2007).

3 Jawor, J. M. & Breitwisch, R. Melanin ornaments, honesty, and sexual selection. *The Auk* **120,** 249–265 (2003).

4 McNamara, M. *et al.* Decoding the evolution of melanin in vertebrates. *Trends Ecol. Evol.* **36,** 430–443 (2021).

5 McGraw, K. J. Melanins, metals, and mate quality. *Oikos* **102,** 402–406 (2003).

6 Galván, I. & Wakamatsu, K. Color measurement of the animal integument predicts the content of specific melanin forms. *RSC Adv.* **6,** 79135–79142 (2016).

7 Liu, S. Y., Shawkey, M. D., Parkinson, D., Troy, T. P. & Ahmed, M. Elucidation of the chemical composition of avian melanin. *RSC Adv.* **4,** 40396–40399 (2014).

8 Li, Q. *et al.* Plumage color patterns of an extinct dinosaur. *Science* **327,** 1369–1372 (2010).

9 Zhang, F. *et al.* Fossilized melanosomes and the colour of Cretaceous dinosaurs and birds. *Nature* **463,** 1075–1078 (2010).

10 Li, Q. *et al.* Reconstruction of *Microraptor* and the evolution of iridescent plumage. *Science* **335,** 1215–1219 (2012).

11 Hu, D. *et al.* A bony-crested Jurassic dinosaur with evidence of iridescent plumage highlights complexity in early paravian evolution. *Nat. Commun.* **9,** 217 (2018).

12 Manning, P. L. *et al.* Pheomelanin pigment remnants mapped in fossils of an extinct mammal. *Nat. Commun.* **10,** 2250 (2019).

13 Lindgren, J. *et al.* Biochemistry and adaptive colouration of an exceptionally preserved juvenile fossil sea turtle. *Sci. Rep.* **7,** 13324 (2017).

14 Gabbott, S. E. *et al*. Pigmented anatomy in Carboniferous cyclostomes and the evolution of the vertebrate eye. *Proc. R. Soc. B* **283,** 20161151 (2016).

15 Lindgren, J. *et al.* Skin pigmentation provides evidence of convergent melanism in extinct marine reptiles. *Nature* **506,** 484–488 (2014).

16 Brown, C. M. *et al.* An exceptionally preserved three-dimensional armored dinosaur reveals insights into coloration and Cretaceous predator-prey dynamics. *Curr. Biol.* **27,** 2514–2521 (2017).

17 Smithwick, F. M., Nicholls, R., Cuthill, I. C. & Vinther, J. Countershading and stripes in the theropod dinosaur *Sinosauropteryx* reveal heterogeneous habitats in the Early Cretaceous Jehol biota. *Curr. Biol.* **27,** 3337–3343 (2017).

18 Vinther, J. *et al.* 3D camouflage in an ornithischian dinosaur. *Curr. Biol.* **26,** 2456–2462 (2016).

19 McNamara, M. E. *et al.* Reconstructing carotenoid-based and structural coloration in fossil skin. *Curr. Biol.* **26,** 1075–1082 (2016).

20 Rossi, V., McNamara, M. E., Webb, S. M., Ito, S. & Wakamatsu, K. Tissue-specific geometry and chemistry of modern and fossilized melanosomes reveal internal anatomy of extinct vertebrates. *Proc. Natl Acad. Sci. USA* **116,** 17880–17889 (2019).

21 Rossi, V., Webb, S. M. & McNamara, M. E. Hierarchical biota-level and taxonomic controls on the chemistry of fossil melanosomes revealed using synchrotron X-ray fluorescence. *Sci. Rep.* **10,** 8970 (2020).

22 Barden, H. E. *et al.* Bacteria or melanosomes? A geochemical analysis of micro-bodies on a tadpole from the Oligocene Enspel Formation of Germany. *Palaeobiodivers. Palaeoenviron.* **95,** 33–45 (2015).

23 Lindgren, J. *et al.* Interpreting melanin-based coloration through deep time: a critical review. *Proc. R. Soc. B* **282,** 20150614 (2015).

24 Jarenmark, M., Sjövall, P., Ito, S., Wakamatsu, K. & Lindgren, J. Chemical evaluation of eumelanin maturation by ToF-SIMS and alkaline peroxide oxidation HPLC analysis. *Int. J. Mol. Sci.* **22,** 161 (2021).

25 Lindgren, J. *et al.* Molecular preservation of the pigment melanin in fossil melanosomes. *Nat. Commun.* **3,** 824 (2012).

26 Colleary, C. *et al.* Chemical, experimental, and morphological evidence for diagenetically altered melanin in exceptionally preserved fossils. *Proc. Natl Acad. Sci. USA* **112,** 12592–12597 (2015).

27 Clements, T. *et al.* The eyes of *Tullimonstrum* reveal a vertebrate affinity. *Nature* **532,** 500–503 (2016).

28 McNamara, M. E., van Dongen, B. E., Lockyer, N. P., Bull, I. D. & Orr, P. J. Fossilization of melanosomes via sulfurization. *Palaeontology* **59,** 337–350 (2016).

29 Lindgren, J. *et al.* Molecular composition and ultrastructure of Jurassic paravian feathers. *Sci. Rep.* **5,** 13520 (2015).

30 Wogelius, R. *et al.* Trace metals as biomarkers for eumelanin pigment in the fossil record. *Science* **333,** 1622–1626 (2011).

31 McNamara, M. E., Briggs, D. E., Orr, P. J., Field, D. J. & Wang, Z. Experimental maturation of feathers: implications for reconstructions of fossil feather colour. *Biol. Lett.* **9,** 20130184 (2013).

32 Rossi, V., Webb, S. M. & McNamara, M. Maturation experiments reveal bias in the chemistry of fossil melanosomes. *Geology* Published online: March 22 (2021). DOI: 10.1130/G48696.1.

33 Glass, K. *et al.* Direct chemical evidence for eumelanin pigment from the Jurassic period. *Proc. Natl Acad. Sci. USA* **109,** 10218–10223 (2012).

34 Ito, S. *et al.* Usefulness of alkaline hydrogen peroxide oxidation to analyze eumelanin and pheomelanin in various tissue samples: application to chemical analysis of human hair melanins. *Pigment Cell Melanoma Res.* **24,** 605–613 (2011).

35 Ito, S., Wakamatsu, K., Glass, K. & Simon, J. D. High-performance liquid chromatography estimation of cross-linking of dihydroxyindole moiety in eumelanin. *Anal. Biochem.* **434,** 221–225 (2013).

36 Glass, K. *et al.* Impact of diagenesis and maturation on the survival of eumelanin in the fossil record. *Org. Geochem.* **64,** 29–37 (2013).

37 Lindgren *et al.* Fossil insect eyes shed light on trilobite optics and the arthropod pigment screen. *Nature* **573,** 122–125 (2019).

38 Lindgren *et al.* Soft-tissue evidence for homeothermy and crypsis in a Jurassic ichthyosaur. *Nature* **564,** 359–365 (2018).

39 Wakamatsu, K., Ito, S., & Rees, J. L. The usefulness of 4-amino-3-hydroxyphenylalanine as a specific marker of pheomelanin. *Pigment Cell Res.* **15,** 225–232 (2002).

40 Wakamatsu, K., Ohtara, K. & Ito, S. Chemical analysis of late stages of pheomelanogenesis: conversion of dihydrobenzothiazine to a benzothiazole structure. *Pigment Cell Melanoma Res.* **22,** 474–486 (2009).

41 Itoh, T., Ito, S., & Wakamatsu, K. Effects of aging on hair color, melanosome morphology, and melanin composition in Japanese females. *Int. J. Mol. Sci*. **20,** 3739 (2019).

42 Ito, S. *et al.* Acid hydrolysis reveals a low but constant level of pheomelanin in human black to brown hair. *Pigment Cell Melanoma Res.* **31,** 393–403 (2018).

43 McNamara, M. E. *et al.* Non-integumentary melanosomes can bias reconstructions of the colours of fossil vertebrates. *Nat. Commun.* **9,** 2878 (2018).

44 Li, Q., Clarke, J. A., Gao, K.-Q., Peteya, J. A. & Shawkey, M. D. Elaborate plumage patterning in a Cretaceous bird. *PeerJ* **6,** e5831 (2018).

45 Slater, T. S. *et al.* Taphonomic experiments resolve controls on the preservation of melanosomes and keratinous tissues in feathers. *Palaeontology* **63,** 103–115 (2020).

46 Donoghue, P. C. & Purnell, M. A. Distinguishing heat from light in debate over controversial fossils. *BioEssays* **31,** 178–189 (2009).

47 Pan, Y., Li, Z., Wang, M. Zhao, T., Xiaoli, W., Xiaoting, Z. Unambiguous evidence of brilliant iridescent feather color from hollow melanosomes in an Early Cretaceous bird. *National Science Review* **9**, nwab227 (2022).

48 Zhao, T., Hu, J., Hu, L., Pan, Y. Experimental maturation of feathers: implications for interpretations of fossil feathers. *Palaios* **35**, 67-76 (2020).

49 Saitta, E.T., Kaye, T.G., Vinther, J. Sediment-encased maturation: a novel method for simulating diagenesis in organic fossil preservation. *Palaeontology* **62**, 135–150 (2019).

50 Saitta, E.T. *et al*. Low fossilization potential of keratin protein revealed by experimental taphonomy. *Palaeontology* **60**, 547–556 (2017).

51 McNamara, M. E. *et al.* The fossil record of insect color illuminated by maturation experiments. *Geology* **41,** 487–490 (2013).

52 Wakamatsu, K., Yokochi, M., Naito, A., Kageshita, T. & Ito, S. Comparison of phaeomelanin and its precursor 5-S-cysteinyldopa in the serum of melanoma patients. *Melanoma Res.* **13,** 357–363 (2003).

53 Ito, S., Del Bino, S., Hirobe, T., & Wakamatsu, K. Improved HPLC conditions to determine eumelain and pheomelanin contents in biological samples using an ion pair reagent. *Int. J. Mol. Sci.* **21,** 5134 (2020).

4.5 Supplementary information

4.5.1 Supplementary text

ToF-SIMS analyses. ToF-SIMS analyses were conducted on untreated and strongly matured feathers and on melanin extracts from these samples. The resulting spectra do not show distinct fragment ion patterns for melanin: instead, spectra are dominated by typical fragment ions for protein (probably derived from feather keratins) and lipids (probably derived from feather waxes). This likely reflects the dispersed distribution of melanosomes in the feathers, rendering it impossible to isolate a region bearing only melanosomes for analysis. ToF-SIMS spectra of the melanin extracts are also dominated by fragment ions for proteins and lipids, with additional peaks for phosphate. In these samples, the protein fragments likely derive from the melanosome membrane and/or protein residues that are adhering to the melanosome surfaces. In turn, these protein residues probably derive from the enzymatic extraction process. The phosphate peaks derive from the phosphate buffer used during the extractions. Collectively, these data suggest that ToF-SIMS is not the most appropriate technique to use for chemical analysis of these biological tissues: the spectral data are effectively swamped by other fragment ions. It is important to note that ToF-SIMS has been applied successfully to analysis of pure synthetic standards of selected eumelanin monomers and their degradation products generated during maturation experiments[1]; the resulting ToF-SIMS data are entirely consistent with AHPO-HPLC data on the samples, confirming the accuracy and validity of AHPO-HPLC for investigation of chemical alteration of melanins.

Melanin chemistry of orange feathers matured at 100°C. Analysis of orange feathers matured at 100°C (n = 3) shows an increase in all melanin markers except TDCA (104 ng/mg, -25%) using AHPO-HPLC (PTCA: 249 ng/mg, +19%; PDCA: 142 ng/mg, +66%; PTeCA: 23 ng/mg, +71%; TTCA: 1395 ng/mg, +35%) compared to untreated feathers. HI-HPLC data show a decrease in both 4-AHP (3320 ng/mg, -15%) and BZ-AA (2121 ng/mg, -18%). HCl-AHPO shows an increase in all melanin markers (PTCA: 65 ng/mg, +11%; PDCA: 29 ng/mg, +79%; PTeCA: 15 ng/mg, +74%; TTCA: 608 ng/mg, +71%; TDCA: 244 ng/mg, +70%). This increase probably reflects natural variation in phaeomelanin content among the samples rather than the use of different HPLC columns for untreated and matured samples. These

data are thus interpreted as evidence of little decrease in phaeomelanin marker concentrations during maturation at 100°C. Given that our data support a higher preservation potential of eumelanin markers, it is expected that black feathers matured at 100°C would show little to no decrease in eumelanin marker concentrations.

3-AHP. HI-HPLC data show small quantities of 3-AHP in untreated black (13 ng/mg) and white (4 ng/mg) feathers and large quantities in orange feathers (1341 ng/mg). 3-AHP increases with progressive maturation in black (200°C: 22 ng/mg; 250°C: 39 ng/mg) and white (200°C: 11 ng/mg; 250°C: 70 ng/mg) feathers but decreases in orange feathers (200°C: 587 ng/mg; 250°C: 152 ng/mg). The progressive increase in black and white feathers likely reflects minor generation of this moiety from non-melanin feather components.

Development of the predictive model. The predictive model is based on data for (a) mean concentrations of individual melanin markers per treatment; (b) standard deviation data for individual markers per treatment (with particular attention to overlap of the range of the data for different treatments); (c) trends in the data for relative concentrations of individual markers (i.e. when expressed as a percentage of the total markers recovered for eumelanin and phaeomelanin, respectively, in a sample). To illustrate, take the case of data from strongly matured eumelanin-dominated systems analysed using HCl pre-treatment. PTCA concentrations are predicted to exceed those for PDCA based on the higher quantities of PTCA remaining following treatment relative to PDCA. With progressive maturation beyond the extent modelled in our experiments, PTeCA may ultimately dominate the melanin signal in fossils given the increase in the PTeCA : PTCA ratio during maturation which is both observed in our AHPO-HPLC data and has been reported previously[2].

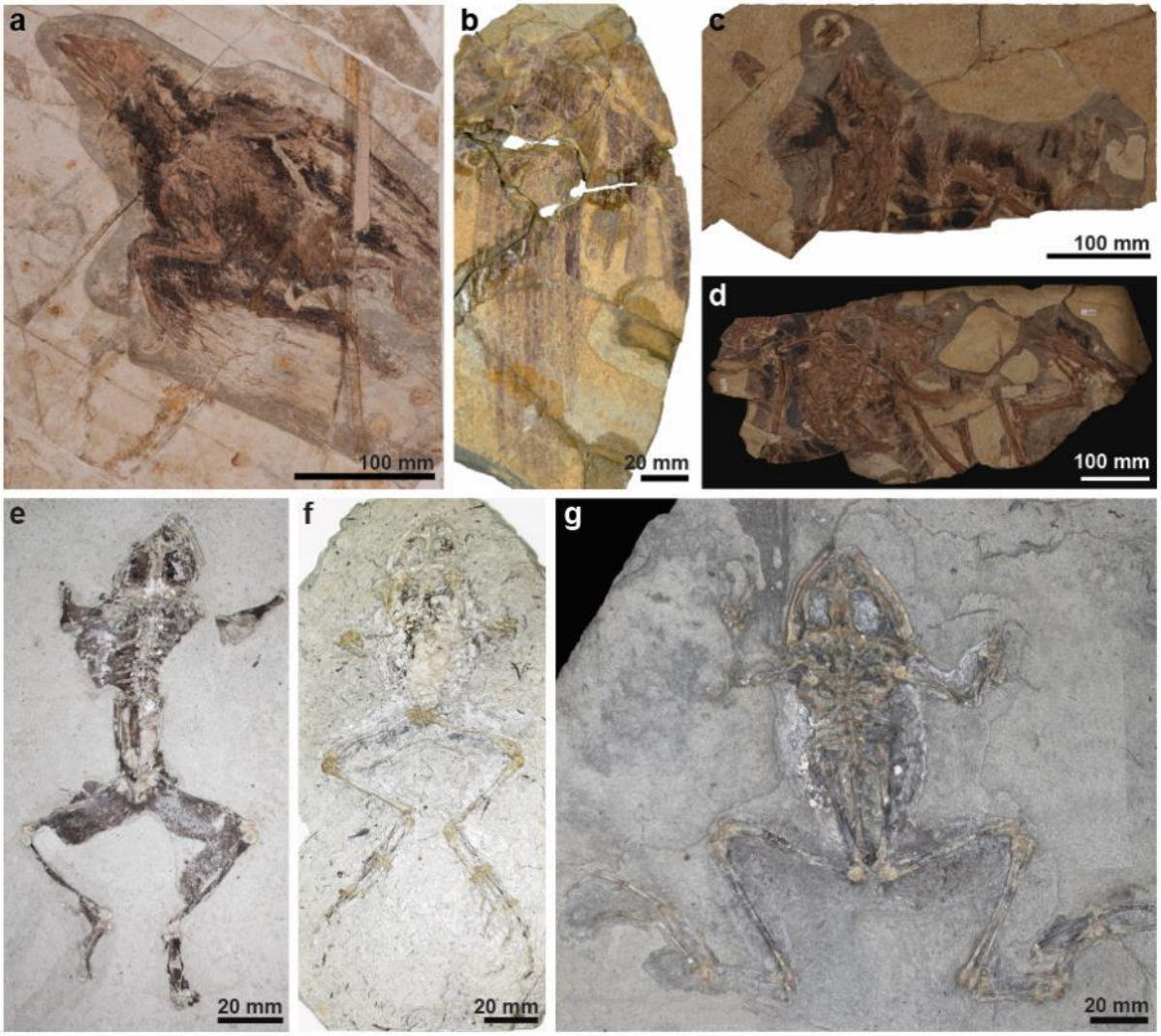


Fig. S4.1 *Photographs of fossil specimens used in this study. a, b Confuciusornis. a IVPP V 13171. b CKGM F 6433. c, d Sinornithosaurus (IVPP V 12811). e–g Pelophylax pueyoi. e MNCN 63778. f MNCN 63773. g MNCN 63694. Scale bars: a 100 mm b 20 mm c, d 100 mm e–g 20 mm. a, c, d from McNamara* et al.[3]*. e, g from McNamara* et al.[4]*.*

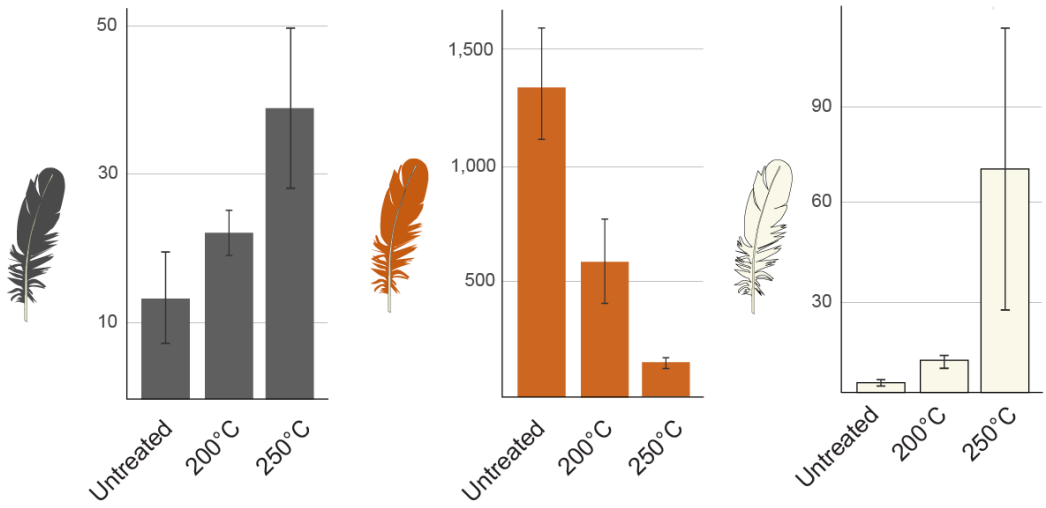


*Fig. S4.2 HI-HPLC data for the phaeomelanin marker 3-AHP for black, orange and white feathers from extant birds with and without thermal treatment. Black and orange feathers are from the domestic chicken (*Gallus gallus*) and white feathers are from the little egret (*Egretta garzetta*).*

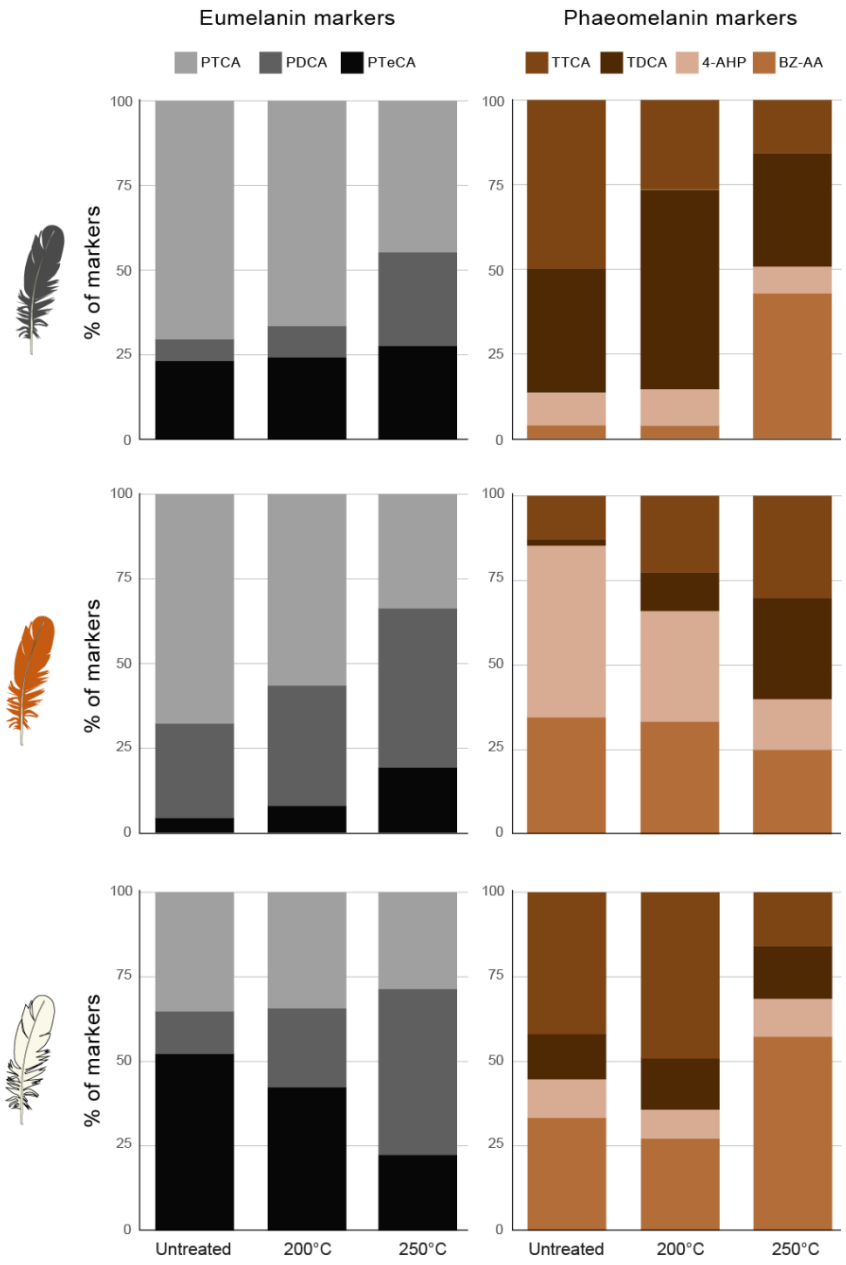


*Fig. S4.3 AHPO- and HI-HPLC data for black, orange and white feathers from extant birds with and without thermal treatment. Eumelanin markers and the phaeomelanin markers TTCA and TDCA are derived during chemical degradation via AHPO. BZ-AA and 4-AHP are derived during HI hydrolysis. Black and orange feathers are from the domestic chicken (*Gallus gallus*) and white feathers are from the little egret (*Egretta garzetta*).*

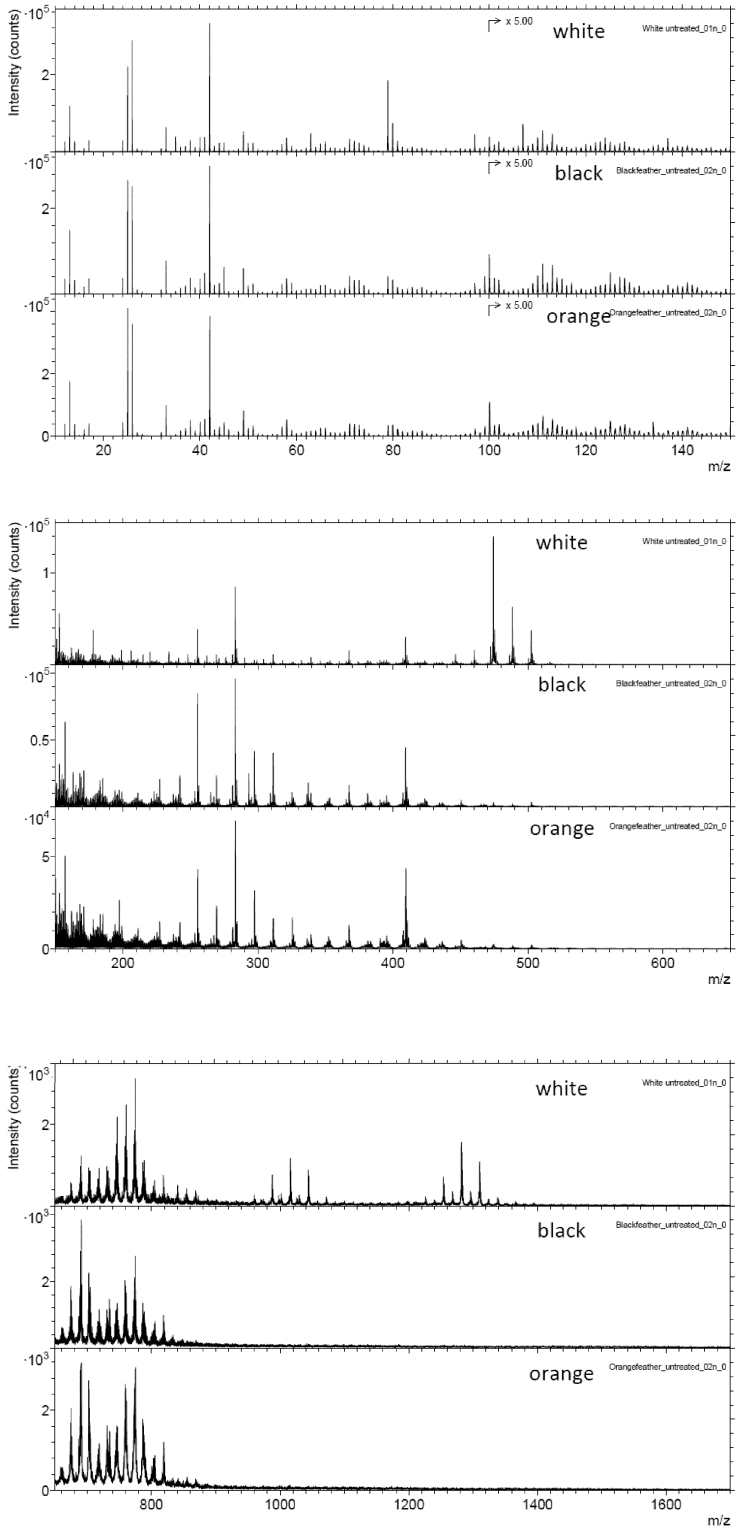


*Fig. S4.4 (part 1) Negative ion ToF-SIMS spectra for untreated black, orange and white feathers from extant birds. Black and orange feathers are from the domestic chicken (*Gallus gallus*) and white feathers are from the little egret (*Egretta garzetta*).*

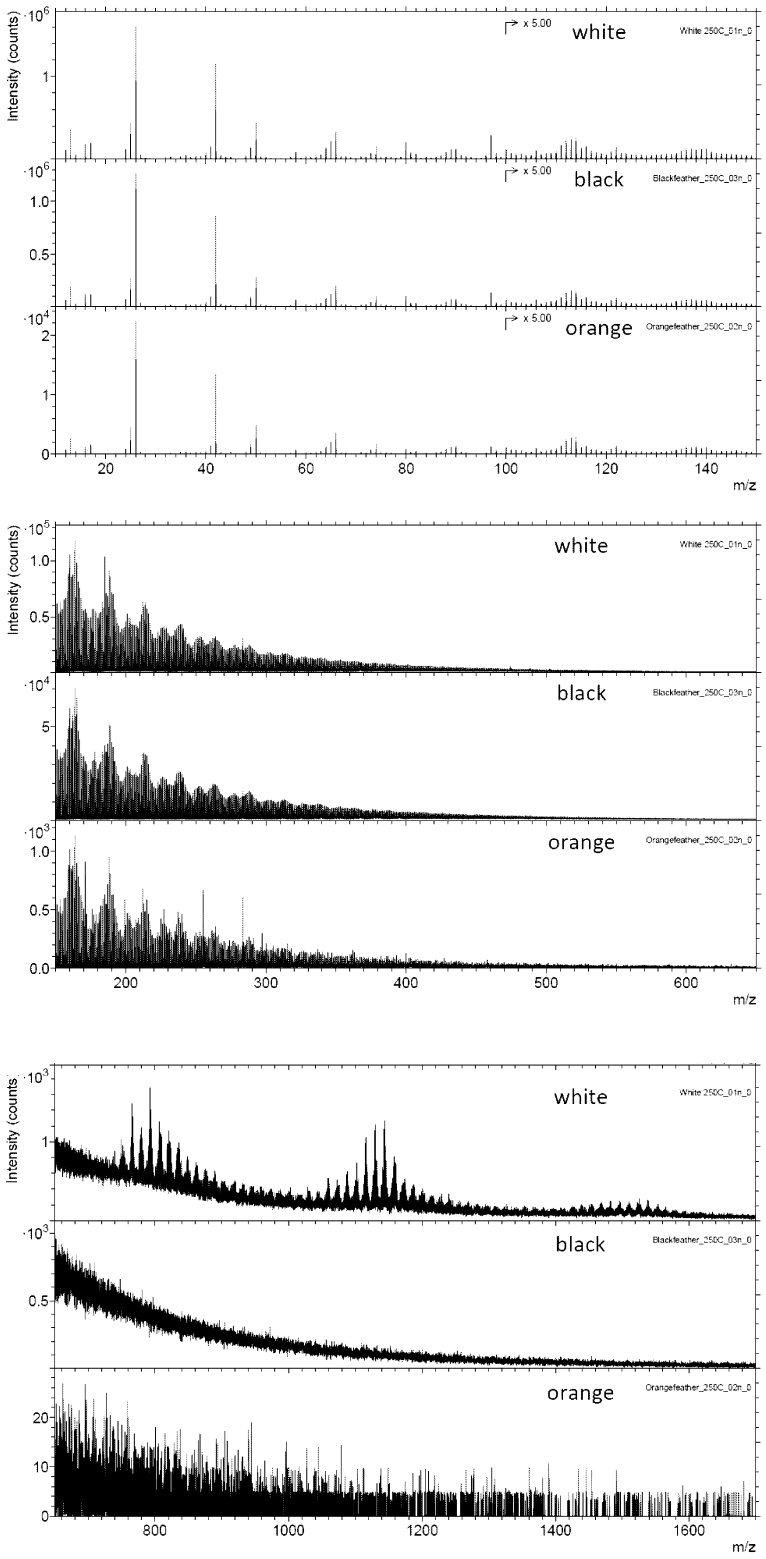


Fig. S4.4 (part 2) *Negative ion ToF-SIMS spectra for black, orange and white feathers from extant birds matured at 250°C for 1 h. Black and orange feathers are from the domestic chicken (*Gallus gallus*) and white feathers are from the little egret (*Egretta garzetta*).*

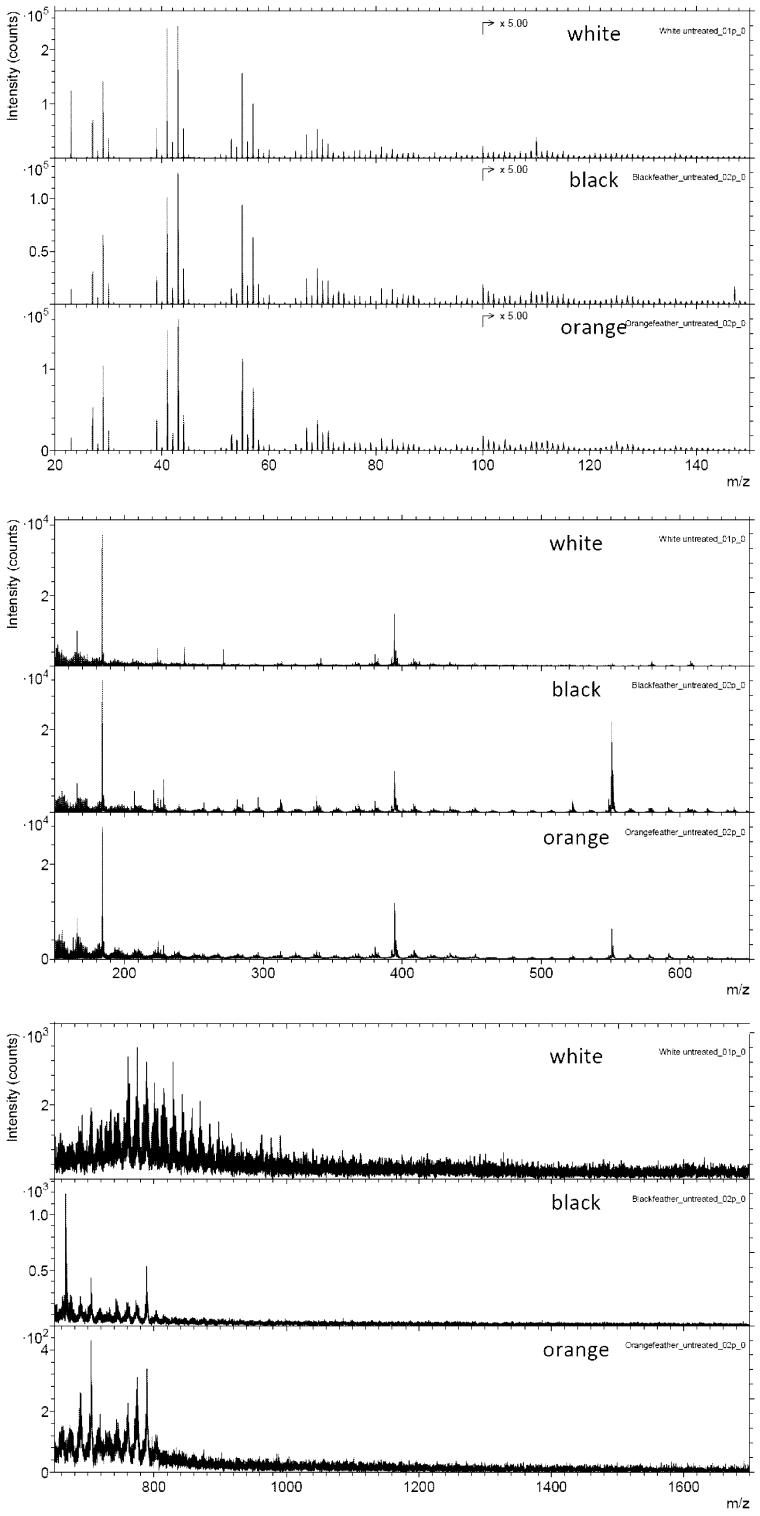


Fig. S4.4 (part 3) *Positive ion ToF-SIMS spectra for untreated black, orange and white feathers from extant birds. Black and orange feathers are from the domestic chicken (*Gallus gallus*) and white feathers are from the little egret (*Egretta garzetta*).*

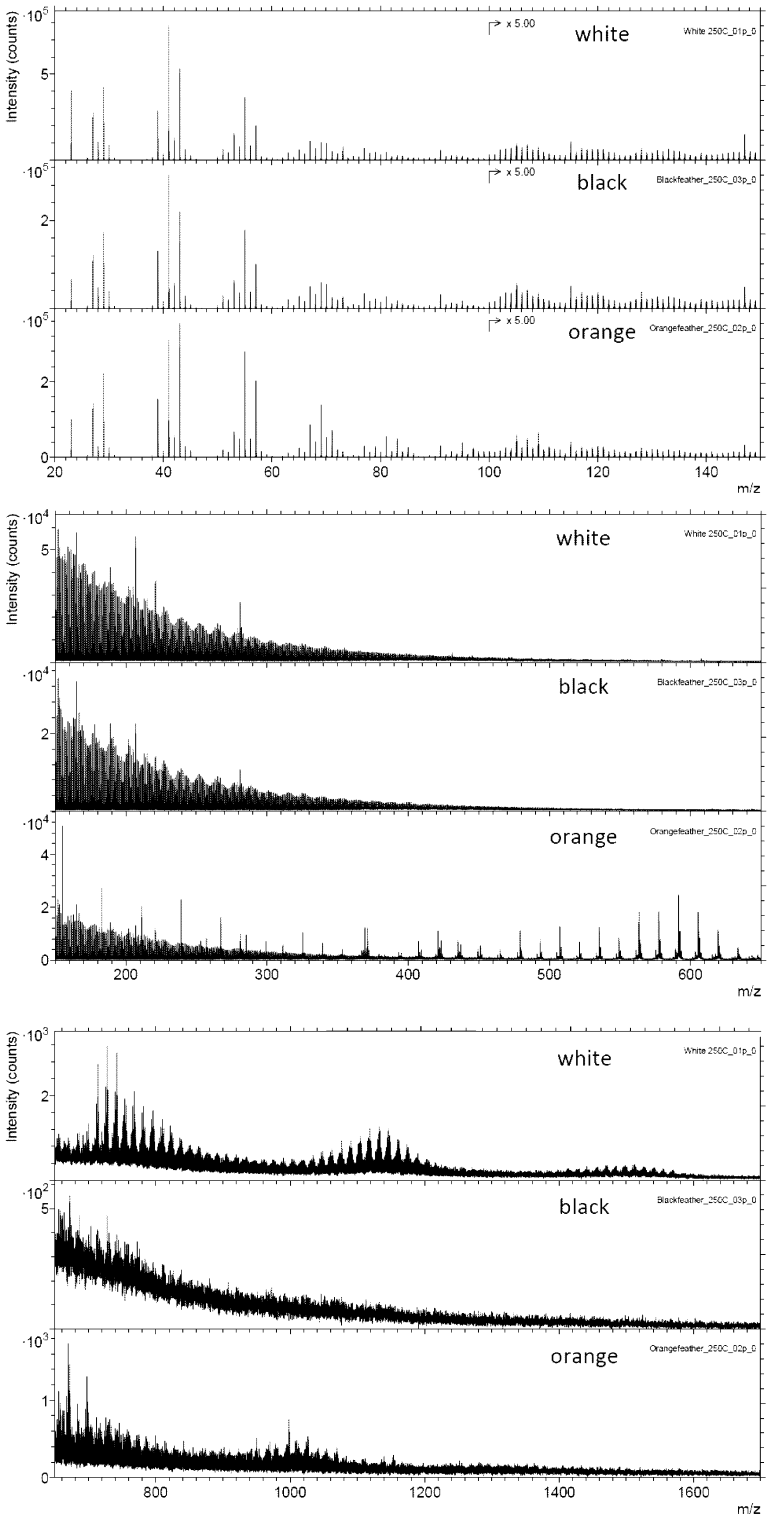


Fig. S4.4 (part 4) *Positive ion ToF-SIMS spectra for black, orange and white feathers from extant birds matured at 250°C for 1 h. Black and orange feathers are from the domestic chicken (*Gallus gallus*) and white feathers are from the little egret (*Egretta garzetta*).*

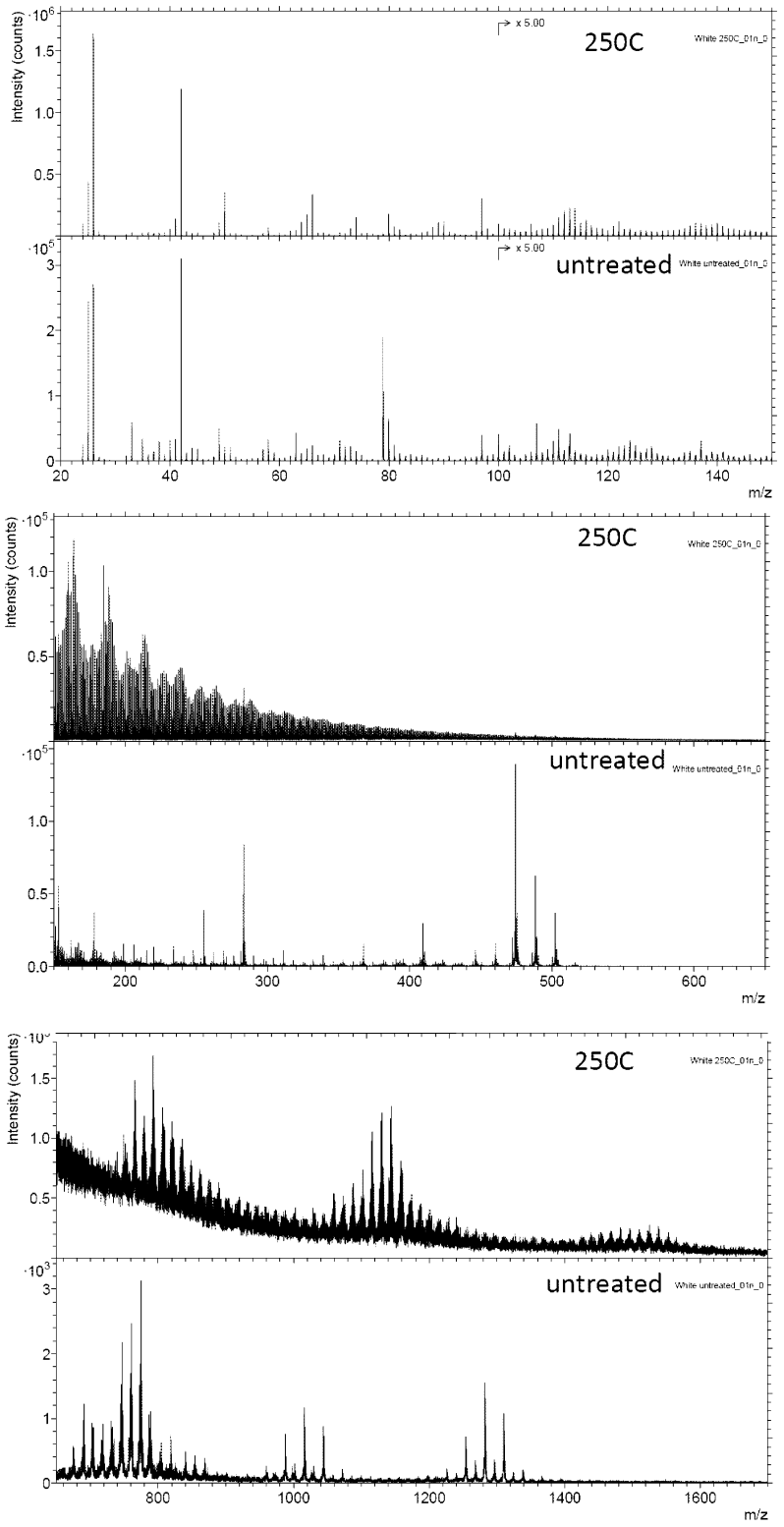


Fig. S4.4 (part 5) *Negative ion ToF-SIMS spectra from melanin extracts of untreated and strongly matured white feathers from* Egretta garzetta*. Matured feathers treated at 250°C for 1 h.*

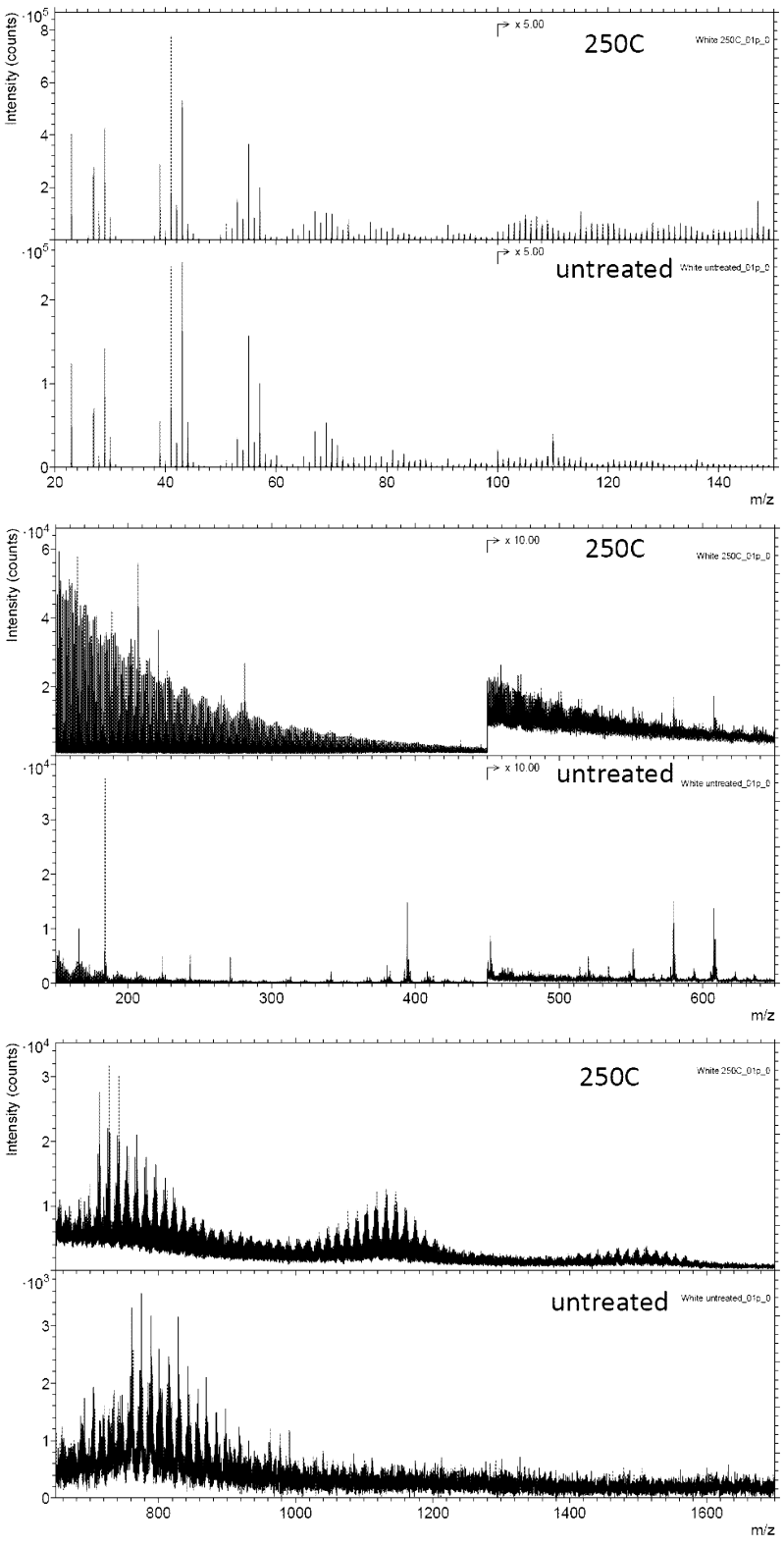


Fig. S4.4 (part 6) *Positive ion ToF-SIMS spectra from melanin extracts of untreated and strongly matured white feathers from* Egretta garzetta*. Matured feathers treated at 250°C for 1 h.*

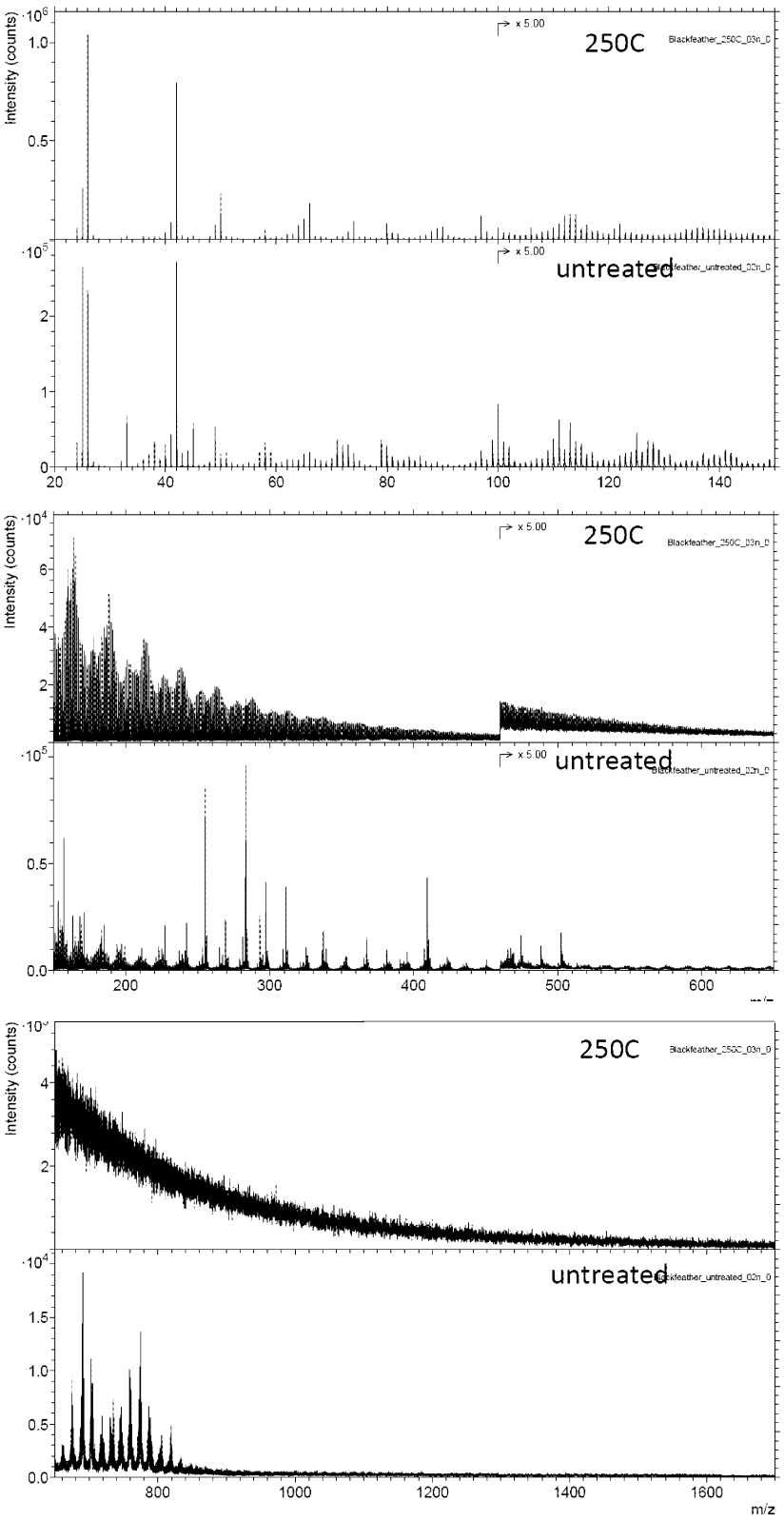


Fig. S4.4 (part 7) *Negative ion ToF-SIMS spectra from melanin extracts of untreated and strongly matured black feathers from* Gallus gallus*. Matured feathers treated at 250°C for 1 h.*

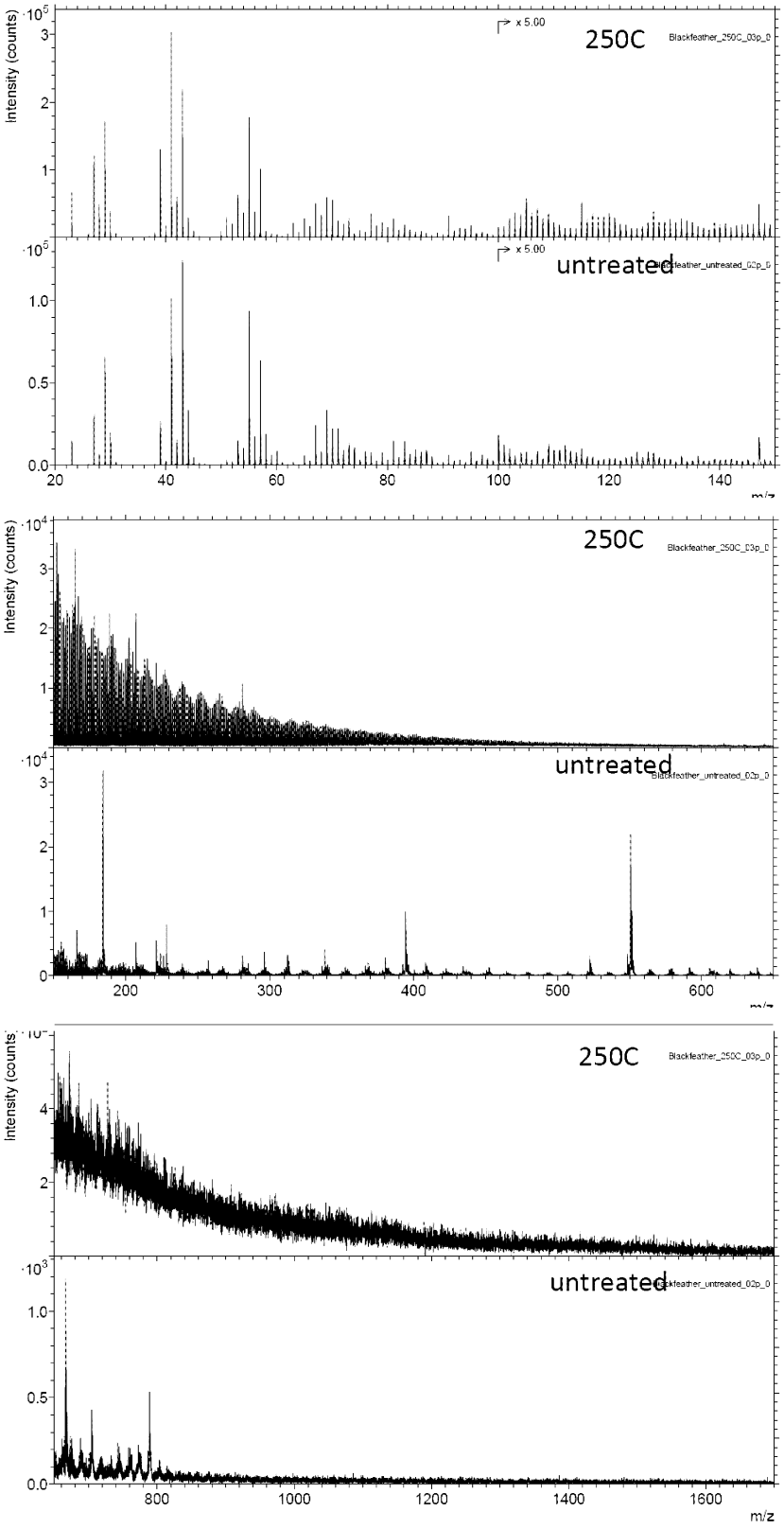


Fig. S4.4 (part 8) Positive ion ToF-SIMS spectra from melanin extracts of untreated and strongly matured black feathers from Gallus gallus*. Matured feathers treated at 250°C for 1 h.*

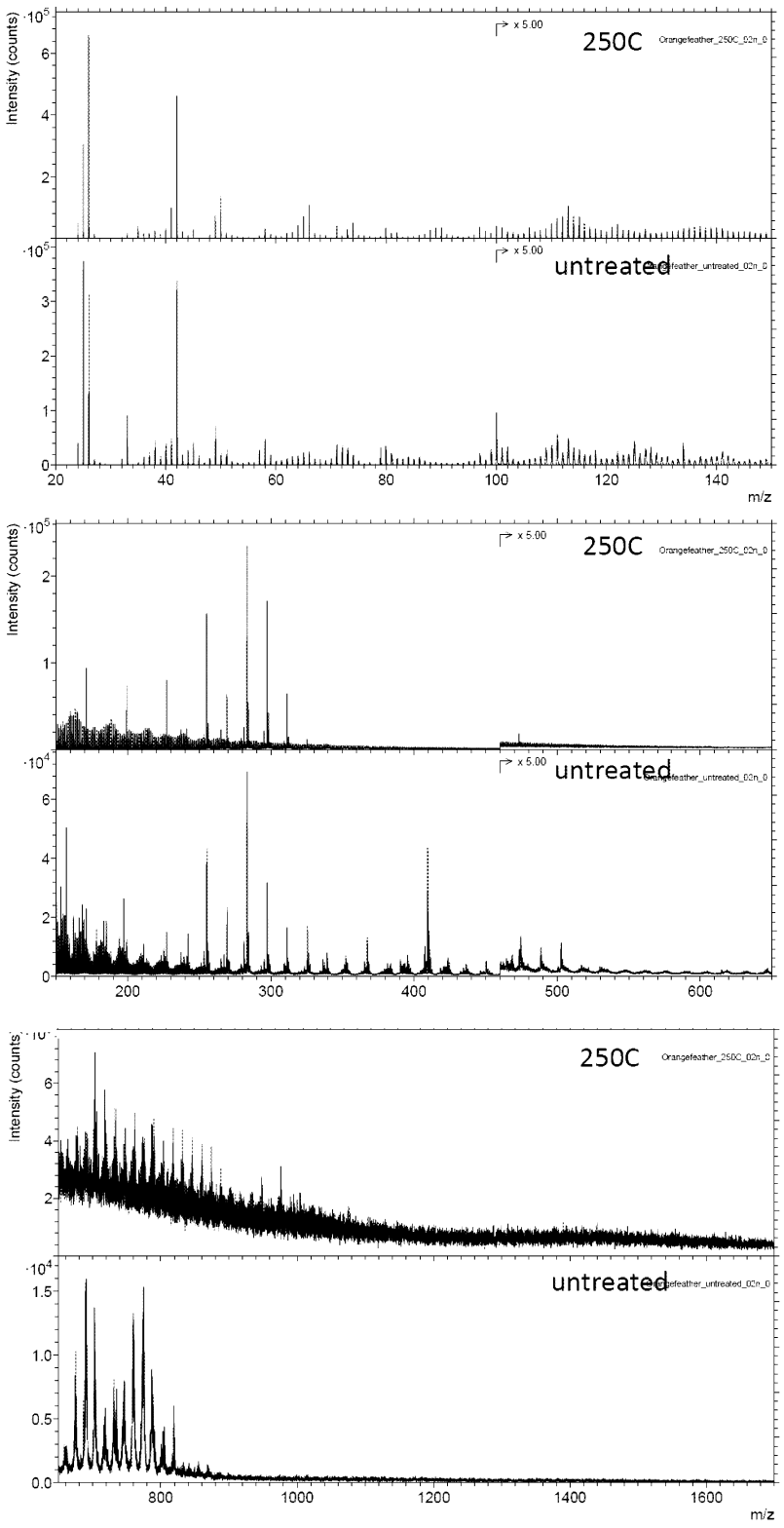


Fig. S4.4 (part 9) *Negative ion ToF-SIMS spectra from melanin extracts of untreated and strongly matured orange feathers from* Gallus gallus*. Matured feathers treated at 250°C for 1 h.*

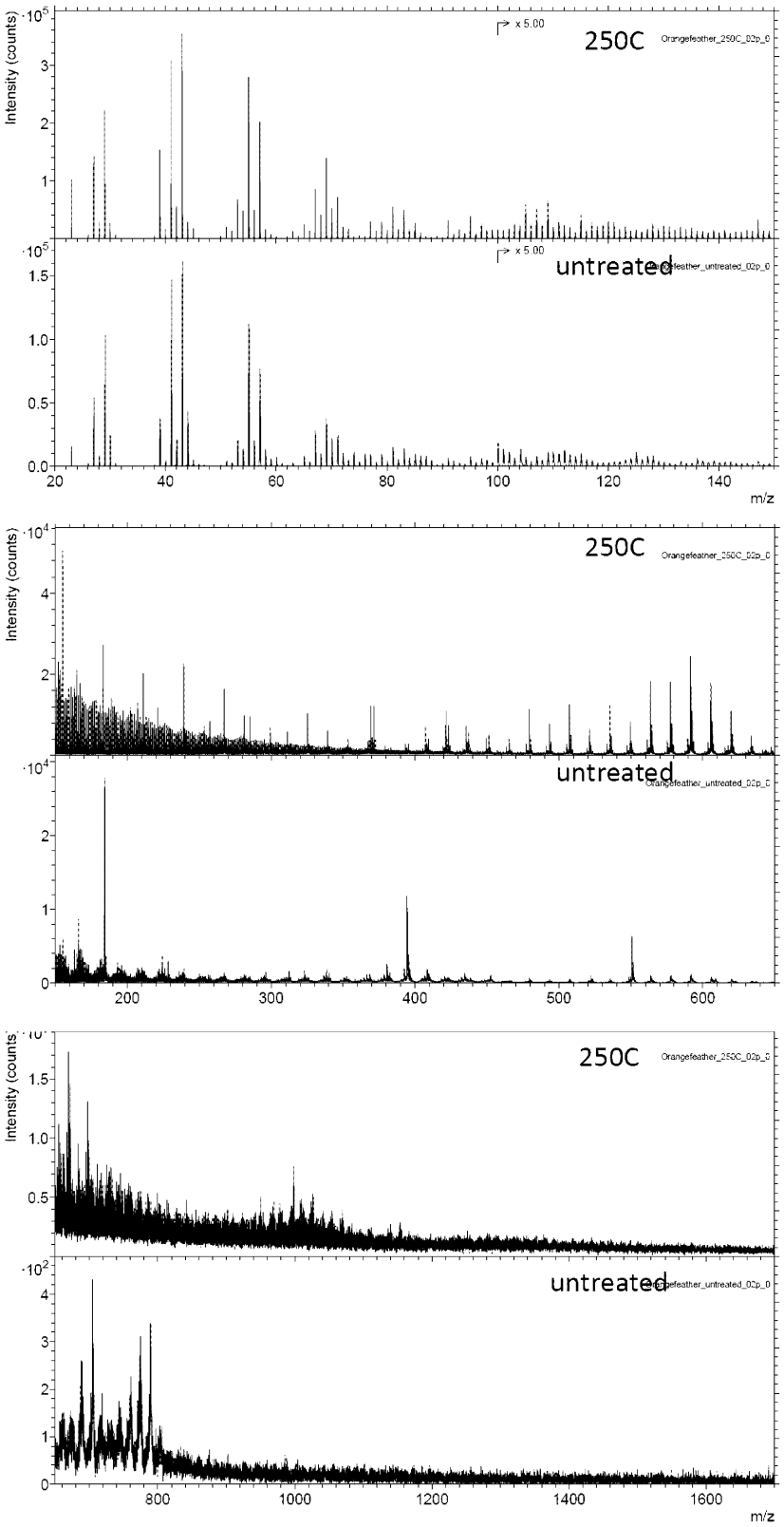


Fig. S4.4 (part 10) *Positive ion ToF-SIMS spectra from melanin extracts of untreated and strongly matured orange feathers from* Gallus gallus*. Matured feathers treated at 250°C for 1 h.*

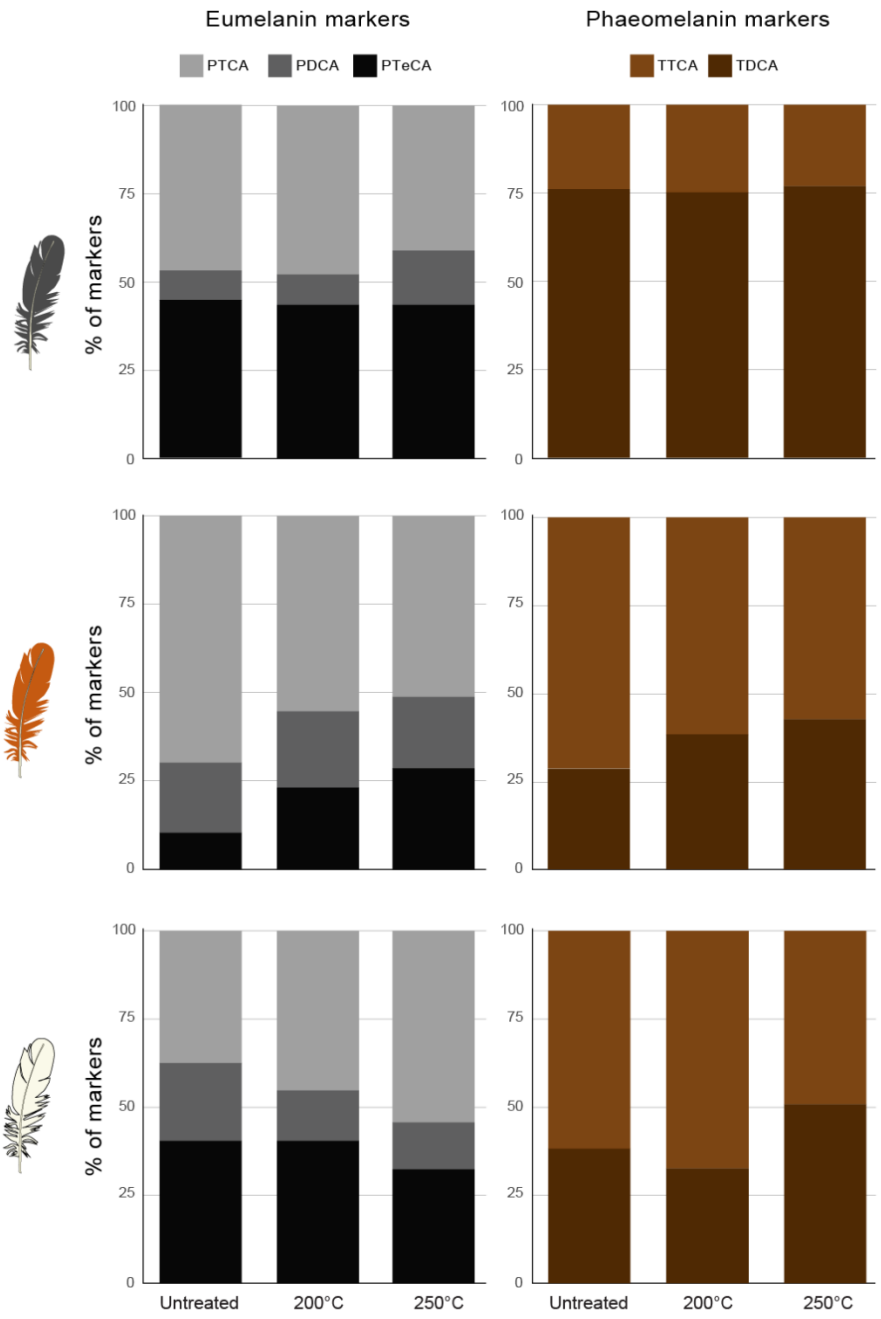


*Fig. S4.5 HCl-AHPO-HPLC data for black, orange and white feathers from extant birds with and without thermal treatment. Melanin markers are derived during chemical degradation via HCl-AHPO. Black and orange feathers are from the domestic chicken (*Gallus gallus*) and white feathers are from the little egret (*Egretta garzetta*). BZ and 4-AHP cannot be analysed following acid treatment.*

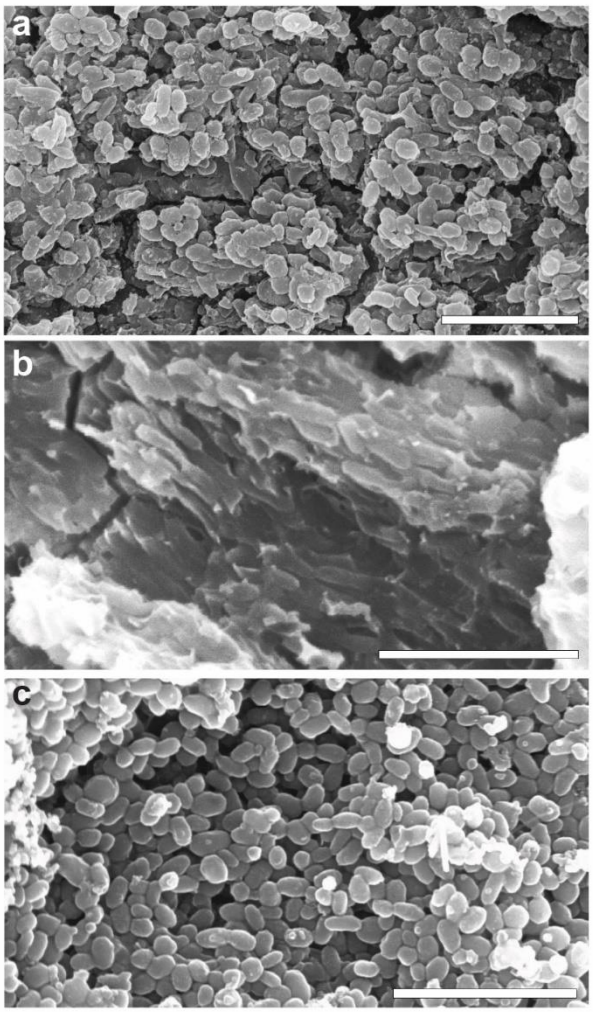


Fig. S4.6 *Scanning electron micrographs of fossil melanosomes in fossil specimens. a* Confuciusornis *(IVPP V 13171). b* Sinornithosaurus *(IVPP V 12811). c* Pelophylax pueyoi *(MNCN 63805), modified from McNamara* et al.[5]*. Scale bars, 5 µm.*

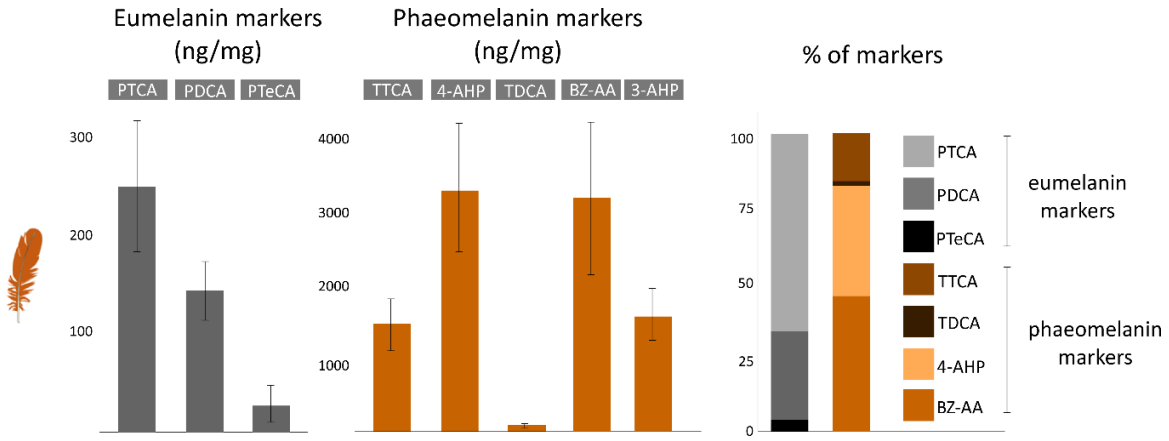


Fig. S4.7 *AHPO- and HI-HPLC data for orange feathers from the common chicken (*Gallus gallus*) matured at 100°C. Eumelanin markers and the phaeomelanin markers TTCA and TDCA are derived during chemical degradation via AHPO. BZ-AA, 3-AHP and 4-AHP are derived during HI hydrolysis.*

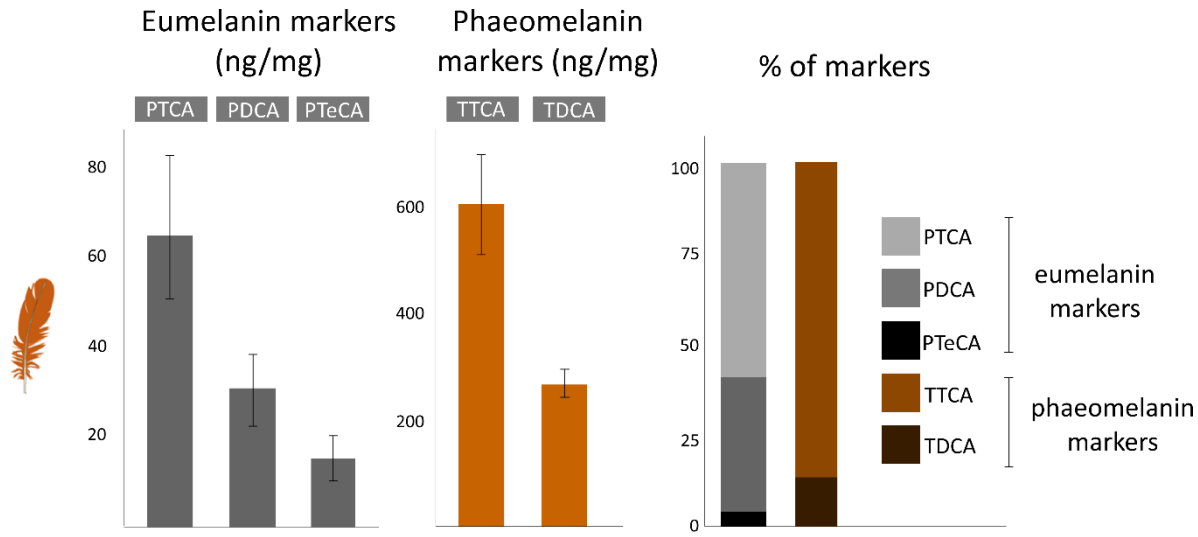


Fig. S4.8 *HCl-AHPO-HPLC data for orange feathers from the common chicken (*Gallus gallus*) matured at 100°C. Melanin markers are derived during chemical degradation via HCl-AHPO. BZ and 4-AHP cannot be analysed following acid treatment.*

Table S4.1 *HPLC-AHPO data for supplementary maturation experiments using orange* Gallus gallus *feathers (n = 3 for experiments with, and without, HCl treatment).*

			(ng/mg)							
Feather type	Treatment	HCl	PTCA	PDCA	TTCA	TDCA	PTeCA	4-AHP	3-AHP	BZ-AA
orange	100°C 1 h	N	249.33 ± 66.91	142.33 ± 29.28	1394.67 ± 257.47	103.8 ± 16.63	23.33 ± 15.4	3319.67 ± 937.05	1392.67 ± 306.78	3352.33 ± 1056.81
orange	100°C 1 h	Y	65.23 ± 19.08	29.27 ± 6.87	607.67 ± 95.21	243.67 ± 28.11	15.47 ± 4.43	n/a	n/a	n/a

1 Jarenmark, M., Sjövall, P., Ito, S., Wakamatsu, K. & Lindgren, J. Chemical evaluation of eumelanin maturation by ToF-SIMS and alkaline peroxide oxidation HPLC analysis. *Int. J. Mol. Sci.* **22,** 161 (2021).

2 Ito, S., Wakamatsu, K., Glass, K. & Simon, J. D. High-performance liquid chromatography estimation of cross-linking of dihydroxyindole moiety in eumelanin. *Anal. Biochem.* **434,** 221–225 (2013).

3 McNamara *et al.* Fossilized skin reveals coevolution with feathers and metabolism in feathered dinosaurs and early birds. *Nat. Commun.* **9,** 2072 (2018).

4 McNamara *et al.* What controls the taphonomy of exceptionally preserved taxa—environment or biology? A case study using frogs from the Miocene Libros Konservat-Lagerstätte (Teruel, Spain). *Palaios* **27,** 63–77 (2012).

5 McNamara *et al.* Soft-tissue preservation in Miocene frogs from Libros, Spain: insights into the genesis of decay microenvironments. *Palaios* **24,** 104–117 (2009).

5. Preservation of corneous beta proteins in Mesozoic feathers

This chapter comprises a paper that is prepared for submission to the journal *Nature.* This chapter is organised as follows: introduction, results and discussion, materials and methods, references and supplementary information.

Candidate contribution to the study. TSS contributed to the design of the study and performed all the experiments. TSS collected and interpreted all S-XANES and FTIR data with assistance. TSS and MNM co-wrote the paper with input from all other authors.

Abstract. Fossil proteins are increasingly valuable tools in evolutionary biology as they can inform on taxonomy[1-3], the innovation of novel tissues[4] and major evolutionary transitions in organismal physiology and ecology[5]. Despite evidence that proteinaceous biomolecules such as collagen can survive for several million years[6], preservation of fossil proteins – or their degraded remnants – on longer timescales is controversial[7]. Fossil keratins (formerly α-keratins) and corneous beta proteins (CBPs; formerly β-keratins) have the potential to yield critical insights into the biomolecular basis of key innovations in the evolution of the vertebrate integument[4, 8]. Reports of CBPs in Mesozoic fossils[4, 9-11], however, conflict with experimental evidence for CBP degradation during fossilization[12-13]. Further, the recent model for molecular modification of feather chemistry during the dinosaur-bird transition does not consider the relative preservation potential of different feather proteins. Here, we use taphonomic experiments to show that feather CBPs can survive thermal maturation. The predominantly β-sheet structure of CBPs, however, is progressively altered to α-helices, suggesting that (α-)keratins and α-helices in fossil feathers are likely artefacts of fossilization. Analysis of fossil feathers demonstrates that this process is independent of geological age, as even Cenozoic feathers comprising β-structures instead show α-helices and disordered structures. As predicted by our experiments, analysis of Mesozoic fossils confirms that evidence of feather CBPs can persist through deep time.

5.1 Introduction

Ancient biomolecules are a powerful source of information on the history of life on Earth[14]. Recent technological advances and better integration of experimental methods[15] have

confirmed the feasibility of biomolecular preservation in deep time[14], yielding essential genetic data for molecular phylogenies[16] and new insights into the timing of key evolutionary transitions[14]. Ancient keratins and CBPs are of particular interest[17] as they define tissue structures that underpin fundamental physiological and ecological strategies and have the potential to inform on the molecular evolution of the vertebrate integument[18]. CBPs are fibrous proteins that, unlike keratins, are rich in the amino acid cysteine. Cysteine promotes extensive cross-linking, and thus confers chemical stability, via disulfide bonds[19]. Feathers in extant birds comprise primarily CBPs[20] (in β-sheet conformation), with minor keratins (with α-helix structure)[21]. Surprisingly, recent studies of feathers from a Jurassic dinosaur[4] and pterosaur[22] have reported a composition dominated by keratins. This has been interpreted as evidence for the posited evolutionary transition[4] between archaic keratin-dominated and CBP-dominated states, but that hypothesis assumes that the original chemistry has not been altered during fossilization[22]. Testing this requires analysis of the molecular alteration of CBP architecture through controlled laboratory experiments in tandem with rigorous taphonomic analysis of fossils[23]. A key unknown is whether the secondary and tertiary structure (defined by interactions between neighbouring CO and NH groups, and amino acid R-groups, respectively) of feather CBPs can survive diagenesis is unknown. Here we resolve this issue using taphonomic experiments based on thermal maturation of feathers from extant birds coupled with data from fossils. We used micro-FTIR and sulfur X-ray spectroscopy to probe the secondary and tertiary structure of feather CBPs. Our results confirm that α-helix conformations (which characterise keratins) in thermally matured feathers are an artefact of maturation. Chemical data from fossil feathers are consistent with our experimental results: fossils that underwent stronger thermal maturation show α-helix-dominated compositions, independent of geological age. Conversely, evidence of β-sheets (characteristic of CBPs) can persist in older fossils that are less thermally matured.

5.2 Results and discussion

5.2.1 Sulfur chemistry reveals degradation of cysteine and CBP tertiary structure

We degraded black feathers from *Gallus gallus* and white feathers from *Egretta garzetta* at 200°C or 250°C in controlled laboratory conditions designed[24] to simulate thermal

maturation during burial while retaining tissue macrostructure, as in our target fossil feathers. Most reports of fossil feather ultrastructures include melanosomes[4,9,22] (organelles rich in melanin *in vivo*) and thus melanin-rich black feathers are the most appropriate analogues for fossils; white feathers are effectively a melanin-free control.

Sulfur X-ray absorption near-edge spectroscopy (XANES) analyses show that spectra for untreated feathers are dominated by a strong broad sulfide peak that can be further resolved into peaks for cystine (disulfide; S-S) and cysteine (thiol; S-H) centred at 2472.92 and 2474.12eV, respectively (Fig. 5.1). The cystine peak is strong in white and especially black feathers. Spectra for both feather colours also show a weak, broad peak for cysteic acid (centred at 2480.92 eV; sulfoxide; S=O) and a weak shoulder for benzothiazole (centred at 2476 eV; S-heterocycle)[25].

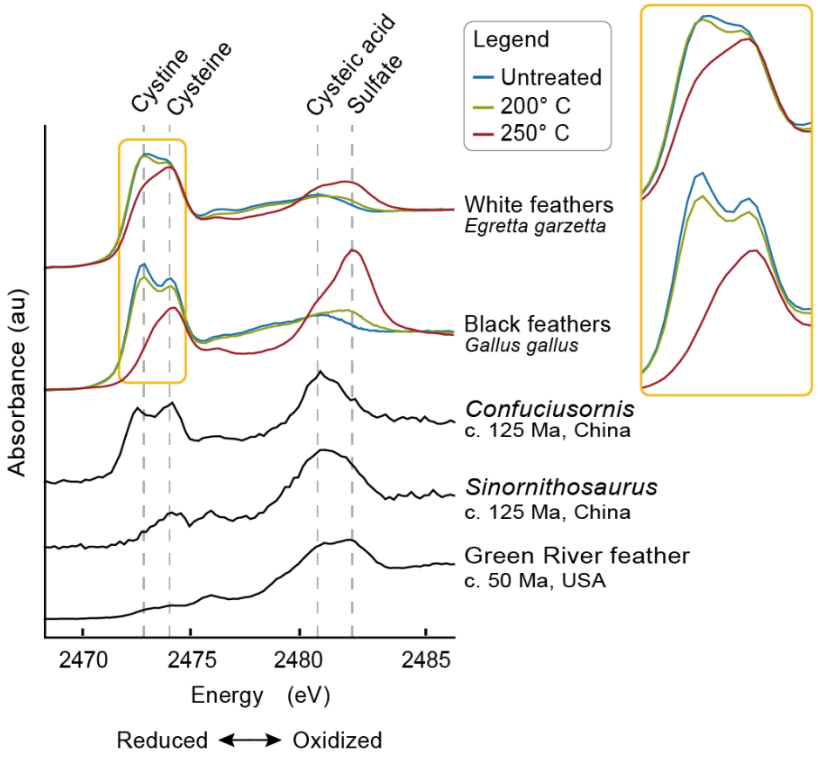


Fig. 5.1 *Sulfur-XANES spectra for fossil feathers and untreated and experimentally degraded white (*Egretta garzetta*) and black (*Gallus gallus*) feathers.*

Following "moderate" maturation at 200°C, spectra for both feather colours closely resemble those of untreated feathers, albeit with a slight reduction in the intensity of the cystine and cysteine peaks and, in black feathers, appearance of a weak broad organic

sulfate (SO_4^{-2}) band (centred at 2482.12–2482.27 eV). In contrast, spectra for "strongly" matured feathers (the 250°C experiment) show a broad peak that incorporates cysteic acid (centred at 2481.12 eV) and, especially in black feathers, organic sulfate (centred at 2482.42 eV). Spectra retain a moderately intense cysteine peak and weak benzothiazole shoulder. The XANES data therefore show a general trend for a transition from reduced (cystine and cysteine) to more oxidised (cysteic acid and sulfate) sulfur species during progressive thermal maturation. Given that CBP disulfide bonds require cystine, which in turn comprises two cysteine moieties, loss of these reduced sulfur species during maturation indicates degradation of CBP tertiary structure.

5.2.2 FTIR reveals degradation of amides and CBP β-sheets

FTIR spectra of untreated feathers are dominated by peaks for amide functional groups, i.e., amides A, B, I, II and III; these bands are the focus of our results (Fig. 5.2 and Supplementary data Table 5.1). All untreated spectra are dominated by amide I (1575–1700 cm^{-1}) and II (1475–1575 cm^{-1}) peaks, with moderate amide A (3115–3360 cm^{-1}) and III (1210–1295 cm^{-1}) peaks and a weak amide B (3015–3115 cm^{-1}) peak. Black feathers show higher absorption than white feathers for all amide bands; the two feather types show substantial differences for peak position only for amides A and II.

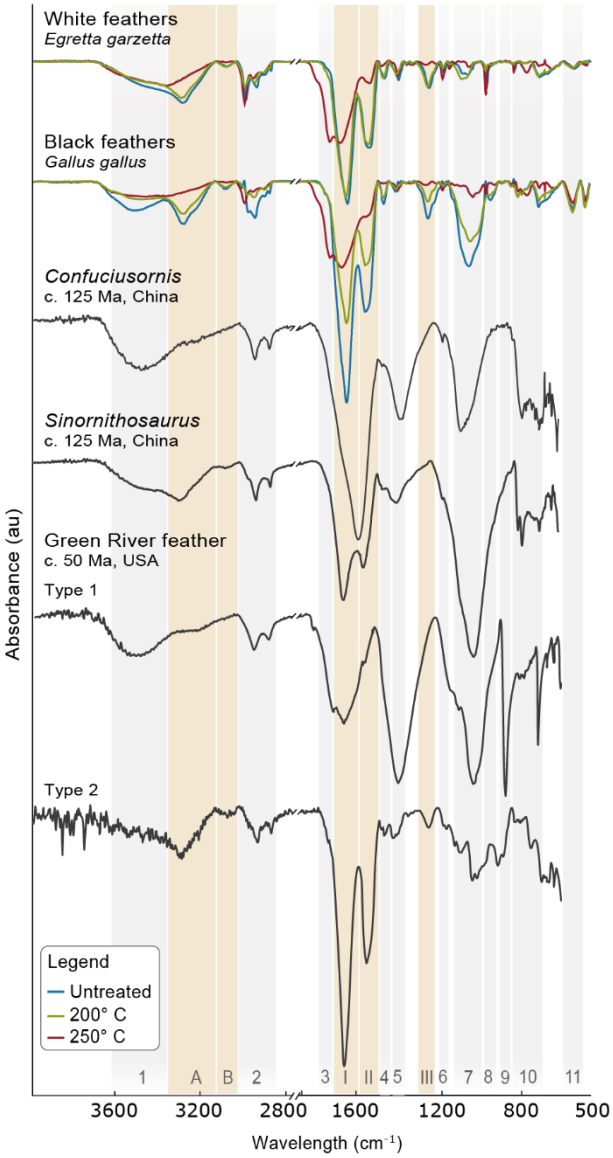


*Fig. 5.2 FTIR spectra for fossil feathers and untreated and experimentally degraded white (*Egretta garzetta*) and black (*Gallus gallus*) feathers. Amide bands are indicated in brown boxes and all other bands in grey boxes.*

Spectra for moderately matured feathers are near-identical to untreated feathers. In contrast, strongly matured feathers lack amides A and B and instead show a new strong peak at ca. 1710 cm^{-1} (band 3). As in untreated feathers, the peak position for amide I is similar in both black and white feathers after strong maturation, albeit shifted to higher wavenumbers; a similar trend characterises changes in amide III. The peak position for amide II is similar in untreated and strongly matured black feathers but shifts to higher wavenumbers for white feathers. These changes in amide peak position likely reflect changes in stereochemistry of the amide local environment.

Deconvolution of the interval encompassing amide I and II in FTIR spectra (1715–1480 cm^{-1}) of untreated feathers reveals peaks corresponding to β-sheets (1495–1496, 1612–1625 and 1626–1641 cm^{-1}; bands i, v and vi), β-turns (1563–1568 and 1670–1684 cm^{-1}; bands iv and ix), α-helices (1531–1561 and 1651–1661 cm^{-1}; bands iii and viii) and random coil structures (1508–1512 cm^{-1}; band ii; Fig. 5.3a, b and Supplementary data Table 5.2).

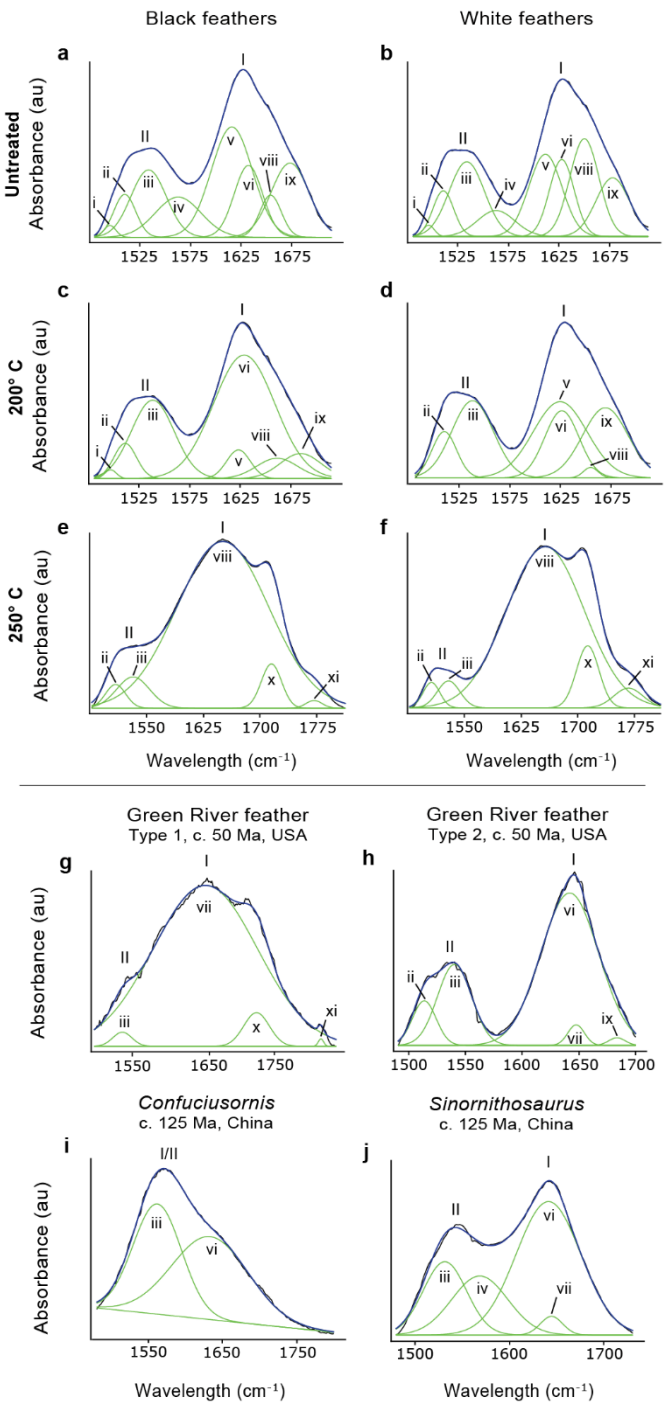


Fig. 5.3 *Deconvoluted amide I and II regions from FTIR data for fossil feathers and untreated and experimentally degraded white (*Egretta garzetta*) and black (*Gallus gallus*) feathers. a – f, feathers from extant birds. a, untreated black feathers. b, untreated white feathers. c, black feathers matured at 200°C. d, white feathers matured at 200°C. e, black feathers matured at 250°C. f, white feathers matured at 250°C. g – j, fossil feathers. g, h, Green River feather (YPM VP 58657). i,* Confuciusornis *(IVPP V 13171). j,* Sinornithosaurus *(IVPP V 12811). Black, processed spectra; green, resolved peaks; blue, deconvolution fit.*

Spectra for black feathers are dominated by the peak for β-sheets in band v (Fig. 5.3a), whereas spectra for white feathers exhibit moderately large peaks in all bands except i and iv, which are weak (Fig. 5.3b). Full width at half maximum (FWHM) measurements indicate that untreated feathers comprise primarily β-structures (black: 67.7%; white: 62.2%) with minor α-helices (black: 23.3%; white: 28.6%).

Following moderate maturation, deconvolution of the amide I+II region reveals that black feather spectra retain a dominant peak for β-sheets (now band vi; Fig. 5.3c and Supplementary data Table 5.2) but lack the peak in band iv for β-turns. All other peaks identified in untreated feathers are present, although peaks in bands v (β-sheets), viii (α-helix) and ix (β-turns) are weaker. Spectra for moderately matured white feathers are similar to untreated examples, although peaks i and iv are absent and peak viii, weaker (Fig. 5.3d). FWHM measurements for black feathers indicate a decrease in β-structure content (black: 56.4%) and increase in α-helix content (black: 34.3%). In contrast, white feathers exhibit near-identical β-structure content (62.4%) to untreated white feathers.

Strong maturation induces major changes in feather amide chemistry. Spectra for black and white feathers are broadly similar; the amide I+II region (now 1815–1480 cm^{-1}) lacks peaks for β-structures and instead is dominated by a peak for α-helices (band viii; Fig. 5.3e, f). Moderate peaks include those for random coil structures, α-helices and C–O bonds in bands ii, iii and xi, respectively, with a weak peak for C–O bonds in band xi. These changes correspond to a substantial increase in α-helix content (black: 69% α-helix; white: 59.6% α-helix).

5.2.3 Degradation of CBP secondary structure

Collectively, the FTIR data reveal dramatic changes in feather amide chemistry. Irrespective of feather colour, degradation is characterised at lower temperatures primarily by loss of β-turns, and at higher temperatures by substantial reduction of amide band intensity, complete loss of β-structures, and dominance of α-helices. Random coil structures (a relatively minor component) persist without dramatic reduction in intensity even after strong maturation. Comparison of relative peak heights indicates higher abundance of α-

helices in strongly degraded, rather than untreated, feathers. The dominance of α-helices in spectra for strongly matured feathers cannot, therefore, solely be explained by the survival of residual α-helix moieties (present as minor components in untreated feathers). Degradation of feather CBPs likely occurs via a multi-step process, whereby loss of β-turns (and probably H-bonding between pleated β-strands in the β-sheet (see Fig. 5.4 for details of protein structure)) facilitates reconfiguration of β-strands into an α-helix conformation. The S-XANES data support this model: the survival of cysteine in strongly matured feathers is consistent with the persistence (as evident in FTIR spectra) of cysteine-rich random coil structures[26]. Despite this, the loss of cystine (in strongly matured black feathers) indicates loss of disulfide bridges in the CBP tertiary structure and thus degradation of CBP β-bundles, β-filaments, dimers and/or β-sheets.

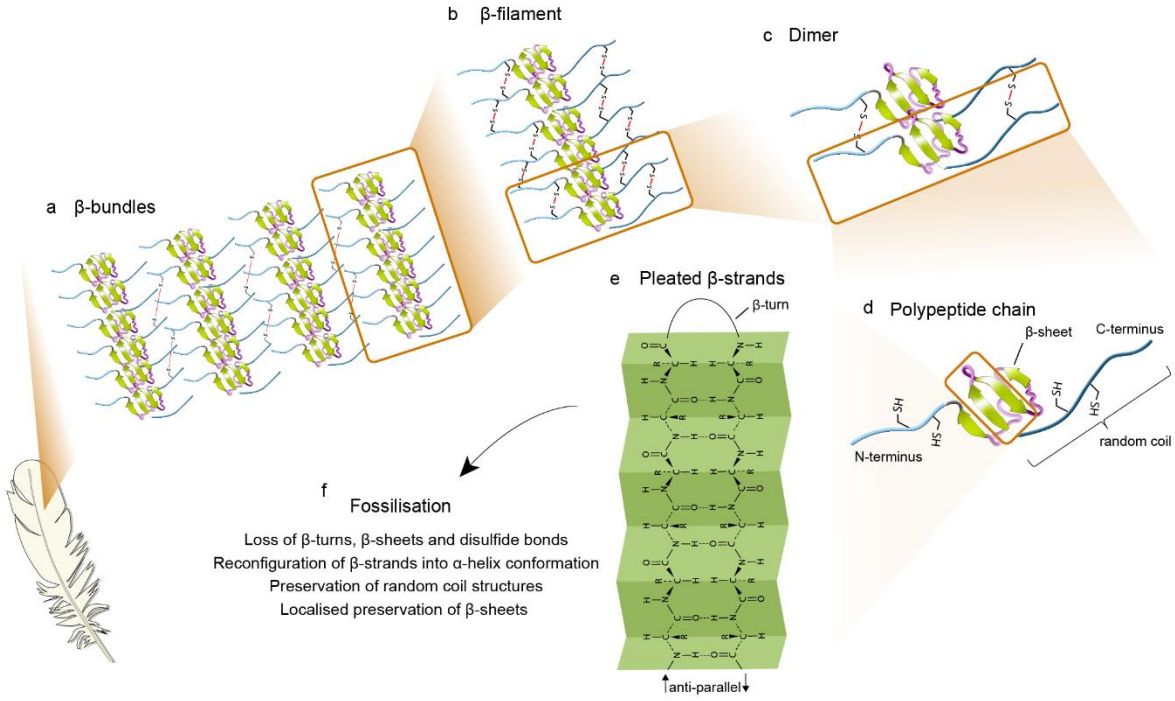


Fig. 5.4 *Schematic representation of the hierarchical structure of feather corneous beta proteins (CBPs). Disulfides can occur in four component structures: β-bundles, β-filaments, dimers and β-sheets. Limited data are available on the orientation of β-strands in CBPs (but see[29]).*

Our experimental data inform interpretations of the fidelity of preservation of fossil feathers. Similar to our strongly matured feathers, S-XANES spectra for a feather from the Eocene Green River biota (Wyoming, USA) feather show a broad band (spanning 2481–2482.4 eV) representing cysteic acid and organic sulfate (Fig. 5.1 and Supplementary data Fig. 5.1). FTIR data reveal heterogeneous preservation. "Type 1" spectra resemble those of strongly matured feathers (i.e., peaks within bands 3, I and II; Fig. 5.2 and Supplementary data Table 5.1): disordered structures dominate (1644 cm^{-1}), with weak peaks for α-helices (1536 cm^{-1}) and no β-structures (Fig. 5.3g and Supplementary data Table 5.2). Type 2 spectra resemble those of untreated or moderately matured feathers (i.e., peaks for amides A, B, I, II and III; Fig. 5.2): β-sheet structures dominate (1641 cm^{-1}), with moderate peaks for α-helices (1539 cm^{-1}) and random coil structures (1512 cm^{-1}) and weak peaks for disordered (1647 cm^{-1}) and β-turn (1683 cm^{-1}) structures (Fig. 5.3h). In contrast, S-XANES spectra for feathers from *Confuciusornis* (Jehol biota, Cretaceous, NE China) show strong, distinct peaks for cystine and cysteine and especially cysteic acid. FTIR spectra for *Confuciusornis* show a strong peak centred between bands I and II (Fig. 5.2); deconvolution of this peak reveals a dominant β-sheet composition (61.3%; 1633 cm^{-1}) with α-helices (38.7%; 1561 cm^{-1}; Fig. 5.3i). S-XANES spectra for *Sinornithosaurus* (Jehol biota, Cretaceous, NE China) show an intermediate composition: they are dominated by cysteic acid with contributions from organic sulfate, and the weak peaks at 2472.92 and 2476 eV likely represent cysteine and benzothiazole, respectively (Fig. 5.1). FTIR spectra for *Sinornithosaurus* show moderate peaks within bands I and II. Deconvolution of the amide region reveals a strong peak for β-sheets (1641 cm^{-1}), moderate peaks for α-helices (1531 cm^{-1}) and β-turns (1568 cm^{-1}) and a weak peak for disordered structures (1644 cm^{-1}). S-XANES spectra for the host sediment for *Sinornithosaurus* and *Confuciusornis* show strong peaks only for sulfate (Supplementary data Fig. 5.2); the spectra for the Green River sediment resemble the spectra for the Green River feather. FTIR spectra for the sediment for the Green River feather are dominated by peaks for C–H, C–O, S–O and/or S=O and contain a very weak peak within amide band I (Supplementary data Fig. 5.3 and Table 5.1). Spectra for the sediment for both fossils from the Jehol biota are similar and dominated by peaks for C–H, C–O, S–O, S=O, C=S and C–C with a very weak peak within amide band I.

This indicates that the fossil feathers are chemically distinct to their respective sedimentary matrices and thus the chemistry of the fossils is endogenous.

These fossil data are consistent with our experimental results but not with previously reported data for *Anchiornis*. The evolutionary model proposed by Pan et al. suggests that *Anchiornis* retains an archaic state for feather chemistry, whereby the feathers comprise primarily keratins (that in turn comprise predominantly α-helix structures)[4]. Phylogenetically more basal taxa should also share this archaic state. Our data, however, show that the feathers of *Sinornithosaurus* (which is basal to *Anchiornis*[22, 27]) comprise primarily β-structures indicative of CBPs. It is unlikely that this composition reflects independent origins of modern feather chemistry (i.e. dominated by feather CBPs) within *Sinornithosaurus* and Avialae. Instead, our experimental data suggest that the keratin-dominated composition of feathers in *Anchiornis* is a taphonomic artefact resulting from thermally-induced alteration of an original β-sheet-rich CBP composition, not an original keratin-dominated state. The chemistry, and thus mechanical properties, of *Anchiornis* feathers were likely already similar to those of extant birds. Our data from other fossil feathers support this hypothesis. In particular, the dominance of α-helix structures (and absence of β-sheets) in spectra from the Green River feather cannot readily be explained using the "archaic α-helix" hypothesis, given that this fossil specimen is younger and from a more derived taxon. Our experiments demonstrate, however, that the most parsimonious explanation for the chemistry of the Green River feather is diagenetic alteration during fossilization. This is supported by the thermal maturation history of the Green River Formation, which is considered to incorporate strong thermal maturation[28].

Our data show that evidence of CBPs can survive in fossil feathers through deep time. Such fossil specimens are thus a rich source of data on the evolution of terrestrial vertebrates and their ecology, providing that data from preserved soft tissues are examined using a taphonomic framework. It is therefore critical that interpretations of the palaeoecology of ancient organisms based on biomolecular data are informed by a holistic understanding of how the fossilization process biases the record of ancient biomolecules and other soft tissue characters.

5.3 Materials and methods

5.3.1 Fossil specimens

This study used an isolated feather (YPM VP 58657) from the Green River Formation (Middle Eocene, USA) and specimens from the Jehol biota (Early Cretaceous, NE China). The latter include a complete specimen (IVPP V 13171) of *Confuciusornis* and a specimen of *Sinornithosaurus* (IVPP V 12811; Supplementary data Fig. 5.1). Institutional abbreviations: IVPP, Institute of Vertebrate Paleontology and Paleoanthropology; YPM, Yale Peabody Museum of Natural History.

5.3.2 Feathers from extant birds

Freshly shed black (*n* = 3) contour feathers from the domestic chicken, *Gallus gallus domesticus*, and white (*n* = 3) primary feathers from the little egret, *Egretta garzetta*, were stored at -80°C prior to experimental treatment. Feathers were sampled according to experimental and analytical needs as described below.

5.3.3 Justification for experimental design

Our goal is to critically assess the preservation potential of feather CBPs using an experimental taphonomic framework. Analysis of experimentally degraded feathers using spectroscopic techniques yields a taphonomic dataset that can be compared to data from fossil feathers. Our experiments were designed specifically to generate appropriate analogues for our target fossil feathers, i.e. thermally matured feathers retaining gross tissue macrostructure (details of rachis, barbs and barbules). Taphonomic experiments require the use of conditions that generate chemical and/or morphological phenomena that are comparable to those preserved in the fossils of interest[23]. There is, however, debate regarding the most appropriate conditions for experimental maturation of feathers. Previous experiments used relatively extreme conditions (up to 250°C/250 bar/24 h) that resulted in liquefaction and partial vaporization of feathers[12, 13]. We do not consider these to represent a valid analogue for fossil feathers, most of which retain (and are identified as feathers on the basis of) several important diagnostic macroscopic and/or

microscopic structures such as rachis, barbs, barbules and melanosomes[9, 30]. Selection of experimental conditions that guarantee survival of these structures is therefore critical to our experiments. Our taphonomic experiments therefore used temperatures of either 200°C or 250°C (similar to those of certain previous experimental studies[24, 31]) that are known to retain gross feather structure.

5.3.3 Maturation experiments

Samples (ca. 10 mm^2) of untreated black and white feathers were wrapped in Al foil and matured in a standard laboratory convection oven at 200°C ± 1°C or 250°C ± 1°C.

5.3.4 X-Ray Absorption Near Edge Structure (XANES) Spectroscopy

Small samples (≥3 mm^2) of untreated and experimentally degraded feathers in addition to fossil material and samples of host sediment were were placed on low-sulfur tape and analyzed at the Stanford Synchrotron Radiation Lightsource (SSRL) using synchrotron X-ray absorption near-edge spectroscopy (XANES) at beam line 6-2. S-XANES data were collected in fluorescence mode using a single element Vortex silicon drift detector set at a scattering angle of ~60°. A $Na_2S_2O_3$ standard with a pre-edge peak at 2472.02 eV was used to calibrate the energy of the monochromator position. Three locations per each sample of feather tissue from extant birds were selected for analysis, yielding a total of nine spectra for each treatment. Multiple locations on each fossil were analysed, yielding 3 spectra for each of the fossil organics and 1 spectrum of the associated sediment; the *Confuciusornis* data, however, results from an individual spectrum. S-XANES standards for selected S-bearing compounds, representing different sulfur species, were prepared by mixing commercially available analytical standards (Sigma Aldrich; ≥98% pure) with BN to obtain a sulfur concentration of ca. 5 wt% in each standard. Data alignment, averaging, background subtraction and normalisation were performed using Athena v. 0.9.26[32].

XANES is a semi-quantitative technique whereby peak intensity indicates the relative abundance of one or more oxidation states for an element of interest. S-XANES is highly informative as it can identify any disulfide moieties present that potentially derive from cysteine. The S-XANES spectra presented here include peaks for cystine (2472.92 eV),

cysteine (2474.12 eV), cysteic acid (2480.92–2481.12 eV) and/or organic sulfate (2482.12–2482.42 eV)[25]. Similar to cysteine, benzothiazole sulfur has an excitation energy of 2474.12 eV and can be observed in spectra only via the presence of a shoulder feature at 2476 eV[25]. For details on the white line energies (i.e., the energy corresponding to the first sharp peak in a XANES spectrum) for analytical standards of selected S-bearing compounds see Supplementary data Fig. 5.4 and Table 5.3.

5.3.5 Fourier Transform Infrared (FTIR) Spectroscopy

Fossil feathers and feathers from extant taxa were analyzed using FTIR. Fossil data were collected in the 4000–600 cm^{-1} range using a PerkinElmer Frontier FTIR spectrometer fitted with a Spotlight 400 microscope. Each spectrum was collected as an average of 8–36 scans. Multiple locations on each fossil were selected for analysis, yielding 4 spectra for fossil organics and sediment; type 2 of the Green River data, however, results from an individual spectrum.

Spectra for untreated and matured feathers were collected in the 4000–500 cm^{-1} range using a universal diamond ATR accessory on the Frontier spectrometer. Given an estimated penetration depth of 2.13 μm for the diamond/KRS-5 crystal it is likely that the FTIR signal captures the entire thickness of the fossil soft tissues (Supplementary data Fig. 5.5 and Table 5.4). Each spectrum was collected as an average of 10 scans. Three locations per each of three replicates per treatment were selected for analysis, yielding a total of nine spectra for each treatment. Absorption of the diamond crystal in the region 2300–1900 cm^{-1} (which does not overlap with the region of interest in this study, i.e. the amide region) was removed. Each spectrum was baseline-corrected using SpectraGryph v. 1.2.7 using the parameters adaptive correction, 15% coarseness and no offset[33]. In addition, interactive baseline correction was performed on data in the region 898–450 cm^{-1} using Spectrum IR v. 10.6.1 (PerkinElmer, USA). This ensured a consistent baseline across the entire scan range to facilitate spectral comparison. Baseline correction can be associated with a very minor shift of up to a few cm^{-1} in the precise position of peaks. Given that any such potential shift is much less (in many cases an order of magnitude less) than the separation between key peaks analysed here, we do not consider any shifts induced by

baseline correction to have introduced error or bias to our data. Each spectrum was standardized to remove sample thickness effects.

FTIR identifies functional groups within a sample via the excitation of bonds by infrared radiation at characteristic wavelengths. Amides are components of proteins and are reflected in spectra primarily via peaks for amide I, II, III, A and/or B. Amide I (1627–1655 cm^{-1}) corresponds largely to C=O stretching whereas amide II (1522–1539 cm^{-1}) reflects mainly N–H bending vibrations; amide III (1232–1239 cm^{-1}) is produced by C–N stretching (bands I, II and III in Fig. 5.2 and Table 5.1). Amides A and B (3267–3281 and 3063–3064 cm^{-1}, respectively) are attributed to the absorption of the N–H stretching vibration (bands A and B in Fig. 5.2 and Table 5.1). Peaks within bands 1, 2, and 4–11 are less informative on amide chemistry and details on their assignment are included in the Supplemental Information.

5.3.6 FTIR deconvolution

Deconvolution was performed on the amide I and II region (1715–1480 cm^{-1} for untreated feathers and feathers matured at 200°C and 1815–1480 cm^{-1} for feathers matured at 250°C) in Origin(Pro) v. 2019b software (OriginLab Corporation, Northampton, MA, USA) to test whether variations in band height and/or shape among experimental treatments reflect differences in protein secondary structure. Deconvolution of spectra for experimentally treated samples was used to compare data from fossil feathers. The spectral range used for deconvolution of fossil feather data varied among spectra (Green River feather type 1: 1815–1500 cm^{-1}; Green River feather type 2: 1700–1490 cm^{-1}; *Confuciusornis*: 1800–1480 cm^{-1}; *Sinornithosaurus*: 1730–1480 cm^{-1}). Peak assignments were made by comparison with the literature[34-36]. Unequivocal structural assignments are difficult to make for peaks within the amide II region and thus some caution is required when assigning structure to peaks (i) and (iii) in our dataset. This, however, does not impact our major results as such peaks are either absent or a minor component of spectra for all treatments. It is possible that our deconvolution includes contributions from amino side chains[37] but these are likely to be minor. Amide I and II bands can consist of peaks attributed to β-sheets (1495–1496, 1612–1625, 1626–1641 and 1641 cm^{-1}), β-turns (1563–1568 and 1670–1684 cm^{-1}), α-helices (1531–1561 and 1651–1661 cm^{-1}), random

coils (1508–1512 cm^{-1}), disordered structures (1644–1647 cm^{-1}) , and C–O (1711 and 1772–1795 cm^{-1}). The percentage of β-structures (the sum of percentage values for β-sheets and β-turns) and α-helices in each feather colour and treatment was calculated using FWHM values.

Acknowledgments. We thank Sharon Bone, Valentina Rossi, Chris Rogers, Thomas Clements, Luke McDonald and Naomi O'Reilly for assistance. This work was supported by ERC Starting Grant H2020-ERC-2014-StG-637691-ANICOLEVO awarded to M.E.M. The use of the Stanford Synchrotron Radiation Lightsource, SLAC National Accelerator Laboratory, is supported by the US Department of Energy, Office of Science, Office of Basic Energy Sciences under contract no. DE-AC02-76SF00515 awarded to M.E.M.

Author contributions. M.E.M. conceived the research and designed the study with T.S.S. T.S.S. and M.E.M. performed S-XANES and FTIR analyses. N.P.E. and S.W. assisted with S-XANES data collection. T.S.S. and M.E.M. wrote the manuscript with input from all other authors.

5.4 References

1. Buckley, M., Collins, M., Thomas-Oates, J., & Wilson, J.C. Species identification by analysis of bone collagen using matrix-assisted laser desorption/ionisation time-of-flight mass spectrometry. *RCM* **23**, 3843–3854. doi:10.1002/rcm.4316 (2009).
2. Buckley, M. Ancient collagen reveals evolutionary history of the endemic South American 'ungulates'. *Proc Royal Soc B* **282**, 20142671. doi:10.1098%2Frspb.2014.2671 (2015).
3. Buckley, M. *et al.* Collagen sequence analysis of the extinct giant ground sloths *Lestodon* and *Megatherium*. *PLoS One* **10**, e0139611. doi:10.1371/journal.pone.0139611 (2015).
4. Pan, Y. *et al*. The molecular evolution of feathers with direct evidence from fossils. *PNAS* **116**, 3018–3023. doi: 10.1073/pnas.1815703116 (2019).
5. McNamara, M. *et al*. Decoding the evolution of melanin in vertebrates. *Trends Ecol* **35**, 430–443. doi:10.1016/j.tree.2020.12.012 (2021).

6. Buckley, M., Lawless, C., & Rybczynski, N. Collagen sequence analysis of fossil camels, Camelops and cf Paracamelus, from the Arctic and sub-Arctic of Plio-Pleistocene North America. *J Proteomics* **194**, 218–225. doi:10.1016/j.jprot.2018.11.014 (2019).
7. Saitta, E.T. *et al.* Low fossilization potential of keratin protein revealed by experimental taphonomy. *Palaeontology* **60**, 547–556. doi:10.1111/pala.12299 (2017).
8. Maderson, P.F., & Alibardi, L. The development of the sauropsid integument: a contribution to the problem of the origin and evolution of feathers. *Am Zool* **40**, 513–529. doi:10.1093/icb/40.4.513 (2000).
9. Pan, Y. *et al.* Molecular evidence of keratin and melanosomes in feathers of the Early Cretaceous bird *Eoconfuciusornis*. *PNAS* **113**, E7900–E7907. doi:10.1073/pnas.1617168113 (2016).
10. Schweitzer, M. *et al.* Beta-keratin specific immunological reactivity in feather-like structures of the Cretaceous Alvarezsaurid, Shuvuuia deserti. *J Exp Zool* **285**, 146–157. (1999).
11. Schweitzer, M.H. *et al.* Keratin immunoreactivity in the Late Cretaceous bird *Rahonavis* ostromi. *J Vertebr Paleontol* **19**, 712–722. doi:10.1080/02724634.1999.10011183 (1999).
12. Saitta, E.T., Kaye, T.G., & Vinther, J. Sediment-encased maturation: a novel method for simulating diagenesis in organic fossil preservation. *Palaeontology* **62**, 135–150. doi:10.1111/pala.12386 (2018).
13. Saitta, E.T., Rogers, C.S., Brooker, R.A., & Vinther, J. Experimental taphonomy of keratin: a structural analysis of early taphonomic changes. *Palaios* **32**, 647–657. doi:10.2110/palo.2017.051 (2017).
14. Briggs, D.E., & Summons, R.E. Ancient biomolecules: their origins, fossilization, and role in revealing the history of life. *BioEssays* **36**, 482–490. doi:10.1002/bies.201400010 (2014)
15. Cappellini, E. *et al*. Ancient biomolecules and evolutionary inference. *Annu Rev Biochem* **87**, 1029–1060. doi:10.1146/annurev-biochem-062917-012002 (2018).
16. Buckley, M. Paleoproteomics: An Introduction to the Analysis of Ancient Proteins by Soft Ionisation Mass Spectrometry. In *Paleogenomics* (eds. Lindqvist, C., & Rajora, O. P.) 31–52 (Springer Switzerland, 2018).

17. Briggs, D.E., Evershed, R.P., & Lockheart, M.J. The biomolecular paleontology of continental fossils. *Paleobiology* **26**, 169–193. doi:10.1017/S0094837300026920 (2000).
18. Zhou, Z. Dinosaurs: what discoveries are truly revolutionary? *Curr Biol* **29**, R720–R722. (2019).
19. Wang, B., Yang, W., McKittrick, J., & Meyers, M.A. Keratin: structure, mechanical properties, occurrence in biological organisms, and efforts at bioinspiration. *Prog Mater Sci* **76**, 229–318. doi:10.1016/j.pmatsci.2015.06.001 (2016).
20. Holthaus, K.B., Eckhart, L., Dalla Valle, L., & Alibardi, L. Evolution and diversification of corneous beta-proteins, the characteristic epidermal proteins of reptiles and birds. *J Exp Zool* **330,** 438–453. doi:10.1002/jez.b.22840 (2018).
21. Alibardi, L. Cornification, morphogenesis and evolution of feathers. *Protoplasma* **254**, 1259–1281. doi:10.1007/s00709-016-1019-2 (2017).
22. Yang, Z. *et al*. Pterosaur integumentary structures with complex feather-like branching. *Nat Ecol Evol* **3**, 24–30. doi:10.1038/s41559-018-0728-7 (2019).
23. Purnell, M.A. *et al.* Experimental analysis of soft-tissue fossilization: opening the black box. *Palaeontology* **61**, 317–323. doi:10.1111/pala.12360 (2018).
24. McNamara, M.E., Briggs, D.E., Orr, P.J., Field, D.J., & Wang, Z. Experimental maturation of feathers: implications for reconstructions of fossil feather colour. *Biol Lett* **9**, 20130184. doi:10.1098/rsbl.2013.0184 (2013).
25. Edwards, N.P. *et al.* Elemental characterisation of melanin in feathers via synchrotron X-ray imaging and absorption spectroscopy. *Sci Rep* **6**, 34002. doi:10.1038/srep34002 (2016).
26. Fraser, R., MacRae, T., & Rogers, G.E. *Keratins: Their Composition, Structure and Biosynthesis*. (Springfield, Thomas, 1972).
27. Pei, R. *et al.* Powered flight potential approached by wide range of close avian relatives but achieved selectively. Preprint at https://www.biorxiv.org/content/10.1101/2020.04.17.046169v1 (2020).
28. Nuccio, V.F., & Roberts, L.N. Thermal Maturity and Oil and Gas Generation History of Petroleum Systems in the Uinta-Piceance Province, Utah and Colorado. In *Petroleum Systems and Geologic Assessment of Oil and Gas in the Uinta–Piceance Province, Utah and Colorado* (ed. USGS Uinta-Piceance Assessment Team) Ch. 4 (U.S. Geological Survey, Denver, 2003).

29. Calvaresi, M., Eckhart, L., & Alibardi, L. The molecular organization of the beta-sheet region in corneous beta-proteins (beta-keratins) of sauropsids explains its stability and polymerization into filaments. *J Struct Biol* **194**, 282–291. doi:10.1016/j.jsb.2016.03.004 (2016).
30. Wogelius, R. *et al.* Trace metals as biomarkers for eumelanin pigment in the fossil record. *Science* **333**, 1622–1626. doi:10.1126/science.1205748 (2011).
31. Slater, T.S. *et al.* Taphonomic experiments resolve controls on the preservation of melanosomes and keratinous tissues in feathers. *Palaeontology* **63**, 103–115. doi:10.1111/pala.12445 (2020).
32. Ravel, B., & Newville, M. Athena, Artemis, Hephaestus: data analysis for X-ray absorption spectroscopy using IFEFFIT. *J Synchrotron Radiat* **12**, 537–541. doi:10.1107/S0909049505012719 (2005).
33. Menges, F. Spectragryph-optical spectroscopy software. Version *1*, 2016-2017. (2017).
34. Barth, A. Infrared spectroscopy of proteins. *Biochim Biophys Acta - Bioenerg* **1767**, 1073–1101. doi:10.1016/j.bbabio.2007.06.004 (2007).
35. Griebenow, K. Secondary structure of proteins in the amorphous dehydrated state probed by FTIR spectroscopy. Dehydration-induced structural changes and their prevention. *Internet J Vibr Spectr* **3,** 1–34. (1999).
36. Abu Tier, M.M., Ghithan, J., Abu-Taha, M., Darwish, S., & Abu-Hadid, M. Spectroscopic approach of the interaction study of ceftriaxone and human serum albumin. *JBSB* **6**, 1–12. doi:10.5897/JBSB2013.0045 (2014).
37. De Meutter, J., & Goormaghtigh, E. Amino acid side chain contribution to protein FTIR spectra: impact on secondary structure evaluation. *Eur Biophys* **50**, 641–651. (2021).

5.5 Supplementary information

5.5.1 Supplementary text

FTIR data. The absorption frequencies provided here are from peak positions observed in this study. An FTIR 'band' refers here to the spectral region in which one or more peaks can occur for a chemical bond (or bonds) that is associated with a functional group (or groups). Each FTIR peak indicates the presence of a particular bond (or bonds) within the sample analysed. The wavelength at which the peak absorbs for a bond (or bonds) corresponds to a functional group (or groups). Peak assignments were made using IRPal v2.0[1]. Peaks for amide functional groups (R–C=O–NH_2) are within bands A (3115–3360 cm^{-1}), B (3015–3115 cm^{-1}), I (1575–1700 cm^{-1}), II (1475–1575 cm^{-1}) and III (1210–1295 cm^{-1}) and are discussed in the main text.

Assignments for moderate and minor peaks in FTIR spectra of untreated and experimentally degraded feathers. The FTIR spectra presented here also reflect the presence of other functional groups via moderate and minor peaks; these band assignments are discussed below.

Moderate peaks in the FTIR spectra are found within bands 2, 3 and 7. Band 2 spans the range 2820–3015 cm^{-1} and, depending on the sample type, includes three to five peaks attributed to CH_x functional groups. Band 3 (1696–1810 cm^{-1}) can feature a single peak within its wavelength range that corresponds to the C=O stretch of carboxylic acid. Band 7 (975–1140 cm^{-1}) can feature one or two peaks that correspond to the stretch of S=O in sulfoxide and/or the stretch of C–O in carboxylic acid/ester.

Minor peaks in the FTIR spectra are exhibited in bands 1, 4–6, 8 and 10. Band 1 (3355–3700 cm^{-1}) can exhibit a single peak that is attributed to the O–H stretch of carboxylic acid. Band 4 (1420–1475 cm^{-1}) can feature a single peak that is potentially associated with stretching vibrations of methyl C–H, aromatic C–C and/or sulfate S=O. Band 5 (1355–1420 cm^{-1}) can feature a single sharp peak corresponds to methyl C–H stretching and/or sulfate S=O stretch. Band 6 (1135–1420 cm^{-1}) can feature a single peak that potentially corresponds to methyl C–H wag, carboxylic acid/ester C–O stretch, thiocarbonyl C=S

stretch and/or sulfone S=O stretch. Band 8 (925–975 cm^{-1}) can feature a single peak that corresponds to N–O amine oxide aliphatics. Band 10 (715–845 cm^{-1}) can exhibit several weak peaks that correspond to out of plane bending of aromatic C–H and/or S–OR esters. A minor peak in band 11 (500–580 cm^{-1}) potentially corresponds to S–S stretch.

5.5.2 Supplementary figures and tables

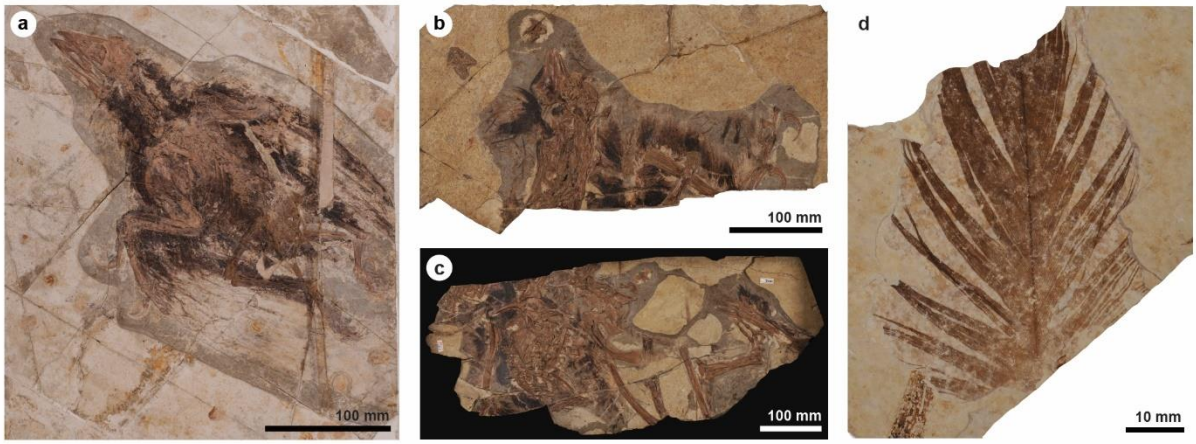


Fig. S5.1 Photographs of fossil feathers. a, Confuciusornis *(IVPP V 13171, Jehol biota, Cretaceous, NE China). b, c,* Sinornithosaurus *(IVPP V 12811, Jehol biota, Cretaceous, NE China). d, Green River feather (YPM VP 58657, Green River biota, Eocene, Wyoming USA).*

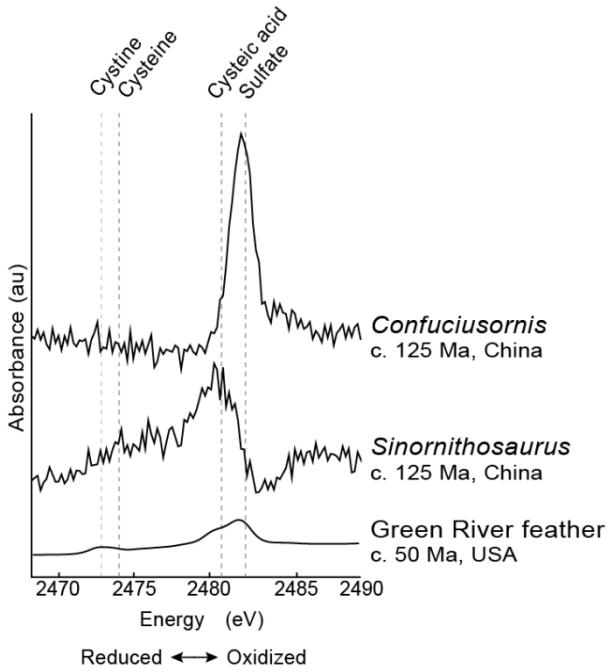


Fig. S5.2 Sulfur-XANES data for sediments hosting fossil feathers. Noisy spectra reflect low sulfur concentrations in the sample.

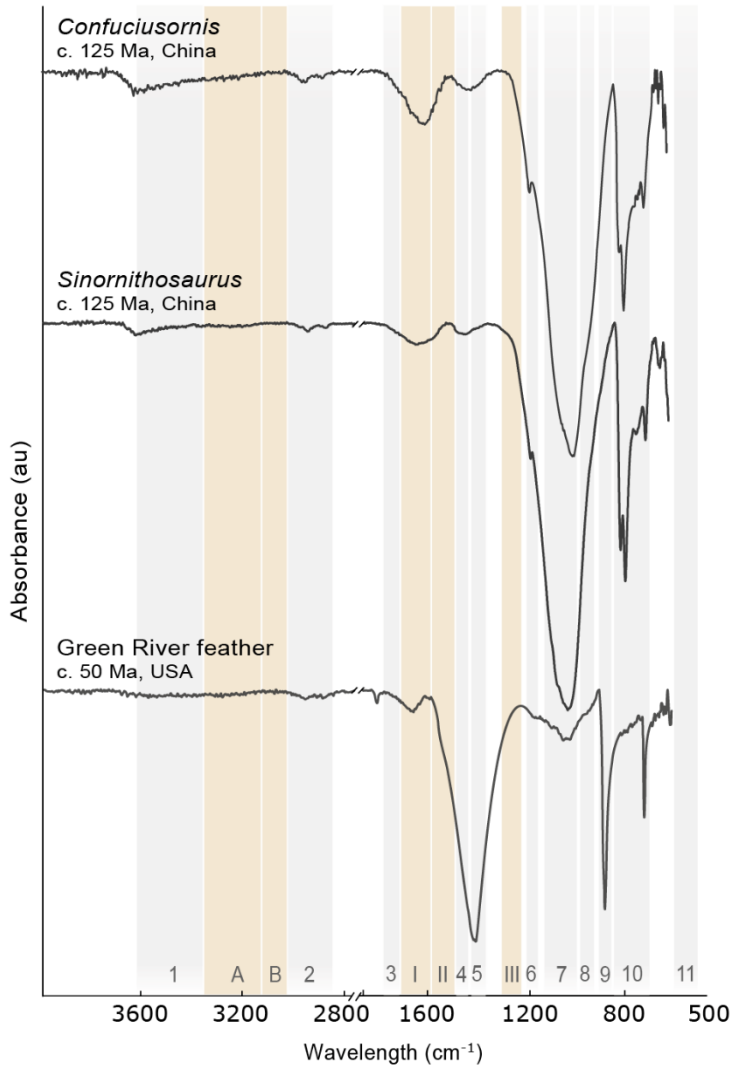


Fig. S5.3 *FTIR data for sediments hosting fossil feathers. Amide bands are indicated in brown boxes and all other bands in grey boxes.*

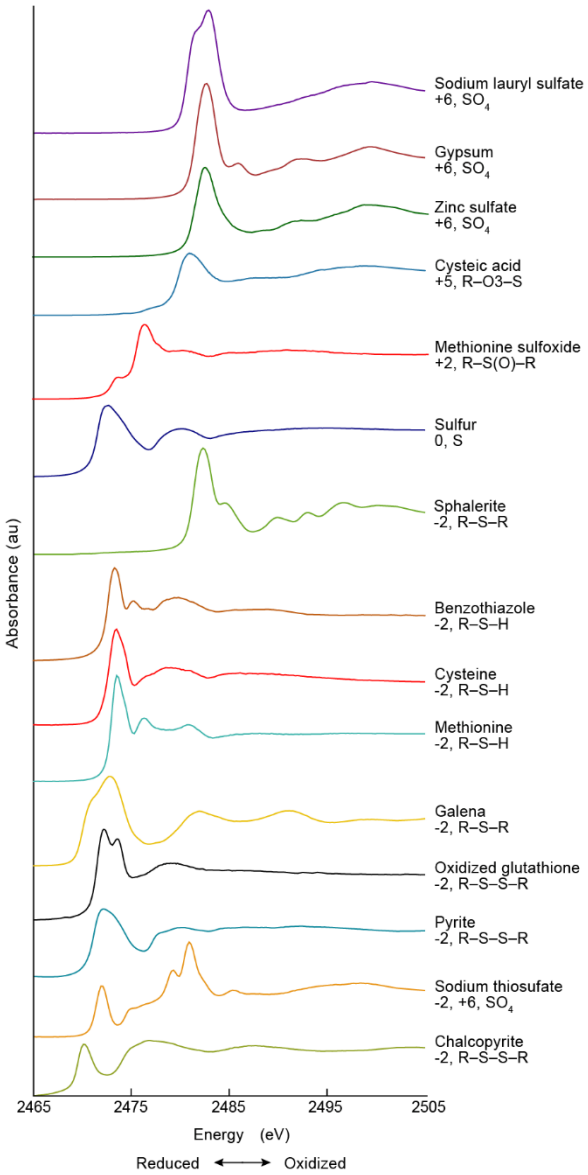


Fig. S5.4 *Sulfur-XANES data for analytical standards for selected S-bearing compounds.*

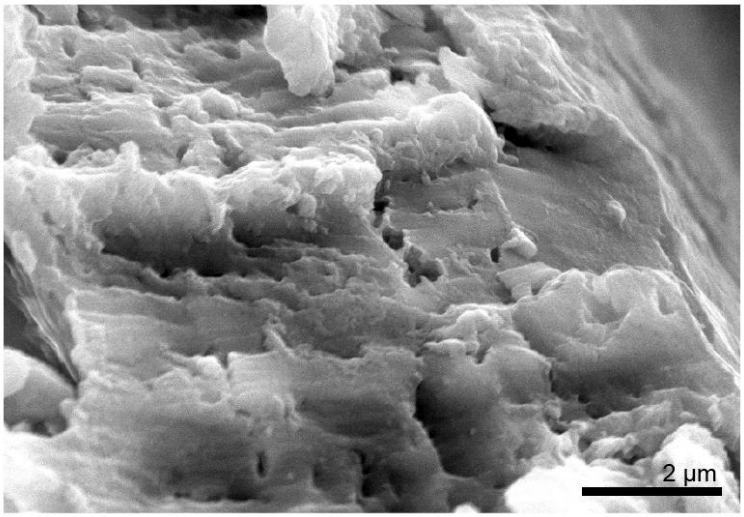


Fig. S5.5 *SEM image of a transverse cross section of a feather barbule (*Gallus gallus*) matured at 200°C. Holes in the barbule mark sites once containing melanosomes*.

Table S5.1 *FTIR peak assignments for untreated and experimentally degraded black (*Gallus gallus*) and white (*Egretta garzetta*) feathers, fossil feathers and host sediment.*

Assignment				Feathers from extant birds						Fossils						
Notation in Figure 2	Band wavenumber (cm^{-1})	Bond	Functional group	Untreated		200°C 1 hour		250°C 1 hour		Green River feather YPM VP 58657			*Sinornithosaurus* IVPP V 12811		*Confuciusornis* IVPP V 13171	
				Black	White	Black	White	Black	White	Feather 1	Feather 2	Sediment	Feather	Sediment	Feather	Sediment
1	3355–3700	O–H	Carboxylic acid	3455	3455	3455	3455	3455	3455	3455	3455	–	3455	–	3475	–
A	3115–3355	N–H	Amide A	3267	3281	3267	3281	–	–	–	3282	–	3294	–	–	–
B	3015–3115	N–H	Amide B	3064	3063	3064	3064	–	–	–	3063	–	3071	–	–	–
2	2820–3015	C–H	CH_2 and CH_3	2922	2972	2925	2971	2973	2973	2922	2918	–	2920	–	2922	–
3	1696–1810	C=O	Carboxylic acid	–	–	–	–	1711	1710	1700	–	–	–	–	–	–
I	1575–1696	C=O N–H	Amide I	1627	1630	1627	1630	1653	1655	1647	1646	1646	1641	1620	–	1588
II	1475–1575	N–H C–N C–C	Amide II	1538	1522	1538	1522	1539	1531	1555	1540	–	1545	–	1572	–
4	1420–1475	S=O C–C C–H	Sulfate Aromatics CH_2 and CH_3	1450	1452	1450	1450	–	–	–	1448	–	–	1435	–	–
5	1355–1420	S=O C–H	Sulfate CH_2 and CH_3	1390	1382	1388	1388	1381	1381	1387	1410	1394	1385	1394	1365	1400
III	1190–1285	C–N	Amide III	1232	1234	1233	1233	1239	1239	–	1239	–	–	–	–	–
6	1135–1190	C–O C–H C=S S=O	Carboxylic acid, ester CH_2 Thiocarbonyl Sulfone	1152	1161	1159	1161	1163	1163	–	1153	–	–	1162	1162	1162
7	975–1140	S=O C–O	Sulfoxide Carboxylic acid, ester	1036	1046, 1072	1028, 1068	1046	1017	1040	1028	1040	1023	1011	1010	1076	985
8	925–975	N–O	Amine oxide	–	953	–	953	953	953	–	–	–	–	–	–	–
9	820–893	C–H S–O	Aromatics S-OR esters	–	–	–	–	–	–	–	–	875	–	–	–	–
10	710–845	C–H S–O	Aromatics S-OR esters	799	–	798	817	756	756	711	745	712	777	777	778	777
11	500–580	S–S	Disulfide	531	532	534	532	531	532	–	–	–	–	–	–	–

Table S5.2 *Deconvolution peak assignments for the amide region of spectra from untreated and experimentally degraded black (*Gallus gallus*) and white (*Egretta garzetta*) feathers and fossil feathers.*

Assignment			Feathers from extant birds						Fossils			
Notation in Figure 2	Wavenumber (cm^{-1})	Secondary structure	Untreated		200°C 1 hour		250°C 1 hour		Green River feather YPM VP 58657		*Sinornithosaurus* IVPP V 12811	*Confuciusornis* IVPP V 13171
			Black	White	Black	White	Black	White	Feather 1	Feather 2	Feather	Feather
i	1495–1496	β-sheet	1495	1495	1496	–	–	–	–	–	–	–
ii	1508–1512	Random coil	1509	1510	1510	1509	1511	1508	–	1512	–	–
iii	1531–1561	α-helix	1533	1533	1538	1537	1534	1531	1536	1539	1531	1561
iv	1563–1568	β-turns	1563	1563	–	–	–	–	–	–	1568	–
v	1612–1625	β-sheet	1616	1612	1623	1625	–	–	–	–	–	–
vi	1626–1641	β-sheet	1632	1628	1628	1626	–	–	–	1641	1641	1633
vii	1644–1647	Disordered	–	–	–	–	–	–	1644	1647	1644	–
viii	1651–1661	α-helix	1654	1651	1661	1655	1653	1661	–	–	–	–
ix	1670–1684	β-turns	1674	1679	1684	1670	–	–	–	1683	–	–
x	1711–1717	C–O	–	–	–	–	1717	1717	1711	–	–	–
xi	1772–1795	C–O	–	–	–	–	1773	1772	1795	–	–	–
	Structural composition (%)	β-structures	67.7	62.2	56.4	62.4	0	0	0	50.1	64.7	61.3
		α-helix	23.3	28.6	34.3	26.1	69	59.6	100	22.9	23	38.7

Table S5.3 *Sulfur-XANES white line energies, oxidation state and chemical nature of analytical standards for selected S-bearing compounds.*

Standard	S-XANES white line energy (eV)	Sulfur oxidation state	Inorganic/organic
Chalcopyrite	2470.2	-2	Inorganic
Sodium thiosulfate	2472.02	-2, +6	Inorganic
Pyrite	2472.1	-2	Inorganic
Oxidized glutathione	2472.92	-2	Organic
Galena	2472.92	-2	Inorganic
Methionine	2473.6	-2	Organic
Cysteine	2474.12	-2	Organic
Benzothiazole	2474.12	-2	Organic
Sphalerite	2482.3	-2	Inorganic
Sulfur	2472.72	0	–
Methionine sulfoxide	2476.5	+2	Organic
Cysteic acid	2481	+5	Organic
Zinc sulfate	2482.5	+6	Inorganic
Gypsum	2482.6	+6	Inorganic
Sodium lauryl sulfate	2482.92	+6	Organic

Table S5.4 *Measurements of cortex thickness in feather barbule (*Gallus gallus*) matured at 200°C.*

SEM image	Cortex thickness (µm)
9_02	0.716
9_02	0.857
9_02	0.686
9_02	0.655
9_08	0.473
9_08	0.681
9_08	0.947
9_08	1.328
9_08	0.672
9_13	0.562
9_13	0.571
9_13	0.434
9_13	0.529
9_13	0.563
9_13	0.614
Average	0.686 ± 0.215

5.5.3 Supplementary references

1. Heeswijk, W.v. (2010). IRPal A tabledriven Infrared Application. v2.0.

6. Degradation experiments reveal a melanin-based bias in the preservation of corneous beta proteins in fossil feathers

This chapter comprises a paper that is prepared for submission to the journal *Current Biology.* This chapter is organised as follows: introduction, materials and methods, results, discussion, references and supplementary information. This chapter compares the chemistry of different coloured feathers using select data from Chapter 5 in addition to new data on experimentally degraded feathers.

Candidate contribution to the study. TSS contributed to the design of the study and performed all the experiments. TSS collected and interpreted all S-XANES and FTIR data with assistance. TSS wrote the paper with input from all other authors.

Abstract. Fossil feathers are critical to understanding feather evolution. Despite evidence of feather corneous beta proteins (CBPs) in fossil feathers, studies to date have not incorporated an understanding of feather taphonomy. Here we use taphonomic experiments to examine the relative impact of decay, sulfurisation, temperature and pressure on the preservation of amides and disulfides, which are key components of the secondary and tertiary structure, respectively, of feather CBPs, in feathers with different melanin chemistry. Our results reveal that the degradation of feather CBPs is controlled primarily by the experimental treatment. The controls on feather CBP tertiary structure preservation are, in decreasing order of importance, temperature, pressure and decay whereas for secondary structure preservation the controls are pressure, temperature and decay. Importantly, is also influenced by melanin content. In contrast to the prevailing paradigm, our data show that the preservation potential of feather CBPs is enhanced in feathers with a low melanin content (especially of eumelanin). Future efforts to detect evidence of feather CBPs in fossils should therefore target phaeomelanic and amelanic fossil feathers, not feathers rich in eumelanin and eumelanosomes. Collectively, the results form the basis for a new integrated model for feather preservation that is firmly grounded in quantitative empirical data and encompasses all major feather components. This model explains variations in the preservation of fossil feathers and represents a major advance in our understanding of the preservation of feathers and of structural proteins. Critically, the model highlights the power of combining systematic and quantitative taphonomic

experiments with a holistic, whole-tissue approach, to resolve long-standing issues relating to the preservation of soft tissues in the fossil record.

6.1 Introduction

Feathers are the most complex integumentary structures in vertebrates with a deep evolutionary history[1]. Recent studies have contributed important insights into feather origins, with new fossil discoveries of feathers in pterosaurs[1, 2] supporting evo-devo hypotheses[3-5] of feather origins in early archosaurs. Fossils have also illuminated the phylogenetic distribution and morphological diversity of feathers in Mesozoic birds, non-avialan dinosaurs and pterosaurs[1, 2, 6, 7]. Despite these advances, other aspects of the feather fossil record are poorly understood, especially the biochemical evolution of feathers. This stems in part from a lack of data, controversial reports of preserved feather chemistry[8-10], and a poor understanding of feather preservation (taphonomy). Studies to date have focussed on two key biochemical components of feathers: melanin pigments[11] and corneous beta proteins (CBPs; previously referred to as β-keratins[3, 12]). Fossil evidence of melanin is widespread, typically as preserved melanosomes (subcellular granules)[13-17] and despite some early debate, is now widely accepted[17]. Preserved evidence of feather CBPs in Mesozoic fossils[8-10], however, is much more controversial: proteins normally degrade over much shorter timespans[18-20] and there is no consensus on CBP preservation among recent experimental studies on feather degradation[21-25]. These issues, plus concerns about false positives in immunohistochemical data[23, 26], collectively cast doubt on reports of CBPs (or keratins) in various Mesozoic birds and feathered dinosaurs[8-10, 27]. New empirical evidence from taphonomic experiments demonstrates that β-sheets in feather CBPs transform to α-helices conformation during thermal maturation (Chapter 5) confirming the hypothesis[1] that alpha helix signatures in fossil feathers are not original[10] but artefacts of fossilization.

Intriguingly, novel spectroscopic evidence of molecular components of feather CBPs in Mesozoic fossil feathers (Chapter 5) support claims that feather CBPs preserve in some fossils, but the controls on preservation are unknown. In particular, whether feather melanin content influences CBP preservation has not been assessed.

Here, we apply spectroscopic approaches to characterise alteration of the secondary and tertiary structure (Chapter 5) of feather CBPs during degradation. We use sulfur x-ray absorption structure (S-XANES) spectroscopy and Fourier transform infrared (FTIR) spectroscopy to characterise the sulfur and amide chemistry, respectively, of experimentally degraded black, white and orange feathers. Our data reveal that feather CBP remnants are more likely to preserve in feathers with little or no melanin, especially, eumelanin. Given that most fossil feathers are preserved as melanosome-rich films, this suggests a major bias in the fossil record against feather CBP preservation.

6.2 Materials and methods

6.2.1 Feathers from extant birds

Freshly shed black (*n* = 3) and orange (*n* = 3) contour feathers from the domestic chicken, *Gallus gallus domesticus*, and white (*n* = 3) primary feathers from the little egret, *Egretta garzetta*, were stored at -80°C prior to experimental treatment.

Feathers of extant birds comprise primarily fibrous feather CBPs that have a β-sheet conformation[12, 28, 29] and are rich in the S-bearing amino acid cysteine. Inter- and intramolecular cross-linking between cysteine moieties via disulfide bonds enhance chemical stability[30]. Minor feather components include intermediate filament-keratins (IF-keratins; previously referred to as α-keratins)[12, 28, 29] that have an α-helix structure and are relatively cysteine-poor[12, 30]. Melanin pigments in feathers[31] are packaged into micron-sized organelles termed melanosomes. Eumelanin comprises a mixture of the indole units 5,6-dihydroxyindole (DHI) and 5,6-dihydroxyindole-2-carboxylic acid (DHICA) and confers grey, dark brown and black colouration[32, 33]. Phaeomelanin comprises the sulfur-bearing units benzothiazine (BT) and benzothiazole (BZ) and confers orange, rufous and some grey tones[15, 33].

6.2.2 Justification for experimental design

The goal of these experiments was to critically assess the relative preservation potential of feather CBPs in feathers that vary in melanin chemistry using an experimental taphonomic

framework. Our experiments used black feathers as proxy for a eumelanin-rich state; orange feathers, as a phaeomelanin-rich state; and white feathers, as an amelanic state; the melanin chemistry of these feathers has already been characterized (note that the white feathers contain minimal concentrations of melanin markers; Chapter 4). Experiments were designed to examine the impact of decay, elevated temperature, elevated pressure and the availability of environmental sulfur on feather CBP degradation. Certain variables were used in isolation (i.e., decay and thermal maturation at 200°C and 250°C); these serve as controls for the experiments where variables are used in combination.

Taphonomic experiments require the use of conditions that generate chemical and/or morphological phenomena that are comparable to those preserved in the fossils of interest[21]. High temperatures and pressures (250°C combined with 250 bar) for extended time intervals (24 h) result in liquefaction and partial vaporization of feather tissue[22, 23, 34]. We do not consider these conditions to represent a valid analogue for fossil feathers as the latter typically retain (and are identified as feathers on the basis of) macroscopic structures such as the rachis and/or vane; microscopic structures such as barbs, barbules and melanosomes are commonly preserved[9, 35]. Experimental conditions that ensure survival of these structures are therefore more appropriate for our experiments.

Our taphonomic experiments used maximum temperatures of 150°C (at 135 bar) or 250°C (without elevated pressure, i.e., at 1 bar) for 1 h that are known[21] to retain gross feather structure. Our experiments used either aluminium foil or sealed Au capsules, which have previously been characterized as systems that are open and closed to diffusion (especially of volatiles from carcasses), respectively[34]. We do not apply these labels to our experiments because the nature and extent of diffusion of decay volatiles, plus the importance of the process to feather CBP degradation, has not been characterized. In contrast to previous studies[34] our experiments did not use sediment. Although the use of a sedimentary matrix has clear benefits (e.g., better approximation of the generic depositional system, enhancing decay rate[36, 37]), it also introduces confounding factors (e.g., grain chemistry, grain size, porosity, permeability and pore water chemistry). These factors potentially impact diffusion of diagenetic fluids and cementation and thus

ultimately, preservation. The impact of sediment during maturation therefore requires systematic hypothesis-based investigation that is beyond the scope of this study.

Our study includes a series of artificial sulfurization experiments. These were designed to test whether the presence of sulfur moieties promotes preservation via sulfurization.

S-XANES and FTIR were used to analyse the feathers because these techniques inform on feather CBP tertiary structure (via the detection of disulfide bonds) and secondary structure (via the detection of amide bonds), respectively (Chapter 5).

6.2.3 Decay experiments

Large samples (ca. 30 mm^2) were dissected from black feathers and placed in individual sterile glass vials, each with 5 mL distilled deionized water (DDW) and with no added inoculum. Vials were capped with Al foil, sealed with parafilm and placed in a Memmert constant temperature incubator at 30°C ± 1°C (Supplementary Figure 6.1). Feathers were sampled after twelve months' decay and stored in 70% ethanol prior to analysis or experimental maturation (see below).

6.2.4 Maturation experiments

Samples (ca. 10 mm^2) of untreated black, orange and white feathers and of feathers decayed for one month were wrapped in Al foil. Smaller samples (ca. 3 mm^2) dissected from untreated black, orange and white feathers, and from black feathers decayed for 12 months, were placed in Au capsules. Foil-wrapped samples were matured in a standard laboratory convection oven at 200°C ± 1°C or 250°C ± 1°C for 1 h. Au capsules were welded shut and placed in a custom-built Strata-Tech water-pressurized cold-seal autoclave at 150°C, 135 bar for 1 h.

6.2.5 Sulfur experiments

Sulfur experiments used the procedure in van Dongen et al.[38]. For feathers of each colour, three replicate samples (each ca. 50 mg, approximately 20 mm^2) were placed in sterile

glass vials with 6 mL of nitrogen-flushed DDW containing 560 mg of NaHS, to which 16 mg of elemental sulfur was added under a nitrogen atmosphere. Vials were sealed with caps and parafilm, placed in a Memmert constant temperature incubator at 45°C and shaken daily by hand for one minute. After four weeks, activated Cu curls (i.e., with added 2N HCl) were added to each vial until oxidation of the Cu ceased. The vials were then stirred for 24 h at room temperature to remove any residual elemental S. Samples were dried under a fume hood and stored at -80°C until analysis.

6.2.6 X-ray Absorption Near Edge Structure (XANES) Spectroscopy

Small samples (≥ 3 mm^2) of untreated and experimentally degraded feathers were placed on low-sulfur tape and analyzed at the Stanford Synchrotron Radiation Lightsource (SSRL) using synchrotron X-ray absorption near-edge spectroscopy (XANES) at beam line 6-2. S-XANES data were collected in fluorescence mode using a single element Vortex silicon drift detector set at a scattering angle of ~60°. A $Na_2S_2O_3$ standard with a pre-edge peak at 2472.02 eV was used to calibrate the energy of the monochromator position. S-XANES standards for selected S-bearing compounds, representing different sulfur species, were prepared by mixing commercially available analytical standards (Sigma Aldrich; ≥98% pure) with BN to obtain a sulfur concentration of ca. 5 wt % in each standard. Data alignment, averaging, background subtraction and normalization were performed using Athena v. 0.9.26[39].

XANES is a semi-quantitative technique whereby peak intensity indicates the relative abundance of one or more oxidation states for an element of interest. The S-XANES spectra presented here include peaks for S-bonds in cystine (S^{-2} in SH; 2472.92 eV), cysteine (S^{-1} in S-S; 2474.12 eV), cysteic acid (S^0 in S-COOH; 2480.92–2481.12 eV) and/or organic sulfate (S^{+6} in $SO_4^{-2}{}_{(org)}$; 2482.12–2482.42 eV)[40]. Benzosulfur is difficult to identify in XANES spectra as its excitation energy (2474.12 eV) is similar to that for cysteine; benzosulfur is, however, associated with a shoulder feature at 2476.3 eV[40]. For details on analytical standards for selected S-bearing compounds see Supplementary Fig. 5.4 and Table 5.3 in Chapter 5.

6.2.7 Fourier Transform Infrared (FTIR) Spectroscopy

Feather samples from all experimental treatments and untreated feathers were analyzed using FTIR. Each spectrum was collected as an average of 10 scans. Three locations per each of three replicates per treatment were analysed, yielding a total of nine spectra for each treatment. Spectra were obtained in the 4000–500 cm^{-1} range using a PerkinElmer Frontier FTIR spectrometer fitted with a universal diamond ATR accessory. The penetration depth of the diamond/Ge crystal at 1000 cm^{-1} is typically 1–2 µm. The thickness of the outer cortex of the feathers analyzed is 0.69 ± 0.22 µm (Supplementary Table 5.4 in Chapter 5). The FTIR signal therefore likely incorporates data from melanosome structural proteins and melanins close to the outer cortex of the feathers. Absorption of the diamond crystal in the region 2300–1900 cm^{-1} (no overlap with the region of interest in this study) was removed and each spectrum was baseline corrected using SpectraGryph v. 1.2.7 (using the following parameters: adaptive correction, 15% coarseness, no offset)[41]. In addition, interactive baseline correction was performed on data in the region 898–450 cm^{-1} using Spectrum IR v. 10.6.1 (PerkinElmer, USA). This ensured a consistent baseline across the entire scan range to facilitate spectral comparison. Each spectrum was normalized via Z-score standardization to remove potential differences in absorption relating to sample thickness and to enable the comparison of peak heights among spectra.

FTIR identifies functional groups within a sample via the excitation of bonds by infrared radiation at characteristic wavelengths. Amide peaks derive from proteins (or amide protein fragments) and are reflected in spectra primarily via peaks in the amide I, II, III, A and/or B regions (see Table 6.2 for bond assignments).

6.3 Results

6.3.1 Sulfur chemistry of experimentally treated feathers

S-XANES data reveal considerable variation in the sulfur chemistry of untreated and experimentally treated black, orange and white feathers (Figure 6.1). Critically, a cystine peak (S-S) is present in all white feathers, even those that are matured; this indicates retention of components of CBP tertiary structure, at least locally.

Spectra for untreated feathers are dominated by a strong broad disulfide peak that can be further resolved into a cystine and cysteine/benzosulfur peak (centred at 2472.92 and 2474.12 eV, respectively; Figure 6.1). The cystine peak is weaker in orange feathers than in white and especially black feathers. This may reflect the selective degradation of cystine in orange feathers by reactive oxygen species (ROS) derived from the phaeomelanin BT unit during irradiation[42, 43]. In contrast, the cysteine/benzosulfur peak is strongest in orange feathers, probably due to the presence of benzosulfur in the phaeomelanin BZ and BT units[33, 40, 44]. S-XANES spectra for orange feathers therefore derive primarily from feather CBPs with a minor phaeomelanin component. Eumelanin lacks sulfur; S-XANES data of black and white feathers thus primarily reveal the sulfur chemistry of feather CBPs. Spectra for all feather types show a minor benzosulfur shoulder (at 2476.3 eV) in addition to a weak, broad cysteic acid peak (centred at 2480.92 eV) with very minor contribution from sulfate (ca. 2482 eV).

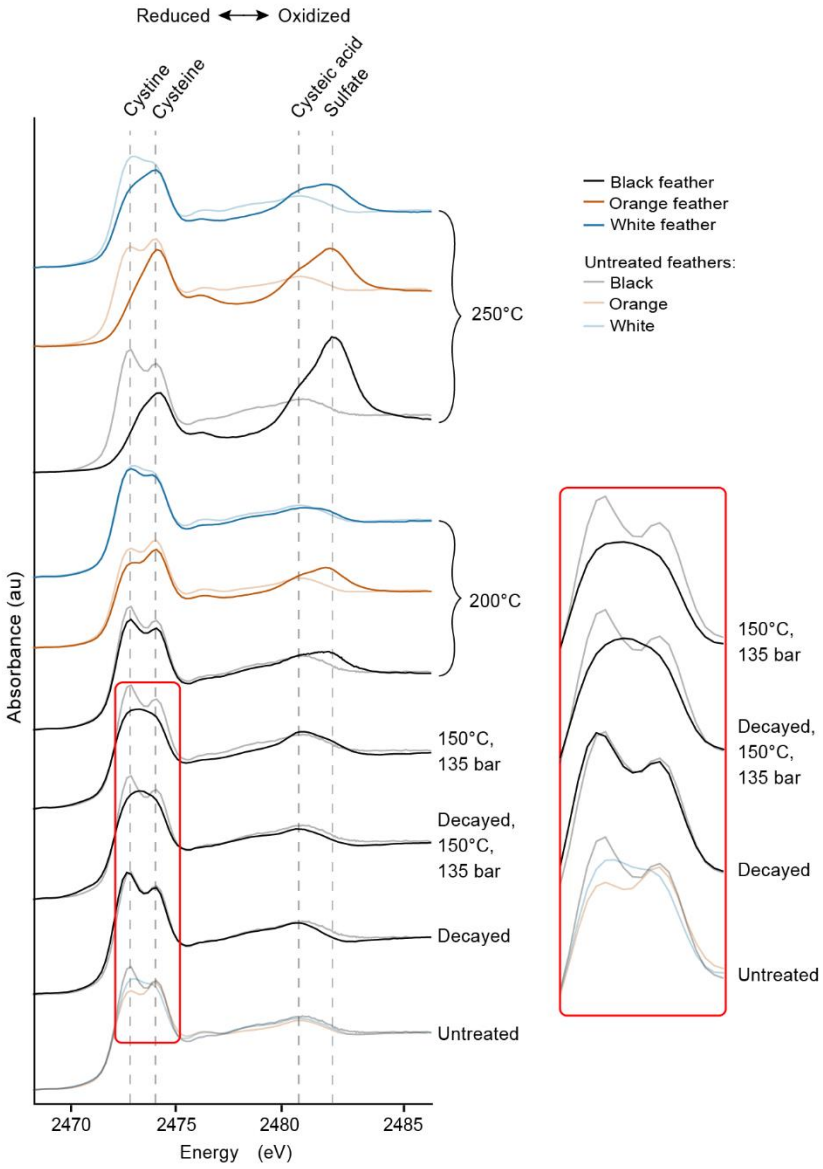


*Fig. 6.1 S-XANES spectra of experimentally degraded black and orange (*Gallus gallus*) and white (*Egretta garzetta*) feathers.*

Spectra for black feathers decayed for 12 months are almost identical to those of untreated black feathers, except slightly weaker peaks for cysteic acid and sulfate.

Black feathers matured at 150°C, 135 bar (without prior decay) display a single broad sulfide peak centred at 2473.32 eV that is slightly weaker than the cystine and cysteine peaks in untreated examples; the benzosulfur shoulder at 2476.3 eV is also weaker. The cysteic acid peak centred at 2480.92 eV is slightly stronger than in untreated black feathers; there is a subtle shift in the band towards higher eV, suggesting a very minor contribution from organic sulfate. Samples decayed for twelve months prior to maturation at 150°C, 135 bar lack a sulfate peak (and a shift in the cysteic acid peak) and exhibit a

slightly stronger sulfide peak, and weaker cysteic acid peak, than samples matured with no prior decay.

Following “moderate” experimental maturation at 200°C, spectra for all feather types closely resemble those of untreated feathers, albeit with a slight reduction in the intensity of the cystine and cysteine peaks and the appearance of a minor broad organic sulfate band (centred at 2482.12–2482.27 eV). Notably, orange feathers exhibit greater alteration of sulfur chemistry (in particular, loss of cysteine and thus disulfide) than black or white feathers when moderately matured (200°C). This could reflect, at least in part, beam damage during XANES analysis.

“Strong” maturation at 250°C induces dramatic changes in the feather spectra, and striking differences among feather types. All strongly matured feather spectra are dominated by an broad organic sulfate peak (centred at 2482.42 eV) that probably includes a strong contribution from cysteic acid. Cystine is absent, cysteine is moderately intense, and there is a weak benzosulfur shoulder.

Spectra for strongly matured orange feathers resemble those for similarly treated black feathers albeit with a stronger cysteine peak and slightly weaker organic sulfate peak (centred at 2482.32 eV).

In contrast, spectra for similarly treated white feathers retain a cystine peak, albeit reduced in intensity relative to untreated white feathers. Spectra show a strong cysteine peak with a weak benzosulfur shoulder; peaks for cysteic acid and especially organic sulfate (strongest at 2482.12 eV) are stronger than in untreated samples.

Principal Component Analysis (Figure 6.2) successfully resolves most of the variation in the dataset (PC2 and PC3 combined correspond to 96.5% of the total variation). PC2 corresponds primarily to variation in cystine and especially organic sulfate (Figure 6.2F). PC3 corresponds primarily to variation in cystine and cysteine/benzosulfur (Figure 6.2F). Most of the data in the chemospace plot are clustered according to both feather colour and experimental treatment.

Black feathers occupy a broad data field characterized by low to high PC2 values and medium to high PC3 values (Figure 6.2B); data groups for most experimental treatments plot separately (except for feathers matured at 200°C and 150°C 135 bar, which each overlap several other fields). Progressive maturation at 150°C (with 130 bar), 200°C and 250°C shifts the data to higher values for both PC2 and PC3, indicating increasing organic sulfate and decreasing cystine and cysteine/benzosulfur content (Figure 6.2C). Somewhat unexpectedly, decayed black feathers show lower PC2 values than untreated feathers, which indicates an increase in cystine and/or a decrease in organic sulfate. Similarly, feathers decayed prior to maturation at 150°C and 135 bar show lower PC2 values than those matured without prior decay (Figure 6.2H).

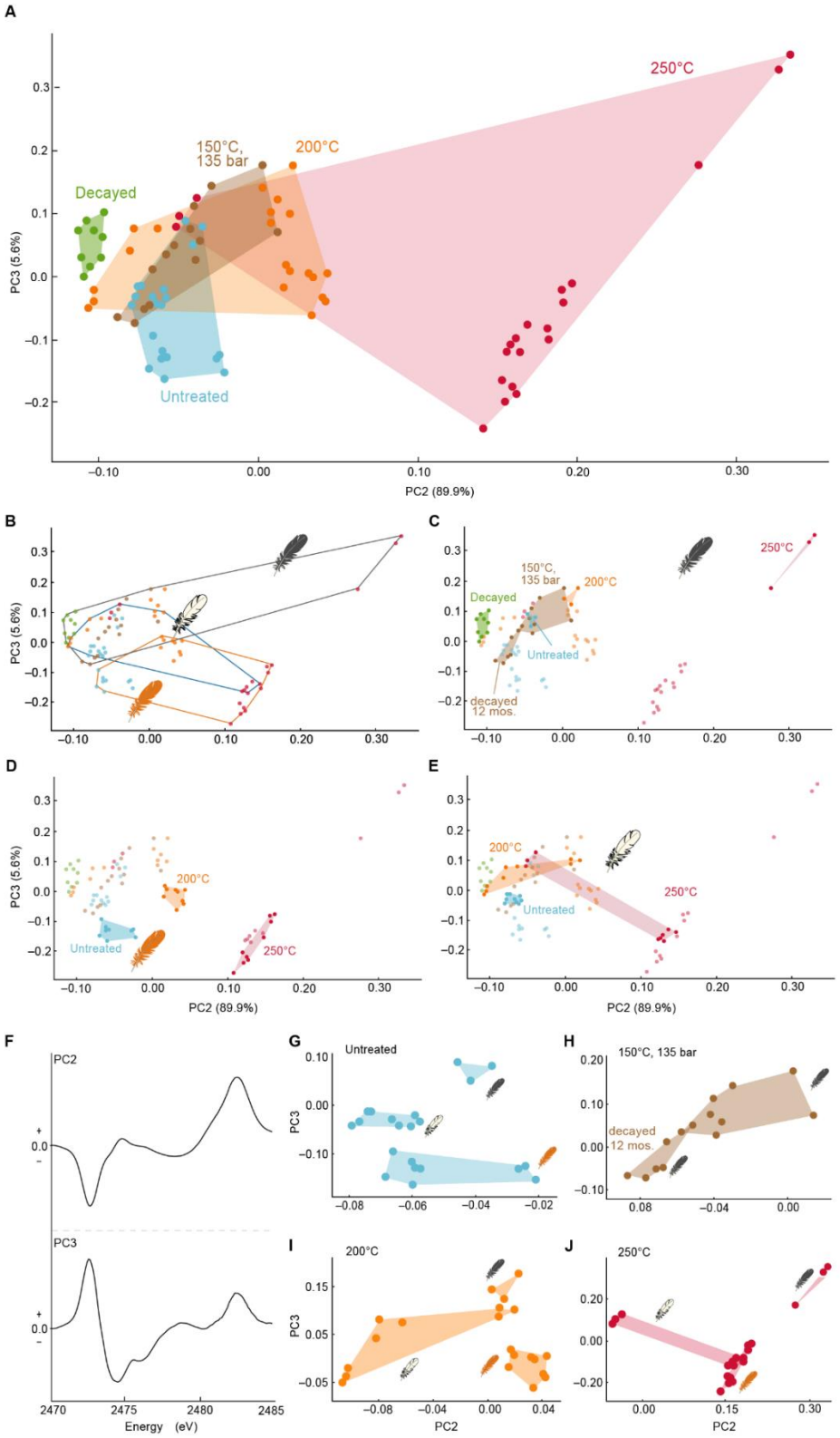


Fig. 6.2 PCA of S-XANES spectra shown in Fig. 6.1. Chemospace plots show data fields for A) different experimental treatments and B) different feather types. Chemospace plots in C–E show data fields for experimental treatments using C) black, D) orange and E) white feathers. F) Spectra for PC2 and PC3. G – H) Chemospace plots of black, orange and white untreated feathers (G) and feathers matured at 150°C, 135 bar (with and without decay (H)), 200°C (I)and 250°C (J).

In contrast to black feathers, orange and white feathers each define small data fields in the chemospace plot (Figure 6.2B). Orange feathers generally show low PC2 and PC3 values; white feathers show low to medium values for PC2 and PC3. Data for different experimental treatments occupy distinct, non-overlapping fields for orange feathers (Figure 6.2D), but there is some overlap for white feathers among data fields corresponding to different maturation treatments (Figure 6.2E). As with black feathers, progressive maturation at 200°C and 250°C shifts the data to higher PC2 values, indicating increasing organic sulfate and decreasing cystine.

Comparison of the data for different feather types reveals important trends. For untreated samples, black feathers plot with high PC2 and PC3 values, reflecting high organic sulfate content, relative to white and orange feathers (Figure 6.2G); white feathers show the lowest PC2 values, and orange feathers the lowest PC3 values. These broad relationships within the chemospace are retained following progressive maturation (Figure 6.2I–J).

6.3.2 Sulfur experiments

The pyrograms of all feathers treated with sulfur are dominated by benzene derivatives, especially toluene (compound 5 in Figure 6.4 and Table 6.1). Other notable components include cholesta-3,5-diene (compound 32), fatty acid methyl esters (compounds 22 and 23), steroid derivatives (including cholestenes: compounds 29 and 30) and nitrogen-containing compounds (Figure 6.3 and Table 6.1). Nitrogen-containing compounds include phenol (compound 15), pyridine (compounds 3, 7 and 11) and pyrrole (compounds 4, 9 and 13) moieties, benzonitrile (compound 16), indole (compound 19), pyrazinediones (compounds 21 and 26) and amides (compounds 24, 27 and 28). Orange feathers contain trace amounts of organic sulfur compounds: 3-methylthietane (compound 1), methylthiophene (compound 6) and thiane (compound 8). Only 3-methylthietane was detected in experimentally treated black feathers; no organic sulfur compounds were detected in white feathers.

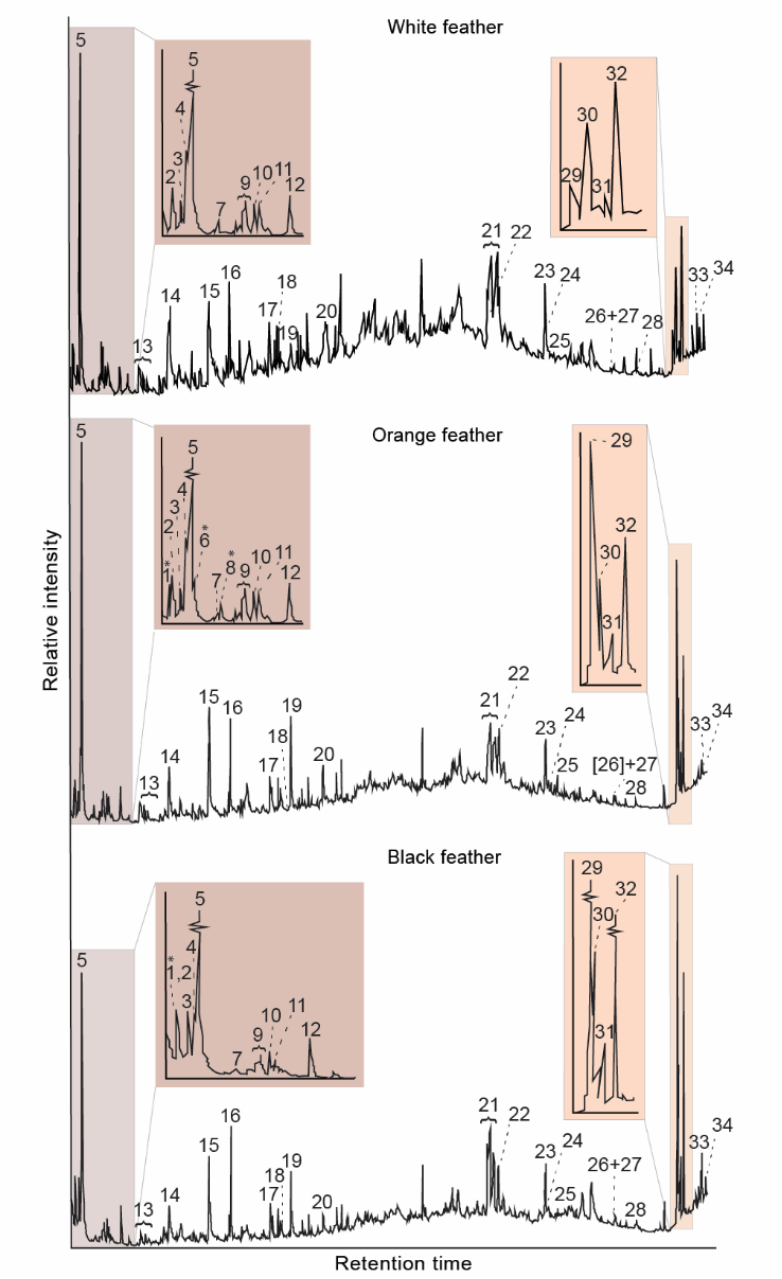


*Fig. 6.3 Py-GC-MS pyrograms of black and orange (*Gallus gallus*) and white (*Egretta garzetta*) feathers degraded in sulfurization experiments.*

Table 6.1 *Peak assignments for py-GC-MS spectra of black and orange (*Gallus gallus*) and white (*Egretta garzetta*) feathers degraded in sulfurization experiments.*

Notation in Figure 3	Compound	Black	Orange	White
1	3-Methylthietane*	x	x	–
2	n-Methylene ethenamine	x	x	x
3	Pyridine	x	x	x
4	Pyrrole	x	x	x
5	Toluene	xxx	xxx	xxx
6	Tethylthiophene*	–	x	–
7	a-Methylpyridine	x	x	x
8	Thiane*	–	x	–
9	Methylpyrroles	x	x	x
10	Ethylbenzene	x	x	x
11	a-Methylpyridine	x	x	x
12	Styrene	x	x	x
13	Dimethyl/ethyl pyrroles	x	x	x
14	Phenol	x	x	xx
15	Methyl phenol	xx	xx	xx
16	Benzonitrile	xx	xx	xx
17	Benzopropanenitrile	x	x	xx
18	Acetylmethylfuran	x	x	xx
19	Indole	x	xx	x
20	Methylindole	x	x	x
21	Isobutylhexahydropyrrolepyrazine-1,4-diones	xx	xx	xx
22	Hexadecanoic acid	xx	xx	xx
23	Octadecanoic acid	xx	xx	xx
24	Hexadecenamide	x	x	x
25	Docosenol	x	x	x
26	Benzylhexahydropyrrolopyrazine-1,4-dione	x	–	x
27	Octadecamide	x	x	x
28	Eicoenamide	x	x	x
29	Cholest-2-ene	xxx	xxx	xx
30	Cholest-3-ene	xxx	xxx	xx
31	Cholesta-4,6-dien-3-ol	xx	xx	x
32	Cholesta-3,5-diene	xxx	xxx	xxx
33	Cholestanol	xx	x	xx
34	Cholesterol	x	x	xx

6.3.3 Amide signals in experimentally treated feathers

FTIR spectra of untreated feathers are dominated by peaks for amide functional groups, i.e., amides A, B, I, II and III; these bands are the focus of our results (Figure 6.4, Table 6.2 and Supplementary Table 6.1). The peak intensity in all major bands varies among feather types and treatments.

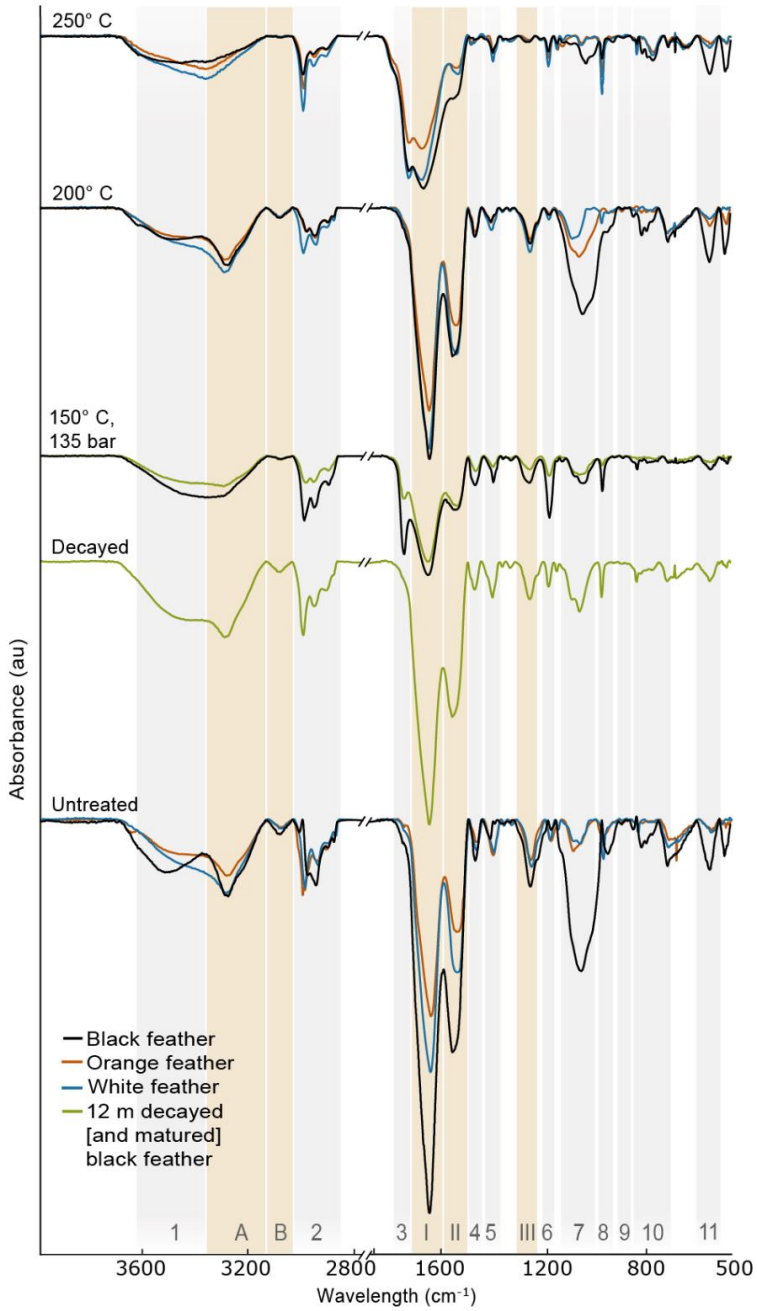


Fig. 6.4 *FTIR spectra of experimentally degraded black and orange (*Gallus gallus*) and white (*Egretta garzetta*) feathers.*

Table 6.2 *Peak assignments for FTIR spectra of experimentally degraded black and orange (*Gallus gallus*) and white (*Egretta garzetta*) feathers.*

		Assignment		Experimental treatment				
Notation in Figure 4	**Band wavenumber (cm^{-1})**	**Bond**	**Functional group**	**Untreated**	**Decayed 12 mos.**	**150°C, 135 bar 1 h**	**200°C 1 h**	**250°C 1 h**
1	3355–3700	O–H	Carboxylic acid	XX	XX	XX	X	X
A	3115–3355	N–H	Amide A	XX	XX	–	X	–
B	3015–3115	N–H	Amide B	X	X	–	X	–
2	2820–3015	C–H	CH_2 and CH_3	XX	XX	XX	XX	XX
3	1696–1810	C=O	Carboxylic acid	–	–	XX	–	XXX
I	1575–1696	C=O N–H	Amide I	XXX	XXX	XX	XXX	XXX
II	1475–1575	N–H C–N C–C	Amide II	XXX	XXX	XX	XXX	XX
4	1420–1475	S=O C–C C–H	Sulfate Aromatics CH_2 and CH_3	X	X	X	X	–
5	1355–1420	S=O C–H	Sulfate CH_2 and CH_3	X	X	X	X	X
III	1190–1285	C–N	Amide III	X	X	X	X	X
6	1135–1190	C–O C–H C=S S=O	Carboxylic acid, ester CH_2 Thiocarbonyl Sulfone	X	X	X	X	X
7	975–1140	S=O C–O	Sulfoxide Carboxylic acid, ester	XXX*	XX	X	XXX*	X
8	925–975	N–O	Amine oxide	–	X	X	–	X
9	710–845	C–H S–O	Aromatics S-OR esters	X	X	–	X	X
10	500–580	S–S	Disulfide	X	X	X	XX	X

All untreated spectra are dominated by amide I (1575–1696 cm^{-1}) and II (1475–1575 cm^{-1}) peaks, with moderate peaks for amide A (3115–3355 cm^{-1}) and III (1190–1285 cm^{-1}) and a weak amide B (3015–3115 cm^{-1}) peak. Band 7 (975–1140 cm^{-1}) is represented by a single strong peak in black feathers but a very weak, bifurcated, peak in orange and white feathers.

Spectra for black feathers matured at 150°C, 135 bar show weaker peaks for all amide bands than untreated feathers; amide A peak is absent and a minor carboxylic acid peak (absent in untreated feathers) appears in band 3 at 1728 cm^{-1}. Spectra for feathers matured at 150°C, 135 bar are near-identical irrespective of whether or not they were decayed prior to maturation. Feathers that were decayed but not matured, however, exhibit weaker peaks in all major bands.

Spectra for feathers matured at 200°C show decreased absorbance across all wavelengths but otherwise are near-identical to untreated feathers.

Maturation at 250°C induces dramatic changes to FTIR spectra of the feathers, notably the loss of amides A and B and the generation of a major peak in band 3.

PCA (Figure 6.5) captures 78.4% of the variation in the dataset. The data for different experimental treatments fall into two broad fields: the 250°C and 150C, 135 bar experiments in the left of the chemospace with low PC2 values, and the rest of the experimental treatments (untreated, decayed, and 200°C) cluster in the right of the chemospace with high PC2 values. Since PC2 accounts for 54% of variation in the dataset, the spread of the data in chemospace confirm that the major changes in feather chemistry are linked to strong maturation, and that maturation under relatively low temperatures but in conjunction with elevated pressure induce similar chemical changes to maturation at a higher temperature and atmospheric pressure. The variation in PC2 corresponds primarily to variation in band 3 (absent at high PC2 values) and amides I, II and III (stronger peaks at high PC2 values; Figure 6.5F). PC3 comprises 24.4% of the variation in the dataset and corresponds primarily to variation in band 7 (no strong peak at lower PC3 values; Figure 6.5F).

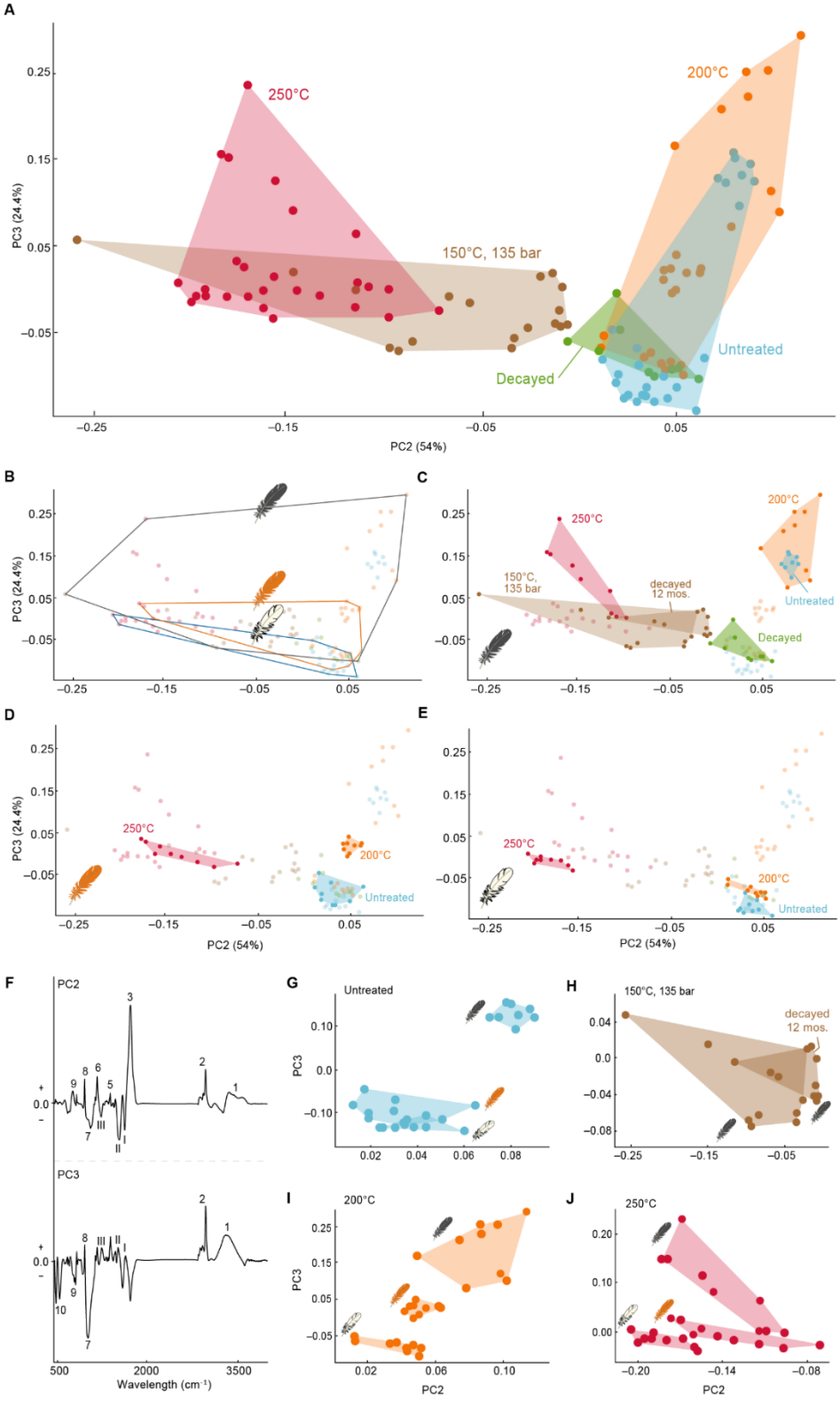


Fig. 6.5 *PCA of FTIR spectra shown in Fig. 6.4. A – B) Chemospace plots show data fields for different experimental treatments (A) and different feather types (B). Chemospace plots in C–E show data fields for experimental treatments using black (C), orange (D) and white (E) feathers. F) Spectra for components 2 and 3. G – J) Chemospace plots for black, orange and white untreated feathers (G) and feathers matured at 150°C, 135 bar (with and without decay (H)), 200°C (I) and 250°C (J).*

Comparison of the data for different feather types reveals important trends. For untreated samples, black feathers plot with high PC2 and PC3 values, reflecting strong peaks for amides I, II and III, relative to white and orange feathers (Figure 6.5G); orange feathers show lower PC3 values, and white feathers, the lowest PC3 values. These broad relationships within the chemospace plot are retained following progressive maturation (Figure 6.5I–J). Collectively, this data indicates that FTIR can differentiate black, white and orange feathers – i.e., feathers with different melanin content – even after strong thermal alteration.

6.4 Discussion

Our previous taphonomic experiments (Chapter 5) provided preliminary data on the response of feather CBPs to thermal maturation. The results revealed that disulfides and amides from feather CBPs in black and white feathers readily survive "moderate" thermal maturation at 200°C, although β-sheets (the dominant secondary structure in feather CBPs) are altered to a-helices during "strong" maturation at 250°C (Chapter 5).

The current study expands the scope of our preliminary dataset both in terms of feather chemistry and experimental parameters. New thermal maturation experiments on orange feathers and new sulfurization experiments provide a comparative basis to assess the impact of melanin chemistry and sulfide availability on feather CBP preservation. Additional experiments using various combinations of decay, temperature and pressure (or select parameters in isolation) inform on the relative impact of these variables using black feathers as a model.

6.4.1 Impact of melanin chemistry

This study reveals that the melanin chemistry of feathers impacts the survival of feather CBPs. Firstly, eumelanin-rich black feathers, phaeomelanin-rich orange feathers and amelanic white feathers respond differently to maturation. This difference is most evident after strong maturation (250˚C), where the disulfide peaks is strongest in white feathers and absent in black feathers, and the sulfate peak is strongest in black feathers. These

results have important implications for the fossil record. Firstly, by confirming that S-XANES can discriminate between feathers with different melanin chemistry even after strong maturation, our data suggest that the technique has potential applications in the determination of original melanin-based colour in fossils.

More important, however, are our data on CBP preservation. Key indicators of feather CBPs (and their degraded remnants) are disulfides and amides. Our experimental data reveal that amides and disulfides from feather CBPs are better preserved in phaeomelanin-rich and, especially, amelanic feathers than in eumelanin-rich feathers. Collectively, our FTIR and S-XANES data indicate that the preservation of feather CBPs is strongly impacted by melanin content; this is probably a strong taphonomic bias in the feather fossil record and may have broader implications for the detection of feather CBPs and potentially other proteins in integumentary and other tissues.

The most plausible underlying chemical mechanism at play is the interaction of melanin degradation products with feather CBPs. Eumelanin contains abundant free carboxylic acid residues[45] that are readily oxidised, yielding CO_2, an oxidant with higher oxidising potential under high temperatures[46]. CO_2 is also produced by the decarboxylation of the eumelanin unit DHICA and the phaeomelanin unit BZ during thermal degradation[47-49]. Our previous experiments showed that DHICA experiences extensive decarboxylation during strong maturation, but not moderate maturation (Chapter 4). This preferential release of CO_2 at higher temperatures produces abundant highly-reactive CO_2[46]. In contrast, decarboxylation of BZ phaeomelanin units occurs progressively from moderate to strong maturation (Chapter 4), likely releasing a substantial portion of CO_2 at lower temperatures that is a weaker oxidant[46]. Feather CBPs are thus more likely to be oxidized during maturation in feathers with a dominant eumelanin composition.

An additional factor is the timing of oxidation (if any). Given that mouldic melanosomes are more likely to form (via oxidation) during early diagenesis, the absence of melanosomes – and thus of melanin during later diagenesis (and presumably higher temperatures) – may further promote the preservation of feather CBPs.

Finally, the metal content of feathers may indirectly impact feather CBP preservation. Eumelanin is typically associated with Cu^{+2} and phaeomelanin, with Zn^{+2}.[40, 44]. Cu^{+2} is a stronger oxidant than Zn^{+2} [50], suggesting that the eumelanin metallome may prefentially promote the oxidation of feather CBPs relative to the phaeomelanin metallome.

6.4.2 Comparison of experimental treatments

Comparative analysis of data from black feathers degraded under different experimental conditions reveals that the primary taphonomic controls differ for feather CBP disulfides and amides.

S-XANES data reveal that the controls on the preservation of feather CBP disulfides – and thus feather CBP tertiary structure – are, in decreasing order of importance, temperature (without pressure), pressure and decay. This finding confirms our preliminary experimental data (Slater et al. in prep.) that showed a striking difference in the response of feather CBPs to thermal maturation at different temperatures. Moderate maturation of feathers results in minor oxidation of disulfides; strong maturation results in the complete loss of disulfides and generation of abundant organic sulfate (Figures 6.1 and 6.2C). The latter changes are more substantial than those exhibited by feathers matured using high temperature-high pressure maturation. Maturation with pressure results in minor oxidation of disulfides (and production of minor organic sulfate (Figures 6.1 and 6.2C)). Unexpectedly, decayed feathers have less organic sulfate than their untreated counterparts.

FTIR data reveal that the controls on the preservation of the amide component of feather CBPs – and thus feather CBP secondary structures – are, in decreasing order of importance, pressure (with temperature), temperature and decay. High temperature-high pressure maturation (using a lower temperature than that used for strong maturation) results in the marked loss of amides and generation of carboxylic acid (band 3 in Figure 6.4, Figure 6.5C). Moderate maturation results in only minor changes to feather chemistry via a slight decrease in amides; strong maturation induces drastic reduction of amides and generation of carboxylic acid (Figures 6.4 and 6.5). Decay (in isolation) reduces amides slightly (Figure 6.4) and reduces carboxylic acid/ester content markedly (band 7 in Figure

6.4); the latter may reflect degradation of free carboxylic acid residues in eumelanin[45]. This decrease in carboxylic acid/ester, which is more substantial than the decrease in carboxylic acid/ester with moderate maturation (Figures 6.4 and 6.5C), is therefore associated here with the degradation of eumelanin and not of feather CBPs. Since there are no other major differences between untreated and decayed feathers, decay is thus considered to have a very minor impact on amide chemistry. Unexpectedly, the decay of feathers prior to high temperature-high pressure maturation results in less amide degradation and less generation of carboxylic acid (band 3 in Figure 6.4, Figure 6.5C).

Collectively, these data suggest that preservation of feather CBPs in fossils is controlled primarily by diagenetic history and not decay. Fossil feathers from deposits with low maximum burial temperatures and pressures are more likely to preserve feather CBP remnants with tertiary and secondary structures; feathers from deposits with a low maximum burial temperature and high maximum burial pressure may preserve evidence of feather CBP tertiary structure but exhibit little evidence of secondary structures.

6.4.3 The impact of ambient sulfur on feather chemistry

The absence of alkylthiophenes indicates that our sulfurization experiments did not result in sulfurization of feathers. This could reflect failure of the experiments due to the specific parameters used, or that feathers are not readily sulfurised, in which case sulfurization is unlikely to contribute to the survival of feather CBPs in the fossil record. Future experiments could test the latter hypothesis, which suggests that sulfur in fossil feather soft tissue is unlikely to be diagenetic but rather should usually indicate original phaeomelanin-rich chemistry.

6.4.4 Implications for the taphonomy of fossil feathers

The absence of disulfides in strongly matured black and orange feathers contrasts with the survival of disulfides in matured white feathers. These data conflict with evidence that black, eumelanin-rich, feathers, are more robust than feathers lacking eumelanin. In particular, our data suggest that melanins do not bind to and stabilise feather proteins, as previously hypothesised[25, 51, 52] and supported by experimental evidence that black

feathers are more recalcitrant than white feathers during decay[53]. The latter conclusion applies to bacterial degradation, however, and not the various combinations of amicrobial decay and maturation investigated here. Other taphonomic experiments reported that only "pigmented" feather tissue yielded an organic residue following maturation[34], but chemical data to support this claim were not provided. A recent study reported tentative evidence that melanin 'blends' with feather tissue[51]. This interpretation, however, is based on TEM images showing indistinct melanosome margins, which could be artefacts. This study therefore provides novel chemical assessment of the impact of melanin content on the preservation of feather CBPs. Based on the experimental data, it is reasonable to expect to recover an amide and cysteine signal in fossil feathers that have not experienced excessively harsh diagenetic conditions, irrespective of melanin content. The preservation of disulfides is predicted to occur preferentially in feathers (or regions thereof) with a low melanin content (especially eumelanin), irrespective of whether this chemistry is original or arose during diagenesis due to oxidation of melanosomes[21].

In sum, the degradation of feather CBPs is primarily controlled by the experimental treatment but, importantly, is also influenced by melanin content. To date, the detection of fossil feather CBPs has focussed on predominantly eumelanic fossil feathers[9, 10, 23, 54]. Our conclusion – that future efforts to detect fossil feather CBPs should target phaeomelanic and especially amelanic fossil feathers – is therefore unexpected. Collectively, the results form the basis for a new integrated model for feather preservation that is firmly grounded in quantitative empirical data and encompasses all major feather components. This model explains variations in the preservation of fossil feathers and represents a major advance in our understanding of the preservation of feathers and of structural proteins. Critically, the model highlights the power of combining systematic and quantitative taphonomic experiments with a holistic, whole-tissue approach, to resolve long-standing issues relating to the preservation of soft tissues in the fossil record.

Acknowledgments. We thank Sharon Bone, Valentina Rossi, Chris Rogers, Thomas Clements, Luke McDonald and Naomi O'Reilly for assistance. This work was supported by ERC Starting Grant H2020-ERC-2014-StG-637691-ANICOLEVO awarded to M.E.M. The use of the Stanford Synchrotron Radiation Lightsource, SLAC National Accelerator Laboratory,

is supported by the US Department of Energy, Office of Science, Office of Basic Energy Sciences under contract no. DE-AC02-76SF00515 awarded to M.E.M.

Author contributions. M.E.M. conceived the research and designed the study with T.S.S. T.S.S. and M.E.M. performed S-XANES and FTIR analyses. N.P.E. and S.W. assisted with S-XANES data collection. B.v.D. performed py-GCMS analyses. T.S.S. and M.E.M. wrote the manuscript with input from all other authors.

6.5 References

1. Yang, Z., Jiang, B., McNamara, M.E., Kearns, S.L., Pittman, M., Kaye, T.G., Orr, P.J., Xu, X., and Benton, M.J. (2019). Pterosaur integumentary structures with complex feather-like branching. Nature ecology & evolution *3*, 24–30.
2. Cincotta, A., Nicolaï, M., Bruno, H., Campos, H. B. N., McNamara, M., D'Alba, L., Shawkey, M. D., Kischlat E.-E., Yans, J., Carleer, R., Escuillié, F. & Godefroit, P. (2022 *accepted*). Melanosomes in simple and branched pterosaur feathers support signalling functions for early feathers. Nature.
3. Alibardi, L. (2017). cornification, morphogenesis and evolution of feathers. Protoplasma *254*, 1259–1281.
4. Dhouailly, D. (2009). A new scenario for the evolutionary origin of hair, feather, and avian scales. Journal of anatomy *214*, 587–606.
5. Dalla Valle, L., Nardi, A., Gelmi, C., Toni, M., Emera, D., and Alibardi, L. (2009). β-keratins of the crocodilian epidermis: composition, structure, and phylogenetic relationships. Journal of Experimental Zoology Part B: Molecular and Developmental Evolution *312*, 42–57.
6. Godefroit, P., Sinitsa, S.M., Dhouailly, D., Bolotsky, Y.L., Sizov, A.V., McNamara, M.E., Benton, M.J., and Spagna, P. (2014). A Jurassic ornithischian dinosaur from Siberia with both feathers and scales. Science *345*, 451–455.
7. Xu, X., Zheng, X., and You, H. (2010). Exceptional dinosaur fossils show ontogenetic development of early feathers. Nature *464*, 1338–1341.
8. Schweitzer, M., Watt, J., Avci, R., Knapp, L., Chiappe, L., Norell, M., and Marshall, M. (1999). Beta-keratin specific immunological reactivity in feather-like structures of

the Cretaceous Alvarezsaurid, Shuvuuia deserti. Journal of Experimental Zoology *285*, 146–157.

9. Pan, Y., Zheng, W., Moyer, A.E., O'Connor, J.K., Wang, M., Zheng, X., Wang, X., Schroeter, E.R., Zhou, Z., and Schweitzer, M.H. (2016). Molecular evidence of keratin and melanosomes in feathers of the Early Cretaceous bird Eoconfuciusornis. Proceedings of the National Academy of Sciences *113*, E7900–E7907.
10. Pan, Y., Zheng, W., Sawyer, R.H., Pennington, M.W., Zheng, X., Wang, X., Wang, M., Hu, L., O'Connor, J., and Zhao, T. (2019). The molecular evolution of feathers with direct evidence from fossils. Proceedings of the National Academy of Sciences *116*, 3018–3023.
11. Hill, G.E., Hill, G.E., McGraw, K.J., and Kevin, J. (2006). Bird coloration: function and evolution, Volume 2, (Harvard University Press).
12. Holthaus, K.B., Eckhart, L., Dalla Valle, L., and Alibardi, L. (2018). Evolution and diversification of corneous beta-proteins, the characteristic epidermal proteins of reptiles and birds. Journal of Experimental Zoology Part B: Molecular and Developmental Evolution *330*, 438–453.
13. Barden, H.E., Bergmann, U., Edwards, N.P., Egerton, V.M., Manning, P.L., Perry, S., van Veelen, A., Wogelius, R.A., and van Dongen, B.E. (2015). Bacteria or melanosomes? A geochemical analysis of micro-bodies on a tadpole from the Oligocene Enspel Formation of Germany. Palaeobiodiversity and Palaeoenvironments *95*, 33–45.
14. Vinther, J. (2016). Fossil melanosomes or bacteria? A wealth of findings favours melanosomes: Melanin fossilises relatively readily, bacteria rarely, hence the need for clarification in the debate over the identity of microbodies in fossil animal specimens. BioEssays *38*, 220–225.
15. D'Alba, L., and Shawkey, M.D. (2019). Melanosomes: biogenesis, properties, and evolution of an ancient organelle. Physiological reviews *99*, 1–19.
16. Roy, A., Rogers, C.S., Clements, T., Pittman, M., Habimana, O., Martin, P., and Vinther, J. (2020). Fossil Microbodies Are Melanosomes: Evaluating and Rejecting the "Fossilized Decay-Associated Microbes" Hypothesis. Bulletin of the American Museum of Natural History, 251–276.

17. McNamara, M., Rossi, V., Slater, T., Rogers, C., Ducrest, A.-L., Dubey, S., and Roulin, A. (2021). Decoding the Evolution of Melanin in Vertebrates. Trends in Ecology & Evolution. *36*, 430–443.
18. Demarchi, B., Hall, S., Roncal-Herrero, T., Freeman, C.L., Woolley, J., Crisp, M.K., Wilson, J., Fotakis, A., Fischer, R., and Kessler, B.M. (2016). Protein sequences bound to mineral surfaces persist into deep time. elife *5*, e17092.
19. Eglinton, G., and Logan, G.A. (1991). Molecular preservation. Philosophical Transactions of the Royal Society of London. Series B: Biological Sciences *333*, 315–328.
20. Bada, J.L., Wang, X.S., and Hamilton, H. (1999). Preservation of key biomolecules in the fossil record: current knowledge and future challenges. Philosophical Transactions of the Royal Society of London. Series B: Biological Sciences *354*, 77–87.
21. Slater, T.S., McNamara, M.E., Orr, P.J., Foley, T.B., Ito, S., and Wakamatsu, K. (2020). Taphonomic experiments resolve controls on the preservation of melanosomes and keratinous tissues in feathers. Palaeontology *63*, 103–115.
22. Saitta, E.T., Rogers, C.S., Brooker, R.A., and Vinther, J. (2017). Experimental Taphonomy of Keratin: a Structural Analysis of Early Taphonomic Changes. Palaios *32*, 647–657.
23. Saitta, E.T., Rogers, C., Brooker, R.A., Abbott, G.D., Kumar, S., O'Reilly, S.S., Donohoe, P., Dutta, S., Summons, R.E., and Vinther, J. (2017). Low fossilization potential of keratin protein revealed by experimental taphonomy. Palaeontology *60*, 547–556.
24. Saitta, E.T., Kaye, T.G., and Vinther, J. (2019). Sediment-encased maturation: a novel method for simulating diagenesis in organic fossil preservation. Palaeontology *62*, 135–150.
25. Moyer, A., Zheng, W., and Schweitzer, M. (2016). Keratin durability has implications for the fossil record: results from a 10 year feather degradation experiment. PlosOne 11 (7): e0157699.
26. Collins, M., Westbroek, P., Muyzer, G., and De Leeuw, J. (1992). Experimental evidence for condenzationreactions between sugars and proteins in carbonate skeletons. Geochimica et Cosmochimica Acta *56*, 1539–1544.

27. Schweitzer, M.H., Watt, J.A., Avci, R., Forster, C.A., Krause, D.W., Knapp, L., Rogers, R.R., Beech, I., and Marshall, M. (1999). Keratin immunoreactivity in the Late Cretaceous bird Rahonavis ostromi. Journal of Vertebrate Paleontology *19*, 712–722.

28. Calvaresi, M., Eckhart, L., and Alibardi, L. (2016). The molecular organization of the beta-sheet region in corneous beta-proteins (beta-keratins) of sauropsids explains its stability and polymerization into filaments. Journal of structural biology *194*, 282–291.

29. Alibardi, L. (2016). The process of cornification evolved from the initial keratinization in the epidermis and epidermal derivatives of vertebrates: a new synthesis and the case of sauropsids. International review of cell and molecular biology *327*, 263–319.

30. Wang, B., Yang, W., McKittrick, J., and Meyers, M.A. (2016). Keratin: Structure, mechanical properties, occurrence in biological organisms, and efforts at bioinspiration. Progress in Materials Science *76*, 229–318.

31. McGraw, K., Safran, R., and Wakamatsu, K. (2005). How feather colour reflects its melanin content. Functional Ecology *19*, 816–821.

32. Wakamatsu, K., and Ito, S. (2002). Advanced chemical methods in melanin determination. Pigment Cell Research *15*, 174–183.

33. Galván, I., and Solano, F. (2016). Bird integumentary melanins: biosynthesis, forms, function and evolution. International Journal of Molecular Sciences *17*, 520.

34. Saitta, E.T., Kaye, T.G., and Vinther, J. (2018). Sediment-encased maturation: a novel method for simulating diagenesis in organic fossil preservation. Palaeontology. *62*, 135–150.

35. Wogelius, R., Manning, P., Barden, H., Edwards, N., Webb, S., Sellers, W., Taylor, K., Larson, P., Dodson, P., and You, H. (2011). Trace metals as biomarkers for eumelanin pigment in the fossil record. Science *333*, 1622–1626.

36. Briggs, D.E., and Kear, A.J. (1994). Decay and mineralization of shrimps. Palaios *9*, 431–456.

37. Sagemann, J., Bale, S.J., Briggs, D.E., and Parkes, R.J. (1999). Controls on the formation of authigenic minerals in association with decaying organic matter: an experimental approach. Geochimica et Cosmochimica Acta *63*, 1083–1095.

38. van Dongen, B.E., Schouten, S., and Sinninghe Damsté, J.S. (2003). Sulfurization of carbohydrates results in a sulfur-rich, unresolved complex mixture in kerogen pyrolysates. Energy & Fuels *17*, 1109–1118.

39. Ravel, B., and Newville, M. (2005). ATHENA, ARTEMIS, HEPHAESTUS: data analysis for X-ray absorption spectroscopy using IFEFFIT. Journal of synchrotron radiation *12*, 537–541.

40. Edwards, N.P., Van Veelen, A., Anné, J., Manning, P.L., Bergmann, U., Sellers, W.I., Egerton, V.M., Sokaras, D., Alonso-Mori, R., and Wakamatsu, K. (2016). Elemental characterizationof melanin in feathers via synchrotron X-ray imaging and absorption spectroscopy. Scientific reports *6*, 34002.

41. Menges, F. (2017). Spectragryph-optical spectroscopy software. Version *1*, 2016–2017.

42. Wakamatsu, K., Ohtara, K., and Ito, S. (2009). Chemical analysis of late stages of pheomelanogenesis: conversion of dihydrobenzothiazine to a benzothiazole structure. Pigment cell & melanoma research *22*, 474–486.

43. Galván, I., and Solano, F. (2015). Melanin chemistry and the ecology of stress. Physiological and Biochemical Zoology *88*, 352–355.

44. Manning, P.L., Edwards, N.P., Bergmann, U., Anné, J., Sellers, W.I., van Veelen, A., Sokaras, D., Egerton, V.M., Alonso-Mori, R., and Ignatyev, K. (2019). Pheomelanin pigment remnants mapped in fossils of an extinct mammal. Nature communications *10*, 1–13.

45. d'Ischia, M., Wakamatsu, K., Napolitano, A., Briganti, S., Garcia-Borron, J.C., Kovacs, D., Meredith, P., Pezzella, A., Picardo, M., and Sarna, T. (2013). Melanins and melanogenesis: methods, standards, protocols. Pigment cell & melanoma research *26*, 616–633.

46. Kawi, S., and Kathiraser, Y. (2015). CO2 as an oxidant for high-temperature reactions. Frontiers in Energy Research *3*, 13.

47. Ito, S., Wakamatsu, K., Glass, K., and Simon, J.D. (2013). High-performance liquid chromatography estimation of cross-linking of dihydroxyindole moiety in eumelanin. Analytical biochemistry *434*, 221–225.

48. Ito, S., Miyake, S., Maruyama, S., Suzuki, I., Commo, S., Nakanishi, Y., and Wakamatsu, K. (2018). Acid hydrolysis reveals a low but constant level of

pheomelanin in human black to brown hair. Pigment cell & melanoma research *31*, 393–403.

49. Jarenmark, M., Sjövall, P., Ito, S., Wakamatsu, K., and Lindgren, J. (2021). Chemical Evaluation of Eumelanin Maturation by ToF-SIMS and Alkaline Peroxide Oxidation HPLC Analysis. International Journal of Molecular Sciences *22*, 161.
50. Vanýsek, P. (2012). Electrochemical series. Handbook of Chemistry and Physics *93*, 5–80.
51. Zhao, T., Hu, J., Hu, L., and Pan, Y. (2020). Experimental maturation of feathers: implications for interpretations of fossil feathers. Palaios *35*, 67–76.
52. Lindgren, J., Moyer, A., Schweitzer, M.H., Sjövall, P., Uvdal, P., Nilsson, D.E., Heimdal, J., Engdahl, A., Gren, J.A., and Schultz, B.P. (2015). Interpreting melanin-based coloration through deep time: a critical review. Proceedings of the Royal Society B: Biological Sciences *282*, 20150614.
53. Goldstein, G., Flory, K.R., Browne, B.A., Majid, S., Ichida, J.M., and Burtt Jr, E.H. (2004). Bacterial degradation of black and white feathers. The Auk *121*, 656–659.
54. Lindgren, J., Sjövall, P., Carney, R.M., Cincotta, A., Uvdal, P., Hutcheson, S.W., Gustafsson, O., Lefèvre, U., Escuillié, F., and Heimdal, J. (2015). Molecular composition and ultrastructure of Jurassic paravian feathers. Scientific reports *5*, 13520.

6.6 Supplementary information

6.6.1 Supplementary text

FTIR data. Use of the term 'band' regarding FTIR spectra refers here to the range of wavelengths in which one or more peaks can occur for a chemical bond (or bonds) that, in turn, is associated with a functional group (or groups). Peak assignments were made using IRPal v2.0[1]. Peaks for amide functional groups (R–C=O–NH_2) are within bands A (3115–3360 cm^{-1}), B (3015–3115 cm^{-1}), I (1575–1700 cm^{-1}), II (1475–1575 cm^{-1}) and III (1210–1295 cm^{-1}) and are discussed in the main text. Further, moderate peaks within bands 3 and 7 are also discussed in the main text.

Assignments of moderate and minor FTIR peaks. An additional moderate peak in FTIR spectra is within band 2. Minor peaks in FTIR spectra are within bands 1, 4–6 and 8–10 (see Supplementary Table 6.1). The assignments of these bands are as follows. Band 2 spans the range 2820–3015 cm^{-1} and, depending on the sample type, includes three to five weak to moderate peaks; it is attributed to C–H stretching vibrations of CH_2 and CH_3 methyl groups. Band 1 (3360–3680 cm^{-1}) is attributed to the O–H stretch of carboxylic acid. A peak in band 4 (1420–1475 cm^{-1}) is potentially associated with stretching vibrations of methyl C–H, aromatic C–C and/or sulfate S=O. A minor sharp peak in band 5 (1380–1420 cm^{-1}) corresponds to methyl C–H stretching and/or sulfate S=O stretch. A minor peak in band 6 (1130–1180 cm^{-1}) potentially corresponds to methyl C–H wag, carboxylic acid/ester C–O stretch, thiocarbonyl C=S stretch and/or sulfone S=O stretch. A peak in band 8 (940–965 cm^{-1}) corresponds to N–O amine oxide aliphatics. Weak peaks in band 9 (715–815 cm^{-1}) correspond to out of plane bending of aromatic C–H and/or S–OR esters. A minor peak in band 10 (495–580 cm^{-1}) corresponds to S–S stretch.

Variation in the position of key peaks among FTIR spectra. Band 2 contributes to variation in the PCA, albeit to lesser degree than peaks within the amide bands and bands 3 and 7 (Figure 6.5F; see main text). Band 2 is therefore included in the following overview of the variation in the position of key peaks among FTIR spectra. Amide bands and bands 2, 3 and 7 all exhibit variation in peak position among different coloured feathers and treatments.

Untreated feathers. The spectrum for untreated black feathers exhibits a peak for amide A at 3267 cm^{-1}, B at 3064 cm^{-1}, I at 1627 cm^{-1}, II at 1538 cm^{-1} and III at 1232 cm^{-1}. Five peaks are present in band 2, with the strongest peak at 2922 cm^{-1}, and one strong sharp peak is displayed in band 7 at 1036 cm^{-1}.

Untreated orange feathers show amide A at 3279 cm^{-1}, B at 3064 cm^{-1}, I at 1628 cm^{-1}, II at 1522 and III at 1236 cm^{-1}. Orange feathers display five weak peaks in band 2 with the strongest peak at 2981 cm^{-1} and two weak peaks in band 7 at 1072 cm^{-1} and 1042 cm^{-1}.

Untreated white feathers possess amide A at 3281 cm^{-1}, B at 3063 cm^{-1}, I at 1630 cm^{-1}, II at 1522 cm^{-1} and III at 1234 cm^{-1}. White feathers possess only four weak peaks in band 2, with the strongest peak at 2972 cm^{-1}, and two weak peaks in band 7 at 1072 cm^{-1} and 1046 cm^{-1}.

Decayed feathers. Compared to untreated black feathers, decayed black feathers display different peak positions for all amides except amide I (1627 cm^{-1}): amide A is at 3279 cm^{-1}, B at 3060 cm^{-1}, II at 1539 cm^{-1} and III at 1235 cm^{-1}. Further, decayed black feathers display the strongest peak at 2972 cm^{-1} within band 2 and two weak peaks at 1070 cm^{-1} and 1041 cm^{-1} in band 7, which contrasts with untreated black feathers. Decayed black feathers exhibit stronger peaks than untreated black feathers within all major bands except band 7.

Feathers matured using high temperature-high pressure maturation. Maturation at 150°C, 135 bar produces differences in the positions of all major peaks compared to untreated black feathers. The peak positions for amides B, I, II and III shift slightly relative to untreated black feathers: amide B is positioned at 3063 cm^{-1}, amide I at 1636 cm^{-1}, amide II at 1523 cm^{-1} and amide III at 1237 cm^{-1}. Unlike untreated black feathers, band 7 displays a very weak peak at 1024 cm^{-1}. Notably, black feathers decayed prior to high temperature-high pressure maturation are near-identical to black feathers matured using temperature-high pressure maturation with no prior decay; feathers from both treatments show three weak peaks within band 2, with the strongest at 2972 cm^{-1}.

Moderately matured feathers. Black feathers matured at 200°C exhibit peak positions different to untreated black feathers in amide III (1233 cm^{-1}) and bands 2 (2925 cm^{-1}) and 7

(1068 cm^{-1} and 1028 cm^{-1}). Compared to untreated black feathers, feathers matured at 200°C display stronger peaks within all major bands except bands 2 and III.

Orange feathers matured at 200°C display peak positions different to untreated orange feathers in amide III (1233 cm^{-1}) and band 7 (1019 cm^{-1} and 1044 cm^{-1}); unlike untreated feathers, band 2 contains only four peaks with the strongest peak at 2924 cm^{-1}. Compared to untreated orange feathers, feathers matured at 200°C display stronger peaks only within bands B, I, II and 7.

Compared to untreated white feathers, those matured at 200°C show different peak positions for amides B (3064 cm^{-1}) and III (1233 cm^{-1}) and band 2 (2971 cm^{-1}). Further, feathers matured at 200°C display stronger peaks only within bands B and 7.

Similar to untreated feathers, key differences among black, orange and white feathers matured at 200°C include variation in the peak positions within most major bands. All major peaks have different positions among the different coloured feathers matured at 200°C, excluding amide B and III in all feathers and amide II in orange and white feathers. Compared to untreated feathers, all feathers exhibit changes in the position of major peaks in band 2 and amide III and, in black and orange feathers, band 7. Peaks within bands B, I, II and 7 are strongest in black feathers and those within bands A, 2 and III are strongest in white feathers; peaks within bands A, I, II and III are weakest in orange feathers.

Strongly matured feathers. Black feathers matured at 250°C show peak positions different to untreated black feathers in amides I (1653 cm^{-1}) II (1539 cm^{-1}) and III (1239 cm^{-1}) and bands 2 (2973 cm^{-1}), 3 (1711 cm^{-1}) and 7 (1017 cm^{-1}). Compared to untreated black feathers, feathers matured at 250°C display stronger peaks only within bands 2 and 3.

Compared to untreated orange feathers, those matured at 250°C display different peak positions for amides I (1656 cm^{-1}), II (1532 cm^{-1}) and III (1232 cm^{-1}) and bands 2 (2973 cm^{-1}), 3 (1710 cm^{-1}) and 7 (1039 cm^{-1}). Further, feathers matured at 250°C display a stronger peak only within band 3.

White feathers matured at 250°C exhibit peak positions different to untreated white feathers in amides I (1655 cm^{-1}), II (1531 cm^{-1}) and III (1239 cm^{-1}) and bands 2 (2973 cm^{-1}), 3 (1710 cm^{-1}) and 7 (1040 cm^{-1}). Compared to untreated white feathers, feathers matured at 250°C display stronger peaks only within bands 2 and 3.

All feathers matured at 250°C display one moderate peak and two weak peaks within band 2 and one weak peak in band 7. Further, all strongly matured feathers exhibit differences in the positions of all major peaks compared to untreated feathers of the same colour. The key difference among spectra for strongly matured black, orange and white feathers is that they display different peak positions within all major bands, excluding band 2 in all feathers and amide III in black and white feathers. Peaks within bands 2, 3 and III are strongest in white feathers and those within bands I, II and 7 are strongest in black feathers; peaks within bands 3, I and II are weakest in orange feathers.

Additional results from the PCA of FTIR spectra. In the PCA, data for untreated and decayed feathers and feathers matured at 200°C partially overlap in the right-hand side of the chemospace plot. Collectively, these treatments show little variation in PC2, corresponding to a minor or absent peak in band 3 and relatively strong amide peaks, and substantial variation in PC3, reflecting differences within band 7. Feathers matured at 150°C, 135 bar and 250°C overlap with each other but with no other treatment. Both treatments sit in the left-hand side of the plot, indicating a strong peak in band 3 and relatively weaker amide peaks; they also show substantial variation in PC3, reflecting differences within band 7.

Black feathers of all treatments exhibit a large data field that spans the entirety of both axes (Figure 6.5B). Untreated black feathers plot at high values in PC2 and mid-values in PC3, indicating the absence of a peak within band 3 and the presence of a strong single peak in band 7 (Figure 6.5C). Decayed black feathers display no overlap with any other treatment and plot at lower PC2 and PC3 values than untreated black feathers, reflecting the presence of two peaks within band 7 in the former. Data for black feathers matured at 150°C, 135 bar with and without prior decay overlap; these treatments plot at even lower PC2 values than decayed (non-matured) black feathers, corresponding to a peak within band 3 and weaker amide I and II peaks in feathers matured at 150°C, 135 bar. Data for black feathers matured at 200°C completely overlap with all untreated black feathers.

Black feathers matured at 250°C plot at low PC2 and high PC3 values, reflecting a peak within band 3, and exhibit little overlap with feathers matured at 150°C, 135 bar (with and without decay).

Orange feathers of all treatments span the majority of PC2 but are restricted to the bottom of PC3 (Figure 6.5B). Untreated orange feathers plot in the bottom-right of the chemospace, indicating an absence of a single strong peak within bands 3 and 7 (Figure 6.5D). Data for orange feathers matured at 200°C plot at slightly higher PC3 values than untreated feathers due to peak position changes in band 2. Feathers matured at 250°C plot at low PC2 and PC3 values, reflecting the presence of a strong peak within band 3 and a weak peak in band 7. Data for orange feathers do not overlap among the different experiments.

White feathers of all treatments occupy the majority of PC2 and, similar to orange feathers, are restricted to the bottom of PC3 (Figure 6.5B). Data for untreated white feathers are situated in the bottom-right of the chemospace, corresponding to the absence of a single strong peak within bands 3 and 7 (Figure 6.5E). White feathers matured at 200°C plot at marginally higher PC3 values than untreated feathers, indicating very little change in amides and bands 2 and 7. The data field for white feathers matured at 250°C plots at low PC2 values, corresponding to a single strong peak in band 3 and, compared to untreated and feathers matured at 200°C, weaker peaks for amides I and II. Data for white feathers do not overlap among the different experiments.

The data for decayed feathers, and feathers matured at 150°C, 135 bar, are for black feathers only. For untreated feathers and feathers matured at 200°C and 250°C, the chemistries of black, white and orange feathers can be compared. The chemospace reveals that the data fields for untreated orange and white feathers overlap at low PC3 values, reflecting the absence of a single strong peak within band 7 in each and similar peak positions within band 2. In contrast, black feathers plot at high PC3 values, indicating a single strong peak within band 7, and at slightly higher PC2 values than orange and white feathers, reflecting differences in the peak positions in band 2 to those of orange and white feathers (Figure 6.5G). Data for black feathers matured at 150°C, 135 bar with and without prior decay overlap, with non-decayed, matured samples occupying a larger data

field than decayed, matured samples (Figure 6.5H); samples decayed prior to maturation plot mostly to the right of non-decayed, matured samples, reflecting a weaker peak in band 3 in most decayed, matured samples. Black, orange and white feathers matured at 200°C do not overlap and are approximately equidistant from each other along both axes (Figure 6.5I). White feathers plot at negative PC3 values, reflecting weak peaks in band 7, whereas black feathers plot at higher PC3 and PC2 values, indicating a single strong peak in band 7 and differences in the peak positions in band 2; orange feathers are intermediate. Black, orange and white feathers matured at 250°C show a similar pattern to feathers matured at 200°C but are closer in proximity to each other and are situated at much lower PC2 values, indicating a peak within band 3.

6.6.2 Supplementary figures and tables



Supplementary Fig. 6.1 *Schematic illustration of experimental decay setup.*

Supplementary Table 6.1 *Identification of peaks in FTIR spectra for experimentally degraded black and orange (Gallus gallus) and white (Egretta garzetta) feathers.*

		Assignment		Experimental treatment										
Notation in Figure 4	Band wavenumber (cm^{-1})	Bond	Functional group	Untreated			200°C 1 hour			250°C 1 hour			Decayed 12 months	150° C, 135 bar 1 hour
				Black	Orange	White	Black	Orange	White	Black	Orange	White	Black	Black
1	3355–3700	O–H	Carboxylic acid	3455	3455	3455	3455	3455	3455	3455	3455	3455	3455	3455
A	3115–3355	N–H	Amide A	3267	3279	3281	3267	3279	3281	–	–	–	3279	–
B	3015–3115	N–H	Amide B	3064	3064	3063	3064	3064	3064	–	–	–	3072	3063
2	2820–3015	C–H	CH_2 and CH_3	2922	2981	2972	2925	2924	2971	2973	2973	2973	2972	2972
3	1696–1810	C=O	Carboxylic acid	–	–	–	–	–	–	1711	1710	1710	–	1728
I	1575–1696	C=O N–H	Amide I	1627	1628	1630	1627	1628	1630	1653	1656	1655	1627	1636
II	1475–1575	N–H C–N C–C	Amide II	1538	1522	1522	1538	1522	1522	1539	1532	1531	1539	1523
4	1420–1475	S=O C–C C–H	Sulfate Aromatics CH_2 and CH_3	1450	1455	1452	1450	1450	1450	–	–	–	1455	1452
5	1355–1420	S=O C–H	Sulfate CH_2 and CH_3	1390	1385	1382	1388	1388	1388	1381	1381	1381	1381	1381
III	1190–1285	C–N	Amide III	1232	1236	1234	1233	1233	1233	1239	1232	1239	1235	1237
6	1135–1190	C–O C–H C=S S=O	Carboxylic acid, ester CH_2 Thiocarbonyl Sulfone	1152	1159	1161	1159	1159	1161	1163	1163	1163	1161	1162
7	975–1140	S=O C–O	Sulfoxide Carboxylic acid, ester	1036	1042, 1072	1046, 1072	1028, 1068	1019, 1044	1046	1017	1039	1040	1041, 1070	1024
8	925–975	N–O	Amine oxide	–	953	953	–	–	953	953	953	953	953	953
9	710–845	C–H S–O	Aromatics S-OR esters	799	–	–	798	756	817	756	756	756	818	818
10	500–580	S–S	Disulfide	531	530	532	534	532	532	531	533	532	532	533

7. Discussion

The main findings of this thesis are: (1) taphonomic processes vary in the extent to which they control the preservation of primary feather components (section 7.1); (2) the intrinsic chemistry of feathers influences the preservation potential of feather CBPs and melanins (section 7.2), and; (3) evidence of phaeomelanin and feather CBPs can survive in deep time (section 7.3). The experimental design and analytical limitations of these main findings are discussed in subsections 7.1.3, 7.2.3, 7.3.2 and 7.3.4. Section 7.4 outlines a new taphonomic model that explains the link between the variable preservation of fossil feathers and biological and geological controls. Finally, section 7.5 discusses the broad limitations of the taphonomic experiments performed here.

7.1 Taphonomic processes vary in the extent to which they control the preservation of primary feather components

The primary components of feathers are feather CBPs – the primary proteins in feathers – and melanins (the latter within melanosomes), which differ in chemistry. Melanosomes are often cited as being particularly resistant to degradation, due to the biopolymeric nature of melanin (Borovansky & Riley, 2011); biopolymers, in turn, are considered more recalcitrant than proteins (Briggs et al., 2000). A taphonomic scenario whereby melanosomes preferentially degrade, yet remnants of proteinaceous feather tissue survive, is therefore somewhat counter-intuitive and is not universally accepted (e.g., see Saitta et al. [2018]). In particular, interpretations of the amorphous to fibrous material that surrounds mouldic melanosomes and 3D melanosomes in some fossils as the organic residue of the proteinaceous feather cortex (Gren et al., 2017; Li et al., 2010; Lindgren et al., 2015b; Pan et al., 2016, 2019; Zhang et al., 2010) are controversial (Saitta et al., 2017a, b, 2018). This controversy largely stems from the absence of data from systematic taphonomic experiments that use appropriate conditions to determine the response of feather components to degradation.

This thesis directly addresses this controversial issue by presenting new empirical data on how feather morphology and chemistry alter during degradation. Importantly, taphonomic processes vary in the extent to which they control the preservation of melanosomes and

proteinaceous feather tissue. As a result, this thesis confirms that taphonomic scenarios, whereby melanin and melanosomes degrade and remnants of proteinaceous feather tissue can survive, exist; notably, all of these melanin-degrading taphonomic scenarios include oxidation. The response of the melanic and protein components of feathers to degradation is discussed in turn below.

7.1.1 The taphonomy of melanin and melanosomes

This thesis provides new empirical data on the taphonomy of melanosomes and melanin. The taphonomic experiments performed here investigate the impact of decay, oxidation and maturation (in isolation and in combination). Data from taphonomic experiments inform on the morphological preservation of melanosomes (based on SEM and TEM micrographs) and the chemical preservation of the melanin molecule (based on AHPO-HPLC data). The results reveal that the factors that control melanosome preservation are, in decreasing order of importance: oxidation, maturation and decay. These factors are discussed separately in the text below.

Oxidation is the primary control on melanosome preservation at least under the experimental conditions used in this study. Electron micrographs show that moulds occur only in oxidised feathers (Figs. 3.2e, 3.3 and 3.4c). AHPO-HPLC data show that oxidised (black) feathers contain a higher number of moulds and substantially fewer PTCA and PTeCA eumelanin markers (Fig. 3.6) than untreated examples (Fig. 4.2), indicating extensive eumelanin degradation. Collectively, morphological and chemical data support the hypothesis that oxidation generates fossil mouldic melanosomes (McNamara, 2013; Vinther, 2016).

The oxidation of melanosomes and the formation of melanosome moulds does not imply complete loss of melanin from feather tissue. Melanosomes are not evident in SEM and TEM micrographs of oxidised feathers. AHPO-HPLC data, however, reveal the presence of eumelanin monomers in oxidised feathers (pathway 5 in Fig. 3.6), although in lower quantities than in untreated feathers (Fig. 4.2). The presence of eumelanin monomers in oxidised feathers suggests that organic residues of melanin can remain regardless of whether the melanosome preserves in 3D (but see Chapter 7.1.3). This raises the

possibility that metals that associate with melanin, whether original or diagenetic (see Chapter 1.7.2), may also remain in fossil feather tissue, regardless of 3D melanosome preservation. Wogelius et al. (2011) report a Cu-melanin complex in an isolated Green River feather that may derive from mouldic melanosomes. Indeed, the regions of the Green River feather that exhibit a Cu signal do not contain 3D melanosomes (Wogelius et al., 2011) but, notably, also do not contain mouldic melanosomes. In a separate report, Lindgren et al. (2015b) provide chemical data on two different regions of *Anchiornis* feathers, both of which include mouldic melanosomes. One region that contains mouldic melanosomes displays a chemical signal consistent with eumelanin in ToF-SIMS data, but Lindgren et al. (2015b) interpret those mouldic melanosomes as the result of sample preparation or disruption. The second region with mouldic melanosomes was interpreted as deriving from melanosome degradation (Lindgren et al., 2015b); those mouldic melanosomes show a chemical signal that is similar to that of the host sediment, albeit with more calcium phosphate (Lindgren et al., 2015b). Reports to date do not, therefore, provide definitive evidence of a eumelanin signal in mouldic melanosomes. Further experiments are required to confirm the hypothesis that remnants of melanin can survive in fossil mouldic melanosomes.

Experimental data suggest that the timing of oxidation is crucial to melanosome survival. Exposure to an oxidant following maturation results in less degradation of melanosomes (Figs. 3.3e–h and 3.4d) and melanin (Fig. 3.6) than where oxidation occurs prior to maturation (Figs. 3.3a–d and 3.6). Notably, maturation following oxidation does not occlude the moulds generated by oxidation, indicating that moulds formed early during diagenesis have the potential to survive in fossils. Mouldic melanosomes in fossil feathers thus most likely indicate the exposure of a fossil to an oxidant early during diagenesis.

It may also be possible to infer the timing of mould formation by considering the alignment of melanosomes in fossil feathers. In *Anchiornis* feathers, 3D melanosomes are aligned, whereas melanosome moulds are not (Lindgren et al., 2015b). This is of interest because eumelanic feathers of extant birds, especially iridescent feathers (Vinther et al., 2008, 2010), can show alignment of eumelanosomes (Carney et al., 2012). Data from fossils and decay experiments indicate that melanosomes can migrate during extended decay when carcasses are disturbed (McNamara et al., 2018). This evidence of melanosome migration,

however, derives from soft internal organs in bloated decaying carcasses filled with decay fluids (McNamara et al., 2018) and may not apply to melanosomes embedded in feather tissue, that is more robust and likely to retain its gross structure during early decay and pre-burial. This potentially conflicts with other experimental data (Saitta et al., 2017a) that demonstrate that melanic feathers decayed in a microbial broth for 50 days resulted in a darkening of the broth during the experiment. The darkening of the microbial broth may indicate that melanin and/or melanosomes migrated into the broth during decay (Saitta et al., 2017a), but, notably, this was not tested using SEM or chemical analysis. If melanosomes can indeed migrate into a solution during decay then melanosomes may also be able to migrate within feather tissue during and following appreciable decay. Saitta et al. (2018) also report a loss of melanosome alignment following sediment-encased maturation. Future work incorporating experiments and fossil analyses would be useful in order to determine whether mouldic melanosome alignment can inform on the timing of oxidation in feathers with structural colouration (see Chapter 8.2).

The variation in fossil melanosome alignment in *Anchiornis* has been used to interpret two separate origins for mouldic impressions in fossils. The interpretation that one structure (moulds) may arise from two different origins, however, is not the most parsimonious explanation. Some of the aligned moulds in *Anchiornis* occur in aluminosilicate clays associated with the fossil feathers and are interpreted as having formed concurrently with the mineralisation of decaying feather fibrils (Lindgren et al. 2015b). Other melanosome moulds also occur in clay minerals associated with the feathers but are not aligned; these are interpreted as potentially of bacterial origin (Lindgren et al., 2015b). Eumelanic, non-iridescent feathers of extant birds, however, often possess melanosomes that are not mutually aligned (Maia et al., 2010); this simple observation could explain the non-aligned mouldic melanosomes in *Anchiornis*. Indeed, the short lifespan of a bacterium and the rapid nature of microbial lysis make it highly unlikely that microbial structure could survive for a sufficient period to generate moulds in clay minerals (unless precipitation of the clays was extremely fast). For example, the average lifespan of *Escherichia coli* is less than one day (Reshes et al., 2008); further, a bacterium undergoes full lysis in less than 30 min (personal observation). The precipitation of clay minerals is thus unlikely to be sufficiently rapid to entomb microbes before full decay of the microbial structure. More importantly, a bacterial interpretation for mouldic melanosomes is not supported by the large body of

research that supports interpretations of fossil microbodies as melanosomes and that refutes a bacterial origin (see Chapter 1.7.1). Oxidation experiments in this thesis clearly demonstrate that melanosome degradation generates mouldic impressions in feather tissue.

Maturation can be constructive or destructive with respect to the preservation of melanosomes and melanin in feathers, depending on the taphonomic scenario. Maturation plays a constructive role in the morphological preservation of melanosomes (as discussed above) and the chemical preservation of eumelanin in feathers when exposed to an oxidant after maturation. Feathers matured prior to oxidation show more melanosomes (Figs. 3.3e–h and 3.4d) in electron micrographs and higher concentrations of melanin markers (Fig. 3.6) in AHPO-HPLC data than feathers matured after oxidation. These data cannot inform on whether thermal maturation with pressure plays a larger role on the preservation of melanosomes and melanin. Unfortunately, the mouldic melanosomes produced via oxidation following high temperature-high pressure maturation were not quantitatively compared to those produced via oxidation following thermal maturation.

Experimental treatment of feathers with maturation only does not degrade melanosome morphology. TEM images show dark, electron-dense melanosomes in both untreated and matured feathers (Fig. 3.4a). Nonetheless, no quantitative comparison on melanosome geometry was made between untreated and matured feathers to test for morphological evidence of melanosome degradation. Critically, McNamara et al. (2013) report that melanosomes shrink up to 20% under maturation conditions of 200°C, 250 bar and 250°C, 250 bar (for 1 hour each). The maturation conditions used in this thesis resemble those used in McNamara et al. (2013). The experimental maturation of feathers, as described in this thesis, therefore likely resulted in melanosome shrinkage but this requires confirmation

The lack of evidence for melanosome degradation via maturation in this thesis contrasts with a recent report by Zhao et al. (2020). In that study the authors describe several stages of melanosome degradation (in experimentally matured feathers) that are not observed in the data presented here. TEM images of matured *Gallus* feathers in Zhao et al. (2020) show three stages of melanosome degradation: (1) disintegration of the melanosome

margins with some melanin granules surrounding the periphery of the melanosome, (2) pale regions of low electron density within the organelle that contrast with dark regions of high electron density and (3) indistinct melanosome margins that may indicate integration of the melanosomal melanin into the surrounding tissue. The second "decay stage" above is of interest because SEM images of black *Gallus* feathers collected as preliminary data for Chapter 3 herein revealed that the melanosomes were hollow. Zhao et al. (2020) do not report hollow melanosomes in *Gallus* but their TEM images of untreated feathers show melanosomes with an electron-lucent core (fig. 6a in Zhao et al. [2020]), i.e., hollow melanosomes. Clearly their second decay stage has the potential to be an original biological feature and not an artefact of degradation. The analysis of melanosomes in experimentally matured feathers from many taxa and with different melanin chemistries may help resolve the full impact of maturation on melanosome and melanin preservation.

Maturation is both destructive and constructive with respect to the chemical preservation of eumelanin in feathers. AHPO-HPLC data show that the PTeCA : PTCA ratio in both orange and black feathers increases with progressive maturation (Fig. 4.2). This result is consistent with previous reports that an increase in the PTeCA : PTCA ratio with maturation indicates an increase in the crosslinking of DHI units (Glass et al., 2013; Ito et al., 2013). The crosslinking of DHI units likely enhances the chemical stability of eumelanin and promotes its preservation in deep time (Glass et al., 2013; Ito et al., 2013). Nevertheless, crosslinking is also a destructive process as it alters the original chemistry of the eumelanin molecule. The data on eumelanin degradation are also consistent with the degradation patterns of eumelanin markers in previous AHPO-HPLC data on matured *Sepia* eumelanin (Jarenmark et al., 2021).

Maturation preferentially degrades phaeomelanin relative to eumelanin. The total concentration of eumelanin markers in matured black feathers shows less of a decrease during maturation than that for phaeomelanin markers in matured orange feathers (Fig. 4.2 and Table 4.1). The data presented here confirm that phaeomelanin markers can survive strong maturation, but it is not clear whether that remnant phaeomelanin has increased preservation potential: it is not possible to test the degree of cross-linking of phaeomelanin monomers

Decay has little impact on melanosome morphology in feathers. Melanosomes do not exhibit obvious differences in geometry in SEM micrographs of untreated and decayed feathers (Fig. 3.2a,f); granted no quantitative comparison was made and ideally this would be tested statistically.

Despite this lack of apparent morphological change during decay, this thesis reveals that melanosomes are not completely immune to change during the decay process. Exposure to an oxidant following decay generates higher quantities of PTeCA markers (pathway 8 in Fig. 3.6) than feathers oxidised without prior decay (pathway 5 in Fig. 3.6). This result indicates that decay prior to oxidation results in more melanin degradation than when feathers are not decayed. This result is potentially due to initial decay of either the melanosome membrane or surrounding proteinaceous tissue, or both.

7.1.2 The taphonomy of proteinaceous feather tissue

The experimental results presented in this thesis also inform on the taphonomy of proteinaceous feather tissue. Electron microscopy, S-XANES and FTIR data reveal that the factors controlling the morphological and chemical preservation of proteinaceous feather tissue are, broadly, in decreasing order of importance: maturation, oxidation and decay. Critically, the experiments show that both morphological and chemical residues of proteinaceous feather tissue survive under all experimental treatments used. Morphological and chemical evidence of proteinaceous feather tissue are therefore likely to survive in deep time.

Maturation is the primary control on the degradation of proteinaceous feather tissue. Electron micrographs show that moderate maturation (200°C for 1 h) results in feather microstructure that is identical to untreated feathers (Figs. 3.2c,f, 3.4 and 3.5a,b); sulfur and amide chemistries are similar to those of untreated feathers (albeit with a reduction in β-turns (Figs. 5.1, 5.2, 5.3, 6.1 and 6.4)).

In contrast, strong maturation (250°C for 1 h) leads to notable changes in proteinaceous feather tissue. This treatment increases sulfate (Fig. 6.1) and reduces amide content (Figs. 5.2 and 6.4). The reduction in amide content reflects a decrease primarily in the quantity

of N–H and C–N bonds within the proteins present. Strong maturation also results in an increase in α-helices and loss of β-sheets and β-turns (Fig. 5.3e,f and Supplementary Table 5.2). This probably reflects the reconfiguration of β-sheets into α-helices and is likely facilitated, at least in part, by the loss of β-turns as follows. Pleated β-strands form a β-sheet structure via β-turns, with H-bonding between the β-strands (Fig. 5.4e). A loss of β-turns could potentially unravel the β-sheet structure and allow reconfiguration of OH bonds to form an α-helix. Critically, random coil structures and cysteine persist following strong maturation (Figs. 5.3e,f, 5.1 and 6.1 and Supplementary Table 5.2). These data confirm that evidence of feather proteins can survive extensive maturation. The mechanisms that are potentially responsible for the survival of evidence of feather proteins, such as encapsulation by lipids during *in situ* polymerisation, are summarised in Chapter 7.4.2.

Incorporation of pressure into the thermal maturation experiments (200°C, 135 bar for 1 h) also leads to notable changes in proteinaceous feather tissue. This treatment results in large regions of exposed melanosomes with no apparent surrounding proteinaceous feather tissue (Fig. 3.2d). High temperature-high pressure maturation under these conditions has a major impact on the preservation of proteinaceous feather tissue, at least locally. Other regions of feathers matured under the same conditions display 3D or mouldic melanosomes with visible proteinaceous feather tissue (Figs. 3.2h and 3.3d,g,h).

High temperature-high pressure maturation (using different conditions of 150°C, 135 bar for 1 h) also impacts feather chemistry but to a lesser extent than strong thermal maturation (250°C for 1 h at atmospheric pressure). FTIR data show a reduction in the amide content of feathers matured using high temperatures and high pressures but the reduction, especially of amides B, I and III, is less than generated by the strong maturation of feathers. S-XANES data show that cystine disulfides remain in feathers matured using high temperatures and high pressures but are absent in strongly matured feathers. The morphology of proteinaceous feather tissue was not examined following maturation under these high temperature-high pressure conditions.

Interestingly, the taphonomic conditions required for the chemical preservation of feather CBPs differ for tertiary and secondary structures of the protein. S-XANES data reveal that

thermal maturation is more detrimental to the preservation of feather CBP tertiary structure than thermal maturation with pressure. In contrast, FTIR data reveal that thermal maturation with pressure is more detrimental to the preservation of feather CBP secondary structures than thermal maturation.

Oxidation alone does not appear to impact the morphological preservation of proteinaceous feather tissue (Fig. 3.2e). The extent to which oxidation impacts on the preservation of feather proteins was not tested.

Decay results in minor changes to feather chemistry. These changes, however, are somewhat counter-intuitive. S-XANES data show that decayed feathers exhibit slightly less sulfate (an indicator of oxidised sulfur from disulfide bonds) than untreated feathers (Fig. 6.1). Further, disulfide peaks are more substantial with decay prior to maturation than in non-decayed, matured feathers (Fig. 6.1). These spectral features are not expected but may be explained by the onset of *in situ* polymerisation. Early stages of decay can initiate *in situ* polymerisation, during which lipids can associate with biomolecules (Gupta et al., 2009). The lipid content of feathers is approximately 0.9% (Zeisler-Diehl et al., 2020). It is possible that the minor amounts of lipids present in feathers associate with and stabilise feather CBPs during the early stages of decay but this requires further testing.

The pH of the decay medium seems to impact feather microstructure. Decay in a solution with a starting pH of 6.0 does not result in any obvious ultrastructural changes to proteinaceous feather tissue. In contrast, decay in a solution with a starting pH of 12.2 results in shrinkage of the feather tissue surrounding melanosomes (Fig. 3.2b). This shrinkage almost certainly reflects chemical alteration of the proteinaceous feather cortex, but the chemistry of these feathers was not tested. Alkaline solutions, however, are reported to cause swelling of hair and feather tissue (Mokrejs et al., 2011; Wang et al., 2021). Alkaline swelling of hair and feather proteinaceous tissue occurs via the weakening of hydrophobic interactions in the polypeptide chains, allowing the reducing agent to damage the protein and liberate cysteine (Wang et al., 2021). Additional analyses are thus required to resolve this inconsistency and understand the chemical reactions responsible for the shrinkage of feather tissue in alkaline conditions observed here.

7.1.3 Barriers to interpreting taphonomic impacts on the preservation of feather components

The term "experimental design" in this thesis refers to various elements of an experiment: the samples chosen for analyses, experiments performed, analytical techniques chosen and the methods by which data was obtained, processed and interpreted. The experimental design and analytical approaches used in this thesis place a series of constraints on the extent to which the results can inform on how taphonomic factors affect feather preservation.

Experimental design. The use of the AHPO protocol in Ito et al. (2011) may influence the results of taphonomic experiments that include an oxidation treatment. The use of this oxidation protocol in isolation (i.e., not in combination with other treatments) does not ensure the degradation of all melanosomes and solubilisation of all melanin in feathers (pathway 5 in Fig. 3.6). Residual melanin markers in oxidised feathers could reflect the complete degradation of some, but not all, of the melanosomes present and the retention of eumelanin molecules that are not membrane-bound. Future analyses are required to test whether mouldic melanosome-bearing matrices can retain chemical evidence of melanin (Chapter 7.1.1).

Other potential limitations of the oxidation protocol are the use of H_2O_2 as an oxidant, the concentration of H_2O_2 and the duration of the oxidation experiments. Data from oxidation experiments demonstrate that melanosomes readily degrade when oxidation precedes maturation, indicating that moulds are more likely to form early during diagenesis. Nevertheless, it is possible that extensive melanosome degradation following maturation is possible but may require exposure to an oxidant for longer durations, interaction with a stronger oxidant or higher concentrations of an oxidant. Such variations in experimental conditions were not tested.

An additional limitation of the taphonomic experiments was the generation of mouldic melanosomes during sample preparation. Initial attempts to visualise the internal structure of feathers used a scalpel to dissect all experimentally treated feathers. This procedure fractured the feather and distributed the melanosomes between the feather part and

counterpart, thus generating abundant moulds that were in fact artefacts of the dissection process. Clearly this has the potential to impact the assessment of melanosome degradation in experimentally treated feathers. Two additional steps were thus added to the sample preparation for SEM and TEM to prevent fracturing: resin-embedding and sectioning of the resin blocks using an ultramicrotome. This modified sample preparation method successfully minimised the artificial generation of mouldic melanosomes based on the absence of moulds in electron microscopy images of non-oxidised samples after resin-embedding and sectioning with an ultramicrotome (Fig. 3.2a–d). The drawback of this method is that it generates a smooth surface of the resin block that can hinder the observation of any intact and 3D melanosomes present (Fig. 3.5a,b). Untreated feathers and feathers thermally matured following decay were therefore fractured without a resin-embedding step to observe the melanosomes (Fig. 3.2f,g). Fractured surfaces show rare voids that are similar in size to the mouldic melanosomes in oxidised feathers (Fig. 3.2f). These voids are interpreted as preparation artefacts since no moulds are visible in the untreated feathers that were resin-embedded and sectioned (Fig. 3.5a,b). Melanosome moulds generated during the fracturing process are thus artefacts of preparation. All oxidised feathers were prepared using the modified sample preparation protocol to ensure that the moulds in the oxidation experiments reflect melanosome degradation and not preparation artefacts. The image in Fig. 3.3d is of an oxidised and matured feather that was fractured due to the poor quality of SEM images taken of the resin-embedded sample.

The results of the experiments described in Chapter 3 inform on the taphonomy of melanosomes (in black feathers) and of their constituent eumelanin. Given the colour of the feathers and the elongated shape of the melanosomes, it is likely that the black feathers analysed primarily contain eumelanin. Melanosomes in the black feathers analysed likely contain minor phaeomelanin, as in the black feathers analysed in Chapter 4 (also from *G. gallus*), but phaeomelanin concentrations were not determined for these particular samples. The experimental data therefore cannot directly explain the impact of oxidation on phaeomelanin and the origins of mouldic "phaeomelanosomes" (spheroidal to sub-spheroidal melanosomes in fossils). There is, however, evidence that phaeomelanin is less resistant to degradation than eumelanin (Colleary et al., 2015; Liu et al., 2005; Wakamatsu & Ito, 2002). It is therefore likely that the same taphonomic scenarios that result in eumelanosome degradation will also degrade phaeomelanosomes. Nevertheless,

it is unclear whether phaeomelanosomes can degrade under other conditions, especially those that do not degrade eumelanin.

This thesis does not address certain important questions regarding feather taphonomy. Sulfurisation is known to contribute to the preservation of fossil melanosomes (McNamara et al., 2016b) and potentially fossil bone marrow (McNamara et al., 2006) and the soft tissues of a mosasaur (Lindgren et al., 2014). It remains unclear whether the sulfurisation of melanosomes involves the eumelanin molecule only or eumelanin plus one or more other melanosome components (e.g., lipids from the organelle membrane and melanosome proteins). If sulfurisation of melanosomes requires lipids or proteins from the melanosome, then sulfurisation can contribute to the preservation of fossil eumelanin only in taphonomic scenarios that are conducive to melanosome preservation. Alternatively, if sulfurisation requires the eumelanin molecule only then sulfurised fossil eumelanin may be more widespread in the geological record than fossil melanosomes. Another important question that this thesis does not address is whether melanosomes containing phaeomelanin can sulfurise.

This thesis also does not elucidate the impact of oxidation on feather chemistry. The data from taphonomic experiments presented here support the identification of melanosome-bearing matrices as the degraded remains of feather tissue. The degraded feather tissue surrounding mouldic melanosomes was presumably exposed to the oxidant(s) that led to melanosome degradation. Experimental data on the impact of oxidation on feather proteins would thus assist in interpreting chemical data on mouldic melanosome-bearing matrices.

Finally, whether heavy metals play a role in the preservation of melanins or feather CBPs is unknown. Previous studies report the presence of heavy metals in fossil feathers (Manning et al., 2013; Pan et al., 2019; Wogelius et al., 2011). Further, Cu is shown to bind to fossil eumelanin in an isolated feather from the Green River formation and in the feathers of *Confuciusornis* (Wogelius et al., 2011). The preservation of archaeological hair (Bertrand et al., 2014) and some soft-bodied fossils in the Burgess Shale (Petrovich, 2001) are interpreted to be due, at least in part, to the association of heavy metals with the tissues

(see Chapters 1.6 and 1.7.2) but whether heavy metals can bind to and stabilise feather proteins is unclear.

Analytical techniques. The analytical techniques used during the research presented here have certain limitations with respect to the characterisation of melanin and melanosome degradation. Foremost, the degradation of non-melanin tissue components can clearly contribute to the AHPO-HPLC melanin signal. The experimental data presented here suggest that these contributions are, however, minimal – at least under the experimental conditions used. AHPO data derived from fossils that experienced a comparable taphonomic history are therefore likely to be broadly representative of the remnant melanin chemistry. Nevertheless, this interpretation does not exclude the possibility that different diagenetic conditions could result in a much greater contribution of non-melanin components to the AHPO signal derived from fossil feathers or other tissues. Additional taphonomic experiments are required to determine the conditions where the risk of non-melanin contributions to the AHPO-HPLC melanin signal is greatest.

A second limitation of the approaches used is that neither SEM nor AHPO-HPLC can determine the organic chemistry of individual melanosomes. Melanosomes in most tissues are considered to contain co-polymers of eumelanin and phaeomelanin (Ito & Wakamatsu, 2008; Ito et al., 2000). Indeed, there is evidence, at least for neuromelanin, that some melanosomes contain a phaeomelanin core surrounded by a eumelanin crust (Bush et al., 2006). Evidence of this casing model stems from photoelectron microscopy data (Bush et al., 2006). Photoelectron microscopy can chemically characterise individual melanosomes by detecting the different oxidation potentials of eumelanin and phaeomelanin (Bush et al., 2006). The results on melanosome and melanin survival presented here may therefore reflect the preservation potential of melanosomes containing eumelanin exclusively, melanosomes with a mixed melanin composition, or both. In addition to photoelectron microscopy, nano-FTIR can also characterise the chemistry of individual melanosomes (Stanic et al., 2018). The distinction between eumelanosomes that are exclusively eumelanic or contain a phaeomelanin core is important in future research as different types of eumelanosomes may vary in their preservation potential.

7.2 Feather intrinsic chemistry influences the preservation potential of feather CBPs and melanins

This thesis suggests that the preservation of melanin and feather CBPs is influenced by the intrinsic chemistry of feathers. The latter includes melanin and melanosomes , feather CBPs, IF-keratins, CBPs, KAPs, melanoproteins, metals and lipids. AHPO-HPLC data on experimentally treated feathers show that the preservation potential of both eumelanin and phaeomelanin differs in both orange and black feathers (Fig. 4.2). Further, S-XANES data demonstrate that a lower phaeomelanin and especially eumelanin content promotes the preservation of feather CBPs (Figs. 6.1 and 6.2). These chemical data highlight the benefits of using whole tissues (rather than pure analytical standards) in taphonomic experiments and are discussed in detail below.

7.2.1 Feather intrinsic chemistry influences melanin preservation

AHPO-HPLC data reveal that melanin monomers show different degradation patterns in black and orange feathers. For instance, the eumelanin marker PTCA (derived primarily from DHICA units) degrades steadily in orange feathers with progressive maturation (i.e., in a stepwise fashion from moderate maturation to strong maturation but degrades markedly in black feathers only with strong maturation. Further, PDCA (reflecting DHI units) increases in black feathers and decreases in orange feathers with moderate maturation but increases in both with strong maturation. The patterns in the data for PTCA and PDCA in orange feathers are not consistent with published mechanisms for the chemical degradation of eumelanin (Ito et al., 2013; Jarenmark et al., 2021). DHI and DHICA units therefore degrade differently in black and orange feathers, with a greater proportional loss of each under moderate maturation conditions than in black feathers.

Similarly, the phaeomelanin markers TTCA and TDCA do not exhibit the same degradation patterns in black and orange feathers. TTCA gradually decreases in black feathers with progressive maturation, whereas in orange feathers it decreases only with strong maturation. TDCA increases in orange feathers with progressive maturation but only in black feathers with moderate maturation.

This variation in the degradation pattern of melanin monomers could reflect one or several factors. Feathers of different colours, i.e., with different dominant melanin chemistry, may differ in the extent to which melanin monomers are crosslinked. AHPO-HPLC provides evidence of greater eumelanin crosslinking in orange feathers than in black feathers via an increasing PTeCA : PTCA ratio with progressive maturation. The experiments with white feathers, however, suggest that we cannot exclude the possibility that the increase in PTeCA in orange feathers may reflect, at least in part, the degradation of non-melanin feather components. Assuming that greater crosslinking leads to a greater preservation potential of molecules, the greater crosslinking in matured orange feathers compared to matured black feathers suggests that eumelanin may be more robust in a phaeomelanin-dominated feather rather than a eumelanin-dominated feather over geological timescales. Such small amounts of eumelanin in a phaeomelanin-dominated feather, however, would be difficult to detect. Greater preservation – and detection – of eumelanin in a phaeomelanin-dominated tissue is therefore not considered the most realistic scenario but the data suggest that it is possible.

Another factor that may contribute to the variation in the degradation of melanin monomers is the DHI : DHICA ratio. The black and orange feathers analysed possess different DHI : DHICA ratios. The eumelanin degradation patterns shown in Chapter 4 resemble AHPO-HPLC data on matured *Sepia* eumelanin rather than synthetic DHI and DHICA and mixtures thereof (Jarenmark et al., 2021); this may reflect a similar DHI : DHICA ratio for natural eumelanin in biological samples. Data on matured synthetic eumelanin suggest that this ratio impacts the degradation patterns of eumelanin markers (Jarenmark et al., 2021). Additional data are needed to confirm whether the DHI : DHICA ratio is similar in all biological samples that are predominantly eumelanic and whether the DHI : DHICA ratio in whole tissues also impacts the survival of eumelanin markers, as it does in synthetic eumelanin (Jarenmark et al., 2021). Additional factors that could potentially explain the different degradation patterns in different coloured feathers include the presence and abundance of the following: melanin co-polymers, melanosome proteins, lipids, other proteins and metals bound to melanins and proteins.

7.2.2 The melanin content of feathers influences the preservation of feather proteins

S-XANES data demonstrate that feather melanin content is linked to the oxidation of disulfides in feather CBPs during maturation. The S-XANES data show that disulfides oxidise gradually in white and orange feathers with progressive maturation but show marked change in black feathers only with strong maturation (Figs. 6.1 and 6.2). Notably, cystine disulfide bonds – indicative of CBP tertiary structure – survive strong maturation only in white feathers; black feathers contain more sulfate and less cysteine than orange and white feathers. Intriguingly, the progressive oxidation of disulfides in orange feathers and the marked oxidation of disulfides only in strongly matured black feathers parallel the chemical alteration of melanin during degradation: phaeomelanin degradation is gradual with progressive maturation whereas major alteration of eumelanin occurs extensively only with strong maturation (Fig. 4.2). The strong oxidation of disulfides in black feathers – and lack of disulfide oxidation in white feathers – may therefore relate to melanin content and potentially melanin degradation (see Chapter 7.4). Ultimately, the experimental data suggest that feather melanin impacts the oxidation of sulfur in feather CBPs, whereby fossil feathers with little to no eumelanin may preferentially retain reduced sulfur species indicative of feather CBPs, relative to feathers with a high phaeomelanin and especially eumelanin content.

These data are in direct conflict with previous taphonomic studies on white and black feathers (Goldstein et al., 2004; Saitta et al., 2018; Zhao et al., 2020). Saitta et al. (2018) report that experimentally matured white feathers degrade completely, leaving no residues of proteinaceous feather tissue. The authors, however, do not provide high-resolution images or chemical data to support these claims. Other studies have also reported that black feathers are more decay-resistant than white feathers (Goldstein et al., 2004; Gunderson et al., 2008). These studies differed substantially to the experimental setup used both in Saitta et al. (2018) and in this thesis, as they focussed on decay by the feather degrading bacterium *Bacillus licheniformis.* In Goldstein et al. (2004) and Gunderson et al. (2008), feathers were sterilised and inoculated with *Bacillus* or 6–12 days at 37°C and the soluble protein content used as a proxy for the extent of decay. Problematically, the soluble proteins from bacteria contributed to the measured soluble protein content. Gunderson et al. (2008) therefore included two additional metrics for analysing the extent of decay: bacterial growth and feather mass; they reported less bacterial growth and reduced loss of feather mass for non-melanised feathers.

Various studies suggest that melanin residues may bind to and stabilise feather proteins, referred to as the 'melanoprotein' hypothesis in this thesis (Lindgren et al., 2015a; Moyer et al., 2016; Zhao et al., 2020). The generation of melanoproteins occurs via interactions of L-dopaquinone with thiols in proteins (García-Borrón et al., 1984). Galván and Solano (2016) propose that the formation of melanoproteins in feathers, and thus stabilisation of feather CBPs, may occur via the interaction of L-dopaquinone with the amino acid cysteine in feather CBPs. Zhao et al. (2020) provide tentative evidence of interaction between melanin and feather tissue. TEM images of experimentally matured feathers show melanosomes with indistinct margins (Zhao et al., 2020), but whether this is evidence of reactions melanin into surrounding tissues is unclear.

7.2.3 Limitations to assessing the impact of intrinsic feather chemistry on the preservation potential of feather CBPs and melanins

The experimental design and analytical techniques chosen for this research place certain constraints on the ability of the results to inform on the influence of the intrinsic feather chemistry on the preservation of melanin and proteins in feathers.

Experimental design. The critical limitation of the experimental design is that not all feather components were analysed. Metals that are bound to melanin (Hong & Simon, 2007) and potentially to feather CBPs (Burger, 1995) could potentially influence the preservation of feather components as metals are known to bind to and stabilise biomolecules (Bertrand et al., 2014; Petrovich, 2001; Wogelius et al., 2011; see Chapters 1.7.2 and 7.1.3), but these were not analysed using e.g., synchrotron-XRF. Another limitation of the experimental design is the use of black feathers that contain small quantities of phaeomelanin and orange feathers with small quantities of eumelanin. The specific feathers used were chosen to approximate endpoints on the eumelanin-phaeomelanin spectrum, but even in this case, avoiding eumelanin-phaeomelanin mixtures was impossible (see Chapter 2.1.1). The feathers analysed permit the assessment of eumelanin degradation in a phaeomelanin-dominated system and vice versa but make it difficult to assess the degradation of eumelanin and phaeomelanin separately in tissues. From an empirical point of view, the use of feather that contain either eumelanin or

phaeomelanin exclusively would be beneficial. The vast majority of tissues, however, contain both pigments so it is not clear whether experiments on tissues containing eumelanin or phaeomelanin only would be biologically relevant.

Analytical techniques. The techniques chosen for this research possess certain analytical limitations.

The FTIR data presented here cannot provide information on each eumelanin, phaeomelanin and proteins individually. An FTIR spectrum will inevitably include contributions, even if minor, from any proteins, eumelanin and phaeomelanin present. ATR-FTIR, which was used to collect the FTIR data here, does not have sufficiently high spatial resolution to probe the chemistry of individual melanosomes and thus the resulting spectra predominantly reflect the chemistry of feather proteins, i.e., amide chemistry (see Chapter 6.2). Nano-FTIR can discriminate between eumelanin and phaeomelanin and probe the chemistry of individual melanosomes. The ability of nano-FTIR to probe individual melanosomes facilitates the analysis of melanosome chemistry only, without feather protein chemistry dominating the IR spectrum. Future attempts to assess the impact of intrinsic feather chemistry on melanin preservation should use nano-FTIR.

There are some minor concerns with the FTIR data processing that warrant consideration. Of primary concern is the strong variation in peak intensity among FTIR spectra, particularly between spectra for black and orange feathers. Differences in peak intensities are important as the intensity of an FTIR peak reflects the concentration of the functional group corresponding to the molecular bond(s). In this thesis, the data were normalised via z-score standardisation (a standard procedure) to remove sample thickness effects and enable the comparison of peak intensities among FTIR spectra (Jardine et al., 2017). It is unexpected that some variation remains in absorption among FTIR spectra. Importantly, it does not seem likely that this difference relates to feather type. Black feathers from *Gallus gallus* show stronger peak intensities across the entire FTIR spectrum than both orange contour feathers from *Gallus gallus* and white primary feathers from *Egretta garzetta.* The variation could therefore indicate some variability in absorption due to melanin content but there is no data in the literature to support this.

Further, there is no literature to suggest that different colours of the same feather type differ in the abundance of functional groups and, in particular, amides – the predominant functional group in the FTIR data presented here. Quantification of FTIR data in future studies could help resolve this issue and potentially experimenting with different standardisation procedures.

Similar to ATR-FTIR, AHPO-HPLC cannot probe the melanin component of feathers exclusively. AHPO-HPLC is widely considered the most diagnostic technique for the identification of melanin (Ito et al., 2011, 2013; Jarenmark et al., 2021; Wakamatsu & Ito, 2002). This thesis, however, shows that the degradation of non-melanin components, especially with strong maturation, generates melanin markers (Figs. 4.2 and 4.3).

The key limitation of S-XANES is its inability to probe the sulfur in feather CBPs exclusively. S-XANES can inform on the sulfur chemistry of feather CBPs only when feather CBPs are the only source of sulfur. The abundance of benzosulfur in phaeomelanin-rich orange feathers makes assessing the contribution of cysteine from feather CBPs to S-XANES spectra difficult. Benzosulfur and cysteine excite at the same energy to produce overlapping peaks (Edwards et al., 2016; Fig. 6.1). Nevertheless, the contribution of cysteine to the cysteine/bensosulfur peak can be estimated by comparing the relative heights of the cysteine/benzosulfur peaks in white and orange feathers. The contribution of benzosulfur to the cysteine/benzosulfur peak in orange feathers is thus minimal compared to the contribution of cysteine to the peak. Notably, eumelanin does not contain sulfur (Ito & Fujita, 1985). Eumelanin-rich black feathers possess minor amounts of phaeomelanin (Fig. 4.2 and Table 4.1); as a result, the contribution of sulfur from phaeomelanin to S-XANES spectra of black feathers is likely to be minor. Further, it is unlikely that feather components other than melanins or feather CBPs contribute to the sulfur in the S-XANES spectra of feathers. IF-keratins in feathers do not contain sulfur (unlike trichocyte IF-keratins, which occur in hair, wool, hoof, horn, claw and baleen [Eckhart & Ehrlich, 2018; Holthaus et al., 2018]). KAPs contain sulfur (Shimomura & Ito, 2005) but are a likely a minor component of mature feathers (Alibardi, 2006; Ng et al., 2012; Wu et al., 2015; see Chapter 1.4.2). Lipids that contain sulfur are termed sulfolipids and occur only in plants (Shimojima, 2011) and the brain, testis and kidneys of mammals (Tadano-Aritomi et al., 2001). The S-XANES data from black and white feathers therefore

reflect predominantly, if not exclusively, the sulfur chemistry of feather CBPs. Comparison of the S-XANES data from black, white and orange feathers reveals that feather CBPs are less oxidised, and thus less degraded, in phaeomelanic orange and amelanic white feathers.

7.3 Evidence of phaeomelanin and feather CBPs can survive in deep time

Reports of chemical residues of phaeomelanin (Brown et al., 2017; Colleary et al., 2015; Manning et al., 2019) and feather CBPs (Pan et al., 2016; Pan et al., 2019; Schweitzer et al., 1999) are few and controversial. The controversial nature of reports of fossil feather CBPs stems – in part – from a lack of data from taphonomic experiments to support the preservation of feather proteins in the fossil record (Saitta et al., 2017a, b, 2018). Data from taphonomic experiments would also provide useful context for reports of chemical residues of phaeomelanin. This thesis demonstrates that chemical residues of phaeomelanin and feather CBPs can survive in deep time based on AHPO-HPLC, HCl-AHPO-HPLC, S-XANES and FTIR data on fossils and experimentally treated feathers from extant birds.

7.3.1 Phaeomelanin can survive extensive maturation

A taphonomic model for the molecular degradation of eumelanin and phaeomelanin is presented here based on AHPO-HPLC and HCl-AHPO-HPLC analyses of experimentally matured feathers. This model supports the data presented in this thesis for the preservation of phaeomelanin monomers in 10 Ma fossil frogs.

The experimental data presented here show that the decrease in total concentration of phaeomelanin markers in orange feathers is more (moderate maturation: -36%; strong maturation: -72%) than the decrease of the total concentrations of eumelanin markers in matured black feathers (moderate maturation: -1%; strong maturation: -62%; see Chapter 4). These data demonstrate that phaeomelanin begins to degrade at lower temperatures than eumelanin and thus presumably begins to degrade earlier during diagenesis. Ultimately, these data suggest that phaeomelanin has a lower preservation potential than eumelanin. A lower preservation potential of phaeomelanin may, in part, explain reports of

fossil phaeomelanosomes preserved exclusively as moulds in feathers of specimens of *Anchiornis* (Li et al., 2010), *Sinornithosaurus* and *Sinosauropteryx* (Zhang et al., 2010). Nevertheless, experimental data show that small amounts of eumelanin and even phaeomelanin monomers can persist after strong maturation (Figs. 4.2 and 4.3).

The use of HCl to demineralise fossil material prior to AHPO-HPLC (Ito et al., 2018; see Chapter 2.6) requires some consideration. The model presented here predicts that eumelanin-dominated feathers (and presumably other fossil tissues) will retain a dominant eumelanin signal after HCl treatment. This eumelanin signal should show PTeCA ≈PTCA > PDCA (Table 4.3) with TDCA > TTCA. Phaeomelanin-dominated fossil tissues should retain a dominant phaeomelanin signal with TTCA > TDCA and accessory should show PTCA > PTeCA >> PDCA. The model predicts the generation of very low concentrations of melanin markers in matured white feathers, which approximate a non-melanic, protein-rich tissue. This artificial melanin signal will be dominated by eumelanin markers, with PTCA > PTeCA >> PDCA. The potential for non-melanin sources to generate melanin markers raises concerns regarding the use of AHPO-HPLC in the detection of fossil melanins. Notably, this artificial signal is enhanced following HCl treatment. This may have broader applications for other analytical approaches: HCl is frequently used as a pre-treatment step for other analytical techniques (Schweitzer et al., 2008) such as Raman spectroscopy (Norell et al., 2020; Wiemann et al., 2018). The potential for HCl treatment to generate chemical signals in AHPO data (and data obtained using other techniques) that could potentially be misinterpreted as biologically informative should thus be explored further.

The experimental data presented here allow the validity of previous reports of fossil phaeomelanin be assessed. During maturation, more BZ-AA is generated (relative to starting conditions) than any other phaeomelanin marker (Fig. 4.2 and Table 4.2). The source of this artificial signal is not clear but the maturation of feathers also results in extensive amide degradation (Figs. 5.2 and 6.4) and oxidation of sulfur in feather CBPs (Figs. 5.1 and 6.1). These data, plus the dominance of feather chemistry by CBPs,are consistent with a protein source for artificially generated melanin markers. BZ-AA alone is therefore not a diagnostic indicator of phaeomelanin (see Chapter 4), and evidence of BZ alone, such as in *Borealopelta* (Brown et al., 2017), does not constitute sufficient evidence for the confident identification of fossil phaeomelanin. Although BZ-AA alone is not

diagnostic, it may, however, form part of a robust signal for fossil phaeomelanin as part of a suite of evidence. For example, the co-occurrence of fossil melanosomes, Zn and benzosulfur (from the BZ phaeomelanin unit) supports fossil phaeomelanin in the Pliocene mouse *Apodemus* (Manning et al., 2019).

Ultimately, the confident identification of phaeomelanin in deep time is important because it has the potential to inform on melanin evolution. Exposure of phaeomelanin to ionising radiation generates ROS that are toxic to organisms (see Chapter 1.3). In fact, a negative correlation exists between the expression of phaeomelanin colouration and the relative brain mass of extant avian species (Galván & Møller, 2011). The costs associated with phaeomelanic colouration thus raise questions regarding the evolutionary pressures that led to its evolution. Galvan et al. (2012) hypothesise that the origin of phaeomelanin is linked to the removal of excess cysteine in the body, which is highly toxic to organisms, via the process of phaeomelanogenesis (see Chapter 1.7.2). Clearly further work is needed but fossil phaeomelanin has great potential to inform on longstanding questions regarding the origins and functional evolution of phaeomelanin.

This thesis presents the oldest chemical evidence of phaeomelanin yet reported, in fossil feathers from the Early-Mid Cretaceous Jehol biota and from fossil frogs from the Late Miocene Libros biota. The chemical signal providing evidence of phaeomelanin in the fossil feathers, however, is not consistent with the model developed in Chapter 4 and is thus considered here to be tentative evidence of phaeomelanin in Mesozoic fossils. Nevertheless, it may be reasonable to expect different eumelanin and phaeomelanin ratios in fossils that experienced intense maturation to those predicted by the model. Importantly, the chemical signal from the fossil frog melanin is most consistent with the taphonomic model developed in Chapter 4. The fossil frog tissues show PTeCA ≈PTCA > PDCA with TDCA > TTCA is present. The eumelanin and phaeomelanin signals suggest that the tissues were originally eumelanin-dominated and are inconsistent with artificial melanin signals.

The preservation of a phaeomelanin chemical signature in the fossil frogs provides evidence of phaeomelanin synthesis in ancient amphibians. Given that phaeomelanin is known to occur in extant reptiles, amphibians, fish and cephalopods (Roulin et al., 2013;

Rogers et al., 2019; Rossi et al., 2019; Wolnicka-Glubisz et al., 2012), our discovery of evidence of phaeomelanin in Mesozoic and Cenozoic fossils opens the possibility for further discoveries in older and more basal taxa. This will help resolve the evolutionary history and origins of phaeomelanin.

7.3.2 Limitations on understanding phaeomelanin preservation

The experimental design and analytical techniques chosen for this research place certain constraints on the ability of the results to inform on the preservation of phaeomelanin.

Experimental design. The thermal maturation experiments using feathers support the preservation of evidence of phaeomelanin in Miocene frogs. It is possible that the response of phaeomelanin markers to maturation may differ between feathers and frog tissues, but further work is necessary to test this hypothesis.

Analytical techniques. AHPO-HPLC is widely considered the most diagnostic assay for the identification of melanin markers following oxidative degradation (Ito et al., 2011, 2013; Jarenmark et al., 2021; Wakamatsu & Ito, 2002). AHPO-HPLC data has been used to support interpretations of fossil eumelanin in organically preserved fossils, such as a Jurassic cephalopod (Glass et al., 2012) and ichthyosaur (Lindgren et al., 2018; see Chapter 1.7.1). This thesis, however, demonstrates that non-melanin sources can contribute to a chemical signal for melanin in matured material (Fig. 4.2). Further, the recovery of eumelanin and phaeomelanin markers in experimentally matured feathers is lower following HCl treatment than when no HCl treatment is used. Further, HCl-AHPO-HPLC is biased against recovery of phaeomelanin (52% recovery of phaeomelanin in orange feathers versus 86% recovery of eumelanin in black feathers). This implies that HCl-AHPO-HPLC data underrepresent actual melanin content, especially of phaeomelanin, in fossils; this bias is compounded by the fact that phaeomelanin degrades faster than eumelanin. To date, chemical residues of fossil phaeomelanin have been reported using S-XANES and ToF-SIMS only (Brown et al., 2017; Colleary et al., 2015; Manning et al., 2019). The absence of evidence of fossil phaeomelanin from HCl-AHPO-HPLC data in many fossils may be due to the use of HCl treatment.

Alternative techniques to AHPO-HPLC can assist in the identification of melanins. ToF-SIMS can identify secondary ion fragmentation patterns that are characteristic of melanins but this technique is not diagnostic (Colleary et al., 2015; Jarenmark et al., 2021). Other techniques that have been successful in generating evidence for the identification of melanin in extant taxa include synchrotron-based photoionisation-MS, GC-MS and Raman spectroscopy (Dernroth et al., 2009; Galván & Jorge, 2015; Galván & Solano, 2015, 2016; Liu, 2014). It is therefore prudent to test techniques that are complementary to HCl-AHPO-HPLC to ensure that minerals and non-melanin organic molecules do not interfere with or contribute to the melanin signal; this is essential for future analyses of fossils for evidence of eumelanin and, especially, phaeomelanin (see Chapter 8.2).

7.3.3 Feather CBPs can survive extensive maturation

This thesis presents chemical evidence of cystine, cysteine, β-sheets and α-helices, which are indicative of remnant feather CBPs, in Mesozoic fossil feathers. Electron microscopy, S-XANES and FTIR data from experimentally treated feathers support these fossil data.

S-XANES and FTIR analyses of Mesozoic fossil feathers reveal evidence for secondary and tertiary structures of remnant feather proteins. Both *Confuciusornis* and *Sinornithosaurus* feathers retain evidence of cysteine, α-helices and β-sheets (Fig. 5.3i); *Confuciusornis* also shows cystine and *Sinornithosaurus* also shows β-turns (Fig. 5.3j). The isolated feather from the Green River Formation shows local preservation of β-sheets, β-turns and α-helices (Fig. 5.3h).

This chemical evidence of fossil feather CBPs is supported by S-XANES and FTIR data on experimentally treated feathers. Cysteine and amides are retained in all experimentally treated feathers and cystine disulfide bonds can survive in matured white feathers. FTIR data show that β-sheets can persist in moderately matured feathers but undergo complete transformation into α-helices with strong maturation. Based on these experimental data it is reasonable to expect an amide and cysteine signal to be retained in most fossil feathers and a cystine signal in at least some fossil feathers. The data also suggest that, if present, β-sheets and cystine will preserve locally, with the predominant secondary structure being α-helices.

The fossil and experimental data in this thesis are consistent with previous reports of remnant proteins in the fossil record. Edwards et al. (2011) interpret the presence of amides, cystine and cysteine (as revealed by S-XANES and FTIR data) in a 50 Ma reptile from the Green River biota (Middle Eocene, USA) as evidence of keratins in fossil skin. In a separate study, Yang et al. (2019) provide FTIR data that suggest the preservation of amides in pterosaur feathers. The amide I peak position is not fully consistent with either an α-helix or β-sheet conformation and is considered to be diagenetic in origin (Yang et al., 2019). This is supported by the experimental data presented in this thesis showing that β-sheets transform to α-helices during maturation. If the α-helix structures in the pterosaur feathers reflect – at least in part –the diagenetic transformation of β-sheets, it implies that pterosaur feathers may have contained feather CBPs, non-specific basal CBPs or a different protein with (at least some) polypeptides in β-sheet conformation.

The data in this thesis provide only partial support for reports of feather CBP remnants in Mesozoic fossils (Pan et al., 2016, 2019; Schweitzer et al., 1999). Although the data in this thesis supports the preservation of feather CBP remnants in Mesozoic fossils, these reports are based on immunohistochemical data that show fluorescence of fossil feathers following incubation with antibodies raised against feather CBPs (Pan et al., 2016, 2019; Schweitzer et al., 1999). Critically, it is unknown whether antibodies can retain their specificity when applied to fossil material. Non-specific antibody binding (where a molecule that lacks the specific epitope for an antibody nonetheless binds that antibody) causes false positive results and is a major concern in immunohistology. In particular, condensation reactions between sugars and proteins during diagenesis can produce melanoidins that can bind to antibodies (Collins et al., 1992). This issue requires further investigation but is beyond the scope of this thesis (Benton et al., 2019; see Chapter 8.2).

Irrespective of the above caveats, analyses of fossil and experimentally treated feathers in this thesis demonstrate that evidence of feather secondary and tertiary structure can preserve in fossils, at least locally. Future analyses of early feathers may thus identify regions with a high fidelity of biochemical preservation that can greatly inform on feather evolution. Of particular interest is the chemistry of feathers in pterosaurs (Yang et al., 2019) and the ornithischian dinosaur *Kulindadromeus* (Godefroit et al., 2014; see Chapter

8.2). Preservation of feather CBPs in pterosaur feathers would support the hypothesis that feather CBPs arose before feathers ca. 250 Ma (Dalla Valle et al., 2009; Dhouailly, 2009; Lowe et al., 2015) – not *after* feathers (Greenwold & Sawyer, 2011; see Chapter 1.4). Evidence of CBPs in the feathers and scales of *Kulindadromeus* (Godefroit et al., 2014), could test the hypothesis that avian scale CBPs evolved from feather CBPs (Dalla Valle et al., 2009; Dhouailly, 2009).

7.3.4 Limitations on understanding the preservation of feather CBPs

The experimental design and analytical techniques chosen to perform the research in this thesis possess certain limitations that warrant consideration.

Experimental design. The experiments in this thesis test whether remnants of feather CBPs can survive in fossil feathers and are detectable using S-XANES and FTIR, but did not target IF-keratins. The degradation of IF-keratins has not been characterised in a taphonomic context, but it is highly likely that they contribute to the FTIR signal presented here. It is possible that IF-keratins may contribute to the S-XANES signal, especially if the proteins contain sulfur, but this cannot be tested as S-XANES and FTIR cannot target IF-keratins to the exclusion of feather CBPs. It is unknown whether the amount of IF-keratins present in feathers varies within and among feathers (as proposed for CBPs [Alibardi, 2016]). If the feathers analysed vary in IF-keratin content, this could potentially explain some of the variations in the S-XANES and FTIR data presented in Chapter 7.2.2. Critically, it is uncertain whether IF-keratins can transform from an α-helix to a β-sheet (Kreplak et al., 2004) conformation under the experimental conditions used here. Confirmation of this process would indicate that β-sheets are not a reliable indicator of feather CBPs in experimentally treated and fossil feathers. A greater understanding of the taphonomy of IF-keratins would be beneficial to the interpretation of chemical data that suggest the preservation of remnant fossil feather CBPs.

An additional limitation is the amount of fossil material that was available for chemical analyses. AHPO-HPLC required the sampling of large amounts of fossil soft-tissue. Despite the relatively small size of the fossil data, the fossils analysed represent diverse taxa and

varied diagenetic histories (see Chapter 2.1) and are thus considered to be appropriate for this thesis.

Analytical techniques. This thesis demonstrates that FTIR and S-XANES are powerful tools for the detection of chemical signals indicative of ancient feather CBPs and can probe secondary and tertiary structures, respectively. Nevertheless, the use of these techniques places certain constraints on the ability to characterise feather CBP degradation and detect remnants of feather CBPs in fossils.

The primary limitation of FTIR is that the process of spectral deconvolution can be vague, with no set protocol. This arises where the chemistry of the sample is unknown. Further, peak assignments for the amide II region are often not unequivocal as the wavelengths at which secondary structures absorb in the region has not been fully characterised (see Chapter 2.8). FTIR deconvolutions thus rely on previous studies and databases of sample spectra, for which the presence and abundance of secondary structure has been characterised. The spectral deconvolution process begins with the selection of peak positions for secondary structures that are likely to be present. The best deconvolution is the one that best fits the data. A sample-specific protocol was developed to improve the reproducibility of the results presented here.

Finally, FTIR cannot target feather CBPs to the exclusion of other proteins. CBPs and, to a lesser extent, IF-keratins, KAPs and melanosome proteins are highly likely to contribute to the FTIR data presented here. Unlike feather CBPs, IF-keratins, KAPs and melanosome proteins are not highly crosslinked. Assuming that crosslinking will make a molecule more robust, it is unlikely that these proteins are more robust than feather CBPs. Further, all of these proteins are relatively minor compared to feather CBPs. It is therefore most likely that the FTIR data here predominantly reflect the chemistry of feather CBPs.

The main limitation of S-XANES is that there is a high demand for access to synchrotron facilities. Obtaining beamtime is thus a highly competitive process and beamtime is limited even for successful applicants. If beam time is granted it is difficult to justify spending an extensive amount of time analysing spatial heterogeneity in sulfur chemistry in an

individual sample. This approach is, however, particularly useful for fossil material where preservation is likely to be heterogeneous (see Chapter 8.2).

An additional limitation of S-XANES is that the analysis of samples using synchrotron radiation can oxidise elements in the sample. The collection of multiple spectra from the same analysis point is important to ensure the use of optimal beam parameters. If the beam parameters are not optimal, successive scans can show signs of beam damage via oxidation of the target element. The optimal beam parameters for this study required different energy step sizes across the scan range to mitigate oxidation (see Chapter 2.7).

Finally, S-XANES data cannot distinguish between disulfides original to feather CBPs and disulfides derived from the diagenetic incorporation of sulfur. If sulfurisation of biomolecules is widespread in organically preserved fossils then a disulfide peak in S-XANES spectra of fossil feathers may not be diagnostic of original cystine. The contribution of sulfurisation to the preservation of feather CBPs – and any molecule other than melanin (McNamara et al., 2016b) – in feathers is, however, unknown. Determining the contribution of sulfurisation to fossil feather preservation is clearly important for future interpretations of S-XANES data from fossil feathers (see Chapter 8.2).

7.4 Model for the preservation of fossil feathers

This thesis demonstrates extensive chemical variation within and among fossil feathers. A taphonomic model is therefore required to explain variations in preservation. This thesis suggests that fossil feathers vary in biochemical preservation due to the extent of thermal maturation and, to a lesser extent, intrinsic biochemistry (see Chapter 6; Fig. 6.2). Future studies may test the following new taphonomic model.

The main features of the model are:

1. Experimental data reveal that the factors that control melanosome and melanin preservation are, in decreasing order of importance: oxidation, maturation and decay. Further, phaeomelanin is less resistant to thermal maturation than eumelanin. Melanosomes and melanin thus preserve where decay is minimal and, most importantly, exposure to an oxidant does not occur prior to intensive

maturation. In particular, evidence of phaeomelanin is more likely to preserve in localities with low maximum burial temperatures.

2. Experimental data reveal that the factors controlling the morphological and chemical preservation of proteinaceous feather tissue are, broadly, in decreasing order of importance: maturation, oxidation and decay. The controls on the morphological preservation of feather tissue in particular are, in decreasing order, thermal maturation using pressure, thermal maturation, oxidation and decay.

   The taphonomic conditions required for the chemical preservation of feather CBPs are nuanced and differ for tertiary and secondary structures of the protein. The controls on the preservation of feather CBP tertiary structure are, in decreasing order of importance, thermal maturation, thermal maturation with pressure and, finally, decay. In contrast, the controls on the preservation of feather CBP secondary structures are thermal maturation with pressure, thermal maturation and, finally, decay.

   Collectively, these data suggest that preservation of feather CBPs in fossils is controlled primarily by diagenetic history and not decay. Fossil feathers from deposits with low maximum burial temperatures and pressures are more likely to preserve feather CBP remnants with tertiary and secondary structures; feathers from deposits with a low maximum burial temperature and high maximum burial pressure may preserve evidence of feather CBP tertiary structure but exhibit little evidence of secondary structures.

3. This feature of the model considers the impact of differences in intrinsic feather chemistry on taphonomy. Preservation of feather CBPs is enhanced where melanin content – especially of eumelanin – is low. This probably reflects elevated levels of CO_2 generated by melanin, especially eumelanin, during diagenesis. This is supported by S-XANES data showing survival of cystine disulfide bonds in white, but not orange or black, feathers after strong maturation. The model is also supported by the presence of relatively more organic sulfate in matured orange and especially black feathers relative to white feathers. To date, the analysis of fossil feathers for protein remnants has focused on eumelanin-dominated feathers (Pan et al., 2016,

2019). It is imperative that future attempts at detecting remnants of feather CBPs in fossils focus on phaeomelanin-dominated tissues or fossil tissues that contain little melanin, which are more likely to preserve feather CBP remnants.

7.4.1 Chemical reactions responsible for the bias in feather CBP preservation

The root cause of the bias in CPB preservation in feathers with different melanin content is intriguing; one, or a combination of, the factors below may apply. One important parameter is the content of free carboxylic acid residues in melanins (d'Ischia et al., 2013). The FTIR data presented here show that untreated black feathers contain substantially more carboxylic acid than orange and especially white feathers (band 7 in Fig. 6.4). Carboxylic acid content decreases in black feathers with progressive maturation; despite this, carboxylic acid content in matured black feathers exceeds that in all matured orange and white feathers. The quantity of free carboxylic acid in melanins is relevant here because oxidation of carboxylic acid releases CO_2; this moiety is a mild oxidant but has greater oxidising potential under high temperatures (Kawi & Kathiraser, 2015). Tissues rich in eumelanin may experience more oxidation than tissues with little or none.

CO_2 is also released upon the decarboxylation of melanins during thermal maturation (Ito et al., 2013, 2018, 2020; Jarenmark et al., 2021). During maturation, BZ units in phaeomelanin undergo decarboxylation to produce TDCA, which releases CO_2. Decarboxylation of DHICA units in eumelanin yields DHI units and free CO_2; this process can be indirectly assessed by examining PTCA markers (which should decrease).

It is interesting to note that patterns in melanin degradation (i.e., decarboxylation as evident in AHPO-HPLC data) occur in tandem with those for CBP degradation (i.e., sulfur oxidation in XANES data). Black feathers show evidence for both processes only at high temperatures (DHICA units show extensive decarboxylation and sulfur oxidation, but not at lower temperatures; Fig. 4.2; Fig. 6.2c). For orange feathers, degradation via the two processes above occurs progressively from moderate to strong maturation conditions (progressive decarboxylation of BZ units (Fig. 4.2) and progressive oxidation; Fig. 6.2d).

The timing of CO_2 release during maturation is important. The total concentrations of BZ decrease by -38% during moderate maturation and a further -47% during strong maturation, resulting in a gradual production of CO_2. A substantial portion of the CO_2 is released at relatively low temperatures and thus has a relatively low oxidising potential (Kawi & Kathiraser, 2015). In contrast, eumelanin DHICA decreases by only -7% during moderate maturation and a further -69% during strong maturation. The majority of the CO_2 released has a high oxidising potential. Note that the CO_2 released via the decarboxylation of DHICA is in addition to the CO_2 released via the oxidation of the free carboxylic acid residues present, which are abundant in black feathers (band 7 in Fig. 6.4). These features collectively may explain the drastic oxidation of sulfur in black feathers with strong maturation. Ultimately, although phaeomelanin begins to degrade earlier and faster than eumelanin during diagenesis, this may enhance the survival of feather CBPs in phaeomelanin-rich feathers relative to eumelanin-rich feathers.

Ultimately, the timing of decarboxylation of melanin – and thus the starting melanin composition of the feather – may be key to the survival of feather CBPs. The survival of cystine disulfides in strongly matured white feathers presumably reflects the lack of melanin monomers present. Although the sulfur oxidation pattern observed in orange feathers may reflect, in part, phaeomelanin degradation (see Chapter 6), the model is supported by data on black and white feathers.

This hypothesis is supported by the presence of organic matrices that bear mouldic melanosomes in fossils. Organic remains of proteinaceous feather tissue are most evident where mouldic melanosomes occur (Li et al., 2010; Zhang et al., 2010). Critically, data in this thesis suggest an early formation of many mouldic melanosomes. Early oxidation of melanin may reduce the production of highly reactive CO_2 at elevated temperatures and, by extension, favour the preservation of remnant feather CBPs.

This model can be tested by future analyses of fossil feathers. The preservation of sulfur (Fig. 5.1), melanin (Fig. 4.4) and amide (Fig. 5.2) chemistries, in addition to protein secondary structures (Fig. 5.3g–j), varies among fossil feathers. Future analyses should focus on fossil feathers that bear mouldic melanosomes, are phaeomelanin-dominated and lack a strong melanin component. Testing this model is essential as it will facilitate

more accurate interpretation of chemical data from fossil feathers and, potentially, allow the confident identification of feather CBP remnants in the fossil record.

This model almost certainly has broader implications for the survival of proteinaceous moieties in the fossil record beyond fossil feathers and feather CBPs. Assuming a generally conserved chemistry for eumelanin and phaeomelanin across vertebrates, it is possible that there is a biochemical bias toward the preservation of proteinaceous remains in tissues with little to no phaeomelanin and, especially, eumelanin. If this bias exists, it places challenges on the identification of suitable fossils – and regions of fossil soft tissues – for analysis. Biochemical analyses of fossil soft tissues often target melanin-rich fossil tissues, perhaps due to their high visibility. Our current lack of widespread and robust evidence for proteins and protein remnants in deep time could, therefore, potentially reflect a sample selection bias. Irrespective of such a bias, the taphonomic model requires robust testing on many types of tissues that differ in melanin content (see Chapter 8.2).

7.4.2 Geochemical mechanisms for fossil feather preservation

Several mechanisms may contribute to the preservation of fossil feathers. These include *in situ* polymerisation, sulfurisation and stabilisation via melanoproteins.

In situ polymerisation is known to play an important role in the preservation of diverse fossil soft tissues (Gupta et al., 2006; Stankiewicz et al., 2000; Stankiewicz et al., 1997; see Chapter 1.8.2). It is possible that the survival of disulfides and amides in the strongly matured and fossil feathers analysed here is due to encapsulation in lipids during *in situ* polymerisation (Cody et al., 2011). Investigating the role of *in situ* polymerisation in the preservation of fossil feathers is beyond the scope of this thesis but warrants future research.

The data presented here suggest that sulfurisation is unlikely to contribute to the preservation of remnant fossil feather CBPs. The sulfurisation protocol used, however, may not be optimal for the sulfurisation of feather tissue (see Chapter 7.5.3). The data presented here are thus equivocal and the role of sulfurization in feather preservation remains unclear.

As described in Chapter 7.2.2, Zhao et al. (2020) claim that indistinct melanosome margins following maturation provide evidence for the reaction of melanosomal melanin with the surrounding tissue; this is a core element of the "melanoprotein hypothesis" that posits that melanin preservation is promoted by reactions between melanin and the surrounding tissue (Lindgren et al., 2015a; Moyer et al., 2016; Zhao et al., 2020). It is unclear, however, whether the indistinct melanosome margins in Zhao et al. (2020) are imaging artefacts. The data presented in this thesis (see the model outlined above and Chapters 7.2.2 and 7.2.3) do not support the melanoprotein hypothesis (but see Chapter 7.5.1).

7.5 Limitations of taphonomic experiments

This section discusses the limitations of the taphonomic experiments presented in Chapters 3–6.

7.5.1 Experimental design

This thesis represents the most comprehensive study of the degradation of feather components in a taphonomic context to date. The studies performed also represent the most controlled set of taphonomic experiments performed on feathers to date and examine the impact of several factors, in isolation and in combination, on the preservation of melanosomes, melanins and feather CBPs in fossil feathers. This thesis also tests the ability of AHPO-HPLC, S-XANES and FTIR to detect chemical signals of melanins and feather CBPs, paving the way for future research on the biochemical fidelity of fossil feathers. Nevertheless, this thesis acknowledges the limitations of the experimental design that apply to all the studies presented and describes them below.

(1) Feathers are natural tissues likely to vary in melanin chemistry. Although black, white and orange feathers were selected based on a visual assessment of feather colour, it cannot be assumed that feathers of similar colour have similar melanin chemistry. Data on black, orange and white feathers in Chapters 3, 5 and 6 derive from three individual feathers for each colour selected at random from a sample set originally selected from extant birds on the basis of homogeneity of colour within and among the feathers in the

set. Data in Chapter 4 are from four (white) or five (black and orange) individual feathers selected at random. The number of samples in all data chapters thus meets the minimum number of replicates required for statistical analyses, which is often considered three. Nevertheless, additional replicates would better indicate the chemical heterogeneity of the melanin component of samples.

(2) The taphonomic experiments presented in this thesis use primary and contour feathers. Different feather types, however, may vary in structural protein chemistry (Holthaus et al., 2018; Kowata et al., 2014; see Chapter 1.4.1). The use of contour feathers for the black and orange feather samples, and the use of primary feathers for the white feather samples, may thus influence the results from experimental data presented in Chapter 6. This issue was mitigated by selective sampling of regions of contour feathers with a closed feather vane and stiff barbs; plumulaceous barb and barbules were not used. The extent to which feather types can vary in structural protein chemistry requires future analyses.

(3) The use of isolated feathers in taphonomic experiments may restrict the relevance of the results to isolated fossil feathers. The decay and maturation of an entire organism may generate a different chemical microenvironment in the plumage than the decay and maturation of an isolated feather.

(4) The metal contents of feathers before and after experimental treatment were not analysed. Metals are implicated in the preservation of fossil melanin (Rossi et al., 2019, 2020, 2021; Wogelius et al., 2011) and extant feathers are known to contain metals (Burger, 1995; Edwards et al., 2016). Future studies may use XRF to test whether the metal composition of feathers can change during diagenesis, whether metals can associate with feather structural proteins and whether metals can contribute to the preservation of remnant proteins in fossil feathers.

7.5.2 Decay

The decay experiments performed in this thesis possess several limitations. The decay of feathers used relatively short durations of up to one year with no added inoculum. S-XANES and FTIR data indicate that feathers decay slowly under these conditions. Most

taphonomic experiments perform decay on taxa or structures that decay rapidly, allowing study of decay on timescales of days to months (Butler et al., 2015; Carlisle et al., 2021; Gabbott et al., 2021; Gupta et al., 2009; Murdock et al., 2014; Sansom, 2014; Sansom et al., 2010). In contrast, the complete decay of feathers with no inoculum is likely to require several years as feather tissues are very robust. Experiments of this length are clearly not compatible with the length of a PhD programme. Future decay experiments should consider ways to expedite decay, e.g., incorporation of an inoculum, sediment, or use of higher decay temperatures. Strategic experimental design would enable the performance of decay experiments, especially those with no added inoculum or sediment and at low temperatures, over longer durations, such as several years. Future studies should investigate the impact of decay on feather components by incorporating metals in decay experiments under a range of pH and Eh conditions. Finally, future analyses should test whether decay can impact on feather chemistry regardless of melanin content via the analysis of decayed white and orange feathers; experimental decay was performed on black feathers only.

7.5.3 Sulfurisation

The sulfurisation protocol used here may not be effective on feathers. This study used a protocol that was previously developed to study the sulfurisation of carbohydrates via the incorporation of sulfur from dissolved sulfides and polysulfides in the ambient environment (Kok et al., 2000; van Dongen et al., 2003, 2006). Critically, these previous studies did not perform sulfurisation experiments on any biomolecules other than carbohydrates. It is thus unclear whether biomolecules other than carbohydrates – in this case, feather CBPs – can be sulfurised using this protocol. Correct implementation of the protocol should be assessed by comparison with a negative control, but unfortunately controls were not assessed in this thesis. In addition to a negative control, sulfurization experiments should use a positive control, i.e., carbohydrates sulfurized, to test for correct implementation of the protocol. Future study of the impact of sulfurisation on the decay and preservation of proteinaceous feather components therefore requires additional experiments. Use of commercially available feather CBPs (in solution) could test the impact of the experimental protocol on isolated CBPs without potential confounding effects of other tissue components; it may also facilitate reactions between the CBPs and ambient

sulfides as the CBPs would be "free" rather than bound within feather tissue. It is also possible that appreciable and measurable sulfurisation can occur only after substantial decay of feather tissue and the generation of a sufficient amount of binding sites to incorporate sulfur. Experiments incorporating a longer duration of decay would thus be useful. In summary, conducting a range of additional experiments that test the feasibility of sulfurisation of feather CBPs, and its impact on feather CBP preservation, will clarify the potential impact of sulfurisation on feather CBP preservation in the fossil record (see Chapter 8.2).

7.5.4 Maturation

The maturation protocols chosen to assess the degradation of feather components possess several limitations. The maturation protocols used here were selected to represent either an open or closed environment (i.e., using foil or Au cells) and are associated with previously reported limitations (Saitta et al., 2018). Maturation of feather tissue in Al foil packets can mature large feather pieces, enabling a large enough sample size to perform certain techniques, such as AHPO-HPLC. Saitta et al. (2018) however, report that entire feather tissues can leak out of Al foil packets. Notably, leakage of tissues out of Al foil packets reflects the excessive duration of the experiment under conditions that do not apply to the study of fossil feathers. Leakage of feather tissue from Al packets did not occur in the experiments in this thesis. Further, Saitta et al. (2018) claim that the non-sealed nature of the Al foil packets allows volatiles to escape. It is uncertain how quickly this process happens, and indeed, how important volatiles are to preservation of feathers. Nevertheless, the escape of volatiles from the packet limits the time during which these chemicals can interact with non-volatiles, i.e., feather components that do not vapourise. Conversely, a completely closed environment is unlikely to apply to most fossils.

Some of the experiments used here involve the maturation of feather tissue in Au capsules. This method provides an extended interval during which volatiles can interact with feather tissue but does not allow the escape of volatiles until the opening of the capsule following the termination of the experiment. Like the premature escape of volatiles, the entrapment of volatiles with non-volatiles over such an extended interval may not be broadly applicable. Fully open conditions, however, are not necessarily more

applicable to fossils due to the impacts of cementation and compaction on porosity and permeability.

Saitta et al. (2018) propose that the use of sediment-encased maturation experiments is most applicable to the fossil record. In fact, the key to determining the best experimental setup for maturation experiments is testing the relevance of volatiles to the preservation of fossil feathers. Determining the type and quantity of volatiles that escape in a fully open system may be achieved by maturing feathers simultaneously while using headspace gas chromatography. This experimental design permits analysis of the emission of volatiles during maturation. Subsequent analysis of the matured feathers can be performed using various analytical chemical techniques, including mass spectrometry, FTIR, Raman and S-XANES. The importance of the sample environment during feather maturation can be tested by comparing the resulting data to data on feathers matured in Al packets and Au capsules.

Finally, the studies presented here would benefit from additional replicates to better characterise any inherent variability in experimental results linked to inherent heterogeneity in feather tissue. In particular, a sample size of at least five is recommended to generate a dataset that meets the requirements of most statistical tests. Notably, entire FTIR and S-XANES spectra are not amenable to statistical tests other than PCA, which does not place a requirement on the number of replicates needed. The need for additional replicates is particularly relevant to strongly matured black feathers, which show greater variation in S-XANES data than orange and white feathers.

Notably, the experiments presented in Chapter 4 did not use high temperature-high pressure maturation. Maturation using high temperature-high pressure requires the use of Au capsules that are small in size. The small nature of the capsules prevents the analysis of the resulting sample using AHPO-HPLC, which requires large amounts of sample.

In addition to being small in size, the Au capsules used for high temperature-high pressure are costly. The conditions of the high temperature-high pressure maturation experiments used in this thesis therefore required careful consideration and justification during the experimental design phase. The use of 200°C, 135 bar (n = 3) experiments in Chapter 3 and

150°C, 135 bar (n = 3) experiments in Chapter 6 was intended to investigate the impact of high temperature-high pressure maturation on the degradation of feather components. Future high temperature-high pressure experiments should perform at least five replicates and use temperatures and pressures different to those used in the experiments here.

Experiments would also benefit from incorporating metal-rich solutions (e.g., using Cu, Zn, S and Ca in isolation and combination) in different concentrations under a range of pH values as melanin is known to preferentially bind certain metals under different pH conditions (Hong & Simon, 2007).

8. Conclusion

8.1 Concluding remarks

This thesis has produced six key findings relating to the taphonomy of feathers. These findings are summarised below.

1) Taphonomic processes vary in the extent to which they impact the preservation of melanin and melanosomes. Importantly, melanosomes degrade preferentially under taphonomic conditions that include oxidation and melanosome moulds are most likely to form early during diagenesis. Decay has less impact on the degradation of eumelanin and melanosomes than oxidation. Maturation (at least the maturation conditions used herein) promotes the preservation of both melanosomes and eumelanin.

2) Taphonomic processes vary in the extent to which they impact the physical and chemical preservation of proteinaceous feather tissue. The controls on the morphological preservation of feather tissue are, in decreasing order, thermal maturation using pressure, thermal maturation, oxidation and decay. The taphonomic conditions required for the chemical preservation of feather CBPs differ for tertiary and secondary structures of the protein. The controls on the preservation of feather CBP tertiary structure are, in decreasing order of importance, temperature, pressure and decay whereas for secondary structure preservation the controls are pressure, temperature and decay. Critically, morphological evidence of proteinaceous feather tissue and, moreover, chemical evidence of feather corneous beta proteins survives the maturation conditions used herein, which are geologically relevant (i.e., retain recognisable feather structures).

3) Changes to the relative concentrations of melanin monomers in tissues during maturation can be predicted. Further, melanin monomers exhibit different degradation patterns in eumelanin-dominated and phaeomelanin-dominated feathers.

4) Chemical evidence of phaeomelanin monomers can survive in Cenozoic and Mesozoic fossils despite the pigment being less robust than eumelanin.

5) Chemical evidence of feather CBPs can survive and be detected in Mesozoic and Cenozoic fossil feathers. In particular, amides – indicative of protein secondary structures – can survive and be detected using FTIR whereas disulfides – indicative of protein tertiary structure – can survive and be detected using S-XANES.

6) Variation in the preservation of fossil feathers can be characterised using a new model that suggests a bias in the preservation of remnant feather CBPs in fossil feathers linked to melanin content. The model predicts that the proteinaceous component of fossil feathers with a dominant phaeomelanin composition – or that lack melanin pigments – will exhibit greater biochemical fidelity than fossil feathers with a dominant eumelanin composition. The model indicates that the preservation of melanosomes and melanin is most likely where decay is minimal and, most importantly, exposure to an oxidant does not occur prior to intensive maturation. The preservation of phaeomelanin is more likely to preserve in localities with low maximum burial temperatures. Fossil feathers from deposits with low maximum burial temperatures and pressures are more likely to preserve feather CBP remnants with tertiary and secondary structures; feathers from deposits with a low maximum burial temperature and high maximum burial pressure may preserve evidence of feather CBP tertiary structure but exhibit little evidence of secondary structures. Finally, the preservation of feather CBPs is enhanced where melanin content – especially of eumelanin – is low.

Collectively, these findings highlight a key issue. Data from experiments suggest a bias toward the preservation of feather CBP remnants in phaeomelanin-dominated and amelanic feathers. The degradation patterns linked to melanin content that are presented here for feather CBPs may apply to the preservation of proteinaceous moieties in other fossil soft tissues. Biochemical analyses of fossil soft tissues often focus on melanin-rich fossil tissues, perhaps due to their high visibility. Our current lack of widespread and robust evidence for proteins and protein remnants in fossils could potentially reflect a bias in the

selection of samples – and regions of fossil soft tissues – for analysis. Future attempts at detecting remnants of feather CBPs – and remnants of proteins in general – in fossils should focus on phaeomelanin-dominated tissues or fossil tissues that contain little melanin.

8.2 Future directions

This thesis proposes several new directions for future study of the taphonomy of fossil feathers and highlights areas of study that are particularly important to the findings of this thesis.

Testing the taphonomic model for feather CBP preservation

Future studies should test the taphonomic model presented in this thesis for the preservation of feather CBP remnants in fossils. Testing of this model is key to the accuracy of future interpretations based on chemical data from fossil feathers. Taphonomic experiments should incorporate the maturation of feathers that differ in melanin content. Chemical data of these experimentally degraded feathers – and of fossil feathers that vary in melanin chemistry – will allow testing of this model. Maturation of other tissues that vary in melanin chemistry may also test whether this model can be extrapolated to other tissues. Further, data from other experimentally degraded tissues will test the possibility that evidence for proteins and protein remnants in fossil soft tissues is due to a bias in analysing eumelanin-rich fossils.

Chemical analyses of primitive fossil feathers

Chemical analyses of primitive fossil feathers will build upon the research presented in this thesis. This thesis presents evidence of remnant fossil feather CBPs in fossil feathers using S-XANES and FTIR. In particular, FTIR and S-XANES analyses of pterosaur feathers and the feathers in *Kulindadromeus* are highly likely to provide key information on the biochemical evolution of feathers. Analyses should also focus on the chemical heterogeneity of primitive fossil feathers and test whether chemical evidence of amides and disulfides, indicative of feather CBPs, is widespread in fossil feathers.

Experimental sulfurisation of feathers

A key limitation of this thesis is the ability to test the contribution of sulfurisation to the preservation of fossil feathers. Performing a controlled set of sulfurisation experiments on feathers and feather CBPs is key to determining whether feather tissue can sulfurise.

Experimental degradation of different feather types

A potential limitation of this thesis is the lack of data on the degradation of feather components in different types of feathers. Incorporating different feather types in future experiments will broaden the dataset presented here. Critically, data on the degradation of different feather types will determine whether the types of feathers used in this thesis (contour black and orange feathers and white primary feathers) impact on the interpretation of a bias toward the preservation of feather CBPs in feathers lacking eumelanin pigments. Resolving this uncertainty will ultimately determine whether the data in this thesis can fully refute the melanoprotein hypothesis.

Testing the use of immunohistochemistry in the detection of fossil feather CBPs

This thesis reports the survival of chemical evidence of feather CBPs in experimentally degraded feathers in addition to remnants of feather CBPs in fossils using FTIR and S-XANES. These findings suggest that controversial reports of remnant feather CBPs in Mesozoic fossils based on immunohistochemical data may be legitimate. The use of immunohistochemistry on fossil feathers must be tested on experimentally degraded feathers to determine whether its use on fossil material is appropriate.

Chemical analyses of fossil soft tissues for phaeomelanin

This thesis presents the oldest evidence of phaeomelanin monomers in the fossil record. Detecting chemical evidence of phaeomelanin in additional fossils will build upon the results presented here. Detecting fossil phaeomelanin in fossil invertebrates may provide key discoveries on the functional evolution of phaeomelanin.

Testing the use of alternative techniques for the detection of fossil melanins

This thesis presents data showing that degraded non-melanin molecules can contribute to a melanin signal using AHPO-HPLC. Techniques complementary to AHPO-HPLC require

testing to ensure that minerals and non-melanin organic molecules cannot produce a chemical signal consistent with melanin.

Testing whether fossil mouldic melanosomes can inform on the timing of oxidation

Future experiments may test whether decay-induced melanosome migration can occur and form non-aligned fossil melanosomes. Further, experiments may test whether decay-induced melanosome migration can occur and produce non-aligned moulds upon melanosome oxidation. Collectively, such decay, maturation and oxidation experiments will confirm whether mouldic melanosome alignment can inform on the timing of oxidation in feathers with structural colouration. An assessment of the melanosome arrangement in melanic feathers of extant birds is required to test this hypothesis.

References

Alibardi, L. (2006). Structural and immunocytochemical characterization of keratinization in vertebrate epidermis and epidermal derivatives. *International Review of Cytology*, *253*, 177–259. https://doi.org/10.1016/s0074-7696(06)53005-0

Alibardi, L. (2016a). Mapping epidermal beta-protein distribution in the lizard *Anolis carolinensis* shows a specific localization for the formation of scales, pads, and claws. *Protoplasma*, *253*(6), 1405–1420. https://doi.org/10.1007/s00709-015-0909-z

Alibardi, L. (2016b). The process of cornification evolved from the initial keratinization in the epidermis and epidermal derivatives of vertebrates: a new synthesis and the case of sauropsids. *International Review of Cell and Molecular Biology*, *327*, 263–319. https://doi.org/10.1016/bs.ircmb.2016.06.005

Alibardi, L. (2017). Cornification, morphogenesis and evolution of feathers. *Protoplasma*, *254*(3), 1259–1281. https://doi.org/10.1007/s00709-016-1019-2

Alibardi, L., & Toni, M. (2008). Cytochemical and molecular characteristics of the process of cornification during feather morphogenesis. *Progress in Histochemistry and Cytochemistry*, *43*(1), 1–69. https://doi.org/10.1016/j.proghi.2008.01.001

Alibardi, L., Dalla Valle, L., Nardi, A., & Toni, M. (2009). Evolution of hard proteins in the sauropsid integument in relation to the cornification of skin derivatives in amniotes. *Journal of Anatomy*, *214*(4), 560–586.

Allen, W. L., Baddeley, R., Cuthill, I. C., & Scott-Samuel, N. E. (2012). A quantitative test of the predicted relationship between countershading and lighting environment. *The American Naturalist*, *180*(6), 762–776. https://doi.org/10.1086/668011

Alleon, J., Bernard, S., Le Guillou, C., Beyssac, O., Sugitani, K., & Robert, F. (2018). Chemical nature of the 3.4 Ga Strelley Pool microfossils. *Geochemical Perspective Letters*, *7*, 37–42. https://doi.org/10.7185/geochemlet.1817

Allison, P. A. (1988). The role of anoxia in the decay and mineralization of proteinaceous macro-fossils. *Paleobiology*, *14*(2), 139–154. https://doi.org/10.1017/S009483730001188X

Ancans, J., Tobin, D. J., Hoogduijn, M. J., Smit, N. P., Wakamatsu, K., & Thody, A. J. (2001). Melanosomal pH controls rate of melanogenesis, eumelanin/phaeomelanin ratio and melanosome maturation in melanocytes and melanoma cells. *Experimental Cell Research*, *268*(1), 26–35. https://doi.org/10.1006/excr.2001.5251

Babarović, F., Puttick, M. N., Zaher, M., Learmonth, E., Gallimore, E.-J., Smithwick, F. M., Mayr, G., & Vinther, J. (2019). Characterization of melanosomes involved in the production of non-iridescent structural feather colours and their detection in the fossil record. *Journal of the Royal Society Interface*, *16*(155), Article 20180921. https://doi.org/10.1098/rsif.2018.0921

Bada, J. L., Wang, X. S., & Hamilton, H. (1999). Preservation of key biomolecules in the fossil record: current knowledge and future challenges. *Philosophical Transactions of the Royal Society of London. Series B: Biological Sciences*, *354*(1379), 77–87. https://doi.org/10.1098/rstb.1999.0361

Barden, H. E., Bergmann, U., Edwards, N. P., Egerton, V. M., Manning, P. L., Perry, S., van Veelan, A., Wogelius, R. A., & van Dongen, B. E. (2015). Bacteria or melanosomes? A geochemical analysis of micro-bodies on a tadpole from the Oligocene Enspel Formation of Germany. *Palaeobiodiversity and Palaeoenvironments*, *95*(1), 33–45. https://doi.org/10.1007/s12549-014-0177-5

Barden, H. E., Wogelius, R. A., Li, D., Manning, P. L., Edwards, N. P., & van Dongen, B. E. (2011). Morphological and geochemical evidence of eumelanin preservation in the feathers of the Early Cretaceous bird, *Gansus yumenensis*. *PloS One*, *6*(10), Article e25494. https://doi.org/10.1371/journal.pone.0025494

Benton, M. J., Dhouailly, D., Jiang, B., & McNamara, M. (2019). The early origin of feathers. *Trends in Ecology & Evolution*, *34*(9), 856–869. https://doi.org/10.1016/j.tree.2019.04.018

Benton, M. J., Zhonghe, Z., Orr, P. J., Fucheng, Z., & Kearns, S. L. (2008). The remarkable fossils from the Early Cretaceous Jehol Biota of China and how they have changed our knowledge of Mesozoic life: Presidential Address, delivered 2nd May 2008. *Proceedings of the Geologists' Association*, *119*(3–4), 209–228. https://doi.org/10.1016/S0016-7878(08)80302-1

Bertrand, L., Vichi, A., Doucet, J., Walter, P., & Blanchard, P. (2014). The fate of archaeological keratin fibres in a temperate burial context: microtaphonomy study of hairs from Marie de Bretagne (15th c., Orléans, France). *Journal of Archaeological Science*, *42*, 487–499. https://doi.org/10.1016/j.jas.2013.11.028

Borovanský, J., & Riley, P. A. (2011). *Melanins and melanosomes: biosynthesis, structure, physiological and pathological functions*. John Wiley & Sons.

Borovanský, J., Hach, P., & Duchoň, J. (1977). Melanosome: an unusually resistant subcellular particle. *Cell Biology International Reports*, *1*(6), 549–554. https://doi.org/10.1016/0309-1651(77)90093-5

Bragulla, H. H., & Homberger, D. G. (2009). Structure and functions of keratin proteins in simple, stratified, keratinized and cornified epithelia. *Journal of Anatomy*, *214*(4), 516–559. https://dx.doi.org/10.1111%2Fj.1469-7580.2009.01066.x

Briggs, D. E. (1995). *Experimental taphonomy. Palaios*, *10*(5), 539–550. https://doi.org/10.2307/3515093

Briggs, D. E. (1999). Molecular taphonomy of animal and plant cuticles: selective preservation and diagenesis. *Philosophical Transactions of the Royal Society of London. Series B: Biological Sciences*, *354*(1379), 7–17. https://dx.doi.org/10.1098%2Frstb.1999.0356

Briggs, D. E. (2003). The role of decay and mineralization in the preservation of soft-bodied fossils. *Annual Review of Earth and Planetary Sciences*, *31*(1), 275–301. https://doi.org/10.1146/annurev.earth.31.100901.144746

Briggs, D. E., & Kear, A. J. (1993). Decay and preservation of polychaetes: taphonomic thresholds in soft-bodied organisms. *Paleobiology*, *19*(1), 107–135. https://doi.org/10.1017/S0094837300012343

Briggs, D. E., & Kear, A. J. (1994). Decay and mineralization of shrimps. *Palaios*, *9*(5), 431–456. https://doi.org/10.2307/3515135

Briggs, D. E., & McMahon, S. (2016). The role of experiments in investigating the taphonomy of exceptional preservation. *Palaeontology*, *59*(1), 1–11. https://doi.org/10.1111/pala.12219

Briggs, D. E., & Wilby, P. R. (1996). The role of the calcium carbonate-calcium phosphate switch in the mineralization of soft-bodied fossils. *Journal of the Geological Society*, *153*(5), 665–668. https://doi.org/10.1144/gsjgs.153.5.0665

Briggs, D. E., Evershed, R. P., & Lockheart, M. J. (2000). The biomolecular paleontology of continental fossils. *Paleobiology*, *26*(S4), 169–193. https://doi.org/10.1017/S0094837300026920

Brown, C. M., Henderson, D. M., Vinther, J., Fletcher, I., Sistiaga, A., Herrera, J., & Summons, R. E. (2017). An exceptionally preserved three-dimensional armored dinosaur reveals insights into coloration and Cretaceous predator-prey dynamics. *Current Biology*, *27*(16), 2514–2521. https://doi.org/10.1016/j.cub.2017.06.071

Brush, A. H. (1978). Avian pigmentation. *Chemical Zoology*, *10*, 141–161.

Buckley, M. (2013). A molecular phylogeny of *Plesiorycteropus* reassigns the extinct mammalian order 'Bibymalagasia'. *PloS One*, *8*(3), Article e59614. https://doi.org/10.1371/journal.pone.0059614

Buckley, M., Lawless, C., & Rybczynski, N. (2019). Collagen sequence analysis of fossil camels, Camelops and c.f. Paracamelus, from the Arctic and sub-Arctic of Plio-Pleistocene North America. *Journal of Proteomics*, *194*, 218–225. https://doi.org/10.1016/j.jprot.2018.11.014

Burger, J. (1995). Heavy metal and selenium levels in feathers of herring gulls (*Larus argentatus*): differences due to year, gender, and age at Captree, Long Island. *Environmental Monitoring and Assessment*, *38*(1), 37–50. https://doi.org/10.1007/BF00547125

Bush, W. D., & Simon, J. D. (2007). Quantification of Ca2+ binding to melanin supports the hypothesis that melanosomes serve a functional role in regulating calcium homeostasis. *Pigment Cell Research*, *20*(2), 134–139. https://doi.org/10.1111/j.1600-0749.2007.00362.x

Bush, W. D., Garguilo, J., Zucca, F. A., Albertini, A., Zecca, L., Edwards, G. S., Nemanich, R. J., & Simon, J. D. (2006). The surface oxidation potential of human neuromelanin reveals a spherical architecture with a pheomelanin core and a eumelanin surface. *Proceedings of the National Academy of Sciences*, *103*(40), 14785–14789. https://doi.org/10.1073/pnas.0604010103

Butler, A. D., Cunningham, J. A., Budd, G. E., & Donoghue, P. C. (2015). Experimental taphonomy of Artemia reveals the role of endogenous microbes in mediating decay and fossilization. *Proceedings of the Royal Society B: Biological Sciences*, *282*(1808), Article 20150476. https://doi.org/10.1098/rspb.2015.0476

Butterfield, N. J. (2003). Exceptional fossil preservation and the Cambrian explosion. *Integrative and Comparative Biology*, *43*(1), 166–177. https://doi.org/10.1093/icb/43.1.166

Calvaresi, M., Eckhart, L., & Alibardi, L. (2016). The molecular organization of the beta-sheet region in corneous beta-proteins (beta-keratins) of sauropsids explains its stability and polymerization into filaments. *Journal of Structural Biology*, *194*(3), 282–291. https://doi.org/10.1016/j.jsb.2016.03.004

Calvin, S. (2013). *XAFS for everyone*. CRC Press.

Cappellini, E., Prohaska, A., Racimo, F., Welker, F., Pedersen, M. W., Allentoft, M. E., de Barros Damgaard, P., Gutenbrunner, P., Dunne, J., Hammann, S., Roffet-Salque, M., Ilardo, M., Moreno-Mayar, J. V., Wang, Y., Sikora, M., Vinner, L., Cox, J., Evershed, R. P., & Willerslev, E. (2018). Ancient biomolecules and evolutionary inference. *Annual Review of Biochemistry*, *87*, 1029–1060. https://doi.org/10.1146/annurev-biochem-062917-012002

Carlisle, E. M., Jobbins, M., Pankhania, V., Cunningham, J. A., & Donoghue, P. C. (2021). Experimental taphonomy of organelles and the fossil record of early eukaryote evolution. *Science Advances*, *7*(5), Article eabe9487. https://doi.org/10.1126/sciadv.abe9487

Carney, R. M., Vinther, J., Shawkey, M. D., D'alba, L., & Ackermann, J. (2012). New evidence on the colour and nature of the isolated *Archaeopteryx* feather. *Nature Communications*, *3*(1), Article 637. https://doi.org/10.1038/ncomms1642

Chen, C.-F., Foley, J., Tang, P.-C., Li, A., Jiang, T. X., Wu, P., Widelitz, R. B., & Chuong, C. M. (2015). Development, regeneration, and evolution of feathers. *Annual Review of Animal Biosciences*, *3*(1), 169–195. https://doi.org/10.1146/annurev-animal-022513-114127

Chen, P.-J., Dong, Z.-M., & Zhen, S.-N. (1998). An exceptionally well-preserved theropod dinosaur from the Yixian Formation of China. *Nature*, *391*(6663), 147-152. https://doi.org/10.1038/34356

Chu, Q., Cai, L., Fu, Y., Chen, X., Yan, Z., Lin, X., Zhou, G., Han, H., Widelitz, R. B., Chuong, C.-M., Wu, W., & Yue, Z. (2014). Dkk2/Frzb in the dermal papillae regulates feather regeneration. *Developmental Biology*, *387*(2), 167–178. https://dx.doi.org/10.1016%2Fj.ydbio.2014.01.010

Chuong, C.-M., Randall, V. A., Widelitz, R. B., Wu, P., & Jiang, T.-X. (2012). Physiological regeneration of skin appendages and implications for regenerative medicine. *Physiology*, *27*(2), 61–72. https://dx.doi.org/10.1152%2Fphysiol.00028.2011

Clements, T., Colleary, C., De Baets, K., & Vinther, J. (2017). Buoyancy mechanisms limit preservation of coleoid cephalopod soft tissues in Mesozoic Lagerstätten. *Palaeontology*, *60*(1), 1–14. https://doi.org/10.5061/dryad.12pn2

Clements, T., Dolocan, A., Martin, P., Purnell, M. A., Vinther, J., & Gabbott, S. E. (2016). The eyes of *Tullimonstrum* reveal a vertebrate affinity. *Nature*, *532*(7600), 500–503. https://doi.org/10.1038/nature17647

Clements, T., Purnell, M., & Gabbott, S. (2019). The Mazon Creek Lagerstätte: a diverse late Paleozoic ecosystem entombed within siderite concretions. *Journal of the Geological Society*, *176*(1), 1–11. https://doi.org/10.1144/jgs2018-088

Cody, G. D., Gupta, N. S., Briggs, D. E., Kilcoyne, A., Summons, R. E., Kenig, F., Plotnick, R. E., & Scott, A. C. (2011). Molecular signature of chitin-protein complex in Paleozoic arthropods. *Geology*, *39*(3), 255–258. https://doi.org/10.1130/G31648.1

Colleary, C., Dolocan, A., Gardner, J., Singh, S., Wuttke, M., Rabenstein, R., Habersetzer, J., Schaal, S., Feseha, M., Clemens, M., Jacobs, B. F., Currano, E. D., Jacobs, L. L., Sylvestersen, R. L., Gabbott, S. E., & Vinther, J. (2015). Chemical, experimental, and morphological evidence for diagenetically altered melanin in exceptionally preserved fossils. *Proceedings of the National Academy of Sciences*, *112*(41), 12592–12597. https://doi.org/10.1073/pnas.1509831112

Collins, M., Westbroek, P., Muyzer, G., & De Leeuw, J. (1992). Experimental evidence for condensation reactions between sugars and proteins in carbonate skeletons. *Geochimica et Cosmochimica Acta*, *56*(4), 1539–1544. https://doi.org/10.1016/0016-7037(92)90223-6

Conway Morris, S. (2008). A redescription of a rare chordate, *Metaspriggina walcotti* Simonetta and Insom, from the Burgess shale (middle Cambrian), British Columbia, Canada. *Journal of Paleontology*, *82*(2), 424–430. https://doi.org/10.1666/06-130.1

Cutler, J., Jiang, D.-T., & Remple, G. (2001). Chemical speciation of arsenic in uranium mine tailings by X-ray absorption spectroscopy. *Canadian Journal of Analytical Sciences and Spectroscopy*, *46*(4), 130–135.

d'Ischia, M., Wakamatsu, K., Napolitano, A., Briganti, S., Garcia-Borron, J. C., Kovacs, D., Meredith, P., Pezzella, A., Picardo, M., Sarna, T., Simon, J. D., & Ito, S. (2013). Melanins and melanogenesis: methods, standards, protocols. *Pigment Cell & Melanoma Research*, *26*(5), 616–633. https://doi.org/10.1111/pcmr.12121

D'Alba, L., & Shawkey, M. D. (2019). Melanosomes: biogenesis, properties, and evolution of an ancient organelle. *Physiological Reviews*, *99*(1), 1–19. https://doi.org/10.1152/physrev.00059.2017

Dalla Valle, L., Nardi, A., Gelmi, C., Toni, M., Emera, D., & Alibardi, L. (2009). β-keratins of the crocodilian epidermis: composition, structure, and phylogenetic relationships. *Journal of Experimental Zoology Part B: Molecular and Developmental Evolution*, *312*(1), 42–57. https://doi.org/10.1002/jez.b.21241

Davis, P. G., & Briggs, D. E. (1998). The impact of decay and disarticulation on the preservation of fossil birds. *Palaios*, *13*(1), 3–13. https://doi.org/10.2307/3515277

De Graaf, W., Sinninghe Damsté, J. S., & de Leeuw, J. W. (1992). Laboratory simulation of natural sulphurization: I. Formation of monomeric and oligomeric isoprenoid polysulphides by low-temperature reactions of inorganic polysulphides with phytol and phytadienes. *Geochimica et Cosmochimica Acta*, *56*(12), 4321–4328.

De Gregorio, B. T., Sharp, T. G., Rushdi, A. I., & Simoneit, B. R. (2011). Bugs or gunk? Nanoscale methods for assessing the biogenicity of ancient microfossils and organic matter. In S. D. Golding & M. Glikson (Eds.), *Earliest life on Earth: habitats, environments and methods of detection* (pp. 239–289). Springer.

Demarchi, B., Hall, S., Roncal-Herrero, T., Freeman, C. L., Woolley, J., Crisp, M. K., Wilson, J., Fotakis, A., Fisher, R., Kessler, B. M., Jersie-Christensen, R. R., Olsen, J. V., Haile, J., Thomas, J., Marean, C. W., Parkington, J., Presslee, S., Lee-Thorp, J., Ditchfield, P., . . . Collins, M. J. (2016). Protein sequences bound to mineral surfaces persist into deep time. *Elife*, *5*, Article e17092. https://doi.org/10.7554/elife.17092

Dernroth, D. N., Rundström, A., & Kågedal, B. (2009). Gas chromatography–mass spectrometry analysis of pheomelanin degradation products. *Journal of Chromatography A*, *1216*(30), 5730–5739. https://doi.org/10.1016/j.chroma.2009.05.063

Dhouailly, D. (2009). A new scenario for the evolutionary origin of hair, feather, and avian scales. *Journal of Anatomy*, *214*(4), 587–606. https://doi.org/10.1111/j.1469-7580.2008.01041.x

Dubey, S., & Roulin, A. (2014). Evolutionary and biomedical consequences of internal melanins. *Pigment Cell & Melanoma Research*, *27*(3), 327–338. https://doi.org/10.1111/pcmr.12231

Dutta, S., Hartkopf-Fröder, C., Witte, K., Brocke, R., & Mann, U. (2013). Molecular characterization of fossil palynomorphs by transmission micro-FTIR spectroscopy: implications for hydrocarbon source evaluation. *International Journal of Coal Geology*, *115*, 13–23. https://doi.org/10.1016/j.coal.2013.04.003

Dyke, G., De Kat, R., Palmer, C., Van Der Kindere, J., Naish, D., & Ganapathisubramani, B. (2013). Aerodynamic performance of the feathered dinosaur *Microraptor* and the evolution of feathered flight. *Nature Communications*, *4*(1), Article 2489. https://doi.org/10.1038/ncomms3489

Eckhart, L., & Ehrlich, F. (2018). Evolution of trichocyte keratins. *Advances in Experimental Medicine and Biology*, *1054*, 33–45. https://doi.org/10.1007/978-981-10-8195-8_4

Edwards, N. P., Barden, H., Van Dongen, B., Manning, P., Larson, P., Bergmann, U., Sellers, W. I., Wogelius, R. (2011). Infrared mapping resolves soft tissue preservation in 50 million year-old reptile skin. *Proceedings of the Royal Society B: Biological Sciences, 278*(1722), 3209–3128. https://doi.org/10.1098/rspb.2011.0135

Edwards, N. P., Manning, P. L., & Wogelius, R. A. (2014). Pigments through time. *Pigment Cell & Melanoma Research*, *27*(5), 684–685. https://doi.org/10.1111/pcmr.12271

Edwards, N. P., Van Veelen, A., Anné, J., Manning, P. L., Bergmann, U., Sellers, W. I., Egerton, V. M., Sokaras, D., Alonso-Mori, R., Wakamatsu, K., Ito, S., & Wogelius, R. A. (2016). Elemental characterisation of melanin in feathers via synchrotron X-ray imaging and absorption spectroscopy. *Scientific Reports*, *6*, Article 34002. https://doi.org/10.1038/srep34002

Eglinton, G., & Logan, G. A. (1991). Molecular preservation. *Philosophical Transactions of the Royal Society of London. Series B: Biological Sciences*, *333*(1268), 315–328. https://doi.org/10.1098/rstb.1991.0081

Feduccia, A., Lingham-Soliar, T., & Hinchliffe, J. R. (2005). Do feathered dinosaurs exist? Testing the hypothesis on neontological and paleontological evidence. *Journal of Morphology*, *266*(2), 125–166. https://doi.org/10.1002/jmor.10382

Feo, T. J., & Prum, R. O. (2014). Theoretical morphology and development of flight feather vane asymmetry with experimental tests in parrots. *Journal of Experimental Zoology Part B: Molecular and Developmental Evolution*, *322*(4), 240–255. https://doi.org/10.1002/jez.b.22573

Feo, T. J., Field, D. J., & Prum, R. O. (2015). Barb geometry of asymmetrical feathers reveals a transitional morphology in the evolution of avian flight. *Proceedings of the Royal Society B: Biological Sciences*, *282*(1803), Article 20142864. https://doi.org/10.1098/rspb.2014.2864

Foth, C. (2020). Introduction to the morphology, development, and ecology of feathers. In C. Foth & O. W. M. Rauhut (Eds.), *The evolution of feathers* (pp. 1–11). Springer, Cham.

Fraser, R. D. B., & Parry, D. A. (2008). Molecular packing in the feather keratin filament. *Journal of Structural Biology*, *162*(1), 1–13. https://doi.org/10.1016/j.jsb.2008.01.011

Fraser, R. D. B., & Parry, D. A. (2011). The structural basis of the filament-matrix texture in the avian/reptilian group of hard β-keratins. *Journal of Structural Biology*, *173*(2), 391–405. https://doi.org/10.1016/j.jsb.2010.09.020

Fraser, R. D. B., & Parry, D. A. (2014). Amino acid sequence homologies in the hard keratins of birds and reptiles, and their implications for molecular structure and physical properties. *Journal of Structural Biology*, *188*(3), 213-224. https://doi.org/10.1016/j.jsb.2014.10.012

Fraser, R. D. B., MacRae, T., & Rogers, G. E. (1972). *Keratins: their composition, structure and biosynthesis*. Thomas.

Fraser, W. T., Lomax, B. H., Jardine, P. E., Gosling, W. D., & Sephton, M. A. (2014). Pollen and spores as a passive monitor of ultraviolet radiation. *Frontiers in Ecology and Evolution*, *2*, Article 12. https://doi.org/10.3389/fevo.2014.00012

Furumura, M., Sakai, C., Potterf, S. B., Vieira, W. D., Barsh, G. S., & Hearing, V. J. (1998). Characterization of genes modulated during pheomelanogenesis using differential display. *Proceedings of the National Academy of Sciences*, *95*(13), 7374–7378. https://dx.doi.org/10.1073%2Fpnas.95.13.7374

Gäb, F., Ballhaus, C., Stinnesbeck, E., Kral, A. G., Janssen, K., & Bierbaum, G. (2020). Experimental taphonomy of fish-role of elevated pressure, salinity and pH. *Scientific Reports*, *10*(1), Article 7839. https://doi.org/10.1038/s41598-020-64651-8

Gabbott, S. E., Donoghue, P. C., Sansom, R. S., Vinther, J., Dolocan, A., & Purnell, M. A. (2016). Pigmented anatomy in Carboniferous cyclostomes and the evolution of the vertebrate eye. *Proceedings of the Royal Society B: Biological Sciences*, *283*(1836), Article 20161151. https://doi.org/10.1098/rspb.2016.1151

Gabbott, S. E., Sansom, R. S., & Purnell, M. A. (2021). Systematic analysis of exceptionally preserved fossils: correlated patterns of decay and preservation. *Palaeontology*, *64*(6), 789–803. https://doi.org/10.1111/pala.12571

Galván, I., & Alonso-Alvarez, C. (2009). The expression of melanin-based plumage is separately modulated by exogenous oxidative stress and a melanocortin. *Proceedings of the Royal Society B: Biological Sciences*, *276*(1670), 3089–3097. https://doi.org/10.1098/rspb.2009.0774

Galván, I., & Jorge, A. (2015). Dispersive Raman spectroscopy allows the identification and quantification of melanin types. *Ecology and Evolution*, *5*(7), 1425–1431. https://doi.org/10.1002/ece3.1453

Galván, I., & Møller, A. (2011). Brain size and the expression of pheomelanin-based colour in birds. *Journal of Evolutionary Biology*, *24*(5), 999–1006. https://doi.org/10.1111/j.1420-9101.2011.02232.x

Galván, I., & Solano, F. (2009). The evolution of eu-and pheomelanic traits may respond to an economy of pigments related to environmental oxidative stress. *Pigment Cell & Melanoma Research*, *22*(3), 339–342. https://doi.org/10.1111/j.1755-148x.2009.00559.x

Galván, I., & Solano, F. (2015). Melanin chemistry and the ecology of stress. *Physiological and Biochemical Zoology*, *88*(3), 352–355. https://doi.org/10.1086/680362

Galván, I., & Solano, F. (2016). Bird integumentary melanins: biosynthesis, forms, function and evolution. *International Journal of Molecular Sciences*, *17*(4), Article 520. https://doi.org/10.3390/ijms17040520

Galván, I., Bonisoli-Alquati, A., Jenkinson, S., Ghanem, G., Wakamatsu, K., Mousseau, T. A., & Møller, A. P. (2014). Chronic exposure to low-dose radiation at Chernobyl favours adaptation to oxidative stress in birds. *Functional Ecology*, *28*(6), 1387–1403. https://doi.org/10.1111/1365-2435.12283

Galván, I., García-Campa, J., & Negro, J. J. (2017). Complex plumage patterns can be produced only with the contribution of melanins. *Physiological and Biochemical Zoology*, *90*(5), 600–604. https://doi.org/10.1086/693962

Galvan, I., Ghanem, G., & Møller, A. P. (2012). Has removal of excess cysteine led to the evolution of pheomelanin? Pheomelanogenesis as an excretory mechanism for cysteine. *BioEssays*, *34*(7), 565–568. https://doi.org/10.1002/bies.201200017

García-Borrón, J., Saura, M., Solano, F., Iborra, J., & Lozano, J. (1984). Water and protein interactions with model melanins. In J. Bagnara, S. N. Klaus, E. Paul, a& M. Schartl (Eds.), *Biological, molecular and clinical aspects of pigmentation* (pp. 91–95). University of Tokyo Press.

Gill-King, H. (1997). Chemical and ultrastructural aspects of decomposition. In W. D. Haglund & M. H. Sorg (Eds.), *Forensic taphonomy: the postmortem fate of human remains* (pp. 93–108). CRC Press.

Glass, K., Ito, S., Wilby, P. R., Sota, T., Nakamura, A., Bowers, C. R., Miller, K. E., Dutta, S., Summons, R. E., Briggs, D. E., Wakamatsu, K., & Simon, J. D. (2013). Impact of diagenesis and maturation on the survival of eumelanin in the fossil record. *Organic Geochemistry*, *64*, 29–37. https://doi.org/10.1016/j.orggeochem.2013.09.002

Glass, K., Ito, S., Wilby, P. R., Sota, T., Nakamura, A., Bowers, C. R., Vinther, J., Dutta, S., Summons, R., Briggs, D. E., Wakamatsu, K., & Simon, J. D. (2012). Direct chemical evidence for eumelanin pigment from the Jurassic period. *Proceedings of the National Academy of Sciences*, *109*(26), 10218–10223. https://doi.org/10.1073/pnas.1118448109

Gluckman, T. L., & Cardoso, G. (2010). The dual function of barred plumage in birds: camouflage and communication. *Journal of Evolutionary Biology*, *23*(11), 2501–2506. https://doi.org/10.1111/j.1420-9101.2010.02109.x

Godefroit, P., Sinitsa, S. M., Dhouailly, D., Bolotsky, Y. L., Sizov, A. V., McNamara, M. E., Benton, M. J., & Spagna, P. (2014). A Jurassic ornithischian dinosaur from Siberia with both feathers and scales. *Science*, *345*(6195), 451–455. https://doi.org/10.1126/science.1253351

Goldstein, G., Flory, K. R., Browne, B. A., Majid, S., Ichida, J. M., & Burtt, E. H., Jr. (2004). Bacterial degradation of black and white feathers. *The Auk*, *121*(3), 656–659. https://doi.org/10.1093/auk/121.3.656

Greenewalt, C. H., Brandt, W., & Friel, D. D. (1960). Iridescent colors of hummingbird feathers. *Journal of the Optical Society of America*, *50*(10), 1005–1013. https://doi.org/10.1364/JOSA.50.001005

Greenwold, M. J., & Sawyer, R. H. (2010). Genomic organization and molecular phylogenies of the beta (β) keratin multigene family in the chicken (*Gallus gallus*) and zebra finch (*Taeniopygia guttata*): implications for feather evolution. *BMC Evolutionary Biology*, *10*(1), Article 148. https://doi.org/10.1186/1471-2148-10-148

Greenwold, M. J., & Sawyer, R. H. (2011). Linking the molecular evolution of avian beta (β) keratins to the evolution of feathers. *Journal of Experimental Zoology Part B: Molecular and Developmental Evolution*, *316*(8), 609–616. https://doi.org/10.1002/jez.b.21436

Greenwold, M. J., & Sawyer, R. H. (2013). Molecular evolution and expression of archosaurian β-keratins: diversification and expansion of archosaurian β-keratins and the origin of feather β-keratins. *Journal of Experimental Zoology Part B: Molecular and Developmental Evolution*, *320*(6), 393–405. https://doi.org/10.1002/jez.b.22514

Gregg, K., & Rogers, G. E. (1986). Feather keratin: composition, structure and biogenesis. In J. Bereiter-Hahn, A. G. Matolsky, & K. S. Richards (Eds.), *Biology of the integument* (pp. 666–694). Springer.

Gren, J. A., Sjövall, P., Eriksson, M. E., Sylvestersen, R. L., Marone, F., Sigfridsson Clauss, K. G., Taylor, G. J., Carlson, S., Uvdal, P., & Lindgren, J. (2017). Molecular and microstructural inventory of an isolated fossil bird feather from the Eocene Fur Formation of Denmark. *Palaeontology*, *60*(1), 73–90. https://doi.org/10.1111/pala.12271

Gueriau, P., Bernard, S., & Bertrand, L. (2016). Advanced synchrotron characterization of paleontological specimens. *Elements*, *12*(1), 45–50. https://doi.org/10.2113/gselements.12.1.45

Gueriau, P., Mocuta, C., & Bertrand, L. (2015). Cerium anomaly at microscale in fossils. *Analytical Chemistry*, *87*(17), 8827–8836. https://doi.org/10.1021/acs.analchem.5b01820

Gunderson, A. R., Frame, A. M., Swaddle, J. P., & Forsyth, M. H. (2008). Resistance of melanized feathers to bacterial degradation: is it really so black and white? *Journal of Avian Biology*, *39*(5), 539–545. https://doi.org/10.1111/j.2008.0908-8857.04413.x

Gupta, N. S., Cody, G. D., Tetlie, O. E., Briggs, D. E., & Summons, R. E. (2009). Rapid incorporation of lipids into macromolecules during experimental decay of invertebrates: initiation of geopolymer formation. *Organic Geochemistry*, *40*(5), 589–594. https://doi.org/10.1016/j.orggeochem.2009.02.005

Gupta, N. S., Michels, R., Briggs, D. E., Evershed, R. P., & Pancost, R. D. (2006). The organic preservation of fossil arthropods: an experimental study. *Proceedings of the Royal Society B: Biological Sciences*, *273*(1602), 2777–2783. https://dx.doi.org/10.1098%2Frspb.2006.3646

Haslam, I. S., Roubos, E. W., Mangoni, M. L., Yoshizato, K., Vaudry, H., Kloepper, J. E., Pattwell, D. M., Maderson, P. F. A., & Paus, R. (2014). From frog integument to human skin: dermatological perspectives from frog skin biology. *Biological Reviews*, *89*(3), 618–655. https://doi.org/10.1111/brv.12072

Haupaix, N., & Manceau, M. (2020). The embryonic origin of periodic color patterns. *Developmental Biology*, *460*(1), 70–76. https://doi.org/10.1016/j.ydbio.2019.08.003

Hellström, A. R., Sundström, E., Gunnarsson, U., Bed'Hom, B., Tixier-Boichard, M., Honaker, C. F., Sahlqvist, A.-S., Jensen, P., Kämpe, O., Siegel, P. B., Kerje, S., & Andersson, L. (2010). Sex-linked barring in chickens is controlled by the CDKN2A/B tumour suppressor locus. *Pigment Cell & Melanoma Research*, *23*(4), 521–530. https://doi.org/10.1111/j.1755-148X.2010.00700.x

Hoekstra, H. (2006). Genetics, development and evolution of adaptive pigmentation in vertebrates. *Heredity*, *97*(3), 222–234. https://doi.org/10.1038/sj.hdy.6800861

Holthaus, K. B., Eckhart, L., Dalla Valle, L., & Alibardi, L. (2018). Evolution and diversification of corneous beta-proteins, the characteristic epidermal proteins of reptiles and birds. *Journal of Experimental Zoology Part B: Molecular and Developmental Evolution*, *330*(8), 438–453. https://doi.org/10.1002/jez.b.22840

Hong, L., & Simon, J. D. (2007). Current understanding of the binding sites, capacity, affinity, and biological significance of metals in melanin. *The Journal of Physical Chemistry*, *111*, 7938–7947. https://doi.org/10.1021/jp071439h

Hou, L.-H., Martin, L. D., Zhou, Z., Feduccia, A., & Zhang, F. (1999). A diapsid skull in a new species of the primitive bird *Confuciusornis*. *Nature*, *399*(6737), 679–682. https://doi.org/10.1038/21411

Hou, L.-H., Zhou, Z., Martin, L. D., & Feduccia, A. (1995). A beaked bird from the Jurassic of China. *Nature*, *377*(6550), 616–618. https://doi.org/10.1038/377616a0

Hu, D., Clarke, J. A., Eliason, C. M., Qiu, R., Li, Q., Shawkey, M. D., Zhao, C., D'Alba, L., & Xu, X. (2018). A bony-crested Jurassic dinosaur with evidence of iridescent plumage highlights complexity in early paravian evolution. *Nature Communications*, *9*(1), Article 217. https://doi.org/10.1038/s41467-017-02515-y

Hudon, J. (2005). Considerations in the conservation of feathers and hair, particularly their pigments. In Alberta Regional Group of Conservators (Ed.), *Fur trade legacy: the preservation of organic materials* (pp. 127–147). Canadian Association for Conservation of Cultural Property.

Hurbain, I., Geerts, W. J., Boudier, T., Marco, S., Verkleij, A. J., Marks, M. S., & Raposo, G. (2008). Electron tomography of early melanosomes: implications for melanogenesis and the generation of fibrillar amyloid sheets. *Proceedings of the National Academy of Sciences*, *105*(50), 19726–19731. https://doi.org/10.1073/pnas.0803488105

Inaba, M., & Chuong, C.-M. (2020). Avian pigment pattern formation: developmental control of macro-(across the body) and micro-(within a feather) level of pigment patterns. *Frontiers in Cell and Developmental Biology*, *8*, Article 620. https://doi.org/10.3389/fcell.2020.00620

Ito, S., & Fujita, K. (1985). Microanalysis of eumelanin and pheomelanin in hair and melanomas by chemical degradation and liquid chromatography. *Analytical Biochemistry*, *144*(2), 527–536. https://doi.org/10.1016/0003-2697(85)90150-2

Ito, S., & Wakamatsu, K. (2008). Chemistry of mixed melanogenesis—Pivotal roles of dopaquinone. *Photochemistry and Photobiology*, *84*(3), 582–592. https://doi.org/10.1111/j.1751-1097.2007.00238.x

Ito, S., Del Bino, S., Hirobe, T., & Wakamatsu, K. (2020). Improved HPLC conditions to determine eumelanin and pheomelanin contents in biological samples using an ion pair reagent. *International Journal of Molecular Sciences*, *21*(14), Article 5134. https://doi.org/10.3390/ijms21145134

Ito, S., Kikuta, M., Koike, S., Szewczyk, G., Sarna, M., Zadlo, A., Sarna, T., & Wakamatsu, K. (2016). Roles of reactive oxygen species in UVA-induced oxidation of 5, 6-dihydroxyindole-2-carboxylic acid-melanin as studied by differential spectrophotometric method. *Pigment Cell & Melanoma Research*, *29*(3), 340–351. https://doi.org/10.1111/pcmr.12469

Ito, S., Miyake, S., Maruyama, S., Suzuki, I., Commo, S., Nakanishi, Y., & Wakamatsu, K. (2018). Acid hydrolysis reveals a low but constant level of pheomelanin in human black to brown hair. *Pigment Cell & Melanoma Research*, *31*(3), 393–403. https://doi.org/10.1111/pcmr.12673

Ito, S., Nakanishi, Y., Valenzuela, R. K., Brilliant, M. H., Kolbe, L., & Wakamatsu, K. (2011). Usefulness of alkaline hydrogen peroxide oxidation to analyze eumelanin and pheomelanin in various tissue samples: application to chemical analysis of human hair melanins. *Pigment Cell & Melanoma Research*, *24*(4), 605–613. https://doi.org/10.1111/j.1755-148x.2011.00864.x

Ito, S., Wakamatsu, K., & Ozeki, H. (2000). Chemical analysis of melanins and its application to the study of the regulation of melanogenesis. *Pigment Cell Research*, *13*(Suppl. 8), 103–109. https://doi.org/10.1034/j.1600-0749.13.s8.19.x

Ito, S., Wakamatsu, K., d'Ischia, M., Napolitano, A., & Pezzella, A. (2011). Structure of melanins. In J. Borovansky & P. A. Riley (Eds.), *Melanins and melanosomes: biosynthesis, Biogenesis, physiological, and pathological functions* (pp. 167–185). Wiley.

Ito, S., Wakamatsu, K., Glass, K., & Simon, J. D. (2013). High-performance liquid chromatography estimation of cross-linking of dihydroxyindole moiety in eumelanin. *Analytical Biochemistry*, *434*(2), 221–225. https://doi.org/10.1016/j.ab.2012.12.005

Jardine, P. E., Abernethy, F. A., Lomax, B. H., Gosling, W. D., & Fraser, W. T. (2017). Shedding light on sporopollenin chemistry, with reference to UV reconstructions. *Review of Palaeobotany and Palynology*, *238*, 1-6. https://doi.org/10.1016/j.revpalbo.2016.11.014

Jardine, P. E., Hoorn, C., Beer, M. A., Barbolini, N., Woutersen, A., Bogota-Angel, G., Gosling, W. D., Fraser, W. T., Lomax, B. H., Huang, H., Sciumbata, M., He, H., & Dupont-Nibet, G. (2021). Sporopollenin chemistry and its durability in the geological record: an integration of extant and fossil chemical data across the seed plants. *Palaeontology*, *64*(2), 285–305. https://doi.org/10.1111/pala.12523

Jarenmark, M., Sjövall, P., Ito, S., Wakamatsu, K., & Lindgren, J. (2021). Chemical evaluation of eumelanin maturation by ToF-SIMS and alkaline peroxide oxidation HPLC analysis. *International Journal of Molecular Sciences*, *22*(1), Article 161. https://doi.org/10.3390/ijms22010161

Ji, Q., Norell, M. A., Gao, K.-Q., Ji, S.-A., & Ren, D. (2001). The distribution of integumentary structures in a feathered dinosaur. *Nature*, *410*(6832), 1084–1088. https://doi.org/10.1038/35074079

Kalinin, A. E., Kajava, A. V., & Steinert, P. M. (2002). Epithelial barrier function: assembly and structural features of the cornified cell envelope. *BioEssays*, *24*(9), 789–800. https://doi.org/10.1002/bies.10144

Kawi, S., & Kathiraser, Y. (2015). CO_2 as an oxidant for high-temperature reactions. *Frontiers in Energy Research*, *3*, Article 13. https://doi.org/10.3389/fenrg.2015.00013

Kishida, R., Aspera, S. M., & Kasai, H. (2021). *Melanin chemistry explored by quantum mechanics*. Springer-Nature.

Kobayashi, T., Urabe, K., Winder, A., Jiménez-Cervantes, C., Imokawa, G., Brewington, T., Solno, F., García-Borrón, J. C., & Hearing, V. J. (1994). Tyrosinase related protein 1 (TRP1) functions as a DHICA oxidase in melanin biosynthesis. *The EMBO Journal*, *13*(24), 5818–5825.

Kok, M. D., Rijpstra, W. I. C., Robertson, L., Volkman, J. K., & Sinninghe Damsté, J. S. (2000). Early steroid sulfurisation in surface sediments of a permanently stratified lake (Ace Lake, Antarctica). *Geochimica et Cosmochimica Acta*, *64*(8), 1425–1436. https://doi.org/10.1016/S0016-7037(99)00430-5

Kowata, K., Nakaoka, M., Nishio, K., Fukao, A., Satoh, A., Ogoshi, M., Takahashi, S., Tsudzuki, M., & Takeuchi, S. (2014). Identification of a feather β-keratin gene exclusively expressed in pennaceous barbule cells of contour feathers in chicken. *Gene*, *542*(1), 23–28. https://doi.org/10.1016/j.gene.2014.03.027

Kreplak, L., Doucet, J., Dumas, P., & Briki, F. (2004). New aspects of the α-helix to β-sheet transition in stretched hard α-keratin fibers. *Biophysical Journal*, *87*(1), 640–647. https://dx.doi.org/10.1529%2Fbiophysj.103.036749

Ksepka, D. T., Clarke, J. A., Nesbitt, S. J., Kulp, F. B., & Grande, L. (2013). Fossil evidence of wing shape in a stem relative of swifts and hummingbirds (Aves, Pan-Apodiformes). *Proceedings of the Royal Society B: Biological Sciences*, *280*(1761), Article 20130580. http://dx.doi.org/10.1098/rspb.2013.0580

Kushimoto, T., Basrur, V., Valencia, J., Matsunaga, J., Vieira, W. D., Ferrans, V. J., Muller, J., Appella, E., & Hearing, V. J. (2001). A model for melanosome biogenesis based on the purification and analysis of early melanosomes. *Proceedings of the National Academy of Sciences*, *98*(19), 10698–10703. https://doi.org/10.1073/pnas.191184798

Li, A., Figueroa, S., Jiang, T.-X., Wu, P., Widelitz, R., Nie, Q., & Chuong, C.-M. (2017). Diverse feather shape evolution enabled by coupling anisotropic signalling modules with self-organizing branching programme. *Nature Communications*, *8*, Article ncomms14139. https://dx.doi.org/10.1038%2Fncomms14139

Li, Q., Clarke, J. A., Gao, K.-Q., Peteya, J. A., & Shawkey, M. D. (2018). Elaborate plumage patterning in a Cretaceous bird. *PeerJ*, *6*, Article e5831. https://doi.org/10.7717/peerj.5831

Li, Q., Clarke, J. A., Gao, K.-Q., Zhou, C.-F., Meng, Q., Li, D., D'Alba, L., & Shawkey, M. D. (2014). Melanosome evolution indicates a key physiological shift within feathered dinosaurs. *Nature*, *507*(7492), 350–353. https://doi.org/10.1038/nature12973

Li, Q., Gao, K.-Q., Meng, Q., Clarke, J. A., Shawkey, M. D., D'Alba, L., Pei, R., Ellison, M., Norell, M. A., & Vinther, J. (2012). Reconstruction of *Microraptor* and the evolution of iridescent plumage. *Science*, *335*(6073), 1215–1219. https://doi.org/10.1126/science.1213780

Li, Q., Gao, K.-Q., Vinther, J., Shawkey, M. D., Clarke, J. A., D'Alba, L., Meng, Q., Briggs, D. E., & Prum, R. O. (2010). Plumage color patterns of an extinct dinosaur. *Science*, *327*(5971), 1369–1372. https://doi.org/10.1126/science.1186290

Lin, G.-W., Li, A., & Chuong, C.-M. (2020). Molecular and cellular mechanisms of feather development provide a basis for the diverse evolution of feather forms. In C. Foth & O. W. M. Rauhut (Eds.), *The evolution of feathers* (pp. 13–26). Springer, Cham.

Lin, S., Foley, J., Jiang, T., Yeh, C., Wu, P., Foley, A., Yen, C. M., Huang, Y. C., Cheng, H. C., Chen, C. F., Reeder, B., Jee, S. H., Widelitz, R. B., & Chuong, C. M. (2013). Topology of feather melanocyte progenitor niche allows complex pigment patterns to emerge. *Science*, *340*(6139), 1442–1445. https://doi.org/10.1126/science.1230374

Lindgren, J., Kuriyama, T., Madsen, H., Sjövall, P., Zheng, W., Uvdal, P., Engdahl, A., Moyer, A. E., Gren, J., Kamezaki, N., Ueno, S., & Schweitzer, M. H. (2017). Biochemistry and adaptive colouration of an exceptionally preserved juvenile fossil sea turtle. *Scientific Reports*, *7*(1), Article 13324. https://doi.org/10.1038/s41598-017-13187-5

Lindgren, J., Moyer, A., Schweitzer, M. H., Sjövall, P., Uvdal, P., Nilsson, D. E., Heimdal, J., Engdahl, A., Gren, J. A., Schultz, B. P., & Kear, B. P. (2015a). Interpreting melanin-based coloration through deep time: a critical review. *Proceedings of the Royal Society B: Biological Sciences*, *282*(1813), Article 20150614. https://doi.org/10.1098/rspb.2015.0614

Lindgren, J., Nilsson, D.-E., Sjövall, P., Jarenmark, M., Ito, S., Wakamatsu, K., Kear, B.P., Schultz, B. P., Sylvestersen, R. L., Madsen, H., LaFountain, J. R., Jr., Alwmark, C., Eriksson, M. E., Hall, S. A., Lindgren, P., Rodríguez-Meizoso, I., & Ahlberg, P. (2019). Fossil insect eyes shed light on trilobite optics and the arthropod pigment screen. *Nature*, *573*(7772), 122–125. https://doi.org/10.1038/s41586-019-1473-z

Lindgren, J., Sjövall, P., Carney, R. M., Cincotta, A., Uvdal, P., Hutcheson, S. W., Gustafsson, O., Lefèvre, U., Escuillié, F., Heimdal, J., Engdahl, A., Gren, J. A., Kear, B. P., Wakamatsu, K., Yans, J., & Godefroit, P. (2015b). Molecular composition and ultrastructure of Jurassic paravian feathers. *Scientific Reports*, *5*, Article 13520. https://doi.org/10.1038/srep13520

Lindgren, J., Sjövall, P., Carney, R. M., Uvdal, P., Gren, J. A., Dyke, G., Schultz, B. P., Shawkey, M. D., Barnes, K. R., Polcyn, M. J. (2014). Skin pigmentation provides evidence of convergent melanism in extinct marine reptiles. *Nature*, *506*(7489), 484–488. https://doi.org/10.1038/nature12899

Lindgren, J., Sjövall, P., Thiel, V., Zheng, W., Ito, S., Wakamatsu, K., Hauff, R., Kear, B. P., Engdahl, A., Alwmark, C., Eriksson, M.E., Jarenmark, M., Sachs, S., Ahlberg, P. E., Marone, F., Kuriyama, T., Gustafsson, O., Malmberg, P., Thomas, A., . . . Schweitzer, M. H. (2018). Soft-tissue evidence for homeothermy and crypsis in a Jurassic ichthyosaur. *Nature*, *564*(7736), 359–365. https://doi.org/10.1038/s41586-018-0775-x

Lindgren, J., Uvdal, P., Sjövall, P., Nilsson, D. E., Engdahl, A., Schultz, B. P., & Thiel, V. (2012). Molecular preservation of the pigment melanin in fossil melanosomes. *Nature Communications*, *3*(1), Article 824. https://doi.org/10.1038/ncomms1819

Lingham-Soliar, T. (2003a). The dinosaurian origin of feathers: perspectives from dolphin (Cetacea) collagen fibers. *Naturwissenschaften*, *90*(12), 563–567. https://doi.org/10.1007/s00114-003-0483-7

Lingham-Soliar, T. (2003b). Evolution of birds: ichthyosaur integumental fibers conform to dromaeosaur protofeathers. *Naturwissenschaften*, *90*(9), 428–432. https://doi.org/10.1007/s00114-003-0448-x

Lingham-Soliar, T., Feduccia, A., & Wang, X. (2007). A new Chinese specimen indicates that 'protofeathers' in the Early Cretaceous theropod dinosaur *Sinosauropteryx* are degraded collagen fibres. *Proceedings of the Royal Society B: Biological Sciences*, *274*(1620), 1823–1829. https://doi.org/10.1098/rspb.2007.0352

Liu, Y., Hong, L., Wakamatsu, K., Ito, S., Adhyaru, B., Cheng, C.-Y., Bowers, C. R., & Simon, J. D. (2005). Comparison of structural and chemical properties of black and red human hair melanosomes. *Photochemistry and Photobiology*, *81*(1), 135–144. https://doi.org/10.1562/2004-08-03-ra-259.1

Liu, S. Y. (2014). Elucidation of the chemical composition of avian melanin. *RSC Advances*, *4*(76), 40396–40399.

Lowe, C. B., Clarke, J. A., Baker, A. J., Haussler, D., & Edwards, S. V. (2015). Feather development genes and associated regulatory innovation predate the origin of Dinosauria. *Molecular Biology and Evolution*, *32*(1), 23–28. https://doi.org/10.1093/molbev/msu309

Maia, R., D'Alba, L., & Shawkey, M. D. (2010). What makes a feather shine? A nanostructural basis for glossy black colours in feathers. *Proceedings of the Royal Society B: Biological Sciences*, *278*(1714), 1973–1980. https://doi.org/10.1098/rspb.2010.1637

Manceau, M., Domingues, V. S., Mallarino, R., & Hoekstra, H. E. (2011). The developmental role of Agouti in color pattern evolution. *Science*, *331*(6020), 1062–1065. https://doi.org/10.1126/science.1200684

Manning, P. L., Edwards, N. P., Bergmann, U., Anné, J., Sellers, W. I., van Veelen, A., Sokaras, D., Egerton, V. M., Alonso-Mori, R., Ignatyev, K., van Dongen, B. E., Wakamatsu, K., Ito, S., Knoll, F., & Wogelius, R. A. (2019). Pheomelanin pigment remnants mapped in fossils of an extinct mammal. *Nature Communications*, *10*(1), Article 2250. https://doi.org/10.1038/s41467-019-10087-2

Manning, P. L., Edwards, N. P., Wogelius, R. A., Bergmann, U., Barden, H. E., Larson, P. L., Schwarz-Wings, D., Egerton, V. M., Sokaras, D., Mori, R. A., & Sellers, W. I. (2013). Synchrotron-based chemical imaging reveals plumage patterns in a 150 million year old early bird. *Journal of Analytical Atomic Spectrometry*, *28*(7), 1024–1030. https://doi.org/10.1039/C3JA50077B

Marshall, C. P., Emry, J. R., & Marshall, A. O. (2011). Haematite pseudomicrofossils present in the 3.5-billion-year-old Apex Chert. *Nature Geoscience*, *4*(4), 240–243. https://doi.org/10.1038/ngeo1084

McCoy, V. E., Gabbott, S. E., Penkman, K., Collins, M. J., Presslee, S., Holt, J., Grossman, H., Wang, B., Solórzano Kraemer, M. M., Delclós, X., & Peñalver, E. (2019). Ancient amino acids from fossil feathers in amber. *Scientific Reports*, *9*(1), Article 6420. https://doi.org/10.1038/s41598-019-42938-9

McCoy, V. E., Soriano, C., & Gabbott, S. E. (2016). A review of preservational variation of fossil inclusions in amber of different chemical groups. *Earth and Environmental Science Transactions of the Royal Society of Edinburgh*, *107*(2–3), 203–211. https://doi.org/10.1017/S1755691017000391

McGraw, K. J. (2006). Mechanics of uncommon colors: pterins, porphyrins, and psittacofulvins. *Bird Coloration*, *1*, 354–398.

McGraw, K., Safran, R., & Wakamatsu, K. (2005). How feather colour reflects its melanin content. *Functional Ecology*, *19*(5), 816–821. https://doi.org/10.1111/j.1365-2435.2005.01032.x

McMahon, S., Anderson, R. P., Saupe, E. E., & Briggs, D. E. (2016). Experimental evidence that clay inhibits bacterial decomposers: implications for preservation of organic fossils. *Geology*, *44*(10), 867–870. https://doi.org/10.1130/G38454.1

McNamara, M. E. (2013). The taphonomy of colour in fossil insects and feathers. *Palaeontology*, *56*(3), 557–575. https://doi.org/10.1111/pala.12044

McNamara, M. E., Briggs, D. E., Orr, P. J., Field, D. J., & Wang, Z. (2013). Experimental maturation of feathers: implications for reconstructions of fossil feather colour. *Biology Letters*, *9*(3). Article 20130184. https://doi.org/10.1098/rsbl.2013.0184

McNamara, M. E., Briggs, D. E., Orr, P. J., Wedmann, S., Noh, H., & Cao, H. (2011). Fossilized biophotonic nanostructures reveal the original colors of 47-million-year-old moths. *PLoS Biology*, *9*(11), Article e1001200. https://doi.org/10.1371/journal.pbio.1001200

McNamara, M. E., Kaye, J. S., Benton, M. J., Orr, P. J., Rossi, V., Ito, S., & Wakamatsu, K. (2018). Non-integumentary melanosomes can bias reconstructions of the colours of fossil vertebrates. *Nature Communications*, *9*, Article 2878. https://doi.org/10.1038/s41467-018-05148-x

McNamara, M. E., Orr, P. J., Alcalá, L., Anadón, P., & Peñalver-Mollá, E. (2012). What controls the taphonomy of exceptionally preserved taxa—Environment or biology? A case study using frogs from the Miocene Libros Konservat-Lagerstätte (Teruel, Spain). *Palaios*, *27*(2), 63–77.

McNamara, M. E., Orr, P. J., Kearns, S. L., Alcalá, L., Anadón, P., & Peñalver-Mollá, E. (2006). High-fidelity organic preservation of bone marrow in ca. 10 Ma amphibians. *Geology*, *34*(8), 641–644. https://doi.org/10.1130/G22526.1

McNamara, M. E., Orr, P. J., Kearns, S. L., Alcalá, L., Anadón, P., & Peñalver-Mollá, E. (2010). Exceptionally preserved tadpoles from the Miocene of Libros, Spain: ecomorphological reconstruction and the impact of ontogeny upon taphonomy. *Lethaia*, *43*(3), 290–306. https://doi.org/10.1111/j.1502-3931.2009.00192.x

McNamara, M. E., Orr, P. J., Kearns, S. L., Alcalá, L., Anadón, P., & Peñalver-Mollá, E. (2016a). Reconstructing carotenoid-based and structural coloration in fossil skin. *Current Biology*, *26*(8), 1075–1082. https://doi.org/10.1016/j.cub.2016.02.038

McNamara, M. E., Rossi, V., Slater, T., Rogers, C., Ducrest, A.-L., Dubey, S., & Roulin, A. (2021). Decoding the evolution of melanin in vertebrates. *Trends in Ecology & Evolution*, *36*(5), 430–443. https://doi.org/10.1016/j.tree.2020.12.012

McNamara, M. E., Saranathan, V., Locatelli, E. R., Noh, H., Briggs, D. E., Orr, P. J., & Cao, H. (2014). Cryptic iridescence in a fossil weevil generated by single diamond photonic crystals. *Journal of the Royal Society Interface*, *11*(100), Article 20140736. https://doi.org/10.1098/rsif.2014.0736

McNamara, M. E., van Dongen, B. E., Lockyer, N. P., Bull, I. D., & Orr, P. J. (2016b). Fossilization of melanosomes via sulfurization. *Palaeontology*, *59*(3), 337–350. https://doi.org/10.1111/pala.12238

Mischke, D., Korge, B. P., Marenholz, I., Volz, A., & Ziegler, A. (1996). Genes encoding structural proteins of epidermal cornification and S100 calcium-binding proteins form a gene complex ("epidermal differentiation complex") on human chromosome 1q21. *Journal of Investigative Dermatology*, *106*(5), 989–992. https://doi.org/10.1111/1523-1747.ep12338501

Mokrejs, P., Svoboda, P., Hrncirik, J., Janacova, D., & Vasek, V. (2011). Processing poultry feathers into keratin hydrolysate through alkaline-enzymatic hydrolysis. *Waste Management & Research*, *29*(3), 260–267. https://doi.org/10.1177/0734242x10370378

Moyer, A. E., Zheng, W., Johnson, E. A., Lamanna, M. C., Li, D.-Q., Lacovara, K. J., & Schweitzer, M. H. (2014). Melanosomes or microbes: testing an alternative hypothesis for the origin of microbodies in fossil feathers. *Scientific Reports*, *4*, Article 4233. https://doi.org/10.1038/srep04233

Moyer, A., Zheng, W., & Schweitzer, M. (2016). Keratin durability has implications for the fossil record: results from a 10 year feather degradation experiment. *PloS One*, *11*(7), Article e0157699. https://doi.org/10.1371/journal.pone.0157699

Murdock, D. J., Gabbott, S. E., Mayer, G., & Purnell, M. A. (2014). Decay of velvet worms (*Onychophora*), and bias in the fossil record of lobopodians. *BMC Evolutionary Biology*, *14*(1), Article 222. https://doi.org/10.1186/s12862-014-0222-z

Muscente, A., Schiffbauer, J. D., Broce, J., Laflamme, M., O'Donnell, K., Boag, T. H., Meyer, M., Hawkins, A. D., Huntley, J. W., McNamara, M., MacKenzie, L. A., Stanley, G. D., Jr., Hinman, N. W., Hofmann, M. H., & Xiao, S. (2017). Exceptionally preserved fossil assemblages through geologic time and space. *Gondwana Research*, *48*, 164–188. https://doi.org/10.1016/j.gr.2017.04.020

Napolitano, A., Di Donato, P., Prota, G., & Land, E. J. (1999). Transient quinonimines and 1, 4-benzothiazines of pheomelanogenesis: new pulse radiolytic and spectrophotometric evidence. *Free Radical Biology and Medicine*, *27*(5–6), 521–528. https://doi.org/10.1016/s0891-5849(99)00098-2

Negro, J. J., Finlayson, C., & Galván, I. (2018). Melanins in fossil animals: is it possible to infer life history traits from the coloration of extinct species? *International Journal of Molecular Sciences*, *19*(2), Article 230. https://dx.doi.org/10.3390%2Fijms19020230

Ng, C. S., Wu, P., Fan, W.-L., Yan, J., Chen, C.-K., Lai, Y.-T., Wu, S.-M., Mao, C.-T., Chen, J.-J., Lu, M.-J. J., Ho, M.-R., Widelitz, R. B., Chen, C.-F., Chuong, C.-M., & Li, W.-H. (2014). Genomic organization, transcriptomic analysis, and functional characterization of avian α-and β-keratins in diverse feather forms. *Genome Biology and Evolution*, *6*(9), 2258–2273. https://doi.org/10.1093/gbe/evu181

Ng, C. S., Wu, P., Foley, J., Foley, A., McDonald, M.-L., Juan, W.-T., Huang, C.-J., Lai, Y.-T., Lo, W.-S., Chen, C.-F., Leal, S. M., Zhang, H., Widelitz, R. B., Patel, P. I., Li, W.-H., & Chuong, C.-M. (2012). The chicken frizzle feather is due to an α-keratin (KRT75) mutation that causes a defective rachis. *PLoS Genetics*, *8*(7), Article e1002748. https://doi.org/10.1371/journal.pgen.1002748

Norell, M. A., Ji, Q., Gao, K., Yuan, C., Zhao, Y., & Wang, L. (2002). 'Modern' feathers on a non-avian dinosaur. *Nature*, *416*(6876), 36–37. https://doi.org/10.1038/416036a

Norell, M. A., Wiemann, J., Fabbri, M., Yu, C., Marsicano, C. A., Moore-Nall, A., Varricchio, D. J., Pol, D., & Zelenitsky, D. K. (2020). The first dinosaur egg was soft. *Nature*, *583*(7816), 406–410. https://doi.org/10.1038/s41586-020-2412-8

Odin, G. P., McNamara, M. E., Arwin, H., & Järrendahl, K. (2018). Experimental degradation of helicoidal photonic nanostructures in scarab beetles (Coleoptera: Scarabaeidae): implications for the identification of circularly polarizing cuticle in the fossil record. *Journal of the Royal Society Interface*, *15*(148), Article 20180560. https://doi.org/10.1098/rsif.2018.0560

Ohtaki, N., & Seiji, M. (1971). Degradation of melanosomes by lysosomes. *Journal of Investigative Dermatology*, *57*(1), 1–5. https://doi.org/10.1111/1523-1747.ep12292038

Ozeki, H., Ito, S., Wakamatsu, K., & Thody, A. J. (1996). Spectrophotometric characterization of eumelanin and pheomelanin in hair. *Pigment Cell Research*, *9*(5), 265–270. https://doi.org/10.1111/j.1600-0749.1996.tb00116.x

Pacton, M., Fiet, N., & Gorin, G. (2006). Revisiting amorphous organic matter in Kimmeridgian laminites: what is the role of the vulcanization process in the amorphization of organic matter? *Terra Nova*, *18*(6), 380–387. https://doi.org/10.1111/j.1365-3121.2006.00702.x

Pahua-Ramos, M., Hernández-Melchor, D., Camacho-Pérez, B., & Quezada-Cruz, M. (2017). Degradation of chicken feathers: a review. *Biotechnology: An Indian Journal*, *13*(6), Article 153.

Pan, Y., Zheng, W., Moyer, A. E., O'Connor, J. K., Wang, M., Zheng, X., Wang, X., Schroeter, E. R., Zhou, Z., & Schweitzer, M. H. (2016). Molecular evidence of keratin and melanosomes in feathers of the Early Cretaceous bird *Eoconfuciusornis*. *Proceedings of the National Academy of Sciences*, *113*(49), E7900–E7907. https://doi.org/10.1073/pnas.1617168113

Pan, Y., Zheng, W., Sawyer, R. H., Pennington, M. W., Zheng, X., Wang, X., Wang, M., Hu, L., O'Connor, J., Zhao, T., Li, Z., Schroeter, E. R., Wu, F., Xu, X., Zhou, Z., & Schweitzer, M. H. (2019). The molecular evolution of feathers with direct evidence from fossils. *Proceedings of the National Academy of Sciences*, *116*(8), 3018–3023. https://doi.org/10.1073/pnas.1815703116

Panzella, L., Gentile, G., D'Errico, G., Della Vecchia, N. F., Errico, M. E., Napolitano, A., Carfagna, C., & d'Ischia, M. (2013). Atypical structural and π-electron features of a melanin polymer that lead to superior free-radical-scavenging properties. *Angewandte Chemie International Edition*, *52*(48), 12684–12687. https://doi.org/10.1002/anie.201305747

Petrovich, R. (2001). Mechanisms of fossilization of the soft-bodied and lightly armored faunas of the Burgess Shale and of some other classical localities. *American Journal of Science*, *301*(8), 683–726. https://doi.org/10.2475/ajs.301.8.683

Pinheiro, F. L., Prado, G., Ito, S., Simon, J. D., Wakamatsu, K., Anelli, L. E.,Andrade, J. A. F., & Glass, K. (2019). Chemical characterization of pterosaur melanin challenges color inferences in extinct animals. *Scientific Reports*, *9*(1), Article 15947. https://doi.org/10.1038/s41598-019-52318-y

Poinar, H. N., Höss, M., Bada, J. L., & Pääbo, S. (1996). Amino acid racemization and the preservation of ancient DNA. *Science*, *272*(5263), 864–866. https://doi.org/10.1126/science.272.5263.864

Preston, L. J., & Genge, M. J. (2010). The Rhynie Chert, Scotland, and the search for life on Mars. *Astrobiology*, *10*(5), 549–560. https://doi.org/10.1089/ast.2008.0321

Preston, L., Shuster, J., Fernández-Remolar, D., Banerjee, N., Osinski, G., & Southam, G. (2011). The preservation and degradation of filamentous bacteria and biomolecules within iron oxide deposits at Rio Tinto, Spain. *Geobiology*, *9*(3), 233–249. https://doi.org/10.1111/j.1472-4669.2011.00275.x

Prum, R. O. (1999). Development and evolutionary origin of feathers. *Journal of Experimental Zoology*, *285*(4), 291–306.

Prum, R. O., & Brush, A. H. (2002). The evolutionary origin and diversification of feathers. *The Quarterly Review of Biology*, *77*(3), 261–295. https://doi.org/10.1086/341993

Prum, R. O., & Dyck, J. (2003). A hierarchical model of plumage: morphology, development, and evolution. *Journal of Experimental Zoology Part B: Molecular and Developmental Evolution*, *298*(1), 73–90. https://doi.org/10.1002/jez.b.27

Prum, R. O., & Torres, R. (2003). Structural colouration of avian skin: convergent evolution of coherently scattering dermal collagen arrays. *Journal of Experimental Biology*, *206*(14), 2409–2429. https://doi.org/10.1242/jeb.00431

Prum, R. O., & Williamson, S. (2002). Reaction–diffusion models of within-feather pigmentation patterning. *Proceedings of the Royal Society of London. Series B: Biological Sciences*, *269*(1493), 781–792. https://doi.org/10.1098/rspb.2001.1896

Qiang, J., Currie, P. J., Norell, M. A., & Shu-An, J. (1998). Two feathered dinosaurs from northeastern China. *Nature*, *393*(6687), 753–761. https://doi.org/10.1038/31635

Reshes, G., Vanounou, S., Fishov, I., & Feingold, M. (2008). Timing the start of division in *E. coli*: a single-cell study. *Physical Biology*, *5*(4), Article 046001. https://doi.org/10.1088/1478-3975/5/4/046001

Rogers, C. S., Astrop, T. I., Webb, S. M., Ito, S., Wakamatsu, K., & McNamara, M. E. (2019). Synchrotron X-ray absorption spectroscopy of melanosomes in vertebrates and cephalopods: implications for the affinity of *Tullimonstrum*. *Proceedings of the Royal Society B*, *286*(1913), Article 20191649. https://doi.org/10.1098/rspb.2019.1649

Rogers, C. S., Webb, S. M., & McNamara, M. E. (2021). Synchrotron x-ray fluorescence analysis reveals diagenetic alteration of fossil melanosome trace metal chemistry. *Palaeontology*, *64*(1), 63–73. https://doi.org/10.5061/dryad.r7sqv9s7q

Rorsman, H., Agrup, G., Hansson, C., Rosengren, A. M., & Rosengren, E. (1979). Detection of phaeomelanins. *Pigment Cell*, *4*, 244–252

Rossi, V., McNamara, M. E., Webb, S. M., Ito, S., & Wakamatsu, K. (2019). Tissue-specific geometry and chemistry of modern and fossilized melanosomes reveal internal anatomy of extinct vertebrates. *Proceedings of the National Academy of Sciences*, *116*(36), 17880–17889. https://doi.org/10.1073/pnas.1820285116

Rossi, V., Webb, S. M., & McNamara, M. E. (2020). Hierarchical biota-level and taxonomic controls on the chemistry of fossil melanosomes revealed using synchrotron X-ray fluorescence. *Scientific Reports*, *10*(1), Article 8970. https://doi.org/10.1038/s41598-020-65868-3

Rossi, V., Webb, S. M., & McNamara, M. E. (2021). Maturation experiments reveal bias in the chemistry of fossil melanosomes. *Geology*, *49*(7), 784–788. https://doi.org/10.1130/G48696.1

Roulin, A., Mafli, A., & Wakamatsu, K. (2013). Reptiles produce pheomelanin: evidence in the eastern Hermann's tortoise (*Eurotestudo boettgeri*). *Journal of Herpetology*, *47*(2), 258–261. https://doi.org/10.1670/12-028

Roy, A., Rogers, C. S., Clements, T., Pittman, M., Habimana, O., Martin, P., & Vinther, J. (2020). Fossil microbodies are melanosomes: evaluating and rejecting the "fossilized decay-associated microbes" hypothesis. *Bulletin of the American Museum of Natural History*, *440*(1), 251–276.

Saitta, E. T., & Vinther, J. (2019). A perspective on the evidence for keratin protein preservation in fossils: an issue of replication versus validation. *Palaeontologia Electronica*, *22*(4), Article 22.3.2E. https://doi.org/10.26879/1017E

Saitta, E. T., Kaye, T. G., & Vinther, J. (2018). Sediment-encased maturation: a novel method for simulating diagenesis in organic fossil preservation. *Palaeontology*, *62*(1), 135–150. https://doi.org/10.1111/pala.12386

Saitta, E. T., Rogers, C. S., Brooker, R. A., & Vinther, J. (2017a). Experimental taphonomy of keratin: a structural analysis of early taphonomic changes. *Palaios*, *32*(10), 647–657. https://doi.org/10.2110/palo.2017.051

Saitta, E. T., Rogers, C., Brooker, R. A., Abbott, G. D., Kumar, S., O'Reilly, S. S., Donohoe, P., Dutta, S., Summons, R. E., & Vinther, J. (2017b). Low fossilization potential of keratin protein revealed by experimental taphonomy. *Palaeontology*, *60*(4), 547–556. https://doi.org/10.5061/dryad.h02q0

Sansom, R. S. (2014). Experimental decay of soft tissues. In M. Laflamme, J. D. Schiffbauer, & S. A. F. Darroh (Eds.), *Reading and writing of the fossil record: preservational pathways to exceptional fossilization: The Paleontological Society Papers* (Vol. PS20, pp. 259–274). Paleontological Research Institution.

Sansom, R. S., Gabbott, S. E., & Purnell, M. A. (2010). Non-random decay of chordate characters causes bias in fossil interpretation. *Nature*, *463*(7282), 797–800. https://doi.org/10.1038/nature08745

Sansom, R. S., Gabbott, S. E., & Purnell, M. A. (2011). Decay of vertebrate characters in hagfish and lamprey (Cyclostomata) and the implications for the vertebrate fossil record. *Proceedings of the Royal Society B: Biological Sciences*, *278*(1709), 1150–1157. https://doi.org/10.1098/rspb.2010.1641

Sansom, R. S., Gabbott, S. E., & Purnell, M. A. (2013). Atlas of vertebrate decay: a visual and taphonomic guide to fossil interpretation. *Palaeontology*, *56*(3), 457–474. https://doi.org/10.1111/pala.12037

Schopf, J. W., Barghoorn, E. S., Maser, M. D., & Gordon, R. O. (1965). Electron microscopy of fossil bacteria two billion years old. *Science*, *149*(3690), 1365–1367. https://doi.org/10.1126/science.149.3690.1365

Schouten, S., de Graaf, W., Sinninghe Damsté, J. S., van Driel, G. B., & de Leeuw, J. W. (1994). Laboratory simulation of natural sulphurization: II. Reaction of multi-functionalized lipids with inorganic polysulphides at low temperatures. *Organic Geochemistry*, *22*(3–5), 825–834.

Schweitzer, M. H., Avci, R., Collier, T., & Goodwin, M. B. (2008). Microscopic, chemical and molecular methods for examining fossil preservation. *Comptes Rendus Palevol*, *7*(2–3), 159–184. https://doi.org/10.1016/j.crpv.2008.02.005

Schweitzer, M. H., Watt, J., Avci, R., Knapp, L., Chiappe, L., Norell, M., & Marshall, M. (1999b). Beta-keratin specific immunological reactivity in feather-like structures of the Cretaceous Alvarezsaurid, *Shuvuuia deserti*. *Journal of Experimental Zoology*, *285*(2), 146–157.

Schweitzer, M. H., Zheng, W., Moyer, A. E., Sjövall, P., & Lindgren, J. (2018). Preservation potential of keratin in deep time. *PloS One*, *13*(11), Article e0206569. https://doi.org/10.1371/journal.pone.0206569

Seilacher, A. (1970). Begriff und bedeutung der Fossil-Lagerstätten: Neues Jahrbuch für Geologie und Paläontologie, Abhandlungen (pp. 34-39).

Shawkey, M. D., D'Alba, L., Xiao, M., Schutte, M., & Buchholz, R. (2015). Ontogeny of an iridescent nanostructure composed of hollow melanosomes. *Journal of Morphology*, *276*(4), 378–384. https://doi.org/10.1002/jmor.20347

Shawkey, M. D., Hauber, M. E., Estep, L. K., & Hill, G. E. (2006). Evolutionary transitions and mechanisms of matte and iridescent plumage coloration in grackles and allies (Icteridae). *Journal of the Royal Society Interface*, *3*(11), 777–786. https://doi.org/10.1098/rsif.2006.0131

Shimojima, M. (2011). Biosynthesis and functions of the plant sulfolipid. *Progress in Lipid Research*, *50*(3), 234–239. https://doi.org/10.1016/j.plipres.2011.02.003

Shimomura, Y., & Ito, M. (2005). Human hair keratin-associated proteins. Journal of Investigative Dermatology Symposium Proceedings, 10(3), 230–233. https://doi.org/10.1111/j.1087-0024.2005.10112.x

Sinninghe Damsté, J. S., Rijpstra, W. I. C., Coolen, M. J., Schouten, S., & Volkman, J. K. (2007). Rapid sulfurisation of highly branched isoprenoid (HBI) alkenes in sulfidic Holocene sediments from Ellis Fjord, Antarctica. *Organic Geochemistry*, *38*(1), 128–139. https://doi.org/10.1016/j.orggeochem.2006.08.003

Shu, D. G., Luo, H.-L., Conway Morris, S., Zhang, X. L., Hu, S.-X., Chen, L., . . . Chen, L. Z. (1999). Lower Cambrian vertebrates from south China. *Nature*, *402*(6757), 42-46.

Smith, B. C. (2011). *Fundamentals of Fourier transform infrared spectroscopy*. CRC Press.

Smithwick, F. M., Nicholls, R., Cuthill, I. C., & Vinther, J. (2017). Countershading and stripes in the theropod dinosaur *Sinosauropteryx* reveal heterogeneous habitats in the Early Cretaceous Jehol Biota. *Current Biology*, *27*(21), 3337–3343. https://doi.org/10.1016/j.cub.2017.09.032

Solano, F. (2020). Photoprotection and skin pigmentation: melanin-related molecules and some other new agents obtained from natural sources. *Molecules*, *25*(7), Article 1537. https://dx.doi.org/10.3390%2Fmolecules25071537

Stanic, V., Maia, F. C. B., de Oliveira Freitas, R., Montoro, F. E., & Evans-Lutterodt, K. (2018). The chemical fingerprint of hair melanosomes by infrared nano-spectroscopy. *Nanoscale*, *10*(29), 14245–14253. https://doi.org/10.1039/C8NR03146K

Stankiewicz, B. A., Briggs, D. E., & Evershed, R. P. (1997). Chemical composition of Paleozoic and Mesozoic fossil invertebrate cuticles as revealed by pyrolysis–gas chromatography/mass spectrometry. *Energy & Fuels*, *11*(3), 515–521. https://doi.org/10.1021/ef9601778

Stankiewicz, B. A., Briggs, D., Michels, R., Collinson, M., Flannery, M., & Evershed, R. (2000). Alternative origin of aliphatic polymer in kerogen. *Geology*, *28*(6), 559–562. https://doi.org/10.1130/0091-7613(2000)28%3C559:AOOAPI%3E2.0.CO;2

Lucas, A. M., & Stettenheim, P. R. (1972). Avian Anatomy-Integument. Washington, DC: US Dept. *Agricult. Handbook*.

Strullu-Derrien, C., Bernard, S., Spencer, A. R., Remusat, L., Kenrick, P., & Derrien, D. (2019). On the structure and chemistry of fossils of the earliest woody plant. *Palaeontology*, *62*(6), 1015–1026.

Stuart-Fox, D., Ospina-Rozo, L., Ng, L., & Franklin, A. M. (2021). The paradox of iridescent signals. *Trends in Ecology & Evolution*, *36*(3), 187–195. https://doi.org/10.1016/j.tree.2020.10.009

Tadano-Aritomi, K., Hikita, T., Suzuki, A., Toyoda, H., Toida, T., Imanari, T., & Ishizuka, I. (2001). Determination of lipid-bound sulfate by ion chromatography and its application to quantification of sulfolipids from kidneys of various mammalian species. *Journal of Lipid Research*, *42*(10), 1604–1608.

Tanaka, G., Parker, A. R., Hasegawa, Y., Siveter, D. J., Yamamoto, R., Miyashita, K., Takahashi, Y., Ito, S., Wakamatsu, K., Mukuda, T., Matsuura, M., Tomikawa, K., Furutani, M., Suzuki, K., & Maeda, H. (2014). Mineralized rods and cones suggest colour vision in a 300 Myr-old fossil fish. *Nature Communications*, *5*(1), Article 5920. https://doi.org/10.1038/ncomms6920

Thomas, D. B., McGoverin, C. M., McGraw, K. J., James, H. F., & Madden, O. (2013). Vibrational spectroscopic analyses of unique yellow feather pigments (spheniscins) in penguins. *Journal of the Royal Society Interface*, *10*(83), Article 20121065. https://doi.org/10.1098/rsif.2012.1065

Thompson, M. (2014). *Everything you need to know about feathers*. The Cornell Lab Bird Academy. https://academy.allaboutbirds.org/feathers-article/

Unwin, D. M., & Martill, D. M. (2020). No protofeathers on pterosaurs. *Nature Ecology & Evolution*, *4*(12), 1590–1591. https://doi.org/10.1038/s41559-020-01308-9

Urabe, K., Aroca, P., Tsukamoto, K., Mascagna, D., Palumbo, A., Prota, G., & Hearing, V. J. (1994). The inherent cytotoxicity of melanin precursors: a revision. *Biochimica et Biophysica Acta*, *1221*(3), 272–278. https://doi.org/10.1016/0167-4889(94)90250-x

van der Valk, T., Pečnerová, P., Díez-del-Molino, D., Bergström, A., Oppenheimer, J., Hartmann, S., Zenikoudakis, G., Thomas, J. A., Dehasque, M., Saglican, E., Fidan, F. R., Barnes, I., Liu, S., Somel, M., Heintzman, P. D.,Nikolskiy, P., Shapiro, B., Skoglund, P., Hofreiter, M., . . . Dalén, L. (2021). Million-year-old DNA sheds light on the genomic history of mammoths. *Nature*, *591*(7849), 265–269. https://doi.org/10.1038/s41586-021-03224-9

van Dongen, B. E., Schouten, S., & Sinninghe Damsté, J. S. (2006). Preservation of carbohydrates through sulfurization in a Jurassic euxinic shelf sea: examination of the Blackstone Band TOC cycle in the Kimmeridge Clay Formation, UK. *Organic Geochemistry*, *37*(9), 1052–1073. http://dx.doi.org/10.1016/j.orggeochem.2006.05.007

van Dongen, B. E., Schouten, S., & Sinninghe Damsté, J. S. (2003). Sulfurization of carbohydrates results in a sulfur-rich, unresolved complex mixture in kerogen pyrolysates. *Energy & Fuels*, *17*(4), 1109–1118. https://doi.org/10.1021/ef0202283

Varejão, F. G., Warren, L. V., Simões, M. G., Fürsich, F. T., Matos, S. A., & Assine, M. L. (2019). Exceptional preservation of soft tissues by microbial entombment: insights into the taphonomy of the Crato Konservat-Lagerstätte. *Palaios*, *34*(7), 331–348. https://doi.org/10.2110/palo.2019.041

Vinther, J. (2016). Fossil melanosomes or bacteria? A wealth of findings favours melanosomes: melanin fossilises relatively readily, bacteria rarely, hence the need for clarification in the debate over the identity of microbodies in fossil animal specimens. *BioEssays*, *38*(3), 220–225. https://doi.org/10.1002/bies.201500168

Vinther, J., Briggs, D. E., Clarke, J., Mayr, G., & Prum, R. O. (2010). Structural coloration in a fossil feather. *Biology Letters*, *6*(1), 128–131. https://doi.org/10.1098/rsbl.2009.0524

Vinther, J., Briggs, D. E., Prum, R. O., & Saranathan, V. (2008). The colour of fossil feathers. *Biology Letters*, *4*(5), 522–525. https://doi.org/10.1098/rsbl.2008.0302

Vinther, J., Nicholls, R., Lautenschlager, S., Pittman, M., Kaye, T. G., Rayfield, E., Mayr, F., & Cuthill, I. C. (2016). 3D camouflage in an ornithischian dinosaur. *Current Biology*, *26*(18), 2456–2462. https://doi.org/10.1016/j.cub.2016.06.065

Voight, J. R., Pörtner, H. O., & O'Dor, R. K. (1995). A review of ammonia-mediated buoyancy in squids (cephalopoda: Teuthoidea). *Marine and Freshwater Behaviour and Physiology*, *25*(1–3), 193–203. https://doi.org/10.1080/10236249409378917

von Meyer, H. (1861). Vogel-Federn und Palpipes priscus von Solnhofen. Neues Jahrbuch für Mineralogie, Geognosie, Geologie und Petrefakten-Kunde 1861:561.

Wakamatsu, K., & Ito, S. (2002). Advanced chemical methods in melanin determination. *Pigment Cell Research*, *15*(3), 174–183. https://doi.org/10.1034/j.1600-0749.2002.02017.x

Wakamatsu, K., Ito, S., & Rees, J. L. (2002). The usefulness of 4-amino-3-hydroxyphenylalanine as a specific marker of pheomelanin. *Pigment Cell Research*, *15*(3), 225–232. https://doi.org/10.1034/j.1600-0749.2002.02009.x

Wakamatsu, K., Ohtara, K., & Ito, S. (2009). Chemical analysis of late stages of pheomelanogenesis: conversion of dihydrobenzothiazine to a benzothiazole structure. *Pigment Cell & Melanoma Research*, *22*(4), 474–486. https://doi.org/10.1111/j.1755-148x.2009.00580.x

Wang, B., Yang, W., McKittrick, J., & Meyers, M. A. (2016). Keratin: structure, mechanical properties, occurrence in biological organisms, and efforts at bioinspiration. *Progress in Materials Science*, *76*, 229–318. https://doi.org/10.1016/j.pmatsci.2015.06.001

Wang, M., Árnadóttir, L., Xu, Z. J., & Feng, Z. (2019). In situ X-ray absorption spectroscopy studies of nanoscale electrocatalysts. *Nano-Micro Letters*, *11*, Article 47. https://doi.org/10.1007/s40820-019-0277-x

Wang, X., Shi, Z., Zhao, Q., & Yun, Y. (2021). Study on the structure and properties of biofunctional keratin from rabbit hair. *Materials*, *14*(2), Article 379. https://doi.org/10.3390/ma14020379

Wellnhofer, P. (2009). *Archaeopteryx: the icon of evolution*. Verlag Dr. Friedrich Pfeil.

Westall, F., de Wit, M. J., Dann, J., van der Gaast, S., de Ronde, C. E., & Gerneke, D. (2001). Early Archean fossil bacteria and biofilms in hydrothermally-influenced sediments from the Barberton greenstone belt, South Africa. *Precambrian Research*, *106*(1–2), 93–116. https://doi.org/10.1016/S0301-9268(00)00127-3

Wiemann, J., Fabbri, M., Yang, T.-R., Stein, K., Sander, P. M., Norell, M. A., & Briggs, D. E. (2018). Fossilization transforms vertebrate hard tissue proteins into N-heterocyclic polymers. *Nature Communications*, *9*(1), Article 4741. https://doi.org/10.1038/s41467-018-07013-3

Wilby, P. R., & Briggs, D. E. (1997). Taxonomic trends in the resolution of detail preserved in fossil phosphatized soft tissues. *Geobios*, *30*(Suppl. 1), 493–502. https://doi.org/10.1016/S0016-6995(97)80056-3

Wogelius, R., Manning, P., Barden, H., Edwards, N., Webb, S., Sellers, W., Taylor, K. G., Larson, P. L., Dodson, P., You, H., Da-Qing, L., & Bergmann, U. (2011). Trace metals as biomarkers for eumelanin pigment in the fossil record. *Science*, *333*(6049), 1622–1626. https://doi.org/10.1126/science.1205748

Wolnicka-Glubisz, A., Pecio, A., Podkowa, D., Kolodziejczyk, L. M., & Plonka, P. M. (2012). Pheomelanin in the skin of *Hymenochirus boettgeri* (Amphibia: Anura: Pipidae). *Experimental Dermatology*, *21*(7), 537–540. https://doi.org/10.1111/j.1600-0625.2012.01511.x

Wu, P., Ng, C. S., Yan, J., Lai, Y.-C., Chen, C.-K., Lai, Y.-T., Wu, S.-M., Chen, J.-J., Luo, W., Widelitz, R. B., Li, W.-H., & Chuong, C.-M. (2015). Topographical mapping of α-and β-keratins on developing chicken skin integuments: functional interaction and evolutionary perspectives. *Proceedings of the National Academy of Sciences*, *112*(49), E6770–E6779. https://doi.org/10.1073/pnas.1520566112

Wuttke, M. (1983). Weichteil-Erhaltung durch lithifizierte Mikroorganismen bei mittel-eozänen Vertrebraten aus den Ölschiefern der Grube Messel bei Darmstadt. *Senckenbergiana Lethaea*, *64*(5–6), 509–527.

Xiao, M., Shawkey, M. D., & Dhinojwala, A. (2020). Bioinspired melanin-based optically active materials. *Advanced Optical Materials*, *8*(19), Article 2000932. https://doi.org/10.1002/adom.202000932

Xing, L., McKellar, R. C., Xu, X., Li, G., Bai, M., Persons, W. S., IV, Miyashita, T., Benton, M. J., Zhang, J., Wolfe, A. P., Yi, Q., Tseng, K., Ran, H., & Currie, P. J. (2016). A feathered dinosaur tail with primitive plumage trapped in mid-Cretaceous amber. *Current Biology*, *26*(24), 3352–3360. https://doi.org/10.1016/j.cub.2016.10.008

Xu, X., & Zhang, F. (2005). A new maniraptoran dinosaur from China with long feathers on the metatarsus. *Naturwissenschaften*, *92*(4), 173–177. https://doi.org/10.1007/s00114-004-0604-y

Xu, X., Norell, M. A., Kuang, X., Wang, X., Zhao, Q., & Jia, C. (2004). Basal tyrannosauroids from China and evidence for protofeathers in tyrannosauroids. *Nature*, *431*(7009), 680–684. https://doi.org/10.1038/nature02855

Xu, X., Tang, Z.-L., & Wang, X.-L. (1999). A therizinosauroid dinosaur with integumentary structures from China. *Nature*, *399*(6734), 350–354. https://doi.org/10.1038/20670

Xu, X., Zhao, Q., Norell, M., Sullivan, C., Hone, D., Erickson, G., Wang, X., Han, F., & Guo, Y. (2009). A new feathered maniraptoran dinosaur fossil that fills a morphological gap in avian origin. *Chinese Science Bulletin*, *54*(3), 430–435. http://dx.doi.org/10.1007/s11434-009-0009-6

Xu, X., Zheng, X., & You, H. (2010). Exceptional dinosaur fossils show ontogenetic development of early feathers. *Nature*, *464*(7293), 1338–1341. https://doi.org/10.1038/nature08965

Xu, X., Zhou, Z.-H., & Prum, R. O. (2001). Branched integumental structures in *Sinornithosaurus* and the origin of feathers. *Nature*, *410*(6825), 200–204. https://doi.org/10.1038/35065589

Xu, X., Zhou, Z., & Wang, X. (2000). The smallest known non-avian theropod dinosaur. *Nature*, *408*(6813), 705–708. https://doi.org/10.1038/35047056

Yang, Z., Jiang, B., McNamara, M. E., Kearns, S. L., Pittman, M., Kaye, T. G., Orr, P. J., Xu, X., & Benton, M. J. (2019). Pterosaur integumentary structures with complex feather-like branching. *Nature Ecology & Evolution*, *3*(1), 24–30. https://doi.org/10.1038/s41559-018-0728-7

Ye, Y., Shen, J., Feng, Q., & Lash, G. G. (2020). Microbial and animal evolution in relation to redox fluctuations in a deep-water setting of South China during the Ediacaran-Cambrian transition (ca. 551–523 Ma). *Palaeogeography, Palaeoclimatology, Palaeoecology*, *546*, Article 109672. https://doi.org/10.1016/j.palaeo.2020.109672

Yu, M., Wu, P., Widelitz, R. B., & Chuong, C.-M. (2002). The morphogenesis of feathers. *Nature*, *420*(6913), 308–312. https://doi.org/10.1038/nature01196

Yue, Z., Jiang, T.-X., Widelitz, R. B., & Chuong, C.-M. (2006). Wnt3a gradient converts radial to bilateral feather symmetry via topological arrangement of epithelia. *Proceedings of the National Academy of Sciences*, *103*(4), 951–955. https://doi.org/10.1073/pnas.0506894103

Zeisler-Diehl, V., Al-Khutabi, E. A. A., Kirfel, G., Schreiber, L., van Echten-Deckert, G., & Herzog, V. (2020). Detection of endogenous lipids in chicken feathers distinct from preen gland constituents. *Protoplasma*, *257*(6), 1709–1724. https://doi.org/10.1007/s00709-020-01544-7

Zhang, F., Kearns, S. L., Orr, P. J., Benton, M. J., Zhou, Z., Johnson, D., Xu, X., & Wang, X. (2010). Fossilized melanosomes and the colour of Cretaceous dinosaurs and birds. *Nature*, *463*(7284), 1075–1078. https://doi.org/10.1038/nature08740

Zhao, T., Hu, J., Hu, L., & Pan, Y. (2020). Experimental maturation of feathers: implications for interpretations of fossil feathers. *Palaios*, *35*(2), 67–76. https://doi.org/10.2110/palo.2019.064

Appendix I

Decoding the evolution of melanin in vertebrates

McNamara *et al*., Trends in Ecology and Evolution (2021)

Available at: https://www.cell.com/trends/ecology-evolution/fulltext/S0169-5347(20)30375-X

Appendix II

Supplementary dataset 1

Available at:
https://datadryad.org/stash/dataset/doi:10.5061/dryad.7290t40

Supplementary dataset 2

Available at:
https://datadryad.org/stash/share/S-MhQ_n5-OThmzG5lkLqWB20y2viwIDyvHBfLKNce2Y